Alternative Chemistries for Etching of Silicon Dioxide and Silicon Nitride

by

Simon Martin Karecki

B.S. Electrical Engineering
Yale University, 1994

Submitted to the Department of Electrical Engineering and Computer Science in Partial Fulfillment of the Requirements for the Degree of

Master of Science
in
Electrical Engineering and Computer Science

at the
MASSACHUSETTS INSTITUTE OF TECHNOLOGY
September, 1996

Signature of Author _____
Department of Electrical Engineering and Computer Science
June 21, 1996

Certified by _____
Professor L. Rafael Reif, Thesis Supervisor
Department of Electrical Engineering and Computer Science
Director, Microsystems Technology Laboratories, MIT

Accepted by _____
Professor Frederic R. Morgenthaler
Chairman, Department Committee on Graduate Students

Alternative Chemistries for Etching of Silicon Dioxide and Silicon Nitride

by

Simon Martin Karecki

Submitted to the Department of Electrical Engineering and Computer Science in Partial Fulfillment of the Requirements for the Degree of

Master of Science
in
Electrical Engineering and Computer Science

at the
MASSACHUSETTS INSTITUTE OF TECHNOLOGY
September, 1996

Abstract

At the present time, the etching of dielectric films in semiconductor processing applications relies almost exclusively on the use of perfluorocompounds (PFCs), gases which are suspected global warming agents. The author's research represents the initial stage of a project whose aim is to identify and characterize possible replacements for PFCs in the two principal etching applications: wafer patterning and plasma enhanced chemical vapor deposition (PECVD) chamber cleaning. These processes, which play essential roles in the manufacture of integrated circuits, use and emit perfluorocompounds in steadily increasing quantities. The scope of the work discussed herein has been to characterize the etch performance of a number of potential replacement candidates for etching silicon dioxide and silicon nitride. The results will be used to screen the candidates for subsequent work, the goal of which will be the development of actual replacement processes for the wafer patterning and chamber cleaning applications respectively. These subsequent stages of this project, portions of which are expected to form the basis of the author's Ph.D. thesis, will build upon the results discussed herein.

A number of potential replacement chemistries from the hydrofluorocarbon (HFC) family has been examined during the course of this work. Statistically designed experiments and neural network analysis were used to develop empirical models of the etch behavior of these compounds in a commercially available magnetically-enhanced reactive ion etch (MERIE) tool. Optical emission interferometry was used to measure etch rates *in-situ*. Films of thermally grown silicon dioxide and stoichiometric chemical vapor deposited silicon nitride on 100 mm boron-doped silicon substrates were used for this study. A five-level, three-variable central composite design (CCD) experimental matrix was employed to study the dependence of film etch rate on process pressure (35-150 mTorr), magnetic field strength (0-100 Gauss), and oxygen flow rate (0-20 sccm) at constant etch gas flow rates (40 sccm) and constant radio frequency power (600 W at 13.56 MHz). 1H-heptafluoropropane (CF_2H-CF_2-CF_3), 2H-heptafluoropropane (CF_3-

$CFH\text{-}CF_3$), and pentafluoroethane (C_2F_5H) were studied in this manner, with octafluoropropane (C_3F_8), a perfluorocompound, being used as a baseline reference gas.

Additional experiments were carried out with these and three other compounds: difluoromethane (CF_2H_2), 1,1,1,2-tetrafluoroethane ($CF_3\text{-}CFH_2$), and trifluoroethylene ($CF_2=CFH$). Whereas the first four compounds listed above have been found to etch both oxide and nitride films under all experimental conditions, the latter three have been found to polymerize heavily, depositing what is believed to be a fluoropolymer film, under some of the same conditions. In these latter experiments, a limited study of the effects of oxygen flow rate (0-45 sccm), etch gas flow rate (15 vs. 40 sccm), process pressure (35 vs. 93 mTorr), as well as chamber condition was carried out in a parameter space where polymerization was suppressed.

It was found that 1H-heptafluoropropane, 2H-heptafluoropropane, and pentafluoroethane etch both films at rates roughly comparable to those of octafluoropropane under a wide window of conditions. Difluoromethane, 1,1,1,2-tetrafluoroethane, and trifluoroethylene have been found to etch under certain conditions (low etch gas flow rate/low process pressure), though at rates generally lower than those of the remaining gases. Net polymer deposition was found to occur at other conditions with these three gases. On the basis of the results presented in this thesis, from a process performance standpoint, 1H- and 2H-heptafluoropropane and pentafluoroethane appear to show the most promise as etch gases that could potentially be used in wafer patterning and chamber cleaning applications. However, additional work is required to verify that these gases can satisfy all the process requirements of each of these applications. In the case of wafer patterning, anisotropy and selectivity to other materials will be of great importance. Chamber cleaning process conditions, on the other hand, tend to be considerably different from those in a wafer patterning process. Chamber cleans typically utilize higher pressure, power, as well as gas flows; thus the viability of these chemicals in this different parameter space needs to be explored. Difluoromethane, 1,1,1,2-tetrafluoroethane, and trifluoroethylene may find limited application in wafer patterning, where polymerization mechanisms sometimes play a key beneficial role in obtaining etch selectivity to other films as well as highly directional etch profiles. However, their usefulness in higher pressure chamber cleaning applications which require high etch rates appears to be marginal.

Finally, the compounds examined in this thesis represent only a portion of the potential replacement candidates that will be evaluated as part of the alternative chemistries project. The evaluation of iodofluorocarbons (IFCs), as well as unsaturated fluorocarbons is also planned.

Thesis Supervisor: Professor L. Rafael Reif
MIT Professor of Electrical Engineering and Computer Science
Director of the Microsystems Technology Laboratories, MIT

Acknowledgments

Thanks go out to my parents, for all the sacrifices they have made to get me where I am today, for all the love and encouragement they have given me over the years, and for always believing that one day I might do something worthwhile, like write a thesis, for instance. Thanks and all my love to Vanessa, for all her patience and understanding, for her never-failing support, for always being there to listen, and - most importantly - for her love and for being a part of my life in so many ways.

Thanks to Professor Rafael Reif, my advisor and the ringleader of our operation, for his leadership and encouragement, for all the advice and guidance, for his confidence in me, and for numerous opportunities to earn frequent flyer miles. Being a part of his research group has truly been a defining experience in my academic life; more importantly, however, it has helped me to grow as a person. I will always be indebted to him. Thanks to Ben Tao, my partner in this project, for his tireless efforts, for his valuable insights, for hours of stimulating discussions, for staying on top of things when the world got hectic, and for his friendship.

Thanks also to Walter Worth, our project manager at SEMATECH, for his support, for his guidance, for being the source of so many invaluable contacts, and for his confidence in our work. And to Dr. Dan Herr, our manager at SRC, for his support and guidance.

To Joe Walsh, Brian Foley, and all the research engineers and staff of the Microsystems Technology Labs for their hard - and often frustrating - work in getting the Precision 5000 up and running, and - perhaps even more importantly - in *keeping* it running; for all their help in times of crisis; and for always being there when their expertise was needed. Thanks also to Bernard Alamariu, Pat Burkhart, and everyone who helped our cause at MTL.

To Linus Cordes, Vicky Diadiuk, Prof. Marty Schmidt, and all those involved in allowing our unconventional processes to enter ICL. To Linus in particular for all his good advice. To Sue Peterson and Sam Crooks at MTL and Paul McQuillan at OSP for making sure that all the important things ran smoothly. Thanks also to Carolyn Zaccaria, Erika Satrape, Diane Hagopian, Kurt Broderick, and Debroah Hodges-Pabon for all their help.

To Igor Tepermeister and Bill Conner at Low Entropy Systems for providing us with the 1000-IS system which proved so valuable in the course of this work, and for their advice and support. Thanks too to Timothy Dalton for his insights and advice, which helped point us in the right direction when the experimental stages were getting underway.

To our SRC Mentors: Avi Kornblit from AT&T (er...Lucent Technologies), Albert Cheng and Charles Lee from TI, and Bruce Huling and Terry Sparks from Motorola. Thanks also to Laurie Beu from Motorola for her advice and encouragement.

To DuPont, for its donation of the NNAPER neural network software which played such a large role in our work, the AEDEPT database, as well as pentafluoroethane and tetrafluoroethane gases. Many thanks, in particular, to Mike Mocella for all his help and support. Thanks to 3M for their donation of octafluoropropane. Thanks also to Nick Esselman from Applied Materials for his help in answering the many questions we had about the Precision 5000.

To all the members of Professor Reif's research group: Rajan Naik, Weize Chen, and Alex Cherkassky for making my experience here a happy one. (And it's not over yet.)

Thanks to Geo, Tim, and all the staff at Cornwall's, for facilitating my trip around the world, as well as John and Pam, the owners, for allowing me to put some nonsense on a plaque

in their fine establishment. Thanks to Yoshi Uchida and Matt Reagan, for all the stimulating debates on the goods and evils of petrol taxes that were held in the said establishment. To Matt Reagan also for endless hours of *X-Files* episodes, all the homebrew, and all kinds of automotive-related advice. I plan to master toe-and-heeling by the time I write my Ph.D. thesis. Thanks to Roger Kermode, Pat Kreidl, Matthew Dyer, and Derek Surka, my housemates, for providing me with such a nice environment in which to take refuge from the world of plasma etching. Thanks to Chris Conley, for being insane enough to undertake the mammoth 48-hr. cross-continent expedition with me during the writing of this thesis. Thanks to Mark Green, Brian Chen, Karen Willcox, and everyone on Thepack for all the friendship and good times.

Finally, thanks to SEMATECH (Project S69g) and the Semiconductor Research Corporation (Contracts 94-MJ-802 and 95-EJ-802) for their funding of this work.

Table of Contents

List of Figures

List of Tables

1. Introduction

The goal of the research presented in this work is the development of alternatives to an environmentally harmful class of substances used in semiconductor manufacturing known as perfluorocompounds. This introductory chapter will review the role that perfluorocompounds play in the semiconductor industry (Section 1.1), discuss the nature of their environmental impact (Section 1.2), and outline the means through which the author's research is intended to play a part in developing a solution to this problem (Section 1.3).

Chapter 2 will attempt to provide a brief overview of the processes in semiconductor manufacturing in which perfluorocompounds are employed. Chapter 3 will discuss the selection of the chemistries that are being considered as replacements for perfluorocompounds in these processes. It will also discuss the properties of the compounds that have been selected. Chapter 4 will be devoted to the details of the experimental procedure that was used. The results of the experiments conducted with alternative chemistries will be presented in Chapter 5. Finally, Chapter 6 will provide some concluding thoughts.

1.1 Perfluorocompounds in the Semiconductor Industry

Perfluorocompound (PFC) chemistries are widely employed as process gases in the semiconductor industry. Their principal application in integrated circuit manufacture is as feed gases in plasma etching processes: patterning of thin films and *in-situ* cleaning of plasma enhanced chemical vapor deposition (PECVD) chambers. A discussion of these processes, as well as of the role of plasma discharges will be deferred until Chapter 2. A loose working definition of a "perfluorocompound" is a fully fluorinated molecule, *i.e.,* one which has all its bonds saturated with fluorine. As a practical matter, most, though not all, of the compounds currently grouped under this umbrella term are fully fluorinated halocarbons. Unsaturated fluorocarbons, *e.g.,* C_2F_4 (CF_2=CF_2), are not considered PFCs, whereas the perfluoroalkanes, *e.g.,* C_2F_6 (CF_3-CF_3) are. PFCs have been found to be effective etchants since they are rich sources of fluorine. Moreover, certain PFCs, namely fully fluorinated halocarbons, possess additional properties that are highly desirable in wafer patterning, such as the potential to form a passivating film in an etching environment. Furthermore, generally speaking, the compounds classified as

PFCs are stable, non-flammable, and (with the exception of NF_3) non-toxic, all of which further enhances their desirability from a process standpoint.

However, PFCs are considered to be very potent global warming gases, as will be discussed in the following section. Thus their use and emission represent an area of concern for the semiconductor industry. Currently, tetrafluoromethane (CF_4), hexafluoroethane (C_2F_6), sulfur hexafluoride (SF_6), nitrogen trifluoride (NF_3), and more recently octafluoropropane (C_3F_8), are the PFCs most heavily used in integrated circuit fabrication. Trifluoromethane (CHF_3), though not strictly a perfluorinated compound, is also a heavily used etchant that shares the same environmental concerns as the PFCs, and is therefore treated as one for practical purposes (see Table 1.3).

PFCs can be used to etch a variety of materials: polysilicon, dielectrics (*i.e.,* silicon dioxide, SiO_2, and silicon nitride, Si_3N_4), as well as refractory metals (*i.e.,* tungsten). Silicon dioxide and silicon nitride patterning and chamber cleaning, however, account for the largest share of PFC usage/emission in semiconductor manufacturing [2]. Of this share, chamber cleaning processes use the larger portion of PFCs. This is in part due to larger gas flows (liters per minute versus cubic centimeters per minute) and longer process times. Table 1.1 shows data released by SEMATECH on 1993 levels of U.S. semiconductor industry PFC purchases. Of the four principal gases included in the study, CF_4 and SF_6 find application primarily in wafer patterning, whereas C_2F_6 and NF_3 are used principally for chamber cleaning. It can be seen, therefore, that chamber cleaning usage does account for larger amounts of PFC purchases. This application, moreover, is reported to be the faster growing one in terms of volumes of gas consumed [2]. Nevertheless, wafer patterning still accounts for a very significant share.

Table 1.1: 1993 U.S. Semiconductor Industry PFC Purchases [1]

	CF_4	C_2F_6	NF_3	SF_6	Total
Estimated U.S. Total (in metric tons)	67	177	18	45	307
% of Total	22	58	6	14	100

As Table 1.2 shows, dielectric films are exclusively dependent on PFCs, while tungsten and polysilicon etch processes are not. As will be discussed in a later section, Section 2.3.1, the only halogen specie which is effective at etching silicon nitride and oxide films is fluorine. Moreover, presently, the only industrially accepted means of delivering fluorine to the etch process is via a PFC feed gas.

Table 1.2: Etch Applications of Perfluorocompounds [2]

Use	Gases
Silicon patterning	C_2F_6, SF_6, NF_3, CF_4, BCl_3, HBr, Cl_2, HCl
SiO_2 patterning	C_2F_6, SF_6, CF_4, CHF_3
Si_3N_4 patterning	CF_4, C_2F_6, SF_6, CHF_3
Tungsten patterning	SF_6, NF_3, Cl_2
SiO_2 and SiN_x PECVD chamber cleaning	C_2F_6, NF_3, SF_6, CF_4

1.2 Environmental Concerns Associated with Perfluorocompounds

The reason behind the increased scrutiny that PFCs have received in recent years is the role they are suspected of playing in global warming. Global warming is defined as an augmentation of what is known as the *natural greenhouse effect* through anthropogenic means. A succinct explanation of the greenhouse effect is given in [3, 6]. Essentially, little of the incoming solar radiation (which is predominantly in the "shortwave" - visible and UV - regions of the spectrum) is absorbed by the atmosphere. Approximately one third of it is reflected back into space by clouds, the air itself and atmospheric particles (which scatter the incoming light), as well as by the earth's surface. The remainder of the incoming energy is absorbed by the earth's surface, which warms up and re-emits some of it as "longwave" (IR) radiation. Without this re-emission, the earth's surface temperature would increase continuously. Whereas visible and UV radiation is not readily absorbed by atmospheric constituents, infrared radiation is. Thus a substantial portion of the outgoing IR emissions is trapped by naturally occurring gases in the atmosphere - mainly water vapor, but also carbon dioxide (CO_2), methane (CH_4), nitrous oxide

(N_2O), and ozone (O_3). These atmospheric constituents then re-emit this trapped energy, approximately half of which escapes into space, while the other half is emitted toward the surface, thus warming it. It is important to remember that, in an unperturbed state, the net outward flux of energy would balance the net incoming flux.

A perturbation in the balance between incoming and outgoing radiation is defined as *radiative forcing*. A radiative forcing effect (a change in outgoing IR radiation from the earth) can thus be attributed to a given gas, which, when present in the atmosphere, absorbs IR radiation and re-emits it toward the surface. The concept of radiative forcing is used to define global warming potential (GWP), a metric by which greenhouse gases, whether naturally occurring or anthropogenic, may be compared. This index is a measure of the time-integrated increase in radiative forcing resulting from an instantaneous release of a unit mass (1 kg) of a given compound in today's atmosphere, relative to that from 1 kg of carbon dioxide [4], which is nominally assigned a GWP of 1. This is quantified in the following equation [5]:

$$GWP_T = \frac{\int_0^T a_i c_i dt}{\int_0^T a_{CO_2} c_{CO_2} dt},$$

where a_i is a coefficient quantifying the instantaneous radiative forcing that results from a unit increase in the atmospheric concentration of a given gas i, c_i is the concentration of that gas in the atmosphere as a function of time, and T is the integration time, *i.e.,* the time after the release through which the calculation is being performed. Typically GWPs are listed for 20, 100, and 500 year time horizons, with the 100 year value being used most commonly. Gases for which GWP values have been calculated include CO_2, N_2O, methane, as well as a number of halogenated compounds, among them PFCs [6].

While present day models of the earth's climate and temperature records taken over the course of the last century do not irrefutably substantiate the existence of a global warming trend, there is substantial evidence for increased concentrations of stable, infrared absorbing gases such as CO_2 and halocarbon compounds in the atmosphere [3,6]. According to the Intergovernmental Panel on Climate Change (IPCC), if total emissions of global warming gases continue at present levels, the consequences could be an increase in global mean temperature by 0.3 °C per decade (which would not be uniformly distributed but rather relatively small at equatorial latitudes and

large in polar regions [3]) and a rise in the global mean sea level of about 6 cm per decade [5]. An increase in total rainfall (which would again not be favorably distributed) is also predicted [3].

PFCs are thought to be potent global warmers because of a confluence of two properties: high stability (and therefore atmospheric longevity) and excellent infrared absorbency [6]. This combination results in long-lived species that are very efficient at trapping and re-emitting longwave radiation emitted by the Earth's surface. A measure of the atmospheric persistence of a compound is its atmospheric lifetime, defined as the exponential decay constant for an atmospheric concentration of that species. (*I.e.,* the lifetime is the time in which a concentration of a given substance is projected to decay to 1/e or ~37% of its initial value.) The calculated atmospheric lifetimes of some of these substances are as high as thousands or tens of thousands of years [6]. Since GWP is a function of both the atmospheric longevity (which manifests itself through the time-dependent coefficient c_i in the above equation) and the infrared absorbency of a compound, it is not surprising that perfluorocompounds possess very high GWPs (see Table 1.3).

Table 1.3: Properties of Greenhouse Gases

Species	Lifetime (years)	Global Warming Potential (100 Yr. Integrated Time Horizon)
CF_4	50,000	6,300
C_2F_6	10,000	12,500
C_3F_8	5,600	6,950
SF_6	3,200	24,900
NF_3	740	8,100
CHF_3	390	12,100
CO_2	50-200	1

All from [6], except C_3F_8 [7, 8], and CHF_3, NF_3 [9].

The use of PFCs in semiconductor processing is problematic for a number of reasons. Many process tools which use these substances have low "conversion efficiencies;" that is, most of the influent feed gas is not reacted and consequently becomes part of the exhaust. While conversion efficiencies as high as 80-90% have been reported for NF_3 in some chamber cleaning

processes, figures as low as 10-15% have been found for CF_4. The PFC used in largest quantities, C_2F_6 has typical conversion efficiencies of 30-40%. [1, 8, 9] Moreover, because these chemicals are so stable, they pass unscathed through the water scrubbers commonly placed on exhaust lines at fabrication facilities [1]. Their stability also makes them difficult to abate through combustion [2].

Presently, PFC usage, and hence emission, in the semiconductor industry is increasing rapidly. This rise stems from a number of reasons, including larger numbers of wafers being processed, greater complexity of processing sequences, which results in an increase in the number of processing steps requiring PFCs, and an overall shift from wet chemical processing toward dry (gas phase) processing, which results in the use of PFCs in new applications [1].

While no regulatory driver - domestic or international - presently exists to mandate reductions in PFC emissions, the emergence of regulatory protocols regarding PFCs is a possibility. Most present anthropogenic greenhouse gas emissions are in the form of gases such as CO_2 and, to a lesser extent, N_2O and CH_4 [6]. Consequently, the initial focus of international attention by bodies such as the United Nations Conference on Environment and Development, which produced the "Framework Convention on Climate Change" in 1992 [10], has been on addressing CO_2 emissions. PFCs, however, are coming under increased scrutiny because of their alarming potency and the relative permanence of their effects. For instance, the 1993 U.S. Climate Change Action Plan, which serves as a policy blueprint for regulatory agencies such as the EPA, specifically calls for reductions in the emissions of halogenated compounds, including PFCs [11]. The EPA is, in fact, presently entering into voluntary agreements with various PFC-emitting industries, including the semiconductor industry, that are aimed at achieving emission reductions. A Memorandum of Understanding addressing PFC emissions has been negotiated between the EPA and various semiconductor manufacturers. A number of companies have already signed this agreement, which, among other terms, commits the signatories to (company-blind) reporting of estimated PFC emissions to the EPA on an annual basis, and striving to reduce their PFC emissions (as normalized to a common unit of production) through process optimization, recycling/abatement, and/or chemistry replacement [12]. In addition to governmental pressure, there are other pressures on the semiconductor industry to reduce PFC emissions, most notably DuPont's sale policy on Zyron®-116 (C_2F_6), which will phase out the

supply of C_2F_6 by DuPont if solutions to reducing emissions of this PFC are not sufficiently mature by year-end 1999 [13].

There are presently several possible avenues which can be followed in an attempt to reduce PFC emissions. These include: process optimization, emission abatement through thermal or plasma destruction, and recovery/recycle. The reader is referred to [14] for an overview of these options. Arguably the most forward-looking solution for the long term, however, would be the replacement of PFCs with compounds that are more environmentally benign. The National Technology Roadmap for Semiconductors has targeted the year 2007 as the date that PFC replacements should be available [15]. The work described in this thesis is intended to facilitate reaching that goal.

1.3 Overview of the Project on Alternative Chemistries

The work that has been performed to constitute the basis of the author's Master's thesis is part of a larger, multi-year program at MIT, whose goal is to provide industrially acceptable long-term solutions to the PFC problem. This work is presently funded by SEMATECH, the semiconductor industry consortium, through a Semiconductor Research Corporation contract under the title "Alternative Chemistries for Wafer Patterning and PECVD Chamber Cleaning." The author's Master's thesis will present results from the initial stage of this project, whose aim is the development of viable alternatives to the PFC-based etching chemistries that are used in both wafer patterning and PECVD chamber cleaning. An experimental plan for all stages of this project, which is expected to span a total of three to four years, has been formulated. As an overview, an outline of this plan, including descriptions of subsequent stages that are expected to form the basis of the author's Ph.D. thesis work, will be presented below. A more detailed description of the initial stage of this project, along with a discussion of the results obtained to date will form the body of this thesis.

The etching of two types of dielectric films, silicon dioxide and silicon nitride, is being investigated. Since the end objective of the project is eventual transfer of technology to semiconductor equipment vendors, it is planned that all stages of the project will be carried out in commercially available, rather than experimental, process tools. An Applied Materials Precision 5000 MERIE (magnetically enhanced reactive ion etcher), presently housed in the Integrated

Circuits Laboratory that is part of the Microsystems Technology Laboratories at MIT, has been used for the work described in this thesis. The Precision 5000 is a widely used commercial etch tool* that is in many ways representative of the current level of commercially available technology.

1.3.1 Preliminary Work - Industry Survey and Literature Search

Prior to the inception of the experimental work, a survey of industry process and ESH (environment, safety and health) professionals and a search of literature were conducted by the author's coworkers (B. A. Tao, L. R. Reif). This was done in an effort to obtain basic information on semiconductor industry PFC usage as well as its research needs in this area. Along with this, an attempt was made to determine what non-perfluorocompound gases, if any, had previously been examined in the role of dielectric etchants, both in industrial and R&D settings. In brief, a determination was made 1). that the development of alternatives for *both* wafer patterning and chamber cleaning processes should be pursued and 2). that the scope of the work should be properly restricted to those processes in which the development of alternatives can make the largest impact, namely dielectric film patterning and dielectric PECVD chamber cleaning. As had been mentioned earlier (Section 1.1), these processes use PFCs most heavily and are moreover exclusively dependent on PFCs, *i.e.,* no production-worthy alternatives are presently thought to be available. While a number of fluorinated compounds besides PFCs had been identified as having been used to etch dielectric films, most were rejected from consideration for this study due to either extreme handling hazards (*e.g.,* ClF_3, BrF_3, BrF_5, IF_5, anhydrous HF, F_2), lack of known suppliers (S_2F_2), or excessive cost (XeF_2). For a more extensive account of the findings of the industry survey/literature search, see [16]. The present list of candidates was drawn from a large database of halogenated compounds which was created after the completion of the search/survey. The criteria according to which the candidates were selected as well as properties of the selected compounds are discussed in Chapter 3.

---

* It should be pointed out that, although the terms "etching" and "etch process" have thus far been used generically in this thesis to describe processes which involve the removal of a film, whether it is in a wafer patterning or a chamber cleaning application, it is common practice to use these terms interchangeably with "wafer patterning." Thus an "etch tool" or an "etcher" refers to a process tool that is dedicated to a wafer patterning application.

1.3.2 Etch Viability Study

The initial stage of the project is an "etch viability" stage, during which a large number of potential replacement chemistries are being tested for etch performance relative to a perfluorinated etchant. Even though this work is being performed in a process tool used for wafer patterning, the experiments carried out during this stage are intended to be simple enough to be generic to both intended applications (wafer patterning and PECVD chamber cleaning). They are also intended to serve as a method for screening the candidate chemistries. Subsequent stages will address the wafer patterning and the chamber cleaning applications separately. These stages will use a smaller subset of the chemistries initially examined. These will be selected largely on the basis of results from the initial stage.

The primary focus of this first stage has been to determine under what conditions, if any, a given candidate chemistry will etch silicon dioxide and silicon nitride. As will be discussed in detail in Section 3.2, three families of chemistries have been selected as potential candidates to be examined: hydrofluorocarbons (HFCs), iodofluorocarbons (IFCs), and unsaturated fluorocarbons. This thesis will discuss experimental results from work carried out with the hydrofluorocarbon family. Six gases: 1H-heptafluoropropane (CF_2H-CF_2-CF_3), 2H-heptafluoropropane (CF_3-CFH-CF_3), pentafluoroethane (C_2F_5H), difluoromethane (CF_2H_2), 1,1,1,2-tetrafluoroethane (CF_3-CFH_2), and trifluoroethylene (CF_2=CFH) have been evaluated, with the PFC octafluoropropane (C_3F_8) being used as a baseline reference. The remaining families of candidate chemistries will be evaluated at a later date.

Etch rate was the principal variable of interest. Blank (unpatterned) thermally grown oxide and LPCVD (low pressure chemical vapor deposition) stoichiometric nitride films were etched. 100 mm boron-doped silicon substrates were used. Etch rate measurements were taken *in-situ* using optical emission interferometry (OEI), a technique developed by Dalton, *et al* [17]. Statistically designed experiments and neural network software were employed to formulate empirically derived etch behavior models for some of the gases. The principal process parameters whose effects were studied were process pressure, magnetic field strength, and oxygen flow rate. The effects of feed gas (etchant) flow rate and chamber condition were also studied. Section 4.2 contains a more detailed discussion of the role of each of these process parameters in the Precision 5000.

1.3.3 Wafer Patterning Study

Once the initial pool of candidate alternatives has been benchmarked for etch performance, separate experimental procedures will be followed for the wafer patterning and PECVD chamber cleaning aspects of the project. It is likely that, because process requirements in the two applications are quite different, the subset of gases used and the solutions that will emerge for each will be different.

The criteria for evaluating the performance of a wafer patterning process are numerous, but four primary parameters which are of fundamental importance in this application are etch rate, uniformity, selectivity, and anisotropy (vertical directionality of the etch). Among other important considerations are loading effects, substrate damage, residual contamination on the wafer, particle generation, wafer-to-wafer process drift, and hardware compatibility, *e.g.,* chamber corrosion or pump oil degradation. The goal of this stage will be to develop effective alternative chemistry etching processes for silicon dioxide and nitride, as defined by the above criteria. The same etch chamber on the Precision 5000 as in the first stage will be used. Thermal oxide and LPCVD nitride films will again be used. Wafers will be patterned with masks containing generic structures of varying dimensions. Different features, such as lines, rectangles, and other geometrically simple structures, in both dense and isolated patterns, will be etched. Etch rates and uniformity will be determined *in-situ* using OEI. The measured etch rates will be used to determine selectivities between the dielectric films and silicon, between the dielectric films and photoresist, as well as between the two dielectric films themselves. Anisotropy will be measured using scanning electron microscopy (SEM). Measurements of fluorine concentration in the plasma will be taken using optical emission spectroscopy (OES). An argon actinometry technique will be used. Concentrations of other species of interest, *e.g.,* CF, CF_2, may also be measured using actinometry. Auger electron spectroscopy (AES) and/or X-ray photoelectron spectroscopy (XPS) will be used to analyze any surface residues that may form. As a final test of the viability of a given etch process, devices and possibly circuits such as ring oscillators may be fabricated using the alternative process. These will then be compared against the performance of similar devices and circuits made using a standard PFC-based etch chemistry.

One of the most important diagnostics in this stage, however, will be effluent characterization using Fourier transform infrared (FTIR) spectroscopy and possibly quadrupole

mass spectroscopy (QMS). Even when gases which themselves pose no short- or long-term environmental hazards are used, undesirable products may be formed in the process chamber. A concern particular to carbon/fluorine chemistries is the possibility of perfluorocarbon formation in the plasma phase through the recombination of F atoms and CF_x fragments. For instance, it has been shown [8] that in processes which utilize larger perfluorocarbon species, *e.g.,* C_2F_6 and C_3F_8, a substantial fraction of the effluent is in the form of CF_4. A process recipe which produces significant amounts of perfluorocarbons is clearly undesirable. Monitoring the composition of the effluent stream will therefore be a critical aspect of the study.

1.3.4 Chamber Cleaning Study

In this stage of the project, a smaller subset of the chemistries evaluated in the initial stage will be used to develop an effective process for cleaning dielectric PECVD chambers. This subset will not necessarily be the same as that to be used in the wafer patterning experiments. The reason for this is that the process requirements for chamber cleaning are different and, in general, simpler than those for patterning. In chamber cleaning, the principal parameter of interest is cleaning time, *i.e.,* etch rate. Selectivity and anisotropy considerations as defined above are, generally speaking, not important. Etch rate and chamber clean time will be measured as a function of process parameters such as rf power, total pressure, and fluorocarbon and oxygen flow rates.

A Novellus Systems Concept One PECVD tool or possibly a PECVD chamber to be installed on the Precision 5000 will be used. (The Precision 5000 platform is capable of serving a dual etch/CVD role.) Typical chamber cleans in PECVD reactors consist of two steps - a high pressure electrode/susceptor clean and a low pressure remote surface clean. Both two step and single step cleans will be performed. Wafer fragments with PECVD oxide or nitride will be placed in various locations in the chamber to monitor the etch rate as a function of location. The etch rates will be measured *ex-situ* using Nanospec®. For all experiments, a deposition process will be performed in the chamber before the cleaning process is run. This pre-coating of the chamber is necessary when wafer fragments are used to avoid loading effects. Additionally, the effectiveness of the cleaning recipe will be measured by the time it takes for the chamber to be cleaned, as determined by OES endpoint detection, a common technique which identifies process

endpoint by recording the change in an emission line from the plasma (typically a fluorine emission line for PFC processes). OES will once again be used to measure concentrations of key species in the plasma. Finally, effluent characterization will be performed using FTIR and possibly QMS.

2. Fluorocarbons and Plasma Processes

The goal of this chapter will be to serve as a preface to later discussions of hydrofluorocarbon etching of dielectrics. The chapter will thus be devoted to reviewing, by way of background, the role of dielectric films in microelectronic fabrication (Section 2.1) and the salient features of plasma discharges in general (Section 2.2). While this latter discussion is not meant to be exhaustive, some key aspects of plasma discharges will be discussed at length - albeit only in first-order detail - in order to present the reader with a reasonably accurate physical picture of the environment that is present in the process chamber during the etch process. This will pave the way for a discussion of the roles of specific process parameters in the Precision 5000 etch tool that was used for the work in this thesis (Section 4.2). The general section on glow discharges will be followed by an overview of the etching of dielectric films in the plasma applications of: wafer patterning (Section 2.3) and PECVD chamber cleaning (Section 2.4). Both of these processes involve the removal of a film through chemical reactions with species generated in a non-equilibrium plasma discharge. An additional component resulting from the bombardment of the etched surface by energetic ions generated by the plasma may also play a key role, depending on the tool configuration and process conditions. As will be seen later, many etch processes, particularly those used for wafer patterning, in fact rely on a synergistic effect between the chemical and physical etch components. (There exists a still different class of etch processes involving plasmas - "sputter etching" - in which films are removed solely through physical bombardment by energetic ions. These processes, however, will not be discussed here.)

Qualitatively speaking, the same etch chemistries may be used to remove the same types of films in both the wafer patterning and the chamber cleaning applications. However, the two applications differ not only in purpose, but also in the process conditions present, the nature of the films being etched, as well as the etch mechanisms themselves. These two applications, along with PECVD itself, represent the major uses of plasma discharges in semiconductor manufacturing. While little attention has been devoted to systematic studies of etching in the chamber cleaning application, there exists a large body of literature, generated by both industry and academia, on plasma wafer patterning processes as well as PECVD. The foregoing chapter will not attempt to review this body of literature, but will instead provide a working description

of plasmas and plasma etch applications, with particular attention to the use of fluorocarbon compounds in the etching of dielectric films.

2.1 Dielectric Films in the Fabrication of Integrated Circuits

The manufacture of integrated circuits is a complex sequence of processing steps. As of this writing, fabrication of advanced integrated circuits may involve more than six weeks of processing and over 100 individual process steps [18]. Integrated circuit manufacture will not be reviewed here, as the reader may be referred to any of a number of excellent textbook sources which give detailed descriptions of typical fabrication sequences [19, 20, 21, 22].

However, it will be pointed out that dielectric films are ubiquitous throughout the structure of a typical IC. For the purposes of this discussion, the term "dielectric films" will be restricted to silicon dioxide and silicon nitride - the two most prevalent types of films, though by no means the only ones used in ICs. In a typical MOS (metal-oxide-semiconductor) system, the many uses of thermally grown silicon dioxide films include gate dielectrics, field insulation between devices, and implant or diffusion masking layers, just to name a few [23]. Deposited silicon oxides are grown via either low pressure chemical vapor deposition (LPCVD) or plasma enhanced chemical vapor deposition (PECVD). Among the uses of these films are: insulation between polysilicon and metal layers, insulation between metal layers in a multi-level metal structure, diffusion sources (when doped), masking layers, and an array of other applications [24, 25]. Silicon nitride, which is deposited through either LPCVD or PECVD, is also widely employed in ICs as: barrier layers, masking layers, passivation, blanket etch stop layers, as well as a number of other applications [26, 27]. The above list is by no means exhaustive and new variations on the uses for oxide and nitride films are constantly being developed. What is clear, however, is that, as device complexity increases, the number of process steps requiring the patterning of oxide and nitride layers will increase, as will the number of steps requiring the deposition of these films through CVD, which will in turn require the cleaning of the deposition chambers. Hence all trends point to ever increasing PFC usage and emission. It should be pointed out here that, while plasma chamber cleaning is commonly associated with the removal of residue films in plasma enhanced CVD chambers, the use of plasmas in cleaning steps has more recently been applied to tube furnaces as well.

2.2 Glow Discharge Processes - a General Description

A plasma, generally speaking, is a partially ionized gas in which the charged species have sufficient concentrations to interact through Coulombic collisions [28]. These charged species are electrons and ionized molecules and atoms. One can broadly differentiate between two types of plasmas. The first is an equilibrium plasma, where the temperatures of the ions and the electrons are equal - examples include the sun and arc welder discharges. What is known as a "plasma" in semiconductor processing usage is actually the second type, described more accurately as a *glow discharge,* or a type of *non-equilibrium plasma*. In such a discharge, the electron temperature is higher than the ion temperature. In a glow discharge used in an IC fabrication application, a typical value for the ion temperature may be 500 K (0.04 eV), while a typical value for the electron temperature may be 23,000 K (~2 eV); in the absence of external heating or cooling of the chamber containing the discharge, the neutrals in the discharge tend to remain close to room temperature [29].

A glow discharge is sustained by the introduction of energy via an electric or magnetic field. Electrons respond rapidly to the applied field, accelerating to high energies relative to those of the more massive ions and neutrals around them. Because of the large difference in mass between the electrons and other species in the discharge, little energy is lost by the electrons in elastic collisions with other particles. This means that the electrons remain energetic enough to produce significant amounts of, ions, free radicals, and other excited species through inelastic collisions with the neutrals. However, since little energy is exchanged between the population of electrons and those of other species, there is little heating of the gas in the discharge, which offers the significant advantage of allowing processing to be performed at low temperatures. [28, 30]

The gases employed in this study are all believed to generate "electropositive" plasma discharges, *i.e.,* the more common type, where the dominant negatively charged species are electrons and where negative ion populations are negligible. A second class - so-called "electronegative" discharges - exists. Representative members are plasmas generated by NF_3 and SF_6. In these plasmas, negative ions are believed to form a dominant portion of the negative species [31], which has complex repercussions on the electrical properties of the discharge. The discussion in this thesis, however, will be limited to electropositive plasmas.

The majority of plasma process tools - whether they are used for wafer patterning or PECVD - that are in use today are so-called "low density" plasma tools, where power is capacitively coupled to the discharge through a radio frequency signal, typically at 13.56 MHz. The most common configuration in such tools is the parallel plate "diode." A schematic representation of an rf diode system is shown in Figure 2.3. Process conditions such as applied rf power, pressure, and gas flow rates differ widely between applications and between different tools. Ranges for these parameters in representative etch and PECVD tools will be given in subsequent sections. Collectively, low density plasmas can be characterized by having plasma (*i.e.,* electron and ion) densities on the order of 10^9 - 10^{11} cm^{-3} and ionization fractions on the order of 10^{-6} - 10^{-3} [30, 32]. This is in contrast to "high density" etch or PECVD tools, which may use inductively coupled rf power input or microwave frequency (2.45 GHz) power input. These tools achieve plasma densities of 10^{10} - 10^{12} cm^{-3} and attain ionization fractions of 10^{-4} to 10^{-1}, *i.e.,* as high as 10% [32].

At the present time, there exists a consensus that future generations of plasma tools for dielectric patterning and film deposition will, in all likelihood, incorporate high density sources. This technology, however, is still not at a mature stage of development. In addition, it does not appear that all future generation processes will require the advantages of finer control over the conditions seen by the wafer and greater efficiency that high density tools provide. At present, conventional (low density) plasma tools are projected to continue to meet many of the needs of the industry in dielectric deposition and etch for years to come [33, 34]. Furthermore, currently installed low density tools, which presently continue to form the bulk of the installed base of plasma process equipment, have projected lifetimes of ten to fifteen years [33,34]. Thus, the focus of the alternative chemistries project will be on low density tools. The intent will be to demonstrate the viability of replacement chemistries in commercially available equipment.

Before moving on to a discussion of the processes of wafer patterning and PECVD chamber cleaning, some detail needs to be added to the description of the discharge in a plasma tool. The bulk of the plasma is always the most positive region in the system. This region, which typically fills most of the space between the electrodes, glows brightly due to the continuous deexcitation of excited species by photon emission. This is also the region where

most of the ionization and dissociation processes occur. This region is, to first order, field free and thus quasi-neutral. Electron and ion densities in the bulk are nearly equal, and are thus characterized by the single parameter - plasma density. Any surface that the plasma wets is at a lower potential than the bulk, hence an electric field exists at all surfaces wet by the plasma. The regions between the plasma bulk and electrodes and other reactor surfaces are called *sheath* regions. These regions are dark, indicating little excitation activity.

2.2.1 Sheath Formation

The reason why the plasma bulk is the most positive region in the system ultimately stems from the fact that electron and ion masses are very different. Sheath formation can be explained by the fact that the lighter electrons can acquire greater energies in response to applied fields and hence can diffuse out of the plasma bulk much more readily than ions. For a more detailed discussion of the following, the reader is referred to [35]. When a plasma is first struck, the walls of the chamber are electrically neutral. To use a simple example, one can visualize sheath formation in a dc discharge at an electrically isolated (floating) surface, designating V_f as the potential of this surface relative to ground and V_p as the potential of the plasma bulk relative to ground. If an electrically isolated surface is exposed to a plasma, initially the electron flux is much larger than the ion flux because the mean electron velocity is much larger than the mean ion velocity. The surface thus builds up a negative charge, which repels incoming electrons and decreases the electron flux. (The ion flux is not increased because it is limited by the arrival rate of ions at the interface of the plasma with the sheath that is being formed, whereas the electrons are being *de*celerated, which prevents the slower ones from reaching the surface altogether.) Since the voltage at the surface V_f is such as to repel electrons, it follows that $V_f < V_p$ and that the sheath potential $(V_p - V_f) > 0$.

The ion and electron fluxes entering the sheath at a floating surface wet by the plasma are:

$$\Phi_i = \frac{n_i \bar{c}_i}{4}, \Phi_e = \frac{n_e \bar{c}_e}{4},$$

respectively, where $n_e = n_i$ = the plasma density, and $\bar{c}_i$ and $\bar{c}_e$ are the mean velocities of the ions and the electrons *in the plasma*. (These velocities are not the classical mean square speeds,

given by $1/2\ mc^2 = 3/2\ kT$, but the mean speeds of the electron and ion populations of the plasma, which - to first order - are the mean speeds of a Maxwellian distribution, given by: $\bar{c} = (8\ kT/\pi m)^{1/2}$.) These fluxes are limited by the arrival rate of each species at the interface. In light of the argument made above, the ion flux cannot increase beyond Φ_i. The ions merely arrive at the surface with greater velocity, but at the same rate. The electron flux, however, is lower at the surface than at the interface, because only those fast enough to overcome the potential barrier of the sheath arrive at the surface. Thus, the number of electrons hitting the surface is reduced:

$$\Phi_{e,surface} = \Phi_e \exp(-\frac{e(V_p - V_f)}{kT_e}) = \Phi_i,$$

where e is the electronic charge, k is Boltzmann's constant, and T_e is the electron temperature. In the steady state, the electron and ion fluxes at the surface must balance. Thus V_f will become fixed at a value appropriate to this condition. Put another way, the voltage drop across the sheath at a floating surface can be related to the mean speeds of the ion and electron populations in the plasma, and this relation is:

$$V_p - V_f = \frac{kT_e}{e} \ln \frac{\bar{c}_e}{\bar{c}_i}.$$

For a floating surface, typical values for electron and ion masses and temperatures give a value V_p - $V_f \approx 15$ V, which is roughly consistent with measured values.

2.2.2 Rf Discharges

In a dc diode system, one of the two electrodes present (termed the *anode*) is typically grounded, while the other (the *cathode*) is coupled to the power supply. Since the anode is at ground potential, the voltage drop between it and the plasma bulk will be small, somewhat less than the floating potential V_p - V_f defined above. The cathode, however, is at supply voltage, which is typically a large negative potential; thus the cathode sheath voltage will be V_{supply} + V_p, much larger than the floating potential. Typically it is on the order of several hundred or thousand volts. The presence of a sheath at the cathode therefore serves to accelerate ions toward the surface, resulting in energetic bombardment of that surface. As will be seen shortly, in wafer patterning applications, this effect plays an important role. Moreover, at the cathode, where a sufficiently large voltage drop exists across the sheath, bombardment by ions with high energies

causes the emission of *secondary electrons* which become accelerated across the sheath, entering the plasma bulk with high energies. It is these electrons which are responsible for sustaining the discharge by promoting more ionization in the bulk region, thus generating more ions and electrons to compensate for those lost to the walls of the system. (For an explanation that goes beyond this first-order discussion, the reader is referred to [28, 36].) The potential distribution in a dc diode discharge is shown in Figure 2.1.

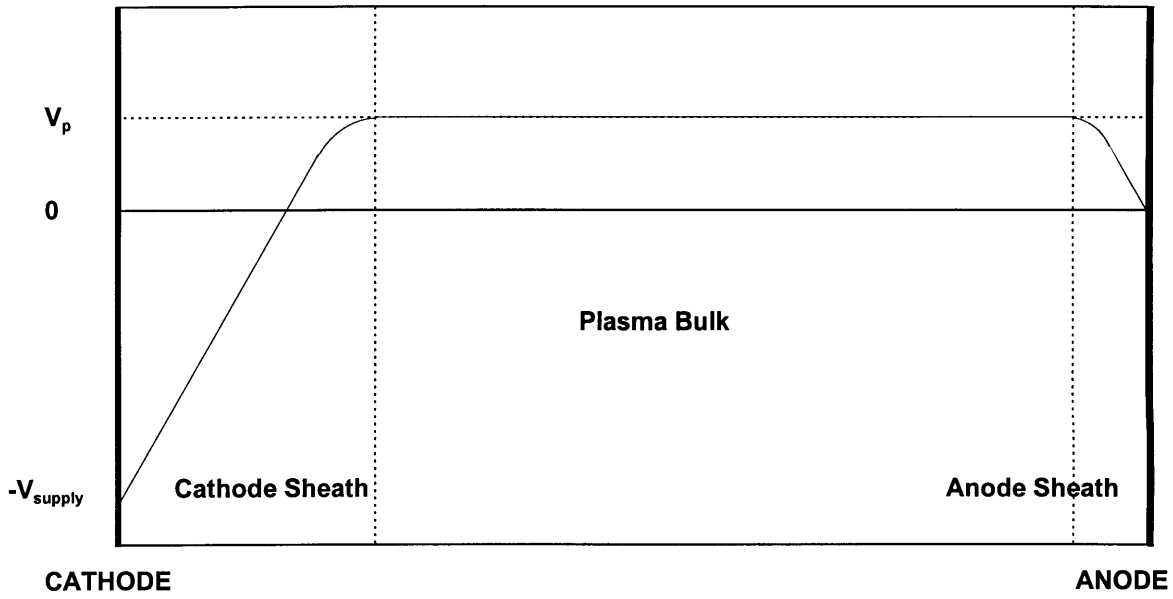

Figure 2.1

The potential distribution in a dc diode glow discharge. The anode is grounded, while the cathode is connected to a large negative supply voltage.

The above discussion is based upon a dc discharge. Dc discharges, however, are limited to systems where both electrodes are conductive. In the situation where an insulating dielectric film is present at one of the electrodes, a dc electron current cannot flow through the film and thus the discharge cannot be sustained. Rf systems overcome this limitation. While rf discharges share a number of essential features with dc discharges, they are also different in several important ways and these differences need to be addressed before this section's first-order discussion of glow discharge processes is reasonably complete.

In rf systems, in addition to the existence of an (rf) sheath voltage at all surfaces being wet by the plasma, there exists an additional dc component at all surfaces that are not at dc ground known as the *dc offset* or the *self-bias*. This voltage, along with the rf sheath voltage which modulates it, determines the energy of the bombarding ions striking those surfaces. This offset arises fundamentally - once again - from the difference between electron and ion masses. In an ac system, the concepts of *anode* and *cathode* continue to be used, though their physical meanings are somewhat different. Neither electrode is now at a "supply" potential. In fact, as will be seen shortly, in a symmetric system (where electrode areas are equal) or even in an asymmetric system (provided that no blocking capacitors are inserted between the power supply and the electrodes), the rf sheath potentials would be equal as well.

If an ac signal were applied to a floating surface exposed to a plasma, the surface would initially draw a much larger electron current on one half of the cycle than the ion current it would draw on the other half. This is because a lighter electron will accelerate to a higher velocity than an ion under the same electric field and thus carry more current. ($\mathbf{J} = ne\mathbf{v}$, where $\mathbf{J}$ is the current density per unit area, n is the concentration of charge carriers, e is the electronic charge, and $\mathbf{v}$ is the velocity at which the carriers are moving.) Were this condition to continue in a steady state, it would violate the principle that (now time-averaged) ion and electron fluxes to the surface must be equal, and would be equivalent to stating that the surface would charge negatively without bound. In order for the fluxes to balance, the duration of the cycle during which electrons are accelerated toward the surface must become shorter so that the time-averaged amount of charge arriving on the surface is equal during both parts of the cycle. This occurs through a shift of the ac waveform at the surface toward more negative values. This shift at a powered electrode is shown in Figure 2.2. The magnitude of this shift is the self-bias. An important consequence of this effect is that the powered electrode in an rf diode system is positive for only a brief fraction of each ac cycle, resulting in almost continuous ion bombardment of the powered electrode. See [37] for a more complete discussion of dc offset in rf discharges.

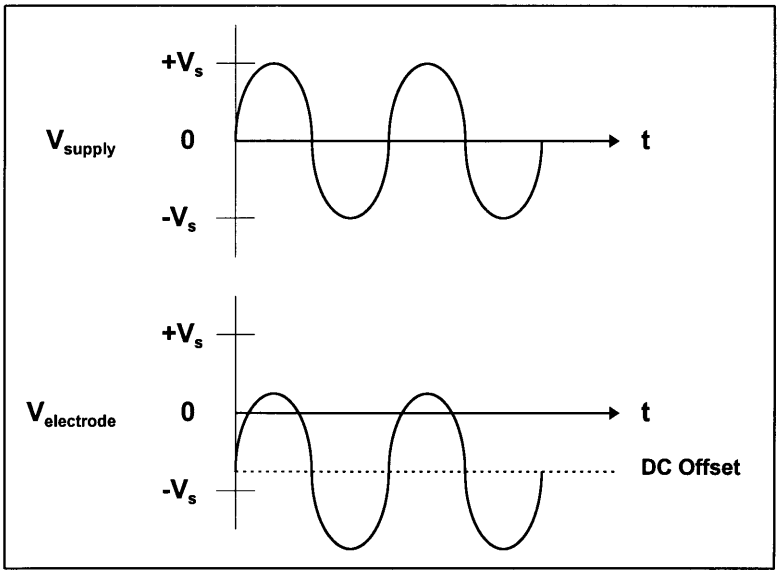

Figure 2.2

Ac voltage waveforms at the generator and at the powered electrode in an rf diode system. The signal at the electrode becomes offset by a dc bias as a result of the tendency of ion and electron fluxes to equalize. The magnitude of the dc bias is such that the net amount of charge incident on the electrode over one cycle is zero. After [37].

What determines the identity of the cathode and the anode? As in dc systems, the cathode is conventionally the electrode with the larger sheath voltage, *i.e.,* the one which is primarily responsible for the emission of secondary electrons to sustain the discharge. Which electrode this turns out to be is not determined by which one is connected to the positive terminal of the supply, but by the *area* ratio of the two electrodes [38]. Were the ac power supply connected directly to the electrodes, the area ratio would not matter. (Both electrode sheaths would sustain the same voltage drop, assuming an equipotential plasma bulk.) However, if a blocking capacitor were to be placed in the circuit between one electrode and the power supply, as is the case in practical systems where a matching network is required to couple the chamber electrodes to the power supply, this would no longer hold true. A "classical" model developed by Koenig and Maissel, based on the assumption that ion current densities at both electrodes are equal, capacitively divides the rf voltage among the two electrode sheaths. The resulting calculation arrives at a fourth-power ratio dependence:

$$\frac{V_1}{V_2} = \left(\frac{A_2}{A_1}\right)^4 .$$

As Maniv has elegantly shown [39], however, the correct assumption (and, arguably, a more intuitive one) is one of equal ion currents at the electrodes, not equal ion current densities, which brings the result to a value that is in much better agreement with experiment [38]:

$$\frac{V_1}{V_2} = \left(\frac{A_2}{A_1}\right)^2 .$$

In either case, the smaller electrode sustains the larger sheath voltage. In practical systems, with the walls of the chamber being grounded, the effective area of the grounded electrode is much larger than that of the powered electrode, thus making the grounded electrode the anode. A typical rf diode configuration is shown in Figure 2.3.

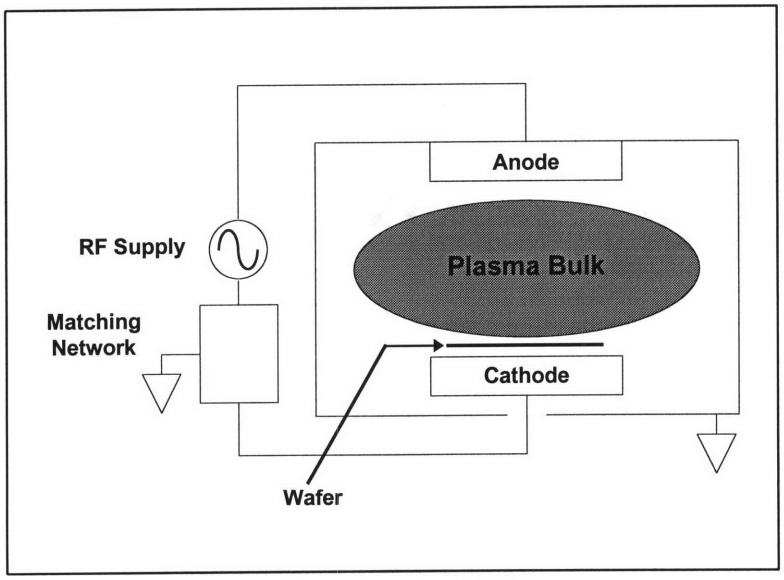

Figure 2.3

An rf diode parallel plate reactor. In this configuration, which corresponds to the Applied Materials Precision 5000 etch tool used in this work, the wafer is shown placed on the powered electrode. The matching network serves to impedance match the generator and its load (the reactor) and consists of reactive circuit components (capacitors and inductors).

2.3 Wafer Patterning

Plasma wafer patterning is a process for transferring lithographically defined features in a masking layer to an underlying film. An example of a pattern transfer sequence is shown in Figure 2.4. This step is ubiquitous throughout the microelectronic fabrication sequence, since feature definition is necessarily a part of the process of forming any device. The reader is referred to [19, 20, 21, 22] for a discussion of photolithography.

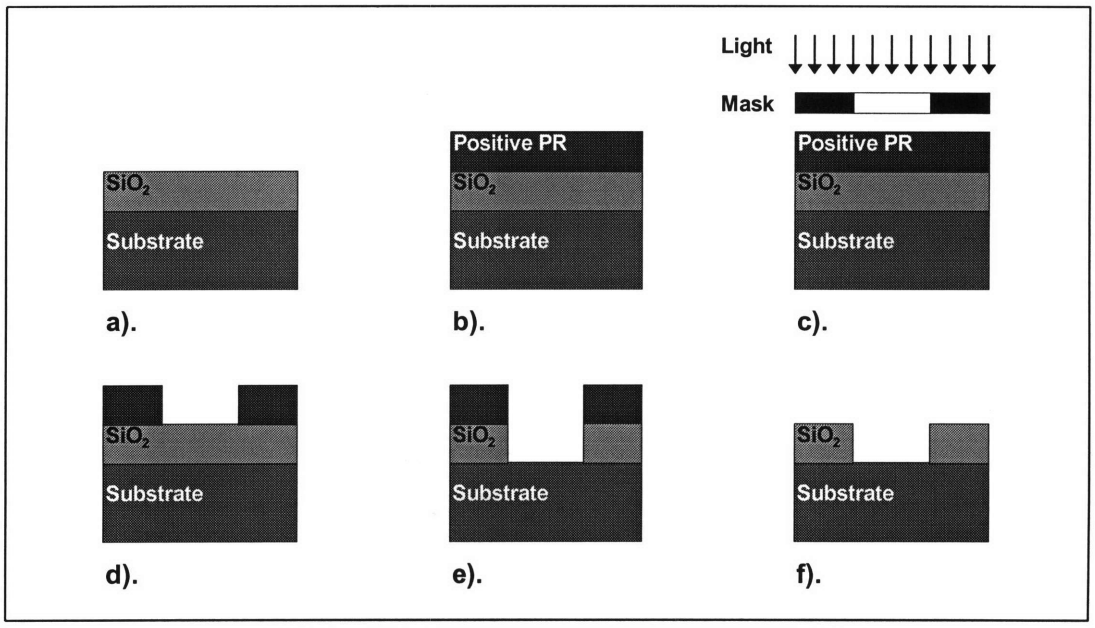

Figure 2.4

A generic representation of photolithographic pattern transfer: a layer to be patterned is coated with photoresist (a, b) and is then exposed to light through a mask (c) and developed (d) - in the case of positive resist (shown here), the exposed parts of the resist layer are removed during development, whereas in the case of negative resist, the unexposed parts are removed; the patterned resist layer then serves as a mask for the etching of the underlying film (e); finally, the resist is removed (f). After[40].

Historically, pattern transfer in semiconductor applications was accomplished through wet chemical processing. This was adequate for large feature sizes (several μm), but because the purely chemical etch produced isotropic profiles (see Figure 2.5), accurate feature definition became difficult as device dimensions shrank and unacceptable loss of critical dimension control became a concern. Plasma processing has proven to be the answer to this problem. Since the trajectories of ions arriving through the sheath at an etched surface are normal, the potential for

highly directional etching exists. An example of an ideal anisotropic profile is shown in Figure 2.5.

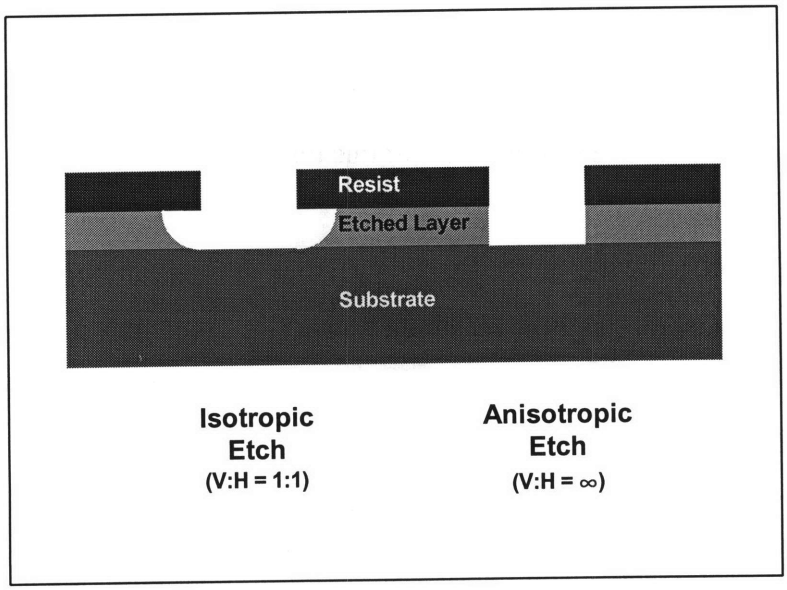

Figure 2.5

Isotropic vs. anisotropic etch profiles.

2.3.1 Process Conditions

Historically, a somewhat arbitrary distinction was sometimes made between two principal types of etch reactor configurations: one known as RIE (reactive ion etching), and the other simply as plasma etching. Some authors (*e.g.,* Flamm [41]) have been more careful to describe these as ion-enhanced plasma etching and chemical plasma etching, respectively. In the former configuration, the wafer is placed on the powered electrode (the cathode), and thus subjected to bombardment by energetic ions. In this configuration, the ion bombardment component is desired and hence the process takes place at low pressures (in the approximate range - 1 mTorr to 0.1 Torr [28]) to minimize ion scattering in the cathode sheath. In the latter configuration, the wafer is placed on the anode, where the sheath voltage is small; moreover, the process typically takes place at relatively high pressures (in the approximate range - 0.1 Torr to 1 Torr [28]). Ion bombardment is minimized and the plasma serves primarily to generate the etchant species [41]. Most present day etch tools are of the former variety, since, as will be seen later, ion bombardment is often necessary to maintain a highly directional etch. The term "reactive ion

etching," however, is a misnomer. It refers to processes which have both a chemical and a physical (ion-induced sputtering) component. It was coined in the belief that ion chemistry played a dominant role in the removal of the film being etched. However, it has since been found that neutrals, rather than ions, dominate the *chemistry* of the process, which is not surprising, given that neutral populations are several orders of magnitude larger than ion populations in typical plasmas. The remainder of this discussion will focus on RIE or ion-enhanced plasma etching.

For etching to proceed, it is generally believed that, as a minimum, three processes must occur sequentially: 1). adsorption of the reactive etch species to the film surface, 2). a reaction to produce an etch product, and 3). desorption of the product [42]. It follows, therefore, that the etch product must be a compound which is volatile, which in practice implies a vapor pressure greater than $\sim 10^{-5}$ or 10^{-4} Torr at the surface of the film [42]. In the case of silicon and silicon-based films, etching is carried out exclusively with halogen-based chemistries. The etch product is believed to be primarily SiM_4, where M is a halogen, but also SiM_x, where $x < 4$. While silicon itself has been successfully etched with fluorine, chlorine, as well as bromine chemistries [42], dielectric etch processes are performed solely with fluorine-bearing species, as opposed to other halogenated compounds. Chlorine and bromine chemistries [43] have been determined to be largely selective to silicon dioxide and nitride. Iodine species have been the subject of some limited studies. To the author's knowledge, these studies have investigated the etching of silicon only. They have indicated that etching of Si is possible, but at lower rates than those experienced with chlorine or fluorine chemistries, and with selectivity to silicon dioxide [44]. This is not surprising, given the lower reactivity of iodine as compared with the other halogens.

Four key parameters are often cited as being most critical to evaluating the performance of a given etch process: etch rate, selectivity to other films, anisotropy, and uniformity across the wafer [28]. A host of other concerns is also important, among them loading effects, substrate damage, residual contamination on the wafer, particle generation, wafer-to-wafer process drift, and hardware compatibility. Since the study discussed in this thesis utilized blank (unpatterned) wafers with a single type of film, a detailed discussion of the results will be restricted to etch rate. However, some of the mechanisms believed to exist in the hydrofluorocarbon discharges that were studied, namely polymerization phenomena and chemistry-dependent effects, do have

rates of these materials are low. When fluorocarbon plasmas are used, all three materials etch readily, with Si exhibiting considerably greater tendencies toward isotropic behavior [45]. A key phenomenon present in these discharges is the tendency for a fluoropolymer layer to form on the surfaces being etched. This phenomenon is perhaps the salient feature of fluorocarbon discharges. Manipulation of the polymerization mechanism through adjustment of process parameters, most notably through altering the chemistry of the discharge itself, is critical to obtaining etch rate enhancement as well as selectivity among these materials. CF_4 has generally been used as the vehicle through which these effects were studied, but the foregoing discussion may be extended to fluorocarbon discharges in general and, in fact, the concepts will be used heavily in the discussion of oxide and nitride etching with hydrofluorocarbon gases.

Polymer Formation [30, 41, 42, 45, 46]. It has been found that a film, regarded to be $(CF_2)_n$ (Teflon®) like, forms on Si and Si-compound surfaces by the adsorption of certain C_xF_y species. CF_x fragments, which are generated by dissociation of the parent fluorocarbon molecule into CF_x and atomic fluorine, as well as unsaturated C_xF_y species (*e.g.*, C_2F_4) that may be formed in the discharge are believed to be responsible. (CF_2, in particular, itself an unsaturate, has been associated with the formation of fluorocarbon layers.) These layers serve as an inhibitor to etching. In the steady state, the formation of this layer and its removal are competing processes and a finite thickness of this film is believed to be present on the surfaces being etched as the etch reaction proceeds. It is possible, however, to drive the conditions in the discharge to a regime where net deposition of the polymer occurs and all etching ceases. This behavior, in fact, was seen repeatedly in a number of the HFC gases that will be discussed in this thesis.

It should be noted that the presence of an inhibiting layer in the steady state during the etch process is believed to be one of the mechanisms that assist anisotropic etching in fluorocarbon plasmas. Whereas, in other types of discharges, ion sputtering of adsorbed reaction products or damage-induced etch-rate enhancement on surfaces exposed to bombardment are believed to play a role [41], in the systems presently under discussion, sidewall passivation by fluoropolymer films is believed to inhibit lateral etching, while vertical etching is allowed to proceed because this film is actively removed, or its formation is suppressed, on surfaces exposed to ion flux.

implications on selectivity and anisotropy. The mechanisms underlying these effects will be discussed in the following section.

The approximate process conditions under which ion-enhanced etching takes place are: pressure ranging from the milliTorr regime to a fraction of a Torr, rf power input ranging up to 1000 W or so, and feed gas flows on the order of tens of sccm (standard cubic centimeters per minute). In the Precision 5000 etch tool used for the author's work, these ranges were: pressure = 35 mTorr to 150 mTorr (200 mTorr for oxygen cleaning steps), rf power = 600 W (750 W for oxygen cleaning steps), and total gas flows ranging up to ~ 60 sccm.

2.3.2 Dielectric Etching with Fluorocarbon Plasmas

While SF_6 and NF_3 are also employed in patterning processes, most dielectric patterning is carried out with fluorocarbon gases. Moreover, all of the gases to be evaluated as part of the alternative chemistries project are also fluorocarbons. The etching of dielectrics with this important class of gases will accordingly feature prominently in the discussion of wafer patterning in general. In industrial applications today CF_4 and CF_3H appear to be the gases of choice. What should be stated at the outset is that the active etchant species in the etching of Si and its compounds by fluorine-containing plasmas is atomic fluorine itself. The mechanisms through which this occurs are, generally speaking, complex and often not well understood. In fact, despite the fact that Si and Si-compound etching in fluorocarbon discharges have been probably the most heavily studied among the various plasma etch systems, one frequently encounters in literature conflicting explanations for any one given phenomenon. Certain key aspects of fluorocarbon discharges, however, have been reasonably well-characterized. The discussion which follows will be an attempt to review some of these features as they pertain to fluorocarbon etching of dielectrics.

When silicon is etched in a fluorine-bearing plasma, the etch reaction has a tendency to proceed isotropically [45]. This is consistent with the observation that F atoms will etch Si readily without the presence of any ion bombardment; silicon dioxide [30, 41, 42] and silicon nitride, on the other hand, are not readily etched by F atoms under such conditions. When subjected to ion bombardment, however, oxide and nitride etch readily in fluorine plasmas and with high anisotropy [30], which is consistent with the fact that the spontaneous or isotropic etch

$$O + CF_2 \rightarrow COF + F$$

where unsaturate levels are suppressed and fluorine atom density is increased. More recent views, however, tend to discount the importance of gas-phase chemistry in favor of a dominant role being played by surface reactions [28].

When oxygen is added to the discharge in amounts larger than some optimum value, a reduction in etch rate occurs. Some authors [30, 45] cite oxygen reactions with the film being etched as inhibiting etching under these conditions. This may occur through competition with fluorine for active sites on the etched layer. While this mechanism may be plausible, simple dilution of the fluorine concentration in the discharge by the presence of large concentrations of another gas is perhaps the more straightforward explanation.

Finally, it should be pointed out that the effects achieved by adding O_2 to a discharge such as a CF_4 plasma can also be attained by incorporating oxygen into the molecular structure of the fluorocarbon feed gas, *e.g.*, COF_2, CF_3OOCF_3, CF_3OCF_3, etc. [46]. This will also be true in the discussion of the role of hydrogen in fluorocarbon plasmas that is about to follow.

Hydrogen Effects [30, 41, 42, 45, 46]. Whereas the presence of oxygen in fluorocarbon plasmas generally tends to enhance fluorine concentrations and improve etch rates, the addition of hydrogen tends to accomplish the opposite. In the gas phase, hydrogen is thought to "scavenge" free fluorine through the reactions [30, 41]:

$$F_2 + H \rightarrow HF + F$$

$$F + H_2 \rightarrow HF + H.$$

Moreover, in addition to reducing fluorine levels directly, hydrogen has also been posited by Flamm to abstract fluorine from fluorocarbon species, producing film-forming precursors, *e.g.*:

$$CF_3 + H \rightarrow CF_2 + HF.$$

Thus the addition of H_2 to a CF_4 plasma promotes the formation of unsaturates (which are believed to be responsible for fluorocarbon deposition) and reduces fluorine concentrations, which in turn may further augment the concentrations of unsaturates if one accepts that fluorine in the gas phase suppresses them.

H_2 addition has been linked to enhanced rates of polymer formation on the etched surfaces by studies in which a silicon surface was subjected to etching in a CF_4/H_2 discharge [42]. It was found that, as H_2 content was increased, etching stopped sooner (at lower H_2

Oxygen Effects [30, 41, 42, 45, 46]. It has been well established that the addition of O_2 to fluorocarbon plasmas can have the effect of dramatically boosting the etch rates of silicon and its compounds. Oxygen is thought to play several roles when added to a fluorocarbon discharge and its effects are intimately connected with the presence of the fluoropolymer layer on the substrate surface. Oxygen is believed to attack this layer. (This author suspects that the mechanism is analogous to the random scission of hydrocarbon polymer chains, which is the process believed to occur in the etching of organic resists by oxygen discharges [30, 45, 47].) This attack has essentially three consequences: 1). the removal of the inhibitor film, which facilitates attack of the underlying Si-based layer by fluorine, 2). the freeing up of gas-phase fluorine that would otherwise be consumed in attacking the polymer, and 3). the direct release of fluorine from the polymer film, which makes more etchant available to attack the Si-based film. Evidence of this has been established through the tracking of increases in optical emission signatures of F and CO, which correlate well with increasing Si etch rate, as oxygen content in a CF_4 discharge is varied [46]. In SiO_2 etching, oxygen present in the film itself is also believed to make a contribution, in that the oxygen liberated from the etched film plays a role in the reactions described above.

Some of the early literature on the subject also mentions possible roles that oxygen may play in the gas phase through oxidation of fluorocarbon fragments to produce CO or COF_2 [42, 46]. Flamm and coworkers [30, 41] discuss a more elaborate mechanism, whereby high F and F_2 levels suppress the concentrations of unsaturated fluorocarbon species in a CF_4 discharge, both in the gas phase and through third-body recombination on surfaces, *e.g.*:

$$F + CF_2 (+ M) \rightarrow CF_3$$

$$F_2 + CF_2 \rightarrow CF_3 + F$$

$$F + C_2F_4 (+ M) \rightarrow C_2F_5$$

$$F_2 + C_2F_4 \rightarrow C_2F_5 + F.$$

Oxygen competes with fluorine in this process, through reactions like:

$$O + CF_2 + M \rightarrow COF_2$$

$$O + CF_2 \rightarrow CO + F_2$$

$$O_2 + CF_2 + M \rightarrow CO_2 + F_2$$

percentages) in the case where the substrate was not subjected to energetic ion bombardment as opposed to the case where it was. This finding suggests the addition of H_2 promotes polymer formation. Where the polymer is removed by bombardment, etching continues to proceed. Without bombardment, at sufficiently high H_2 percentages, the polymer layer is allowed to build up at a rate that outcompetes the etch mechanism and etching ceases. This mechanism is consistent with the "scavenging" and unsaturate promotion effects discussed above.

Why one would wish to intentionally induce greater polymerization in a discharge becomes clear from the observation that the suppression of etching is more pronounced with some materials (Si) than with others (SiO_2, Si_3N_4) [45]. A partial explanation for this phenomenon has been offered for the oxide case by Coburn and coworkers [42, 46], who posit that the polymer layer forms preferentially on Si as opposed to SiO_2. The argument is rooted in two observations: 1). experiments have shown that the carbon-containing layer does indeed accumulate more slowly on Si than on SiO_2 and 2). when SiO_2 is etched in a pure CF_4 discharge, the presence of CO, CO_2, and COF_2 is detected in the effluent. The conclusion is that the difference is caused by the liberation of oxygen from the silicon dioxide, which reacts with carbon in the fluorocarbon layer, a mechanism mentioned earlier in this discussion. By this argument, as conditions are pushed toward increasing polymerization, Si surfaces are subjected to increasing rates of fluoropolymer deposition, while SiO_2 surfaces "offset" the buildup of polymer, staving off the onset of net deposition. Indeed, experiments have shown that, as H_2 content in a CF_4 plasma is increased, the SiO_2 etch rate drops off, but the Si etch rate does so even more precipitously, leading to a high SiO_2-Si selectivity window [46].

It has been observed that SiO_2-to-Si selectivity can be enhanced through mechanisms other than H_2 addition, namely through the use of other fluorocarbon precursors which are more likely to promote polymerization (C_3F_8, C_2F_4), the addition of other sources of hydrogen (CH_4, C_2H_4), or the addition of other "unsaturated" species (C_2H_4, C_2F_4) [45, 46]. Coburn's argument above is readily extended to these plasmas, as it is not dependent on the presence of hydrogen itself, but merely on the existence of conditions which enhance polymer formation. It should be pointed out that conspicuously absent from the above discussion is an explanation which is applicable to silicon nitride films, which have also been observed to etch faster than Si in polymerizing plasmas.

In any case, the concept which has emerged is the notion of "fluorine deficient" plasmas. Whereas the fluorine "scavenging" explanation involving hydrogen appears adequate for H_2 containing plasmas or gases like CF_3H, a more general model is necessary to explain why certain fluorocarbon chemistries are more apt to polymerize than others. This model, though simplistic and lacking additional physical insight beyond what was already discussed in this section, has gained a great deal of currency. It is the "relative stoichiometry" concept or fluorine/carbon ratio model.

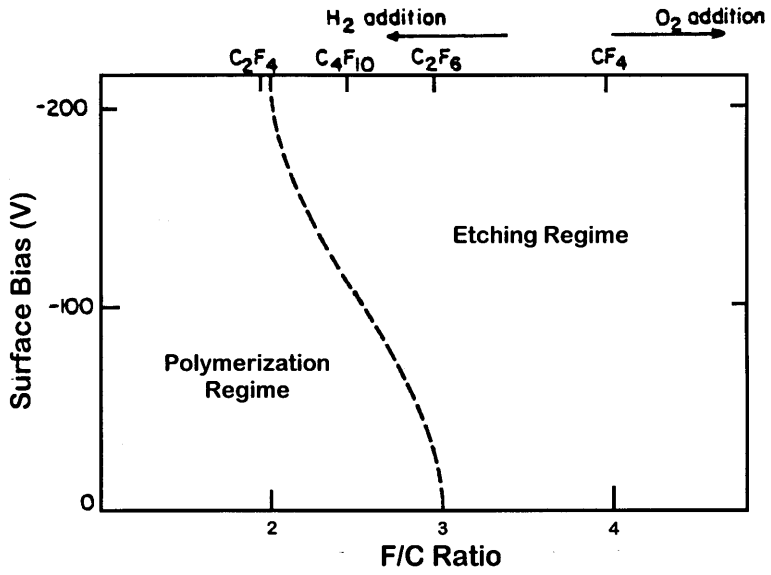

Figure 2.6

Fluorine/carbon rations for several fluorocarbon gases. After [46].

F/C Ratio Model and Polymerization [42, 45, 46]. The essential message of the F/C ratio model is conveyed in Figure 2.6. The F/C ratio model ties in the phenomena discussed earlier by stating, quite simply, that lower fluorine concentrations relative to carbon concentrations tend to promote polymerizing behavior. What is the F/C ratio a ratio of? The region in the plasma where this ratio is appropriate to take is, naturally, the region near the substrate. The ratio of the fluorocarbon feed can be regarded as a starting point. This ratio is then modified by processes such as those discussed earlier in this section, *e.g.,* fluorine scavenging by hydrogen or fluorine liberation from fluoropolymer films by oxygen. The effective F/C ratio therefore excludes the relatively unreactive molecular species in the region of

interest (*i.e.*, CF_4, C_2F_6, HF, SiF_4, CO_x, COF_2, etc.) [42]. In essence, "fluorine deficient" plasmas tend to contain lower concentrations of etchant species and higher concentrations of polymer-forming precursors. In actuality, F/C ratios are not calculated, except as ballpark figures. The concept is merely used as a means of characterizing the polymerizing tendencies of a plasma.

Before leaving the subject, one ought to point out that the border line between etching and polymerization regimes is by no means well defined and will differ from system to system. However, the shift of this boundary toward lower F/C ratios with higher ion bombardment (see figure 2.6) is well-established and provides a consistent representation of the fact that etching may be sustained in the presence of large populations of film precursors if a means for the suppression of film formation (*e.g.*, bombardment of the surface) is present. The concept is particularly useful when discussing oxide/nitride to silicon selectivity, which is believed to be maximized when operating close to the onset of net polymer deposition.

Silicon Nitride Etching. Little has been said explicitly about the etching of silicon nitride in fluorocarbon plasmas up to this point, except that, insofar as it is a silicon-containing film, the same general mechanisms are expected to take place as those occurring in Si and SiO_2 etching. Nitride etching in fluorocarbon plasmas has sometimes been described as exhibiting behavior intermediate to that of Si and SiO_2 [45, 48]. It should be pointed out that large differences sometimes exist between the quality of plasma-deposited (PECVD) nitride films, which tend to have a composition given by SiN_x:H, and films deposited at higher temperatures by LPCVD, which are typically intentionally silicon-rich or stoichiometric (Si_3N_4). The non-stoichiometric plasma films tend to be less dense, more porous, and sometimes have significant hydrogen content (depending on the gaseous precursors used). It has been reported that, not surprisingly, these films etch more readily than LPCVD nitrides [45, 48]. This is consistent with the presence of hydrogen and a lower degree of Si-N bonding [30]. Some authors report that the addition of N_2 to a CF_4 discharge selectively enhances the etch rate of nitride relative to oxide. The mechanism cited is the scavenging of N atoms from the etched surface by gas phase atomic nitrogen to from N_2 [49]. In the experiments carried out as part of the author's thesis work, LPCVD nitride and thermal oxide films were used; they exhibited analogous etch behavior under some conditions, but significant differences were found at others, particularly with respect to trends in behavior as a function of oxygen content in the discharge (see Chapter 5). See Section

5.1.1, in particular for a discussion of some additional factors thought to be involved in the etching of nitride.

2.4 PECVD and PECVD Chamber Cleaning

The other major plasma application used is semiconductor processing is plasma enhanced chemical vapor deposition (PECVD). In chemical vapor deposition, reactant gases are introduced into a chamber where they are decomposed thermally (often at temperatures of several hundred °C) and react on a surface to form a film. The most prevalent variant is low pressure CVD (LPCVD). A detailed treatment of CVD processes is not germane to this discussion and the reader is once again referred to standard texts for a comprehensive description [19, 20, 21, 22]. Plasma enhanced CVD is a variant wherein the thermal energy input required to dissociate the feed gas and promote the formation of a quality film on the substrate is partially replaced by the introduction of energy from the plasma. While PECVD still occurs at elevated temperatures, these temperatures are typically a few hundred degrees lower than those required in the analogous LPCVD processes. As an example, LPCVD silicon nitrides are deposited at 700-900 °C, while PECVD nitrides tend to use the 300-400 °C range [50]. Whereas PECVD films are often of poorer quality than LPCVD films, the low temperature processing advantage makes them suitable for deposition of layers over Al (Al-Si eutectic temperature = 577 °C [51]). Thus PECVD films are ubiquitous throughout interconnect structures.

The cleaning of PECVD chambers is typically accomplished with similar etchants to those used for patterning the deposited films. However, since there are no anisotropy or selectivity requirements (except for selectivity to the materials of construction in the chamber), the choice of available chemistries is, in principle, greater. High throughput, hence high etch rate, is the primary criterion for evaluating process performance. Today, C_2F_6 and NF_3 are the gases used in largest volumes for the cleaning of dielectric deposition chambers [2]. To the author's knowledge, few systematic studies on the mechanisms of the etch process under chamber cleaning conditions have been published. These conditions tend to be rather different than those present in wafer patterning processes. As an example, in a Novellus Concept One PECVD tool, a standard C_2F_6 clean process operates at: pressure = 2.7 Torr, rf power = 2800 W, etch gas flow = 1600 sccm, oxygen flow = 1600 sccm [52]. In addition, while wafer patterning

3. Selection of Candidate Chemistries

This chapter will discuss the process by which the chemistries to be evaluated as potential alternatives to PFCs were chosen. When the survey of previous work in the field was concluded, a database containing a large number (~100) of halogenated compounds was created and a list of candidates was drawn up on the basis of criteria to be discussed in Section 3.1. Three families of chemistries were ultimately selected for testing - hydrofluorocarbons (HFCs), iodofluorocarbons (IFCs), and unsaturated fluorocarbons. Their properties will be discussed in Section 3.2.

3.1 Selection Criteria

As had been pointed out earlier, fluorine is believed to be the only halogen capable of effectively etching dielectric films. Thus the pool of potential candidate replacement chemistries was limited to fluorine-bearing substances. Two requirements for any potential replacement were clear from the outset: acceptable process performance (*i.e.,* comparable to that of established PFC etchants) and lower environmental impact than that of the PFCs. However, since process performance in the case of previously unexplored chemistries is impossible to determine *a priori*, the only determination in this matter than could be made was by means of inference from the structure of the molecule and the behavior of analogous species. Moreover, while long-term global environmental impact is necessarily a key concern, given the motivation for this work, shorter-term local effects, namely toxicity, reactivity, and other handling and safety issues, are also of importance if a given compound is to be readily accepted in industrial usage. Thus the principal criteria in the selection process became the chemical structure of the compound and environmental, safety, and health (ESH) considerations.

From the environmental standpoint, the two main criteria were global warming potential and ozone depleting potential (ODP).[†] Chemistries with no ODP and, obviously, low or no

---

[†] The ozone depleting effect is sometimes confused with the global warming phenomenon. Ozone depletion involves the destruction of stratospheric ozone by halogens (Cl, Br, I, though not F) released from species stable enough to reach the stratosphere. The halogen, once released, can cycle through a reaction of the following type many times, destroying more ozone [5]: $O_3 + Cl \rightarrow ClO + O_2$

$ClO \rightarrow Cl + O.$

processes typically run for times on the order of half a minute to a minute, chamber clean cycles last several minutes. Finally, even though the same chemistry may be used, the mechanisms by which etching occurs are believed to be different. In a patterning process, the CF_x layer that forms on etched surfaces may itself be a significant source of fluorine in the etch - fluorine which has been made available to etch by ion-enhanced processes such as those described in the previous section. The high-pressure etching that occurs during chamber cleans, on the other hand, is thought not to be significantly ion-enhanced but mainly chemical in nature [53].

GWP were desired. From a health standpoint, long-term effects were given the highest priority. Thus, following the suggestion of the SEMATECH Global Warming Prioritization Technical Advisory Board (PTAB), strongly carcinogenic, teratogenic, or mutagenic substances were excluded. Chemistries that were very highly toxic, corrosive, or that possessed other extreme handling hazards were also not selected. However, the mere presence of toxicity or handling hazards was not used as a criterion for rejection. This is because, even though one would ideally like to implement solutions which are as stable and benign from a handling and safety standpoint as compounds like CF_4 or C_2F_6, it is unlikely that alternative chemistries that fit this description will be found. The reason for this is that those halogenated compounds which are stable enough not to present concerns in terms of toxicity, reactivity, or corrosiveness tend to be very stable atmospherically as well. A number of halogenated compounds exist which pose no long-term environmental threat, but these tend to be reactive, and thus toxic, highly reactive, or corrosive. In short, there exists a basic tradeoff. However, it is the author's belief that there exist several classes of fluorinated compounds which may carry an acceptable level of handling risk and meet the environmental criteria outlined above. These compounds are described below. It should be pointed out that the toxicity ratings for each compound in Tables 3.1-3 are qualitative assessments based primarily on acute toxicity information available in Materials Safety Data Sheets. Hence they should be treated only as rough indicators. Appendix 2 provides more detailed information on the compounds in Tables 3.1-3.

3.2 Families of Chemistries to Be Evaluated

Based on the above criteria, the author and his coworkers have identified three families of fluorinated compounds to be used in the experimental stages of the project: hydrofluorocarbons (HFCs), iodofluorocarbons (IFCs), and unsaturated fluorocarbons. All these chemistries are carbon-based; the author has found that, generally speaking, inorganic fluorides tend to have much greater handling concerns associated with them than fluorocarbon chemistries and are thus less likely to gain industrial acceptance.

3.2.1 Hydrofluorocarbons

Hydrofluorocarbons are, in a sense, the next logical step in an attempt to move away from perfluorinated species. As can be seen from Tables 1.3 and 3.1, comparison of HFC lifetimes and GWPs with those of their fully fluorinated counterparts indicates that modification of the fluorocarbon molecule by replacement of fluorine with hydrogen leads to lower atmospheric stability. However, it should be noted that, although HFC GWP values are in general much lower than those reported for perfluorocompounds (except in the case of CHF_3, an HFC, but nearly as stable as perfluorinated compounds), these values are still significant. On the other hand, an attractive property of HFCs is the fact that they are relatively easy to handle. Generally speaking, they have slight or negligible toxic effects and are not corrosive. Most are also non-flammable. The use of several HFCs, namely CF_2H_2, C_2F_5H, and $C_2F_4H_2$ [27, 54,55], in mixtures used for dielectric etching has already been reported. It has been found that, for patterning applications, these HFCs may be an attractive alternative for some processes because they provide high selectivity to silicon. Preliminary work with C_2F_5H and $C_2F_4H_2$ indicated that their etch rates may be too slow for chamber cleaning applications, however [55].

Table 3.1: Properties of Selected HFCs [6,56]

$C_xF_yH_z$	Line Formula	Name	Halocarbon number	Flamm.	Toxicity	GWP_{100}	Boiling Point	Lifetime	Used as Etchant?
CF_2H_2		difluoromethane	32	Y	toxic	580	-51.7 °C	6 yrs.	Y
C_2F_5H	CF_3-CF_2H	pentafluoroethane	125	N	slight	3200	-48.5 °C	36 yrs.	Y
$C_2F_4H_2$	CF_2H-CF_2H	1,1,2,2-tetrafluoro-ethane	134	N	slight	1200	-19.7 °C	11.9 yrs.	
	CF_3-CFH_2	1,1,1,2-tetrafluoro-ethane	134a			1300	-26.5 °C	14 yrs.	Y
C_3F_7H	CF_2H-CF_2-CF_3	1H-heptafluoro-propane	227ca	N	slight	?	-16.3 °C	?	
	CF_3-CFH-CF_3	2H-heptafluoro-propane	227ea			3300	-15.2 °C	41 yrs.	
C_2F_3H	CF_2=CFH	trifluoroethylene	1123	Y	N/A	?	-51.0 °C	?	

As Table 3.1 indicates, to the best of the author's knowledge, 1H- and 2H-heptafluoropropane as well as trifluoroethylene had not been previously examined in any etch

applications. The compounds in this table were the ones evaluated in this study, with the exception of the symmetric isomer of tetrafluoroethane (1,1,2,2-tetrafluoroethane, FC-134). Previous work [55] with FC-134a reported highly polymerizing behavior in a Precision 5000 etch tool. SiO_2 etch rates of ~3000 Å/min in FC-134a were reported, but only at high magnetic fields (see Section 4.2.4 for a discussion of this process parameter). As a result, FC-134a was given lower priority as a potential replacement to be evaluated, and FC-134 was not deemed to be sufficiently dissimilar to warrant investigation.

Table 3.2: Properties of Selected IFCs [56]

$C_xF_yI_z$	Line Formula	Name	Flamm.	Toxicity	Vapor Pres. @ 20 °C	Boiling Point	Used as Etchant?
CF_3I		iodotrifluoromethane	N	irritant	85 psi	-22.5 °C	Y
CF_2I_2		diiododifluoromethane	N				
C_2F_5I	CF_3-CF_2I	iodopentafluoroethane	N	irritant	35 psi	12-13 °C	
$C_2F_4I_2$	CF_2I-CF_2I	1,2-diiodotetrafluoroethane	N	irritant / toxic	N/A	112-113°C	
	CF_3-CFI_2	1,1-diiodotetrafluoroethane			N/A	N/A	
C_3F_7I	CF_2I-CF_2-CF_3	1-iodoheptafluoropropane	N	N/A	N/A	40 °C	
	CF_3-CFI-CF_3	2-iodoheptafluoropropane			7.1 psi	38 °C	
C_2F_3I	CF_2=CFI	iodotrifluoroethylene	N	irritant	N/A	30 °C	

3.2.2 Iodofluorocarbons

A second group of fluorocarbons that will be investigated as part of the alternative chemistries project is the iodofluorocarbon family. One property of the compounds in this family is that the iodine in the $C_xF_yI_z$ molecule tends to photolyze easily, due to the weakness of the C-I bond. This has favorable implications for the atmospheric instability of these molecules. The atmospheric lifetime for CF_3I, for instance, is estimated to be only several days [57], as opposed to hundreds or thousands of years. It should be noted that unlike F, and like Br and Cl, atomic iodine is an effective ozone-destroying agent. However, IFCs are believed to be so short-lived in the atmosphere, that their ozone depleting capacity is negligible. It should also be pointed out that there exist very large natural sources of iodocarbons. "These sources are so

large that it would be difficult for human activities to approach them, in sharp contrast to chloro- and bromocarbons." [57]. The calculated 20-year GWP for CF_3I is less than 5. CF_4 and CF_3H, by comparison, have 20-year GWP values of 4,100 and 9,200, respectively [6]. The calculated ozone depleting potential for this gas is also small: less than 0.008 (conservatively) and probably less than 0.0001, relative to $CFCl_3$ (FC-11), which is assigned a value of 1 as a reference [57, 58]. Thus long-term environmental problems do not appear to be a concern.

As a family, IFCs are also non-flammable; in fact, some have been used for fire-fighting applications [59]. While toxicity concerns tend to be higher than those associated with HFCs (IFC material safety data sheets describe them as irritant to eyes, mucous membranes, and the respiratory tract), relatively speaking, IFCs do not appear to be particularly threatening to human health. (An exception may be 1,2-diiodotetrafluoroethane ($C_2F_4I_2$), which does appear to have substantial toxic effects in rats. See Appendix 2.) A possible difficulty in using some of the heavier iodine-containing compounds, however, is their high boiling points and low vapor pressures (see Table 3.2). Heated lines will probably need to be used to avoid condensation and/or mass flow controller damage. Compounds like $C_2F_4I_2$ will almost certainly require a bubbler or liquid injection as a means of delivery. CF_3I and C_2F_5I, however, have reasonably low boiling points and are thus attractive from a facilities standpoint. Another possible drawback in using IFCs stems from the fact that iodine is likely to be easily liberated in the plasma, which may have hardware compatibility implications. In particular, the use of iodinated species in wet pump vacuum systems can lead to pump oil degradation. The etch viability of these chemicals is less certain than that of the HFCs: only one of the chemicals in this family appears to have been used for etching, namely, CF_3I for silicon trenches [60]. In general, relatively little research effort appears to have been expended on the investigation of IFCs in plasma applications. However, lack of serious handling concerns combined with the low atmospheric stability of these compounds (stemming from the weakness of the C-I bond) makes them very attractive candidates for this study. In a sense, IFCs represent an apparent exception to the "tradeoff principle" noted earlier.

3.2.3 Unsaturated Fluorocarbons

The third principal family of fluorinated compounds to be characterized during the etch viability stage is the unsaturated fluorocarbon family. These compounds contain double or triple carbon-to-carbon bonds, which make them considerably more reactive than perfluoroalkanes. No atmospheric lifetimes or GWPs have yet been calculated for these molecules, but they are expected to be very short-lived. The compounds in Table 3.3 are more toxic and/or otherwise reactive than those in the previously discussed categories. C_2F_4, in particular, can polymerize explosively in the presence of oxygen. It can also explode at high pressures if not stabilized with inhibitors. While it does not appear to have any acutely toxic effects, a report recently released has identified it as a suspected carcinogen [61]. (Its inclusion on this list is primarily for it to serve as a model compound for this family, as well as for other derived species, *i.e.*, C_2F_3H and C_2F_3I. Because of the severe handling issues associated with this compound, it is unlikely to be accepted as a PFC replacement in industrial applications.) Fortunately, the other compounds listed in Table 3.3 appear to be more stable and somewhat easier to handle. In terms of etch viability, some of these compounds have been tested successfully in wafer patterning applications. C_2F_4 and C_3F_6 have been used for etching of SiO_2 in high density ECR (electron cyclotron resonance) and inductively coupled plasmas. In keeping with predictions based on their low F/C ratio, they have been found to polymerize heavily, and thus etch oxide with good selectivity (about 50:1) to silicon [62,63].

Table 3.3: Properties of Selected Unsaturated Fluorocarbons [56]

C_xF_y	Line Formula	Name	Flamm.	Toxicity	Boiling Point	Used as Etchant?
C_2F_4	*CF_2=CF_2*	*tetrafluoroethylene*	*Y*	*low*	*-76.3 °C*	*Y*
C_3F_6	CF_3-CF=CF_2	hexafluoropropylene	N	moderate	-29.5 °C	Y
C_4F_6	CF_3-C≡C-CF_3	hexafluoro-2-butyne	?	irritant	-24.6 °C	
C_4F_6	CF_2=CF-CF=CF_2	hexafluoro-1,3-butadiene	N	moderate	6.0 °C	
c-C_4F_6	CF_2-CF_2-CF=CF-	hexafluorocyclobutene	N	high	3-5.5 °C	
C_4F_8	CF_3-CF=CF-CF_3	octafluoro-2-butene	N	moderate	1.2 °C	

3.2.4 Inorganic Fluorides

One will notice that the basic approach to chemistry selection was modification of a perfluorocarbon molecule to achieve lower expected atmospheric stability. In perfluorocarbons, the key to this stability is the strength of the C-F bond. In the case of the HFCs and IFCs, reduction of the compound's stability is accomplished through substitution of a more weakly bonded specie in what remains a relatively fluorine-rich molecule. In the case of the unsaturated fluorocarbons, the introduction of double or triple bonds achieves this purpose. Some molecules in the above tables (C_2F_3H and C_2F_3I) benefit from both forms of atmospheric "stability lowering." Conspicuously absent from the above discussion are chlorine or bromine substituted fluorocarbons (chlorofluorocarbons and bromofluorocarbons). These compounds, though structurally analogous to IFCs, do not benefit from the unique weakness of the C-I bond in IFCs (which gives the latter the ability to photolyze easily to give off iodine) and are therefore quite stable. Moreover, despite the fact that chloro- and bromofluorocarbons have been used successfully to etch dielectrics, they are potent ozone depleting substances *and* also have substantial global warming potentials (*e.g.,* CF_3Br: $GWP_{100} = 5{,}600$; CF_3Cl: $GWP_{100} = 11{,}700$ [6]). Hence from an environmental standpoint, they are clearly not desirable.

A question that needs to be addressed, however, is why the list of candidates is limited to only organic (*i.e.,* carbon-based) fluorides. While it is true that in wafer patterning applications, the presence of carbon facilitates the formation of passivating films which play important roles in providing anisotropy and selectivity, these issues are not relevant to chamber cleaning applications. Moreover, anisotropic etching of dielectrics has been demonstrated even in the absence of passivating polymer films (*e.g.,* with NF_3 with SiO_2 [30]). Unfortunately, nearly all inorganic fluorides which were initially considered were deemed to have high health or safety risks associated with them. It was decided, therefore, that the search for alternatives should initially concentrate on compounds with lower levels of risk and only move to highly reactive ones if other possibilities have been exhausted. Table 3.4 contains an overview of a number of inorganic fluorides that were excluded because of health/safety issues.

Table 3.4: Health/Safety Issues Associated with Selected Inorganic Fluorides [56]

Compound	Health/Safety Issues
BF_3	highly toxic
PF_3	highly toxic
PF_5	highly toxic, easily hydrolyzed - corrosive
clef	highly toxic, very strong oxidizer, corrosive
ClF_3	highly toxic, very strong oxidizer, corrosive
ClF_5	highly toxic, corrosive, explosive
BrF_3	highly toxic, very strong oxidizer, corrosive
BrF_5	highly toxic, very strong oxidizer, reacts violently with water
IF_5	highly toxic, very strong oxidizer, reacts violently with water
F_2	toxic, extremely powerful oxidizer, corrosive
HF	toxic; corrosive
SF_4	highly toxic, corrosive, reacts violently with water
N_2F_4	powerful oxidizer; heat, shock, or blast can detonate it under pressure
COF_2	toxic, easily hydrolyzed
F_2O	highly toxic, explodes on contact with water, powerful oxidizer, unstable
F_2O_2	may explode from heat, shock or friction, powerful oxidizer, unstable
NO_2F	toxic, corrosive, easily hydrolyzed, powerful oxidizer
S_2F_{10}	highly toxic
SeF_4	hydrolyzed violently by water, high boiling point

More detailed information on the three families of chemistries that have been selected for testing can be found in a report included in this thesis as Appendix 2.

4. Experimental Approach

This chapter will discuss the experimental scheme that was used in the evaluation of the HFCs. The films that were grown for use in this study will be discussed in Section 4.1. The Applied Materials Precision 5000 etch tool will be described, along with key process parameters, in Section 4.2. This will be followed by a discussion of the principal diagnostic technique used in this work - optical emission interferometry (Section 4.3). It was originally intended that all of the gases would be characterized using design-of-experiments ("DOE") methodology. However, three of the gases (CF_2H_2, $C_2F_4H_2$, and C_2F_3H) were found to polymerize heavily (resulting in net deposition of polymeric films) in the parameter space defined by the experimental matrix. More limited studies were therefore carried out with these gases in a parameter space that was less conducive to polymerization. The remaining gases were also evaluated in this space for comparison. The experimental plan used in these studies is discussed in Section 4.4. The results of the experiments described in Section 4.4 will be discussed at length in Chapter 5.

4.1 Films

It was determined that high quality, stoichiometric films, rather than plasma-deposited films, should be used in this study, as such films are generally more resistant to removal by etching. In the case of silicon dioxide, thermally grown SiO_2 was used.[‡] The target thickness for these films was ~ 11,000 Å. Actual films ranged in thickness from approximately 10,400 Å to 11,700 Å, as measured by Nanospec®, depending on the lot. Wafers were processed in lots of 25, or double lots of 50. An LPCVD process was used for the silicon nitride films.[§] Since LPCVD nitride tends to have high tensile stress, a target thickness of only ~5,000 Å was chosen. Actual film thicknesses, as measured by Nanospec®, ranged from approximately 5,100 Å to almost 5,500 Å. Wafers were processed in double lots of 50 or a quadruple lot of 100 at one time. For

---

[‡] The oxide films were grown in ICL (Integrated Circuits Laboratory) furnace tubes B1, B2, or B5, using wet oxidation recipe 223 at 1150 °C, 1 atm, with 3 lpm O_2 and 6 lpm H_2. (Adjustable step lengths: step 7 = 10 min., step 8 = 2 hrs.)

[§] The nitride films were deposited in ICL furnace tube A5, using SiH_4 / NH_3 recipe 460 at 775 °C, 300 mTorr, with 150 sccm NH_3 and 50 sccm $SiCl_2H_2$. (Adjustable step length: step 8 = 3 hrs.)

the SiO_2 films, all substrates used were 100 mm boron-doped p-type Si, with resistivities specified as ranging from 2.5 to 4 Ω-cm ($N_A \approx 3 - 5.5 \times 10^{15}\,cm^{-3}$). For the Si_3N_4 films, these substrates were used, as well as 100 mm boron-doped p-type Si wafers with resistivities specified as 6 to 12 Ω-cm ($N_A \approx 1 - 2.5 \times 10^{15}\,cm^{-3}$).

4.2 Applied Materials Precision 5000 Etch Tool

The Precision 5000 is a loadlocked, single wafer process platform that can be configured with up to four etch or (PE)CVD chambers. The unit used for this study (System #6166) was fitted with two etch chambers, one dedicated to polysilicon etching, one to dielectrics - see Figure 4.1. Only the dielectric etch chamber was used. The gases supplied to this chamber that were used in the course of this work were: CF_4 (20 sccm mass flow controller), O_2 (100 sccm MFC), Ar (100 sccm MFC), and the fluorocarbon gases being evaluated. The latter were supplied through an additional 250 sccm MFC. (All MFC sizes are given as calibrated for N_2. See Appendix 3 for gas conversion factors for the compounds used in the study.) The additional line was connected to a six-valve manifold, which enabled up to six process gases to be connected at any given time and greatly facilitated switching between gases.

The Precision 5000 etch chambers are of the capacitively coupled rf diode type, configured in the RIE ("ion-enhanced etching") mode, with the wafer sitting on a susceptor which is the powered cathode. The excitation frequency used is 13.56 MHz. The feed gas is introduced through a gas distribution plate (showerhead) incorporated into the chamber lid. A turbomolecular pump, backed by a mechanical pump, maintains vacuum in the chamber. Helium backside cooling as well as a heat exchanger are provided to maintain the wafer, the cathode, and the chamber walls at a constant temperature. Temperature effects, however, were not studied in the course of this work. Thus the He cooling pressure was set at a default value of 4 Torr for all runs and wall as well as cathode temperatures were not monitored. Default settings for the heat exchanger were used. A significant feature of the design of the Precision 5000 etch chamber is magnetic enhancement. The chamber is equipped with four magnet coils, arranged around the walls of the chamber. Two coils facing each other form a set; the two sets are 90 degrees out of phase. A rotating magnetic field whose lines of flux are parallel to the surface may thus be generated. This configuration is often referred to as MERIE (magnetically enhanced reactive ion

etcher). The role of the magnetic field will be discussed shortly. In addition to magnetic field strength (given on the Precision 5000 in units of Gauss, which are, strictly, units of magnetic flux density), other principal process parameters which can be controlled on the Precision 5000 are: rf power, process pressure, gas flow rates, and, naturally, step duration. Each of these variables will be discussed in turn.

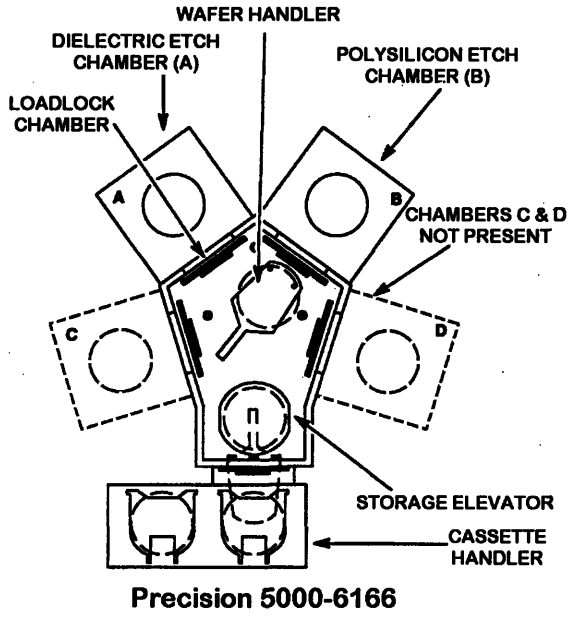

Figure 4.1

Schematic of the Applied Materials Precision 5000 platform (System #6166) housed in the Integrated Circuits Laboratory at MIT, shown configured with two process chambers, both for etch. After [64]

Each etch run used a two-step recipe: a 15 s gas flow and pressure stabilization step, during which all the process parameters except rf power were set to the desired values, and a variably-timed etch step. The plasma was not struck until the end of the stabilization step. A 200 W/s power ramp was used during plasma ignition and extinction. Significant pressure fluctuation was observed during the first ~5 s after plasma ignition; hence recording of the interferometric signal (see Section 4.3) was not initiated until 5 seconds after ignition. Initially, an attempt was made to use a constant time for all etch runs (120s). However, as will be

discussed shortly, sometimes not enough cycles of the interferometric signal were collected during this period. A variably timed etch step was therefore adopted, where the duration of the etch was determined by the amount of film etched, *i.e.,* the number of cycles in the recorded interferometric signal. All processing was performed in a manual mode for maximal flexibility.

4.2.1 Power

The effect of applied rf power in a diode etcher is among the more straightforward. In a diode system, the sheath voltage and dc self-bias are determined by the electrical characteristics of the system and cannot be adjusted independently of the power input. Thus ion energy (a direct function of sheath voltages) and ion flux (a function of the degree of feed gas dissociation) are inexorably linked. Increasing power therefore increases the plasma density and thereby the production of reactive species and hence the fluxes of these species to the substrate; it also increases the energy of the ions incident on the substrate. The net effect tends to be an increase in etch rate. A drawback to using very high power levels, however, is substrate damage due to excessive ion bombardment.

4.2.2 Pressure

In the Precision 5000 etch chamber, process pressure is maintained independently of feed gas flow rates by means of a throttle at the entrance to the turbo pump foreline. The effect of varying pressure is not as straightforward as that of power input. Increasing pressure can cause etch rate to rise or to drop. It can also profoundly affect the polymerization mechanisms in plasmas that are prone to polymerize, affecting polymer formation rates and moving the process from net etching to net deposition regimes.

Generally speaking, the most important first-order effect of increasing pressure is to increase the concentrations of all reactants, and hence to increase the fluxes of all species to the surface, which tends to increase etch rates. However, if the process is dominated by polymerization kinetics, increasing pressure can boost polymer deposition rates. To the extent that relative partial pressures of the species within the discharge remain constant as total pressure varies, the reactions that they are involved in should exhibit a first-order dependence with pressure. Thus the chemical components of etching are believed to increase linearly with

pressure. On the other hand, some authors, *e.g.*, [30], support the view that polymer formation may be initiated by reactions such as the dimerization of CF_2:

$$CF_2 + CF_2 (+ M) \rightarrow C_2F_4 (+ M).$$

They will argue that, because the rate laws for such reactions are second- (or higher) order with pressure (*e.g.*, $r = kN_{CF2}^2 (\propto P^2)$), polymerization phenomena will become more important, relative to first-order reactions such as etching of an Si-based film by F atoms, at higher pressures.

Increasing pressure can, moreover, induce more complicated changes in the plasma. At higher pressures, ion bombardment energies are reduced [30]. For one thing, there is greater ion scattering due to collisions in the sheath [65]. Additionally, both the dc self-bias and the rf sheath voltage tend to decrease. The decrease in rf sheath voltage results from a decrease in the effective rf voltage driving the plasma. The relation between the two is estimated by [66]:

$$V_{sheath,\ rf} = |V| \sin \phi,$$

where V is the rf voltage driving the plasma and ϕ is the phase angle between the rf voltage and the rf current. Work carried out with Cl_2/HBr plasmas in the Precision 5000 [65] shows that measured rf voltage is indeed found to decrease with increasing pressure. Other experiments in the same system show that the magnitude of the dc self-bias also decreases with increasing pressure [65, 67].

As pressure increases, plasma density is believed to increase, simply due to higher gas density [68]. On the other hand, at higher pressures, the plasma also tends to be "cooler," *i.e.*, the electron energy distribution function (EEDF) shifts toward lower energies [30]. This shift occurs because, at higher pressures, the electron population in the plasma experiences more energy loss through collisions. Thus the net effect on etch rate can be complicated.

The EEDF is a concept that has not been previously introduced, but it is simply the distribution of electrons with respect to energy. (To first order, this distribution is Maxwellian. The high energy tail, however, is believed to be better modeled by a Druyvesteyn distribution [28].) The EEDF is an important concept because it can be used to calculate the number of electrons that are energetic enough to cause events which require a certain energy threshold, for instance excitation and ionization. Dissociation, excitation, and ionization potentials on the order of a few eV to ~20 eV are common [28]. Thus a shift of the EEDF to lower energies implies a

smaller high energy tail, and hence a decrease in the frequency of excitation, ionization, and dissociation events.

4.2.3 Feed Gas Flow Rate

The following discussion is based on the "classical" argument about flow rate effects, as given by Chapman [69]. In the simplest of all models, etch rate can be viewed as being limited by the supply of the reactant (active etch species) at the surface. If one were to assume that the time spent by these species in the chamber was large on the scale of the time it took for them to arrive at the surface, adsorb, and react, the etch rate would be limited by the rate at which the reactant that is consumed were replenished - and thus by the rate of generation of the active etch species in the plasma. With increased etch gas flow, the etch rate would increase in some monotonic fashion as reactant concentrations increased, until it saturated at a value limited by the rate of reaction itself. However, the concentration of the active etch species at the surface (where it matters) is also affected by the pumping speed. At constant total pressure, two regimes are posited to exist in all systems: a low flow rate regime and a high flow rate regime. In both cases, the etch rate is assumed to be limited by the supply of reactant at the surface, not the rate of reaction. In the low flow rate regime, increasing the flow rate increases observed etch rates. This does not imply that 100% conversion of the feed gas is achieved. Rather, it merely indicates that increasing the flow rate of the feed gas increases the supply of active etchant species in the region near the surface where they are available to etch. However, as flow rate increases, at a constant total pressure, the pumping speed (*amount* of material pumped out per unit time) also must increase to compensate. Even if one were to assume that generation of active etchant species from the feed gas were instantaneous, in the asymptotic limit of infinitely high flows and pumping speeds, all of the etchant thus produced would immediately leave the chamber without having the opportunity to react. Thus the pumping speed effect results in a monotonic decrease in etch rate as a function of feed gas flow. Figure 4.2 illustrates this. The overall flow rate effect is believed to be the product of the two curves.

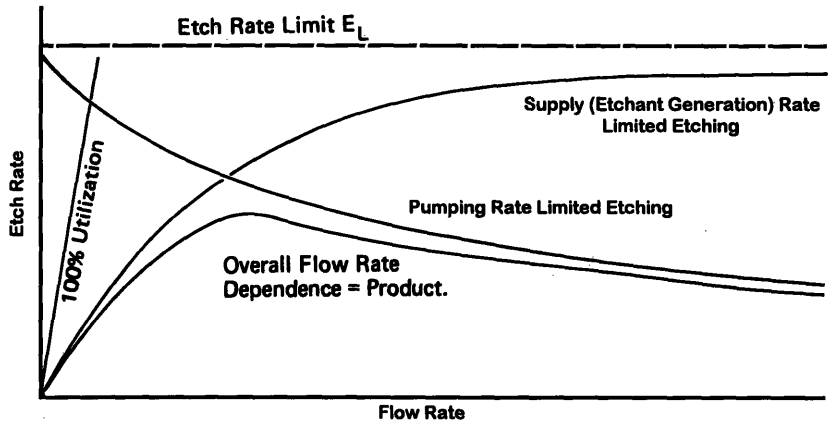

Figure 4.2

The effect of etch gas flow rate on the etch rate. Overall behavior is believed to follow the product of the etchant generation rate and the pumping rate curves. After [69].

This brings the discussion to the concept of *residence time*, defined as [70]:

$$\tau = \frac{PV}{Q},$$

where P is the pressure, V is the chamber volume (fixed), and Q is the total flow rate of the feed gas. One can see that, in the preceding discussion, the low flow rate / low pumping speed regime, corresponds to high residence times, while the high flow rate / high pumping speed regime corresponds to low residence times. This criterion is often useful in a discussion of etch behavior.

4.2.4 Magnetic Field

The magnetic field in the Precision 5000 causes charged particles to experience a Lorentz force:

$$\mathbf{F} = e\mathbf{E} + e(\mathbf{v} \times \mathbf{B}),$$

where e is the electronic charge, $\mathbf{E}$ is the strength of the electric field experienced by the particle, $\mathbf{v}$ is its velocity, and $\mathbf{B}$ is the magnetic flux density in the region through which the particle is moving. Of the two principal types of charged species present in electropostive plasmas: electrons and positive ions, it turns out that only the electrons respond to the magnetic field to any measurable degree.

The explanation for this begins with that fact that a charged particle in a magnetic field, once in motion, will acquire a gyration, whose radius r is given by:

$$r = \frac{mv}{eB},$$

where m is the mass of the particle, v its speed, and B the magnitude of the magnetic flux density it is experiencing. The mean free path of the particle is given by:

$$\lambda = \frac{v}{\upsilon},$$

where υ is the collision frequency. (In practice, this frequency is the frequency of collisions with neutrals in the plasma.) If the radius of the orbit is larger than the mean free path, no net effect is seen. However if the opposite is the case, then the particle acquires a gyrating motion perpendicular to the lines of magnetic flux. At the magnetic flux densities available in the Precision 5000 (0 to 100 Gauss nominally, 0 to ~150 Gauss maximum attainable) the former is the case for the more massive positive ions, while the latter is true for the electrons. See [71] for a discussion of these effects. This gyration has the effect of noticeably increasing the time that electrons stay resident in the plasma, which increases the number of collisions they experience; it also reduces their loss rate due to recombination at the walls. Thus the net effect is a substantial increase in plasma density [72, 73], which tends to result in higher fluxes of active etchant species being generated and thus increases etch rate dramatically.

A drawback to the use of magnetic enhancement in a configuration such as that in the Precision 5000 is that the presence of the B-field results in non-uniformities in the plasma. See [74] for a more detailed discussion. This results in: nonuniformities in the environment seen by the wafer surface, differences in dc self bias across the wafer, charging effects caused by potential differences induced across the wafer, and damage to devices being patterned. (This damage is believed to be caused by phenomena such as tunneling currents through the gate dielectric.) The spatial nonuniformities can be seen with the naked eye as an increase in optical emission from those regions where the plasma density is greater. To reduce the effects of lateral plasma non-uniformity, the B-field in the Precision 5000 is rotated. (In this study, the default frequency of 0.5 Hz was used.) Nevertheless, substantial radial nonuniformity is still present in MERIE systems if process conditions are not chosen carefully.

Workers have reported that increasing B-field in a magnetically enhanced system tends to decrease the magnitude of the dc self-bias [73, 75] and the rf voltage driving the plasma [76] (implying a decrease in the rf sheath voltage). Thus while increasing B-field has the effect of increasing production of reactive species in the plasma, it also decreases mean ion energy. The decrease in self-bias is explained by Yeom and Kushner as being the result of a decrease in electron mobility in the presence of the magnetic field [73]. Lower electron flux to the surfaces wet by the plasma (resulting from their confinement by the gyration motion they undergo) implies that lower dc bias is needed (see discussion in Section 2.2.2). In the Precision 5000, in terms of the net effect on etch rate, however, this is more than compensated for by higher fluxes of reactive etch species.

4.2.5 Chamber State

The condition of the chamber during the etch process can vary between two runs with an otherwise identical recipe. Often, the chamber condition can be sufficiently different to effect significant variation in etch rate. There have been few systematic studies on this topic. Nevertheless this is a very important parameter. In industrial practice, the potential for process drift as a result of chamber state variation is recognized in the use of extensive "seasoning" (*i.e.*, the running of dummy processes to bring the chamber to a steady state condition) after any maintenance step which potentially alters the chamber environment. Wet cleans (whereby the chamber is opened to atmosphere and cleaned mechanically with solvents) as well as more frequent plasma cleans are two such steps. In a research tool such as the Precision 5000 used for this project, the use of different chemistries by other users also has the potential to alter the condition of the surfaces in the chamber.

What is meant by "chamber state," is the amount and nature of chamber wall residues that have been deposited in the course of processing. These deposits have the potential to alter the chemistry of subsequent processes through mechanisms such as consumption of etchant species, liberation of etchant species that have been incorporated into the film, or any number of other complex interactions with the chemistry of the plasma that can alter the concentrations of important species in the discharge. Chemistries which polymerize heavily appear to warrant particular attention. At times, the deposition of polymer can be rapid enough to result in a

coating of the chamber viewports which is thick enough to be perceptible by the naked eye after a single run. It should be pointed out that, on grounded or electrically isolated surfaces, the beneficial effect of ion bombardment in removing the polymer film is largely absent. Thus even chemistries which may not appear to result in significant polymer buildup on the wafer surface can cause the condition of the chamber walls to be altered. While a systematic study of this effect was not carried out as part of the work described in this thesis, an effort had been made to determine the severity of "memory" (process drift) effects in the chamber for one of the of the chemistries which were found to polymerize most heavily. In addition, as will be discussed shortly, center point replication was used in the designed experiment matrices in this work in order to track process drift.

4.3 Diagnostics: Optical Emission Interferometry

A powerful new technique for *in-situ* measurement of etch (and deposition) rates in plasma tools was employed in the course of this work. This method, optical emission interferometry (OEI), was developed by Dalton and coworkers [77] and since commercialized by Low Entropy Systems (Boston, MA). OEI relies on the principles of interferometry to determine the change in the thickness of a film that is being etched or deposited. Its innovation lies in the use of the light of the plasma itself to provide the interferometric signal. The collection of this light at an appropriate frequency with a CCD (charge coupled display) camera enables spatially resolved, *in-situ* measurements to be taken. Comparison of results obtained with this technique against data taken by Nanospec®, generally showed excellent correlation between the two methods. Some exceptions to this (typically for process conditions in a narrow window around the boundary of etching and net deposition) will be discussed later.

The advantages of an *in-situ* etch rate monitor include immediate detection of process drift, a considerable savings in time and effort over *ex-situ* methods, and the capability to measure every wafer in a lot and use it as a monitor for the next, resulting in savings through the elimination of monitor wafers and rework [18]. 1000-IS, a commercially available OEI system made by Low Entropy Systems (LES), was used in the course of this study. After an initial series of trials to verify its performance against a conventional *ex-situ* technique (Nanospec®), OEI was used exclusively for the measurement of etch rates in the designed matrix experiments

(which, as will be discussed later, were carried out with gases that exhibited low levels of polymer formation). In subsequent experiments where net polymer deposition was encountered, OEI was used in conjunction with Nanospec®.

The CCD camera, connected directly to an I/O board in a PC used for data acquisition, was mounted on the lid of the dielectric etch chamber of the Precision 5000 directly above a viewport in the chamber lid. In the 1000-IS system, the CCD array contains 753 x 244 (H x V) pixels of dimensions 11.5 x 27 μm (H x V). All of these pixels may be used for acquisition, resulting in the collection of full frames representing an image of the wafer being processed. However, in order to maximize temporal sampling rate by reducing the number of regions processed, a circular grid of regions (2 adjacent pixels per region) was defined and only data from these points was collected. The regions were arranged in a concentric pattern of four rings, with regions in the outermost ring being located just inside a 6 mm exclusion zone at the wafer edge.

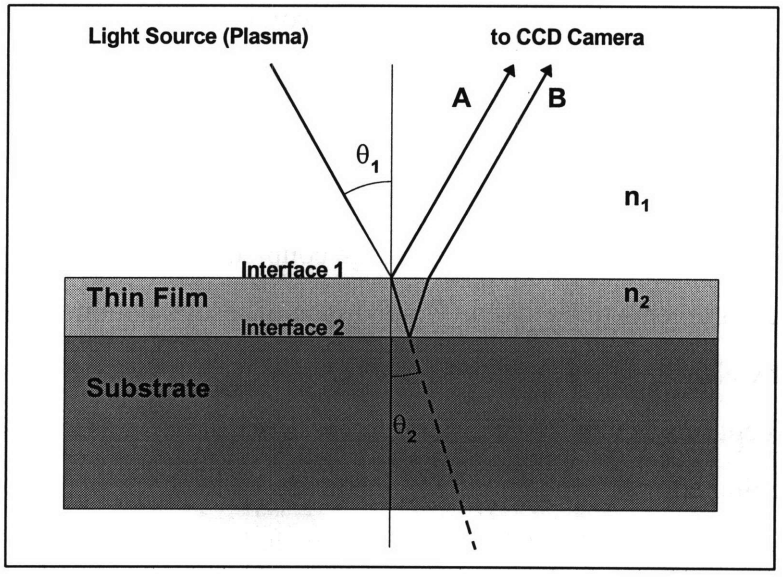

Figure 4.3

The basics of thin film interferometry as applied in the 1000-IS system: light from the plasma is reflected at both interfaces of the thin film being measured; as a result of the difference in distances traveled by beams A and B, a difference in phase between the two beams forms; the resulting interferometric signal is detected as a change in the intensity of the light seen by the CCD array. After [78].

In the 1000-IS system, interferometric signal is collected at a specific wavelength of light determined by a bandpass filter mounted on the camera lens. As will be apparent from the foregoing discussion of interferometry, it is desirable to employ the shortest wavelength available at which there is sufficient light. In a glow discharge of the type found in an etch reactor, good choices for this wavelength are emission wavelengths of the active etch species, in this case fluorine. A 486 nm filter (part 486-FS-10-25, Andover Corp., Salem, NH), corresponding to a strong fluorine emission line, was used.

The determination of etch/deposition rates by the 1000-IS software is based on the principles of interferometry [78]. Interferometry is the use of a difference in phase between two waves of light to determine a difference in the distance they have traversed. The use of the technique in the measurement of a film is predicated on the existence of optical interfaces where the index of refraction of the medium through which the light travels changes. Films which absorb little light at the wavelength of measurement are best suited to the technique. Silicon dioxide as well as silicon nitride both meet this criterion. As Figure 4.3 shows, a portion of the light incident on interface 1 will be reflected, while a portion of it will be transmitted through the film. The transmitted portion will undergo another reflection at interface 2. In principle, the difference in the paths traveled by waves A and B can be related to the thickness of the film if its index of refraction and the geometry of the situation (incident angle, θ_1) are known. However, the 1000-IS system cannot measure this difference directly; therefore it does not provide a means for measuring the absolute thickness of the film itself. What it can provide is the change in that thickness as the interference signal evolves over time. The interference is produced by the superposition of the signals reflected at interfaces 1 and 2. If the difference in the optical paths is an integral number of wavelengths, constructive interference will result and the detected signal will be at a maximum. If the difference in paths is equal to n + ½ wavelengths, where n is an integer, destructive interference will result and the detected signal will be at a minimum. Thus, as a film is etched or deposited and its thickness changes, the detected signal will fluctuate between these extrema in a sinusoidal manner. The period of this signal can be related to the etch rate, *ER*, by [78]:

$$ER = \frac{\lambda}{2n_2 \cos\theta_2 T},$$

where λ is the wavelength of the light, n_2 is the index of refraction of the film, θ_2 is the angle of refraction in the film, and T is the period of the detected signal. In the setup used for this work, the camera was mounted along the normal to the wafer; thus eliminating the geometric term in the equation.

The period of the time-varying signal is accurately determined from the frequency of the periodicity of the time domain waveform [78]. The 1000-IS software uses FFT (fast Fourier transform) techniques to accomplish this. A very useful feature of this method is its ability to filter out noise as well as other periodic signals. This is particularly important in MERIE systems, where a periodic signal generated by the magnetic field or one of its harmonics is superimposed on the time domain waveform of the interferometric signal.**

It is apparent from the above discussion that at least one, but preferably more than one, cycle must be collected in order to obtain enough data points to map out the time domain waveform. In practice, the requirement for a good quality fit is a minimum of 1.5 cycles. This requirement translates to a minimum thickness for the films being etched or deposited. In the case of SiO_2 (n = 1.45), one period of the signal corresponds to ~1675 Å; in the case of Si_3N_4 (n = 2.00), one period corresponds to ~1215 Å. Hence there was an advantage in using thicker films to allow the etch to proceed for a longer time in order that more cycles could be collected and a higher quality fit obtained.

4.4 Experimental Plan

Seven gases were studied during the course of this work: 1H- and 2H-heptafluoropropane, pentafluoroethane, difluoromethane, 1,1,1,2-tetrafluoroethane, and trifluoroethylene, with the PFC octafluoropropane used as a baseline reference. 1H-heptafluoropropane, 2H-heptafluoropropane, difluoromethane, and trifluoroethylene were

** The following settings were used in the 1000-IS software during analysis of data: *Rate Analysis:* FFT+Fit, Low Pass Filter Manual, OE All Divide, peaked sine, n=1.45 (oxide), n-2.00 (nitride), n=1.35 (fluoropolymer); *Uniformity Analysis:* exclusion = 6 mm, outlier rejection = 3 sigma.

purchased from PCR, Inc. (Gainesville, FL). Octafluoropropane was supplied by 3M Specialty Chemicals. Tetrafluoroethane and pentafluoroethane were supplied by DuPont. The purity of all gases was 99% or higher. The trifluoroethylene was inhibited with <0.1% of dipentene. The inhibitor was not removed. See Appendix 3. Except as noted below, all tests were carried out on both oxide and nitride substrates.

The decision to use octafluoropropane, rather than more common PFC gases such as tetrafluoromethane or hexafluoroethane, was motivated in large part by recent industrial interest in this gas as an emerging etchant for the cleaning of PECVD chambers. Recent work at Novellus Systems, Inc. shows that C_3F_8 is potentially significantly more efficient in this role than C_2F_6 [52]. There does not appear to exist a large body of information on the use of this particular substance for etching in the literature. Chen and Lee reported studying the optical emission characteristics of C_3F_8/O_2, C_2F_6/O_2, and CF_4/O_2 plasmas used to etch undoped polysilicon in a capacitively coupled RIE system [79]. They found that larger oxygen concentrations are needed to achieve the maximum fluorine emission intensity as the F/C ratio of the feed gas decreases. They also found that CF_2 emission intensities are strongest in C_3F_8 and weakest in CF_4 at all levels of oxygen content, suggesting greater tendency to polymerize in C_3F_8. The CF_2 signal was found to decrease with O_2 addition in all three gases. All these results are consistent with the previously described models (see Section 2.3.2). Others have studied the polymerization behavior of C_3F_8, as well as CF_4, C_2F_6, and C_2F_4, with and without the addition of hydrogen [80, 81]. D'Agostino *et al* reported strongest concentrations of fluorine and weakest concentrations of CF and CF_2 in CF_4 and, conversely, strongest concentrations of CF and CF_2 and weakest concentrations of fluorine in C_2F_4 - with C_2F_6 and C_3F_8 exhibiting intermediate behavior [80]. He reported that high ratios of [F] to [CF_x] resulted in etching of silicon, its compounds, as well as the $(CF_x)_n$ deposited fluoropolymer layer, while low ratios were associated with the formation of the polymer.

4.4.1 Designed Matrix Experiments - the Central Composite Design

Three hydrofluorocarbon gases - 1H- and 2H- heptafluoropropane, and pentafluoroethane, with octafluoropropane as a reference were examined using a central composite design (CCD) experimental matrix. The results were analyzed using NNAPER

(Neural Network Analyzer of Process Evaluation Responses) developed by E.I. du Pont de Nemours and Company. The results of the experiments described in this and the following two sections are discussed in Section 5.1.

Design-of-Experiments ("DOE") methodology has a number of advantages over traditional "one-at-a-time" approaches. One of the principal limitations of "one-at-a-time" experiments is the fact that they fail to account for interaction effects between two variables. *I.e.,* an increase in input variable A and an increase in input variable B may each independently result in an increase in the output variable being monitored, but, to use an extreme example, increasing both these together may result in a *decrease* in the output variable because of a more complex interaction between the inputs. "One-at-a-time" experiments are inadequate for evaluating this type of process as the interaction cannot be captured. Statistically designed experiments overcome this limitation because they allow for the monitoring of the interactions between the variables; that is, they measure the effects of simultaneously varying more than one variable. As will be seen in the following chapter, a complex process such as a plasma etch involves a number of such interaction effects.

A number of different statistically designed experimental methodologies exist. References such as [82, 83, 84, 85, 86] describe these, along with the statistical theory behind them. Only a brief discussion will be included here. Arguably the most exhaustive of these designs is the *full factorial* matrix. The full factorial can quantitatively extract apparent interactions between all the input variables. The full factorial matrix is in principle also the most thorough in exploring any given experimental *parameter space*. A major disadvantage of the full factorial scheme, however, is its cost. An n variable matrix which explores each variable at k levels requires n^k runs, making full factorial schemes impractical for experiments with large numbers of variables. *Fractional factorial* designs which explore the same parameter space as a corresponding full factorial trade the capability to resolve more complex, higher order interaction effects for greater economy by sampling the space more sparsely in a carefully selected manner. Other common designs, such as *Box-Behnken* designs and *central composite* designs (CCD), are even more efficient. The scheme utilized in this work was the central composite design, chosen because it allows for exploration of a wide parameter space at a large number of levels with remarkable economy.

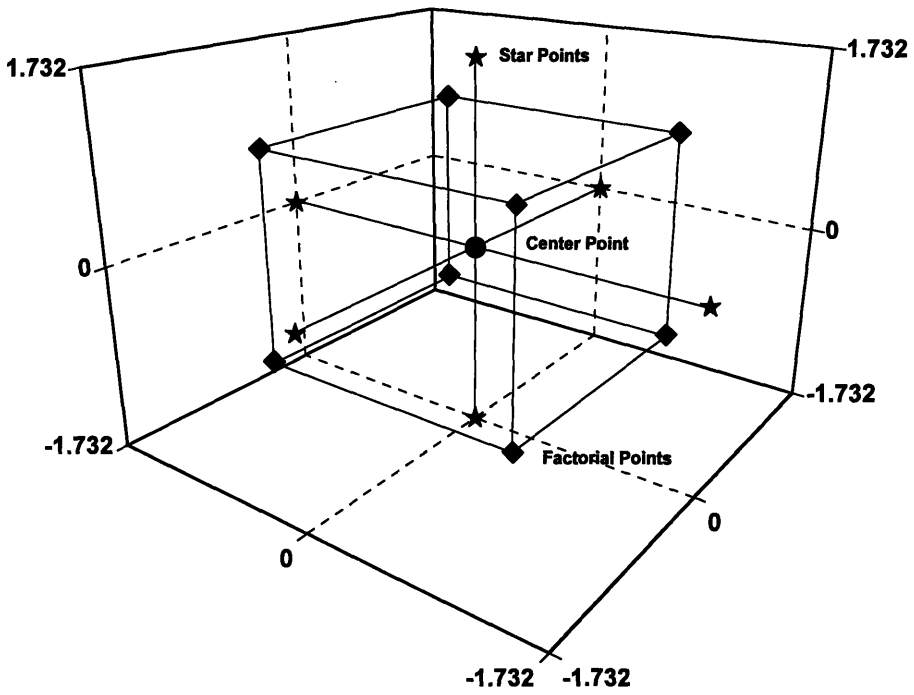

Figure 4.4

The 3 variable, 5 level central composite design matrix.

In this work, a three variable, five level matrix requiring a minimum of fifteen runs (excluding center point replicates) was used. A three variable, five level full factorial scheme, by comparison, requires 243 runs. The tradeoffs are decreased thoroughness and decreased capability to resolve higher order interactions. However, in real physical systems, the effects of interactions of order higher than two (*i.e.*, interactions between more than two variables) tend to be small relative to first and second order effects, making the use of sparse designs such as the CCD viable. The central composite design used is shown in Figure 4.4. The scheme is made up of three components: a central point, designated by variable levels (0,0,0), a two level, three variable full factorial experiment (eight points), designated by the set of variable levels $<\pm1,\pm1\pm1>$, and a set of six axial or "star" points lying along the axes of the parameter space, designated by the set $<\pm\alpha,0,0>$ and its permutations. The coefficient α is chosen so that the design is "rotatable," *i.e.*, so that all points are equidistant in the parameter space from the center point. For a three variable CCD, a simple exercise in geometry shows that $\alpha = \sqrt{3} = 1.732$.

Alternately, the CCD can be characterized as being based on a face centered cube design with a central point, where the axial points are pushed out from <±1,0,0> to <±α,0,0>.

4.4.2 Designed Matrix Experiments - Selection of Variables

The input parameters chosen for this study were process pressure, magnetic field, and oxygen flow rate. The effects of two of these, pressure and oxygen flow rate, along with a third, the flow rate of argon gas added to the discharge, were studied in preliminary tests carried out with octafluoropropane and 2H-heptafluoropropane. Only oxide substrates were used for the preliminary study. These tests used the same thermal oxide wafers as those described in Section 4.1. Some results from these tests are shown in Figures 4.5 and 4.6.

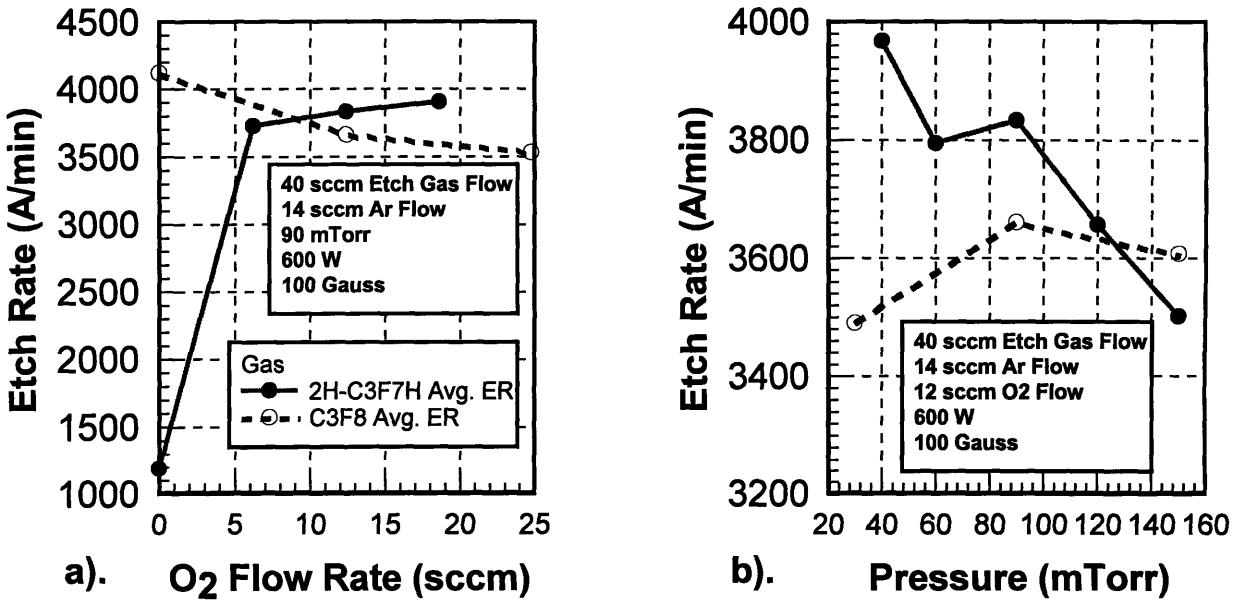

Figure 4.5

Preliminary tests with octafluoropropane and 2H-heptafluoropropane on thermal oxide substrates: oxide etch rate vs. a). O_2 flow rate (at 90 mTorr); b). pressure (at 12 sccm O_2 flow).

In the preliminary tests, it was found that, while the etch rate of SiO_2 in octafluoropropane decreases with the addition of oxygen (probably due to dilution or the effect of decreased residence time at higher total flows), the etch rate in 2H-heptafluoropropane increases dramatically with the addition of small amounts of O_2, suggesting a tendency toward

polymerizing behavior in the absence of oxygen. Indeed, net polymer deposition in the absence of oxygen was found to take place with 2H-heptafluoropropane in tests carried out at 0 Gauss magnetic field (see Figure 4.6[††]). This observation is consistent with the mechanisms postulated in Section 2.3.2. The effect of pressure appeared to be quite different for the two gases, as is shown in Figure 4.5. A more detailed discussion of pressure effects with these gases will be provided in the following chapter. The effects of argon addition (data not shown) appeared to be ambiguous and relatively small.

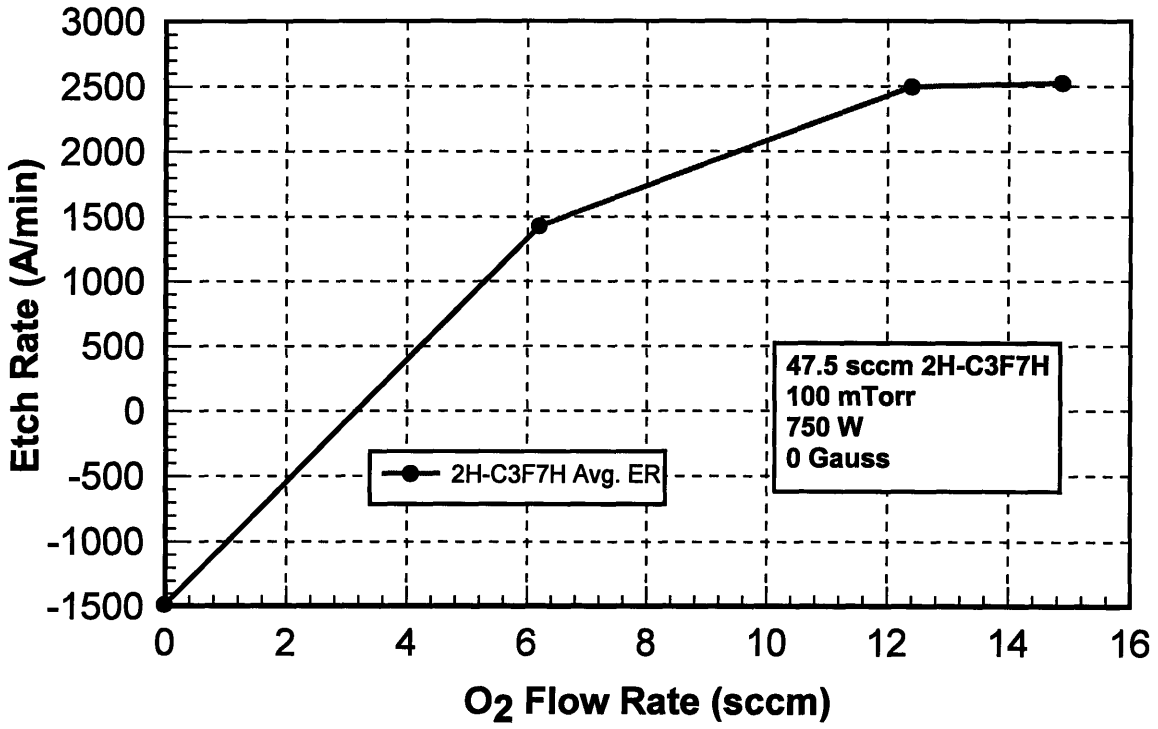

Figure 4.6

Preliminary tests with 2H-heptafluoropropane on thermal oxide substrates: oxide etch rate vs. O_2 flow rate without magnetic enhancement. Net deposition of what is believed to be a fluoropolymer film is shown as negative etch rate.

[††] Deposition rates were determined using Nanospec® and later OEI assuming an index of refraction of 1.35 (bulk Teflon®, $(CF_2)_n$). See Sections 5.2, 5.3.

In summary, it was determined that the addition of argon did not appear to have a significant effect on the etch behavior of the two gases studied, whereas the addition of oxygen did appear to affect etch rates substantially. Oxygen flow rate was therefore chosen as one of the input parameters to be studied more thoroughly. Pressure was found to have a complex effect, and was therefore also chosen as a matrix variable. Finally, a comparison of Figures 4.5a and 4.6 shows that the presence of a magnetic field can also significantly affect etch behavior. Thus magnetic field was chosen as a matrix variable as well. The effects of fluorocarbon gas flow rate as well as chamber condition were not studied in these preliminary experiments, but were subsequently found to be important. Because chamber condition is difficult to characterize by a set of continuous, as opposed to discrete, variables, it is ill suited to be included in a designed experiment matrix such as the one used in this study. Fluorocarbon gas flow rate, however, could be incorporated, and, in fact, it is the author's intent to expand the CCD matrix to a four variable scheme that will include fluorocarbon gas flow rate during the testing of iodofluorocarbons and unsaturated fluorocarbons which is to follow. Finally, the effects of rf power input (see Section 4.2.1) are believed to be fairly well understood, in comparison with the other variables; thus the effects of varying power were not studied in the preliminary experiments, nor was power varied in the subsequent matrix experiments.

Upon examination, the preliminary data shown above indicates that 2H-heptafluoropropane is capable of etching oxide at rates comparable to those of octafluoropropane and that 2H-heptafluoropropane polymerizes heavily at low flows of oxygen and no magnetic field, producing - under certain conditions - net deposition of what is presumed to be a $(CF_x)_n$ fluoropolymer layer. The highest oxide etch rates achieved in these initial experiments were approximately 4000 Å/min.

In the matrix experiments, the ranges for the variables studied were: 35 to 150 mTorr for process pressure, 0 to 20 sccm for oxygen flow rate, and 0 to 100 Gauss for magnetic field. The magnetic field values were determined by the range of available settings on the Precision 5000 tool. Operation above 100 Gauss is possible. Dalton has studied the effects of magnetic field on an HBr/Cl_2 polysilicon etch process over the range 0 to 140 Gauss. However, the etch rate trends seen above 100 Gauss were qualitatively the same as those seen below 100 Gauss [87]. Moreover, prolonged operation at high magnetic fields was reported to result in reliability

problems involving the magnetic coils [88]. The oxygen flows were selected to cover a range from 0 to 50% of the fluorocarbon feed gas flow, which was fixed at 40 sccm, a value consistent with those reported in earlier studies involving etch processes in the Precision 5000 [55, 89]. The lower limit of the process pressure was taken to be the lowest pressure that could be reliably sustained by the system given the flows of gas being used. The upper limit was chosen on the basis of earlier studies by other authors [55, 89]. The actual experimental matrix used in this part of the work, as defined by the three parameters discussed above, is shown in Figure 4.7. The significance of the test points and center point replicates shown in the figure will be discussed in the following section.

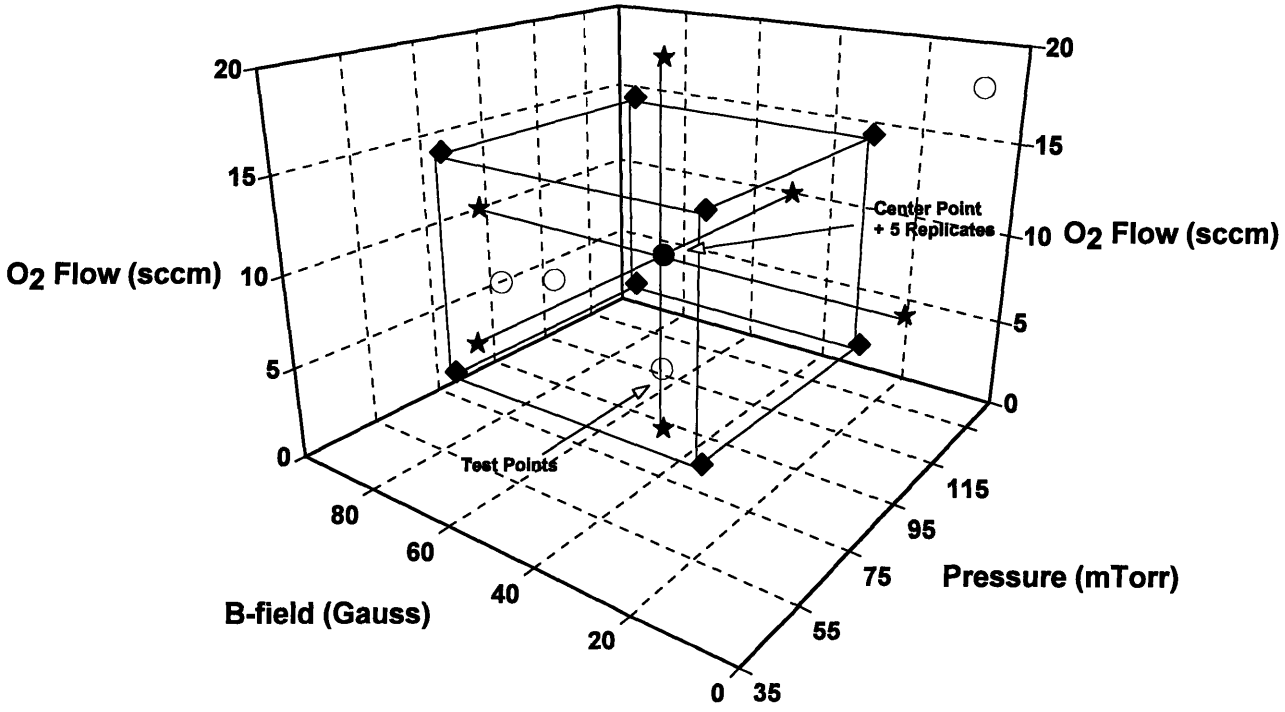

Figure 4.7

The actual experimental matrix used in this study: a CCD design with a total of 6 center point replicates and 4 pseudo-random test points (24 runs total).

4.4.3 Designed Matrix Experiments - Neural Network Analysis

The data generated by the CCD matrix experiments was evaluated using the NNAPER software. A 24-run scheme based on the 15-run CCD matrix described above was employed for each of the two types of dielectric films. Thus the evaluation of each gas required 48 runs. The

roles of the additional points in this scheme, which was generated by a design advisor feature of the software, will be discussed shortly.

Neural networks are an alternative to response surface methodology (RSM) techniques, which generate empirical models from experimental data by fitting response to polynomial expressions. Generally speaking, a polynomial expression of order n is required to fit interaction effects of order n. Since three variable or higher order interactions are often discounted, quadratic polynomials tend to result in sufficiently good fits. A limitation of polynomial curve fitting methods, however, is that they are inherently limited to a single kind of mathematical model of the responses being evaluated.

Neural networks, on the other hand, do not presume the relationship of the response to the input variables to be constrained to follow any particular mathematical form, such as a polynomial expression. Instead of attempting to fit the input-output relationships to a mathematical expression in a single transformation, neural networks rely on connecting inputs with outputs through multiple transformations using a network of nodes ("neurons") with weighted connections ("synapses"). The neuron is a structure which sums its (weighted) inputs and processes them through a function that provides non-linearity, such as a "squashing" function [90, 91]. In principle, the precise form of this function is somewhat arbitrary, as long as it is bounded and nonlinear. The synapses are the links where the neural learning is embedded through weights assigned to the connections. NNAPER, in particular, uses a three-layer back propagation neural network [91], whose basic structure is shown in Figure 4.8. This type of network consists of: a layer of input variables, corresponding to process inputs, such as pressure, gas flows, etc.; and two layers of "neurons" - a layer of output responses, corresponding to process outputs, such as etch rate, and a "hidden" layer of intermediate nodes, each connected to each input and output through weighted links ("synapses"). Thus the network provides a two-level transformation between inputs and outputs, which is arguably a more accurate reflection of a real physical system, such as a plasma, than a single transformation approach. This is because in such a system there too exists a layer of "hidden" variables, such as plasma density, concentrations of individual species, sheath voltages, etc. Adjusting the process inputs (pressure, flows, etc.) directly impacts these intermediate variables, which, in turn, affect the measurable output variables. Nevertheless, it should be pointed out that, even though the intermediate nodes

in a multi-level neural network can be thought of as a means of approximating this relationship, in actuality, they are only constructs which do not specifically correspond to any "hidden" plasma properties in particular [90].

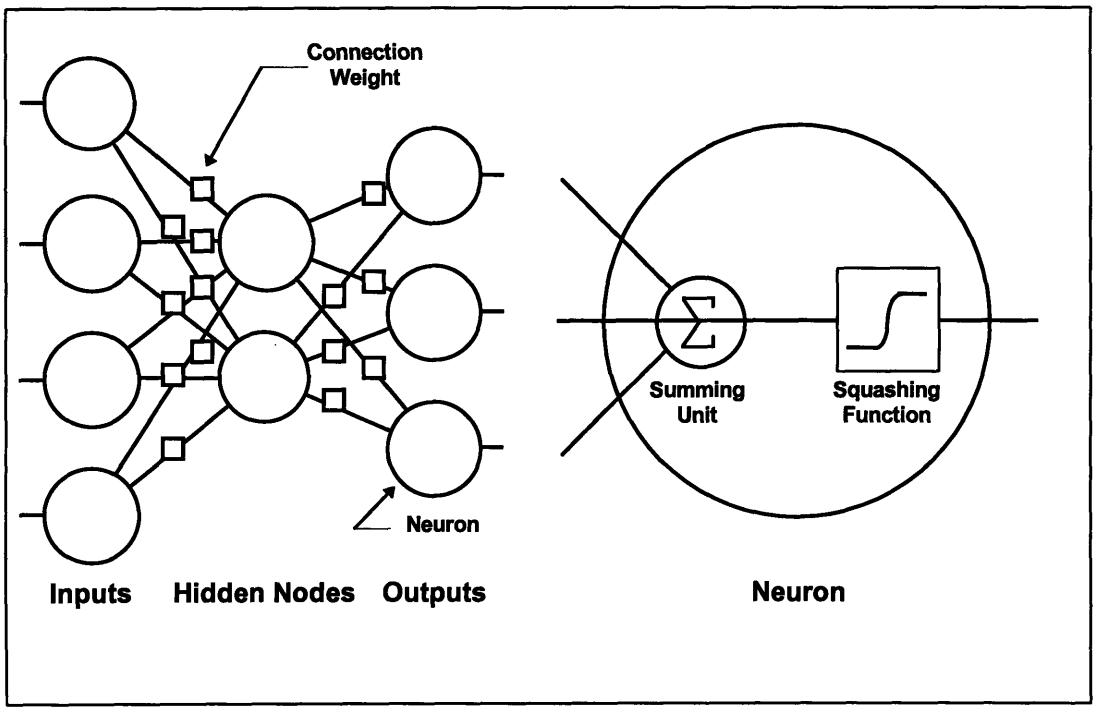

Figure 4.8

An example of the three-layer back propagation network used by NNAPER: a four-input, three-output model, with two hidden nodes. Each hidden and output node is a neuron which consists of a summing unit and a "squashing function," *i.e.*, $y(x) = 1/(1 + e^{-ax})$. The inputs are merely placeholders for data. After [90, 91]

To solve a given network, NNAPER can use historical data, which can, in principle, have been collected in an arbitrary manner, or it can generate an experimental procedure based on the number of controlled inputs and observed outputs desired by the user, then allow the user to provide the network with experimental data generated by this procedure. In either case, the structure of a given model (number of inputs, outputs, and hidden nodes) is determined by the user before NNAPER is provided with the experimental information needed to solve the network. The weights are generated through the process of solving the model. The number of inputs and outputs is obviously constrained by the physical variables selected for a given experiment. The number of hidden nodes, however, can be varied, if the network is large

enough, in order to produce the most accurate fit to the data, and this, in fact, is recommended in practice. The network used in the present work, however, had only three inputs (magnetic field, oxygen flow, pressure) and a single output (average etch rate); the number of hidden nodes was fixed at two. The model that is built by NNAPER can then be used to generate a set of output response values for any point in the parameter space sampled by the experiment.

Table 4.1: NNAPER Experimental Matrix

Run	Type	Pressure (mTorr)		Magnetic Field (Gauss)		O_2 Flow (sccm)	
		NNAPER	Actual Setpoint	NNAPER	Actual Setpoint	NNAPER	Actual Setpoint
1	C	92.5	93	50	50	10	10
2	C	92.5	93	50	50	10	10
3	C	92.5	93	50	50	10	10
4	S	35	35	50	50	10	10
5	S	92.5	93	0	0	10	10
6	S	150	150	50	50	10	10
7	S	92.5	93	50	50	0	0
8	S	92.5	93	100	100	10	10
9	S	92.5	93	50	50	20	20
10	T	96.531	97	81.79	82	6.43	7
11	C	92.5	93	50	50	10	10
12	F	59.323	60	21.15	21	15.77	15
13	F	59.323	60	78.85	79	15.77	15
14	T	149.389	149	7.822	8	17.677	18
15	F	125.678	126	21.15	21	15.77	15
16	F	59.323	60	21.15	21	4.23	5
17	C	92.5	93	50	50	10	10
18	T	57.185	57	63.339	63	10.265	11
19	F	59.323	60	78.85	79	4.23	5
20	F	125.678	126	78.85	79	15.77	15
21	F	125.678	126	78.85	79	4.23	5
22	T	85.519	86	45.927	46	4.517	6
23	C	92.5	93	50	50	10	10
24	F	125.678	126	21.15	21	4.23	5

The experimental design generated by NNAPER is typically a central composite design. For a three variable experimental matrix, 24 runs are required. The design incorporates nine additional points into the matrix, along with the 15 required for the three variable CCD. Of these, five are center point replicates, which are intended to track process drift or "memory" effects (*i.e.*, the influence of unknown variables) through the course of the experiment. The remaining four are "test" points interspersed throughout the parameter space of the matrix. The test points are generated in a pseudo-random pattern that assures that they are sufficiently well spread out throughout the parameter space. NNAPER solves the network twice: once using only the "training data" (the fifteen point CCD structure plus the center point replicates), then once again using all of the points. A comparison of the two outcomes is a test of the program's predictive capabilities. In general, the incorporation of the additional test points improves the fit of the model to the experimental data, but a well-behaved system should provide a reasonable model with only the training data. The 24 run CCD-based NNAPER matrix used for this study is shown in Table 4.1. Table 4.2 gives a summary of the matrix experiments that were conducted.

Table 4.2: Summary of Matrix Experimental Series

Gas	Oxide Matrix Runs (Lot: Wafer #)	Nitride Matrix Runs (Lot: Wafer #)	Figures
C_3F_8	**3**:1-24	**3**:1-24	A1.1-3, A1.4-6
2H-C_3F_7H	**4**:1-6, 8-16, 18-24, **2**:13, 17	**7**:1-24	A1.7-9, A1.10-12
1H-C_3F_7H	**5**:1-6, 8-23, **10**:25	**5**:1-24	A1.13-15, A1.16-18
C_2F_5H	**6**:1-6, 8-25	**6**:1-24	A1.19-21, A1.22-24

4.4.4 Non-Matrix Experiments

Three of the gases tested - 1,1,1,2-tetrafluoroethane, difluoromethane, and trifluoroethylene - were found to polymerize when tested at the center point of the matrix (600W, 93 mTorr, 50 Gauss, 10 sccm O_2 flow, 40 sccm etch gas flow), depositing what is believed to be a $(CF_x)_n$ fluoropolymer layer. Tetrafluoroethane and trifluoroethylene merely deposited a film on

the wafer and the chamber walls. The deposition rates on the wafer were generally similar with SiO_2, Si_3N_4, as well as blank Si substrates (see Table 4.3), though some variation was observed.

Table 4.3: Fluoropolymer Deposition Rates for C_2F_3H and $C_2F_4H_2$ Measured at the Matrix Center Point

Substrate	Trifluoroethylene Deposition Rate (Å/min)		1,1,1,2-Tetrafluoroethane Deposition Rate (Å/min)	
	Top	Center	Top	Center
Blank Si	2177	2456	1433	1606
	2216	2545	1473	1650
SiO_2	2008	2425	1150	1440
	2073	2487		
Si_3N_4	2096	2370	1360	1614

With an SiO_2 substrate, the difluoromethane plasma, on the other hand, was observed to burn the deposited film off the surface of the wafer, causing it to peel and flake. With a blank Si wafer, it left a gray, sandpaper-like deposit of indeterminate thickness. Because the difluoromethane center point recipe proved so unstable, it was not run with an Si_3N_4 substrate. Interestingly enough, this behavior was not observed with trifluoroethylene, which, like difluoromethane, is also a flammable gas.

This behavior prompted a decision not to test these gases in the parameter space of the matrix, but to carry out more limited tests in a process window where net etching, rather than polymer deposition, would take place. Trials conducted with trifluoroethylene were used to identify such a regime. Subsequent to this, experiments were carried out with the three polymerizing gases in which the dependence of etch rate on oxygen flow was studied, with the remaining variables (rf power, etch gas flow, magnetic field, and pressure) fixed. For comparison purposes, the remaining four gases were then evaluated using this experimental procedure as well. Additionally, some limited tests to determine the effects of pressure, etch gas flow, and chamber condition were also carried out. All the above experiments are summarized in Table 4.4. The remainder of this section describes the experimental scheme that was used,

whereas the results are discussed in Section 5.2. With the exception of the initial trifluoroethylene polymerization study, where only oxide wafers were used, all experimental series used both oxide and nitride substrates.

Effects of Process Variables on Polymerization. Four series of trials (# 1a-d - see Table 4.4) were conducted with trifluoroethylene. In order to identify a regime in which the process could be driven toward net etching, the effects of pressure, oxygen flow, magnetic field strength, and etch gas flow were studied in "one-at-a-time" experiments using trifluoroethylene with SiO_2 substrates. Rf power was fixed at 600 W. Pressure was varied from 35 to 150 mTorr. Magnetic field was varied from 0 to 100 Gauss. Oxygen flow was varied from 0 to 20 sccm. When not being varied, these parameters were fixed at their center point values in the central composite matrix used earlier: 93 mTorr for pressure, 50 Gauss for magnetic field, and 10 sccm for oxygen flow. The etch gas flow rate was initially 40 sccm. Etch gas flow rate was then separately varied (in Series # 1d) from 10 to 40 sccm, with pressure at 35 mTorr, magnetic field at 50 Gauss, and oxygen flow at 10 sccm.

Oxygen Flow Rate Study. In brief, low pressure, low etch gas flow, as well as high magnetic field and high oxygen flow were found to suppress polymerization in the trifluoroethylene tests. On the basis of these trials, a regime in which polymerization was suppressed, characterized by low pressure and low etch gas flow, was identified and a set of process conditions was chosen for a more careful study of all seven gases. It was decided that it would be most informative to study the effects of oxygen flow in greater detail in this next series of trials, since this parameter has been known to have such a profound effect on the polymerization behavior of fluorocarbon gases (see Section 2.3.2). In the next sets of runs (Series # 2-15), rf power (600 W), magnetic field[‡‡] (50 Gauss), pressure (35 mTorr), and etch gas flow (15 sccm) were fixed, while oxygen flow rate was varied from 0 to 45 sccm (a 3:1 O_2 to etch gas ratio).

Supplementary Experiments: Pressure and Etch Gas Flow Effects. In addition to these trials, additional tests were carried out to gain more insight into the effects of pressure and

etch gas flow rate on etching and polymerization behavior. In the case of etch gas flow (Series #16, 17), a two-level comparison was made between flows of 15 sccm and 40 sccm with all seven gases. The remaining parameters in this study were held at the following values: rf power - 600 W, magnetic field - 50 Gauss, pressure - 35 mTorr, oxygen flow - 10 sccm. The 40 sccm data for octafluoropropane, 1H- and 2H-heptafluoropropane, and pentafluoroethane was taken from the matrix runs that had been performed earlier.

In the case of pressure (Series #18, 19), a similar two-level comparison was made using all seven gases at pressures of 35 mTorr and 93 mTorr. The remaining parameters were held at: rf power - 600 W, magnetic field - 50 Gauss, etch gas flow - 40 sccm, oxygen flow - 10 sccm. The data for octafluoropropane, 1H- and 2H-heptafluoropropane, and pentafluoroethane was also taken from the earlier matrix runs.

Supplementary Experiments: Memory (Chamber Condition) Effects. It had earlier been established that the so-called non-polymerizing gases (1H- and 2H- heptafluoropropane, pentafluoroethane, and octafluoropropane) did not exhibit process drift or "memory" effects (see Section 5.1.4). This was ascertained through a comparison of etch rate data taken in the center point replicate runs. Nevertheless, even with these gases, an attempt to insure that chamber condition did not affect the measured results was made by performing an oxygen clean[§§] before each series of runs, then seasoning the chamber for 10 min with the center point recipe using a blank Si wafer.

Trifluoroethylene was the first polymerizing gas to be evaluated in some detail. Two series of replicate runs using trifluoroethylene with oxide substrates were performed to verify the reproducibility of the data (Series # 20, 21). Pronounced discrepancies were found in measured etch rates between pairs of replicate runs taken in these series. The differences between otherwise identical replicate points in these runs were the sequence in which they were

---

[‡‡] Since operating at high magnetic fields is generally not practiced, mainly due to poor etch uniformity, magnetic field was fixed at an intermediate value, rather than at a high value, as would be indicated by the results of the trifluoroethylene study.

[§§] Standard O_2 clean recipe: 60 sccm O_2, 5 sccm CF_4, 700 W, 200 mTorr, 0 Gauss, 900 s, although times greater than 900 s (based on visual inspection of residue on chamber viewports) and oxygen flows of 80 sccm were sometimes also used.

performed and the state of the chamber when a given series was started. Subsequently, data from trifluoroethylene series which were used in the oxygen flow rate study - designated here as Series # 23 (same runs as Series # 8 for oxide) and # 25 (consisting of portions of Series # 15 for nitride) - was also compared to runs performed during the early trials with trifluoroethylene.

In all, three data sets were collected with trifluoroethylene: 1). two series with oxide films (Series # 20, 21) where oxygen flow rate was varied from 0 to 48 sccm (at 600 W, 93 mTorr, 50 Gauss, and 40 sccm etch gas flow); 2). two series with oxide films (Series # 22, 23(8)) where oxygen flow rate was varied from 0 to 45 sccm (at 600 W, 35 mTorr, 50 Gauss, and 15 sccm etch gas flow); and 3). two series with nitride films (Series # 24, 25(15)) where oxygen flow rate was also varied from 0 to 45 sccm (also at 600 W, 35 mTorr, 50 Gauss, and 15 sccm etch gas flow). (See Table 4.4.) It was found that the condition of the chamber at the start of a given run, as characterized by the presence or absence of polymeric deposits on the chamber surfaces, did indeed appear to be responsible for large drifts in the process, or "memory" effects. Chapter 5 discusses the results of all the above experiments in detail.

Table 4.4: Summary of Non-Matrix Experimental Series

Gases	Varied Parameters	Ranges	Fixed Parameters	Films	Series # (Oxide)	Runs (Oxide) (Lot: Wafer #)	Series # (Nitride)	Runs (Nitride) (Lot: Wafer #)
C_2F_3H	Pressure	35 - 150 mTorr	600 W, 50 G, 10/40 sccm O_2/etch gas	SiO_2	1a	**8**:1, 2, 4		
	Magnetic field	0 - 100 Gauss	600 W, 93 mT, 10/40 sccm O_2/etch gas		1b	**8**:1, 3, 6		
	Oxygen flow	0 - 20 sccm	600 W, 93 mT, 50 G, 40 sccm etch gas		1c	**8**:1, 5, 7		
	Etch gas flow:	10 - 40 sccm	600 W, 35 mT, 50 G, 10 sccm O_2		1d	**8**:2, 13, 14-15		
all	Oxygen flow (14 series)	0 - 45 sccm	600 W, 35 mT, 50 G, 15 sccm etch gas	SiO_2, Si_3N_4	2	**9**:9, 11-17 *(C_3F_8)*	9	**8**:25, **9**:1-7*(C_3F_8)*
					3	**10**:9-16 *(1H-C_3F_7H)*	10	**9**:25, **10**:1-7 *(1H-C_3F_7H)*
					4	**9**:18-25 *(2H-C_3F_7H)*	11	**9**:9-16 *(2H-C_3F_7H)*
					5	**10**:1-8 *(C_2F_5H)*	12	**9**:17-24 *(C_2F_5H)*
					6	**7**:15-22 *(CF_2H_2)*	13	**8**:6-13 *(CF_2H_2)*
					7	**9**:1-8 *($C_2F_4H_2$)*	14	**8**:14-21 *($C_2F_4H_2$)*
					8	**8**:22-25, **7**:2-5 *(C_2F_3H)*	15	**10**:8-15 *(C_2F_3H)*

Table 4.4: Summary of Non-Matrix Experimental Series (con't)

Gases	Varied Parameters	Ranges	Fixed Parameters	Films	Series # (Oxide)	Runs (Oxide) (Lot: Wafer #)	Series # (Nitride)	Runs (Nitride) (Lot: Wafer #)
all	Etch gas flow (2 series)	15 vs. 40 sccm	600 W, 35 mT, 50 G, 10 sccm O_2	SiO_2, Si_3N_4	16	7:3, 8:2 *(C_2F_3H)* 9:5, 10:20 *($C_2F_4H_2$)* 7:19, 10:18 *(CF_2H_2)* 10:5, 6:4 *(C_2F_5H)* 9:22, 4:4 *(2H-C_3F_7H)* 10:13, 5-4 *(1H-C_3F_7H)* 9:14, 3:4 *(C_3F_8)*	17	8:10, 10:19 *(C_2F_3H)* 8:18, 10:21 *($C_2F_4H_2$)* 10:12, 17 *(CF_2H_2)* 9:21, 6:4 *(C_2F_5H)* 9:13, 4:4 *(2H-C_3F_7H)* 10:4, 5:4 *(1H-C_3F_7H)* 9:4, 3:4 *(C_3F_8)*
all	Pressure (2 series)	35 vs. 93 mTorr	600 W, 50 G, 10/40 sccm O_2/etch gas	SiO_2, Si_3N_4	18	8:1, 2 *(C_2F_3H)* 7:1, 10:20 *($C_2F_4H_2$)* 10:18 *(CF_2H_2)* 6:1, 4*(C_2F_5H)* 4:1, 4 *(2H-C_3F_7H)* 5:1, 4 *(1H-C_3F_7H)* 3:1, 4 *(C_3F_8)*	19	10:16, 17 *(C_2F_3H)* 8:23, 10:21 *($C_2F_4H_2$)* 10:19 *(CF_2H_2)* 6:1, 4*(C_2F_5H)* 4:1, 4 *(2H-C_3F_7H)* 5:1, 4 *(1H-C_3F_7H)* 3:1, 4 *(C_3F_8)*
C_2F_3H	Oxygen flow (2 series)	0 - 48 sccm	600 W, 93 mT, 50 G, 40 sccm etch gas	SiO_2	20	8:1, 5, 7-9, 12		
					21	7:6-11		
	Oxygen flow (4 series)	0 - 45 sccm	600 W, 35 mT, 50 G, 15 sccm etch gas	SiO_2, Si_3N_4	22	8:16-21	24	4:24, 3:25, 8:1-5
					23	8:22-25, 7:2-5	25	10:8-10, 12, 15

5. Results and Discussion

Following the outline of the discussion in Section 4.4, this chapter will discuss the results of the experimental work carried out for this thesis. Section 5.1 will cover the designed matrix experiments, while Section 5.2 will treat the non-matrix data. The discussion will focus on trends seen in the etch and polymerization behavior of the seven gases studied as a function of pressure, gas flows, magnetic field strength, and chamber condition. In Section 5.3, Auger electron spectroscopy (AES) data from some of the wafers will be discussed. Finally, Section 5.4 will to provide a summary and attempt to draw some broader conclusions about the implications of this work.

5.1 Designed Matrix Experiments

In this section, the behavior of four gases - octafluoropropane, 1H- and 2H-heptafluoropropane, and pentafluoroethane - as a function of the three matrix variables - pressure, magnetic field, and oxygen flow rate - will be examined. Sections 2.3 and 4.2 provide a discussion of the mechanisms that these variables are believed to affect. The figures in this section will be used to supplement the discussion with relevant graphical information as appropriate; however, for a complete graphical representation of the NNAPER models of the parameter space explored in these experiments, the reader is referred to Appendix 1. The reader is reminded that the results presented in this section, while generated from experimental data, are nevertheless the output of the NNAPER software, and hence *models* of the behavior of each of the gases. All etch rates reported in this section are average etch rates across the wafer.[***]

[***] As a rule, it is recommended that raw, rather than processed, data be used for inputs to the NNAPER model. However, a comparison of an octafluoropropane model generated with raw etch rate data taken at eight locations across the wafer and one generated with average etch rate data showed that using average etch rate as a single network output did not detract from the quality of the model.

5.1.1 Octafluoropropane Results

Magnetic Field. The effect of increasing magnetic field strength[†††] with both oxide and nitride films was a pronounced increase in etch rate. This increase is consistent with the principal effect that increasing magnetic field strength is known to have - increasing plasma density - which, in turn, is believed to increase the concentrations of active etch species, principally fluorine. This increase is observed at both high and low oxygen flows and both high and low pressures (see Figures A1.2, A1.3 for oxide; A1.5, A1.6 for nitride).

Oxygen Flow. The effect of oxygen addition appears to be quite different in the case of oxide than in that of nitride. In the case of oxide, the addition of oxygen generally seems to cause a decrease in etch rate. (See Figures A1.1, A1.3.) The lack of an observed etch rate increase with the addition of oxygen suggests 1). that, in the parameter space where this effect is seen, octafluoropropane does not polymerize heavily enough to inhibit the etch process and oxygen is not needed to overcome the effects of polymer formation (as the principal benefits of adding oxygen are believed to be the suppression of polymer formation and the removal of polymer film) and/or 2). that polymerization still occurs and oxygen still plays the usual role, but other mechanisms dominate. Since, as will be discussed shortly, the interaction of oxygen flow rate and pressure effects appears to be most reasonably explained by invoking a polymerization mechanism, the author is disinclined to rule out the presence of polymerization altogether. However, since the beneficial effect of polymer suppression by oxygen does not appear to be the dominant one, one is led to believe that the decrease in etch rate can probably be attributed to dilution/decreased residence time effects that accompany higher total flows. This decrease appears to be most pronounced at low pressures and medium to high B-fields. This latter observation is consistent with the data from non-matrix Series # 1, which will be discussed in Section 5.2.1, where trifluoroethylene was found to polymerize *less* heavily at low pressures and high magnetic fields.

[†††] The term "magnetic field strength" will be used as a matter of convenience, even though technically the unit used (Gauss) is a unit of magnetic flux density. Generally speaking, in a non-ferromagnetic medium, magnetic field strength (**H**) and magnetic flux density (**B**) are related by: $\mathbf{B} = \mu_0\mathbf{H}$, where μ_0 is the permeability of free space.

An apparent exception to this behavior is seen at high B-fields and high pressures, where the model predicts a slight increase in etch rate as a function of oxygen flow (3610 Å/min to 3630 Å/min for 0-20 sccm O_2 at 100 Gauss and 150 mTorr). *Prima facie*, these results may be interpreted as suggesting that polymer formation plays a more significant role under the above conditions and that oxygen plays a more prominent role in affecting the etch rate by suppressing polymerization. However, because the magnitude of this apparent increase is so small, it seems more likely that the observed effect may be better interpreted as an insensitivity of the etch process to the presence of additional oxygen flow at these conditions.

The behavior of the octafluoropropane/silicon nitride system appears to be more straightforward. Adding oxygen increases etch rate at all B-field and pressure values, which suggests perhaps that polymer formation is taking place on nitride and that oxygen is needed for its suppression. At high values of B-field, the increase in etch rate appears to level off. (See Figures A1.4, A1.6.) It is interesting that oxygen addition in the nitride system has an effect opposite to that in the oxide system. One possible explanation for this may involve preferential deposition of polymer film on nitride, as opposed to oxide, surfaces under the same conditions. In fact, a comparison of Figures A1.1-3 with A1.4-6 indicates that oxide does generally etch faster with octafluoropropane than does nitride under the same conditions. (Two regions that appear to be exceptions to this rule have been observed at 93 mTorr, high oxygen flows and low B-fields and at 50 Gauss, high oxygen flows and low pressures.) Other workers, however, have used X-ray photoelectron spectroscopy (XPS) to observe preferential deposition on silicon dioxide as opposed to silicon nitride surfaces in remote $CF_4 + H_2/CH_4$ discharges [92][‡‡‡]. A second possible mechanism may involve an active role on the part of oxygen in removing the nitrogen from the film [93]. Despite the fact that this mechanism was postulated on the basis of work carried out with plasma deposited nitride, not LPCVD nitride, the applicability of these findings to LPCVD films may be reasonably good, for the authors claim low hydrogen content

---

‡‡‡ Evidence for the presence of this effect in this study is mixed. Subsequent non-matrix experiments indicate that, at least in a regime of *net* polymer deposition, under some conditions, the deposition rates on oxide and nitride are fairly similar (see Sections 4.4.4 and 5.2.2: Table 4.3, and Figures 5.13, 5.14), under some conditions, the oxide rate is higher (see Section 5.2.3: Figures 5.15a, b), and under other conditions, the nitride rate appears to be higher (see Sections 4.4.4 and 5.2.4: Table 4.3, and Figures 5.16a, b).

and a high degree of stoichiometry in their nitride films, characteristics which are also found in LPCVD films. Surface analysis techniques can be employed to help resolve this question. In any case, further efforts are clearly necessary if the oxygen dependencies in the oxide and nitride octafluoropropane etch processes are to be better understood.

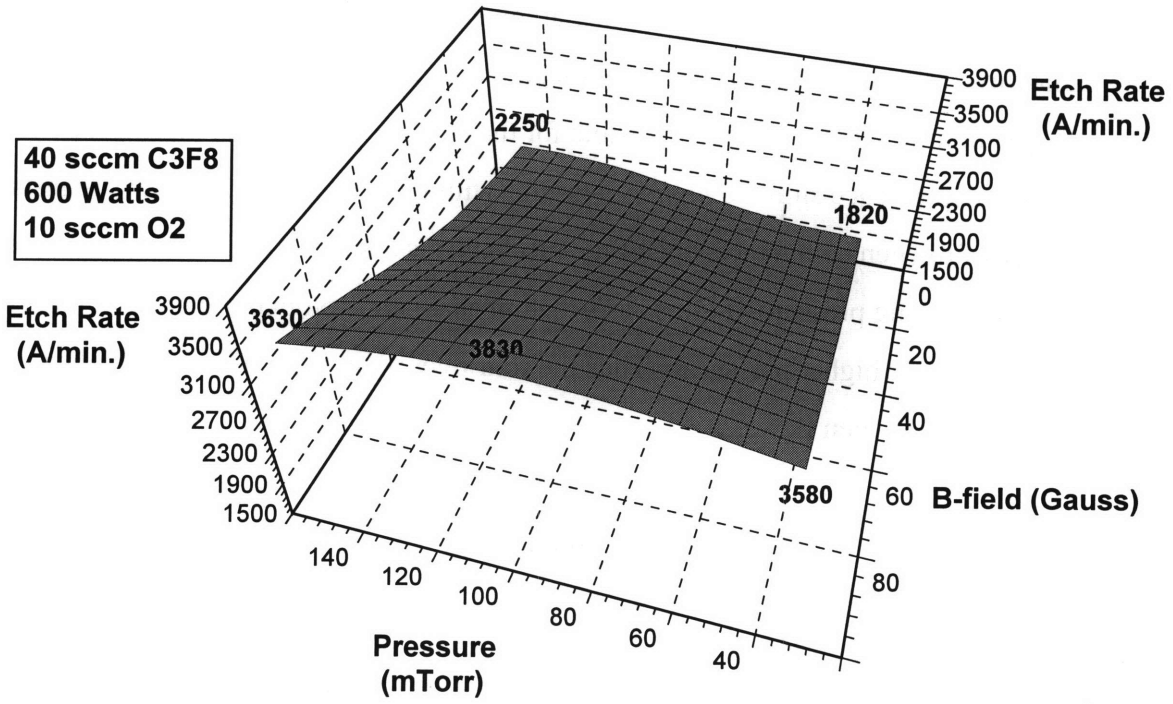

Figure 5.1

Modeled silicon dioxide etch rate in octafluoropropane at 10 sccm O_2 flow, showing the shift of the pressure fold-over point toward lower pressures with increasing magnetic field.

Pressure. The effects of pressure appear to be complex. In the oxide system, a maximum in etch rate is seen over the studied range (35-150 mTorr). The initial increase in etch rate with increasing pressure is probably attributable to increased concentrations of etchant species, whereas the observed decrease at higher pressures may be due to increased ion scattering in the sheaths, and therefore reduced ion energies (accompanied by reduced rf and dc sheath voltages), and/or an increase in polymerization, whose kinetics are believed to be of second order with pressure. The location of this fold-over point moves toward lower pressures with increasing B-field (see Figures 5.1, A1.1, A1.2) and toward higher pressures with increasing oxygen flow (see Figures 5.2, A1.1, A1.2). The fact that the onset of the negative dependence on pressure

comes at *lower* pressures with increasing magnetic field suggests that increasing the magnetic field augments a pressure effect associated with etch rate decrease. This is consistent with the observation made in Section 4.2.4 that increasing B-field lowers dc bias and rf sheath voltage. Thus, one can speculate that at higher fields the decrease in the etch component due to ion bombardment, which is also associated with higher pressures, may be augmented, which would suggest that this effect should be seen sooner (*i.e.,* at lower pressures). It should be pointed out once again, however, that the *dominant* effect of magnetic field strength increase is a *net* increase in etch rate. A similar argument appears plausible for the oxygen effect. That the onset of negative pressure dependence shifts to *higher* pressures with increasing oxygen flow suggests that the presence of oxygen counteracts one of the mechanisms associated with etch rate decrease as a function of increasing pressure. In this case, that mechanism is probably increased tendency toward polymerization at higher pressures. Thus the fold-over point is seen later (at higher pressures) with higher oxygen flows.

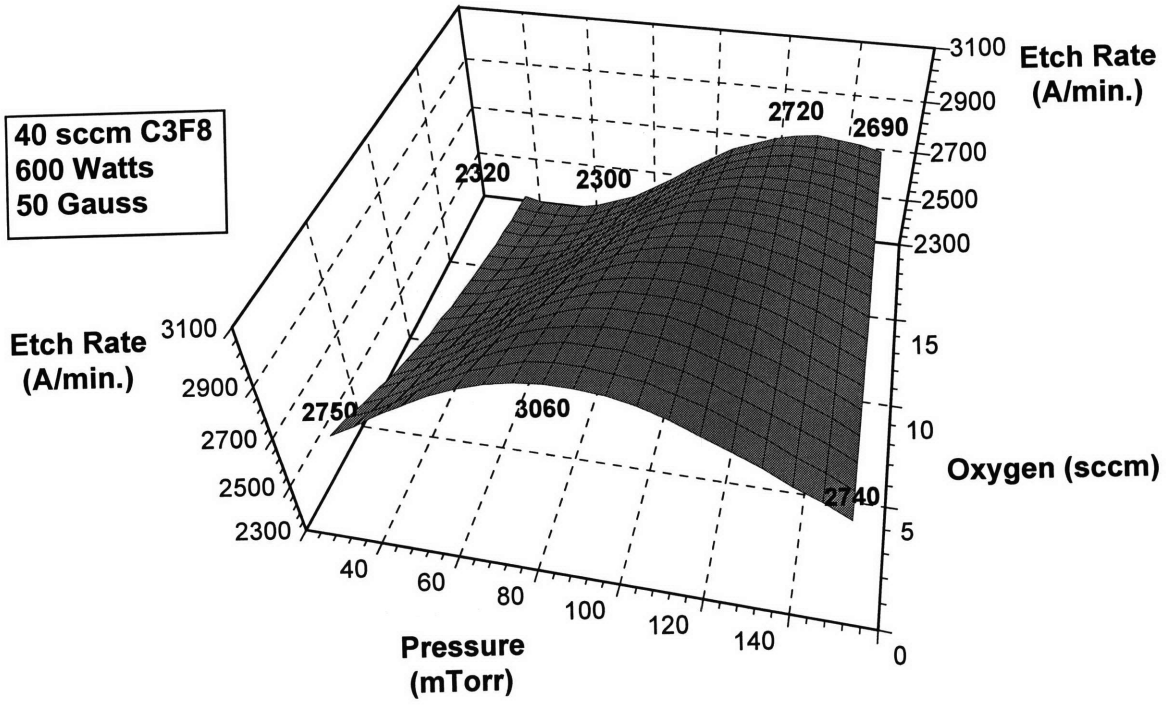

Figure 5.2

Modeled silicon dioxide etch rate in octafluoropropane at 50 Gauss. The shift of the fold-over point toward higher pressures with increasing oxygen flow is clearly visible.

The pressure dependence of the octafluoropropane/nitride system, on the other hand, is generally positive, suggesting perhaps that increased concentrations of etchant species are probably responsible for the increase in etch rate with pressure. However, at high oxygen flows and high magnetic fields, etch rate becomes nearly insensitive to pressure (see Figures A1.4, A1.5).

The maximum average oxide etch rate with octafluoropropane in the parameter space explored is given by the model to be 3900 Å/min, at 100 Gauss, approximately 80 mTorr, and 0 sccm O_2. The maximum average nitride etch rate is given to be 3220 Å/min, at 100 Gauss and 20 sccm O_2, across the pressure range of 35-150 mTorr. With the exception of the following regions: 93 mTorr, high oxygen flows/low B-fields and 50 Gauss, high oxygen flows/low pressures, oxide generally etches faster with octafluoropropane than does nitride under the same conditions. The highest measured oxide:nitride etch rate ratio (ERR) , as determined by comparing average etch rates from oxide and nitride runs at the same conditions is 2.05 at 93 mTorr, 50 Gauss, 0 sccm oxygen.

5.1.2 1H- and 2H-Heptafluoropropane Results

Magnetic Field. The behaviors of the two isomers of heptafluoropropane generally follow very similar trends. Increasing magnetic field has the expected effect of substantially increasing both oxide and nitride etch rates with both isomers. In the case of oxide, the increase with magnetic field is more pronounced at low oxygen flows, particularly with the 1H isomer. In the case of nitride, the increase actually begins to reach a plateau at high oxygen flows. (See Figures A1.8, A1.9 [2H oxide]; A1.11, A1.12 [2H nitride]; A1.14, A1.15 [1H oxide]; and A1.17, A1.18 [1H nitride].)

Oxygen Flow. The addition of oxygen has a generally positive effect in all four systems studied, suggesting that polymerization mechanisms play an important role and that oxygen is necessary to counteract the formation of the polymeric film. In the oxide case, the etch rate increases with oxygen flow under all conditions, but begins to plateau at high oxygen flows. (See Figures A1.7, A1.9 [2H]; A1.13, A1.15 [1H].) With 2H-heptafluoropropane, the model actually predicts a fold-over at high oxygen flows and a slight negative dependence (see Figures A1.7, A1.9). This may be an artifact of the model; however it is also very plausible that a fold-

over point would be seen, since at high ratios of oxygen to etch gas flow, the oxygen appears to serve mainly as a diluent (see Section 5.2.2). At any rate, since the beneficial effect of adding oxygen appears to saturate, it appears that there is a point in any given parameter region where the introduction of additional oxygen no longer aids the suppression of polymer formation and/or the liberation of additional fluorine. With both gases, the onset of the plateau is seen to move toward lower values of O_2 flow with increasing B-field and toward higher values of O_2 flow with increasing pressure. The reasons for this do not appear obvious; however, some speculative explanations may be offered here. The shift toward *higher* values of oxygen flow with pressure may perhaps be related to an increase in residence time associated with the increase in pressure, whose effects may offset those of the decrease in residence time that comes with increasing oxygen flows. The shift toward *lower* values with increasing B-field may be attributed to the emergence of a condition where oxygen is no longer necessary, or at least less necessary, to suppress polymer formation and/or liberate fluorine because the same is accomplished through the generation of larger numbers of fluorine radicals at higher B-fields.

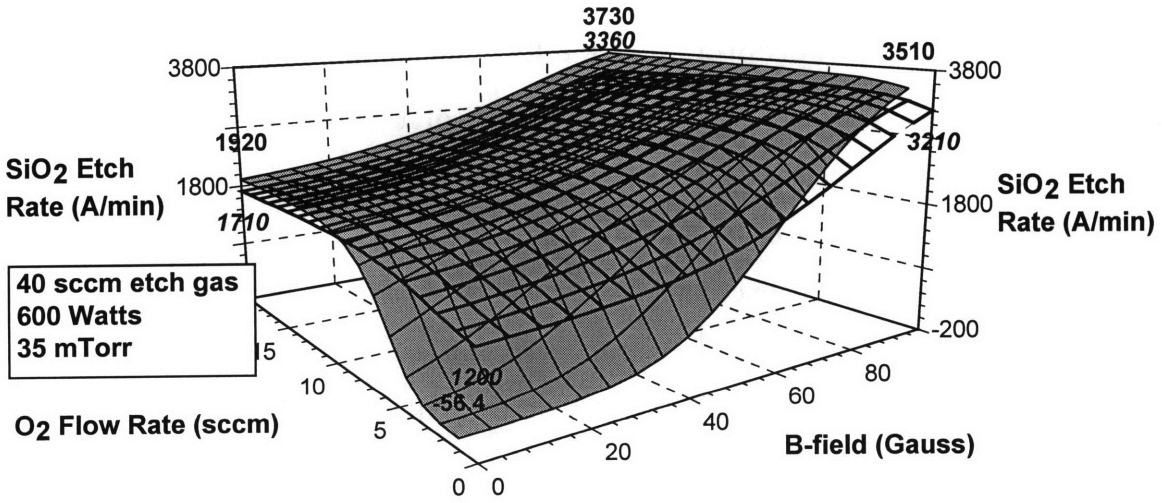

Figure 5.3

Comparison between the modeled oxide etch behaviors of 1H- (solid fill) and 2H-heptafluoropropane (no fill) at 35 mTorr, showing similar behavior except in the low oxygen flow/low B-field regime, where the 1H isomer is predicted to cause net deposition.

Most interestingly, where the oxide etch behaviors of the 1H and 2H isomers diverge is in the low magnetic field, low oxygen flow regime. In the case of 1H-heptafluoropropane, the

model predicts a net deposition regime, with deposition rates up to approximately 60 Å/min. (This value is, naturally, only a estimate, since the model is not explicitly aware of the nature of the deposited film and merely predicts "negative" etching.) In the case of the 2H isomer (CF_3-CFH-CF_3), the model predicts net etching at rates on the order of 1100-1200 Å/min. (See Figures 5.3, A1.9, A1.15.) Thus, while the two gases behave very similarly in oxygen-rich environments, in the absence of large quantities of oxygen, the 1H isomer (CF_2H-CF_2-CF_3) appears to polymerize more heavily. This suggests that the position of the hydrogen atom in the heptafluoropropane molecule can have a pronounced effect on the relative numbers of film deposition precursors, as opposed to etch species, that are formed. Interestingly enough, the presence of a higher magnetic field at the low oxygen condition seems to compensate for lack of oxygen, perhaps via the generation of large numbers of fluorine radicals relative to polymer precursors.

The effect of oxygen addition with both isomers in the case of silicon nitride is also generally positive, suggesting that oxygen plays a role in suppressing polymerization and/or liberating fluorine. As with oxide, etch rate begins to plateau at high oxygen flows in the presence of high magnetic fields. Under most conditions, oxide tends to etch faster than nitride with both gases. However, as had been shown above, at low oxygen flows and low magnetic fields with the 1H isomer, oxide etching is predicted to cease, while nitride etching is still possible, albeit at slow rates. (See Figures A1.10, A1.12 [2H]; A1.16, A1.18 [1H].)

Pressure. The pressure dependencies of the two gases appear to be ambiguous. In the 2H/oxide system, the etch rate dependence on pressure is slightly negative at low oxygen flows and low magnetic fields, visibly negative at low oxygen flows and high magnetic fields, slightly positive at high oxygen flows and low magnetic fields, and more positive at high oxygen flows and high magnetic fields. In the 1H/oxide system, the pressure dependence is generally negative at all conditions except low oxygen flows and low magnetic fields, where the predicted net deposition regime is encountered and the process appears quite insensitive to pressure. In the 2H/nitride case, the pressure dependence is negative at low oxygen flows and low magnetic fields, has a minimum at low oxygen flows and high magnetic fields, is positive at high oxygen flows and low magnetic fields, and is relatively insensitive with a slight maximum at high oxygen flows and high magnetic fields. In the 1H case, the nitride etch behavior as a function of

pressure is insensitive at low magnetic fields, is slightly negative at low oxygen flows and high magnetic fields, and is again relatively insensitive at high oxygen flows and high magnetic fields. This suggests that either the pressure behaviors are truly quite complex, or, more probably, that the etch behavior of these gases is, for the most part, relatively insensitive to pressure variation over the range of 35 to 150 mTorr. The apparent complexities may be due to experimental noise. An exception to this may be the 2H/oxide low oxygen/high B-field region, where the negative dependence is more pronounced (a difference of 850 Å/min over the range 35-150 mTorr). Otherwise, as Figures A1.7, A1.8 (2H oxide); A1.10, A1.11 (2H nitride); A1.13, A1.14 (1H oxide); and A1.16, A1.17 (1H nitride) make it apparent, etch rate variations as a function of pressure, where they do seem to occur, tend to be ~600 Å/min or smaller, often negligible.

The maximum oxide etch rates given by the model are 3730 Å/min for the 1H isomer (at 100 Gauss, 35 mTorr, and 20 sccm O_2) and 3560 Å/min for the 2H isomer (at 100 Gauss, 150 mTorr, and 10 sccm O_2). The corresponding maximum nitride etch rates are 2300 Å/min for the 1H isomer (in a plateau of the parameter space approximately defined by 94-100 Gauss, 61-150 mTorr, and 20 sccm O_2) and 2430 Å/min for the 2H isomer (at 100 Gauss, 86-118 mTorr, and 20 sccm O_2). Oxide generally etches faster than nitride with both gases, with the exception of low oxygen flow/low B-field conditions with the 1H isomer, where net deposition is predicted on oxide surfaces. The highest measured 1H oxide:nitride ERR is 3.05-3.06, measured at 60 mTorr/21 Gauss, 60 mTorr/79 gauss, 126 mTorr/21 Gauss, and 126 mTorr/79 Gauss, all at 5 sccm oxygen. With 2H, however, the highest measured ERR is 5.41 at 93 mTorr, 50 Gauss, 0 sccm oxygen.

5.1.3 Pentafluoroethane Results

Magnetic Field. Once again, the effect of increasing magnetic field strength was, predictably, a significant increase in etch rate in both the oxide and nitride systems. In the nitride system, this increase begins to level off slightly at high oxygen flows. (See Figures A1.20, A1.21 [oxide]; A1.23, A1.24 [nitride].)

Oxygen Flow. In the pentafluoroethane/oxide system, the etch rate reaches a maximum over the range of 0 to 20 sccm oxygen flow. Hence, initially a beneficial effect probably associated with the suppression of polymerization and/or fluorine liberation is occurring, but at

higher values of oxygen flow, the etch rate saturates. The subsequent decrease in etch rate is probably due to the reduced residence time/dilution effects mentioned earlier. The fold-over point moves to lower values of oxygen flow with increasing B-field, occurring around 9-10 sccm at 0 Gauss and moving to 4-6 sccm at 100 Gauss. The same explanation as that offered earlier for the heptafluoropropane gases may hold. Pressure, however, has virtually no effect on the location of the fold-over point. In the nitride case, the oxygen effect is less complex. A monotonic increase in etch rate is observed, leveling off somewhat at high values of B-field. (See Figures A1.19, A1.21 [oxide]; A1.22, A1.24 [nitride].)

Figures 5.4 and 5.5 show a cross-section of the modeled parameter space at 50 Gauss and 80 mTorr. The oxygen flow dependence of each of the gases is shown. In the case of oxide, the saturation of etch rate with increasing oxygen flow for the three hydrogen-containing gases is clearly visible.

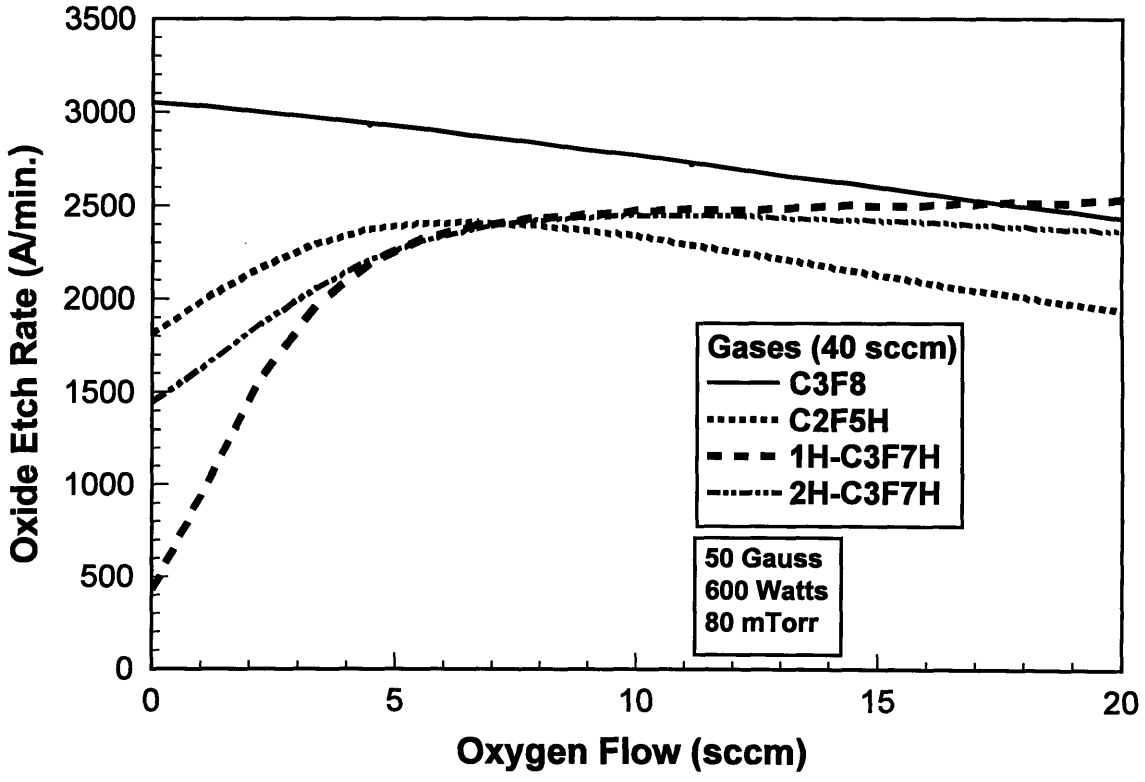

Figure 5.4

Modeled silicon dioxide etch rates as a function of oxygen flow for all four gases used in the matrix experiments.

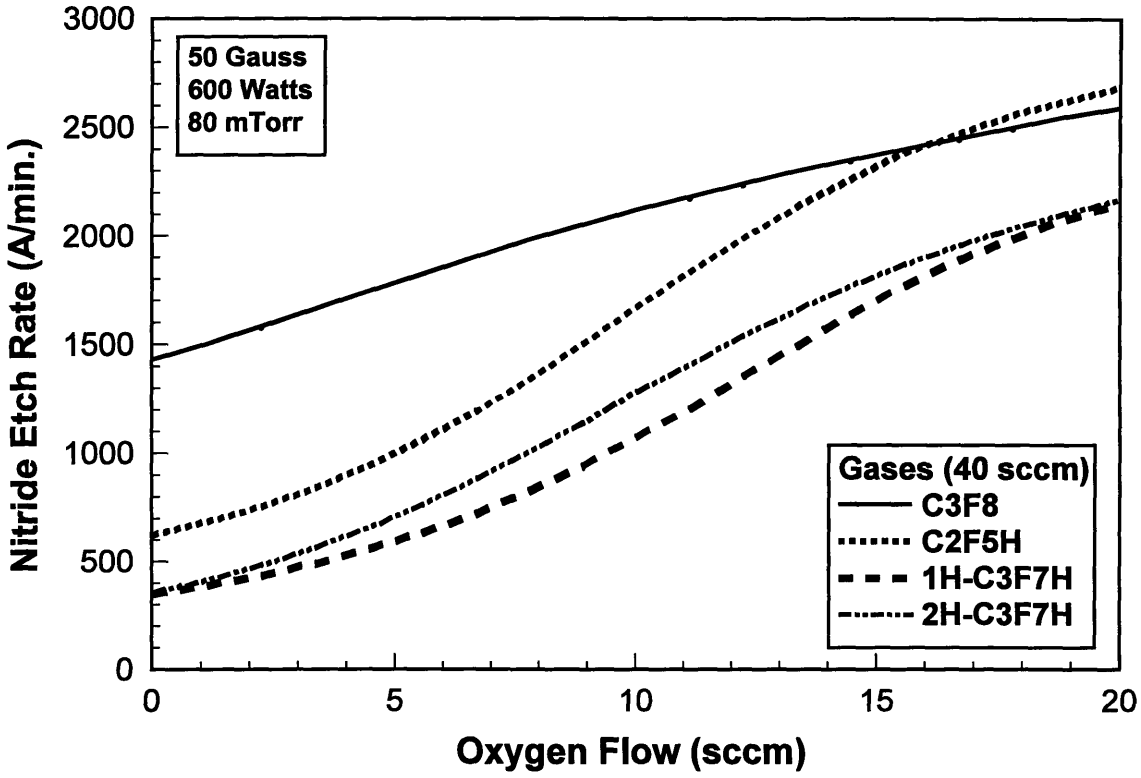

Figure 5.5

Modeled silicon nitride etch rates as a function of oxygen flow for all four gases used in the matrix experiments.

Pressure. The etch rate dependence on pressure has been observed to be either weakly positive or insensitive with both materials etched. In the oxide case, at low oxygen flows and low magnetic fields, the dependence is insensitive, becoming weakly positive with an increase in either variable. In the nitride case, the etch rate is, for all practical purposes, insensitive to pressure variation. (See Figures A1.19, A1.20 [oxide]; A1.22, A1.23 [nitride].)

The maximum average oxide etch rate given by the model is 3550 Å/min (at 100 Gauss, 150 mTorr, and 5-6 sccm O_2). The maximum nitride etch rate is 2840 Å/min (at 100 Gauss, 146-150 mTorr, 20 sccm O_2). In contrast to the other gases in the matrix study, pentafluoroethane appears to possess a large region in the parameter space studied where nitride films etch faster than oxide films. At high oxygen flows and low to medium B-fields, modeled nitride etch rates are higher than oxide etch rates for all pressures; at high oxygen flows; high B-fields, and low pressures, the rates are comparable (see Figures A1.19-24). The maximum oxide:nitride ERR (4.05) is found at the 93 mTorr, 50 gauss, 0 sccm oxygen condition, whereas the maximum

nitride:oxide ERR (1.33) is seen at a test point at 148 mTorr, 8 Gauss, and 18 sccm of oxygen, a low B-field, high oxygen condition.

5.1.4 Memory Effects

In order to observe any process drift due to change in chamber condition during the matrix experiments, center point replicates were incorporated into the matrix (see Sections 4.4.3, 4.4.4). Runs 1, 2, 3, 11, 17, and 23 in the 24 run matrix were center point runs. Figure 5.6 shows the variation in average etch rate for each gas as a function of run number. As will be discussed later, the principal factor thought to contribute to a change in chamber condition is the deposition of fluoropolymer on chamber surfaces. In the case of octafluoropropane, the two heptafluoropropane isomers, and pentafluoroethane, however, no significant memory effects due to a presumed change in chamber condition are observed, suggesting that these gases do not deposit significant amounts of polymeric residue in the chamber under the conditions studied. As Figure 5.6 also shows, at the center point of the matrix, oxide etch rates all fall in a relatively narrow range for the four gases, whereas nitride etch rates are all markedly lower and vary more considerably from gas to gas.

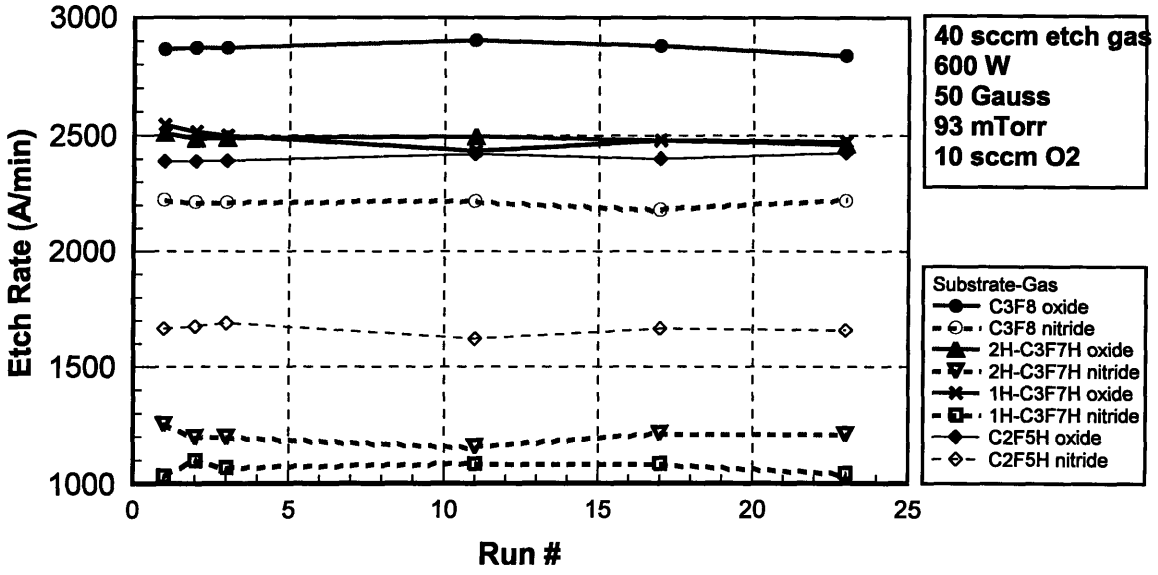

Figure 5.6

Etch rate variation at the center point of the matrix as a function of run number.

5.2 Non-Matrix Experiments

This section reports the results of the experimental series described in Section 4.4.4 and listed in Table 4.4. These tests were conducted to evaluate those HFC gases - trifluoroethylene, 1,1,1,2-tetrafluoroethane, and difluoromethane - which were found to polymerize at the center point of the matrix heavily enough to cause net deposition. For purpose of comparison, the remaining four gases were also tested under the same conditions. OEI was used to measure etch/deposition rate. Nanospec® was used to verify the OEI results. In general, the two methods had excellent correlation. However, in a few cases (where the process was on the borderline between etch and deposition regimes) OEI data was of insufficient quality to be useful, generally because the periodicity of the interferometric signal was too long to be measured within the window of the etch run. In these cases, Nanospec® data was used. In runs where net deposition was observed, the index of refraction used to calculate the thickness of the film was 1.35, that of bulk polytetrafluoroethylene, $(CF_2)_n$ (Teflon®), Section 5.3 discusses AES (Auger electron spectroscopy) data taken from several wafers used in the experiments discussed in this chapter. Qualitative analysis of residue films on wafer surfaces from runs with a "polymerizing" as well as a "non-polymerizing" gas shows that the composition of the residue appears to be primarily carbon and fluorine. While this does not demonstrate that the polymer layer is necessarily $(CF_2)_n$, or even $(CF_x)_n$, it does indicate that the assumption of a $(CF_x)_n$ composition is reasonable. One should point out that it is also possible that, with the HFC gases, the composition of the polymer film could be $(CF_xH_y)_n$, since hydrogen is present in the discharge. Workers [94] have, in fact, cited studies where gases such as CF_4, + H_2, CF_3H, and C_2F_6 + H_2 have produced CF_xH_y polymer films, where x = 0.03 to 0.34 and y = 0.73 to 1.55, depending on the gas.

5.2.1 Trifluoroethylene Polymerization Study (Non-Matrix Series # 1a-d)

In order to locate a suitable process regime in which the etch behavior of the polymerizing gases listed above could be observed, it was necessary to carry out several sets of trials to determine the effects of various process variables on polymer deposition rate, with the intent of identifying a set of conditions which would tend to promote net etching rather than polymerization. Trifluoroethylene with oxide substrates was employed for this study. In Series # 1a (see Figure 5.7a), pressure was varied over the range explored in the matrix experiments,

with the remaining variables (etch gas flow, oxygen flow, rf power, and B-field) held at their center point values. In Series # 1b, 1c, the same was done with magnetic field and oxygen flow, respectively (see Figures 5.7b, 5.7c). Rf power was not varied, but trifluoroethylene flow rate was - in Series # 1d (see Figure 5.7d). Here oxygen flow and magnetic field were held at their center point values, but, for reasons given in the discussion below, pressure was lowered to 35 mTorr. Series # 1a-c were performed after the chamber was subjected to an oxygen clean (900s, 200 mTorr, 700 W, 0 Gauss, 80 sccm O_2, 5 sccm CF_4), then a 10 min (net deposition) seasoning step using trifluoroethylene at the matrix center point conditions with a blank Si wafer. Series # 1d was performed at the conclusion of Series # 1a-c, after another oxygen clean and another 10 minute seasoning step, both same as before. It was observed that, as Figures 5.7a-d indicate, polymerization tends to be suppressed at lower pressures, lower etch gas flow rates, higher B-fields, and higher oxygen flows. All the trends observed were very pronounced and monotonic.

The effect of oxygen in suppressing polymer formation has been well established in literature (see Section 2.3.2). Oxygen is believed to attack the polymer layer, thus helping expose the underlying film to the etchant species (fluorine), as well as making more fluorine available to etch the silicon-based film by liberating fluorine incorporated in the fluoropolymer and preventing the fluorine present near the surface from being consumed in the etching of the polymer layer. (Some authors also discuss gas-phase mechanisms by which oxygen is thought to interact with CF_x species to liberate more fluorine [30, 41, 46].) At any rate, there is good evidence in literature that, when added in appropriate quantities, oxygen acts to increase concentrations of atomic fluorine [46], a principal mechanism for this in discharges such as those in this study being the interaction with the polymer layer. Nevertheless, as the matrix experiments have shown, oxygen addition can have pronouncedly different effects on the process, depending on the etch gas used and the film being etched. Oxygen flow rate was therefore chosen as the variable of interest for subsequent tests.

The effect of magnetic field on polymer formation has not been extensively studied in literature. It is well known, however, that increasing magnetic field in a system such as the Precision 5000 has the effect of substantially increasing plasma density. This translates to higher etch rates mainly due to higher fluxes of etchant species (*i.e.,* fluorine) produced by more frequent dissociation events in the discharge. It is believed that polymer formation in

fluorocarbon plasmas is caused by the adsorption of unsaturated species, such as certain CF_x fragments, which are thought to be polymer precursors [41, 45, 46]. It may be the case that as plasma density increases, electron impact collisions dissociate more of the fluorocarbon etch gas, as well as perhaps the unsaturated species, resulting in an increase in fluorine concentrations, which leads to etching of the polymer layer, and partially offsets the deposition mechanism. In practical applications on the Precision 5000, the magnetic field strength is often determined by the level of non-uniformity across the wafer that can be tolerated, and thus large values of B-field are typically not used. For this reason, it was decided that the magnetic field be fixed at an intermediate value (50 Gauss) for subsequent experiments, despite the observation that higher values appear to suppress deposition.

The observed increase in polymer deposition with increasing pressure may be consistent with the explanation that, while etch rate tends to have a first order dependence on pressure (due to greater concentrations of etchant species at higher pressures), polymer formation kinetics may have a second-order dependence, suggested by mechanisms such as [30]:

$$CF_2 + CF_2 (+ M) \rightarrow C_2F_4 (+ M),$$

where the reaction rate is $r = kN_{CF2}^2 (\propto P^2)$. Thus at higher pressures, deposition mechanisms may dominate if large concentrations of fragments such as CF_2 are present. Once the process is in that regime, increasing pressure will likely result in an increase in deposition rate. Moreover, at higher pressures, ion bombardment, which aids in film removal and offsets deposition, occurs with lower energies because sheath voltages are lower and because there is more frequent ion scattering in the sheaths [30, 65]. A pressure setting of 35 mTorr - the lowest that could be reliably maintained by the Precision 5000 etch chamber across a variety of conditions - was chosen for the tests to follow. This setting was also used for the trifluoroethylene flow rate experiments.

It is interesting that reducing the trifluoroethylene flow rate from 40 sccm to 10 sccm reduced the deposition rate, then moved the process into a net etching regime. The etch rate continued to increase with lower flow rate over the range of flows studied. One possible explanation for this observed behavior may involve the residence time of the species in the system. It may be the case that, in the regime in which this data was collected, at lower flows (and hence higher residence times [70]), the fluorocarbon feed gas is more completely

dissociated, resulting in larger concentrations of atomic fluorine relative to CF_x polymer precursors and related species. More detailed studies are needed, however, to verify this. A flow rate setting of 15 sccm was chosen for later tests.

All the above trends are consistent with the mechanisms that have been postulated in Sections 2.3.2, 4.2.2, 4.2.3, and 4.2.4, as well as with the effects that have been observed in the earlier matrix experiments. In summary, the conditions chosen for subsequent runs, in which oxygen flow was varied, were: 600 W, 50 Gauss, 35 mTorr, and 15 sccm etch gas flow rate. At low flow rates of trifluoroethylene, net etching of SiO_2 was observed with a maximum etch rate of 1886 Å/min at 10 sccm of the etch gas, 35 mTorr, 50 Gauss, and 10 sccm oxygen flow. Fluorocarbon deposition rates as high as 3279 Å/min were observed with trifluoroethylene in the Series # 1 tests for the 0 sccm oxygen flow condition at 93 mTorr, 50 Gauss, and 40 sccm etch gas flow.

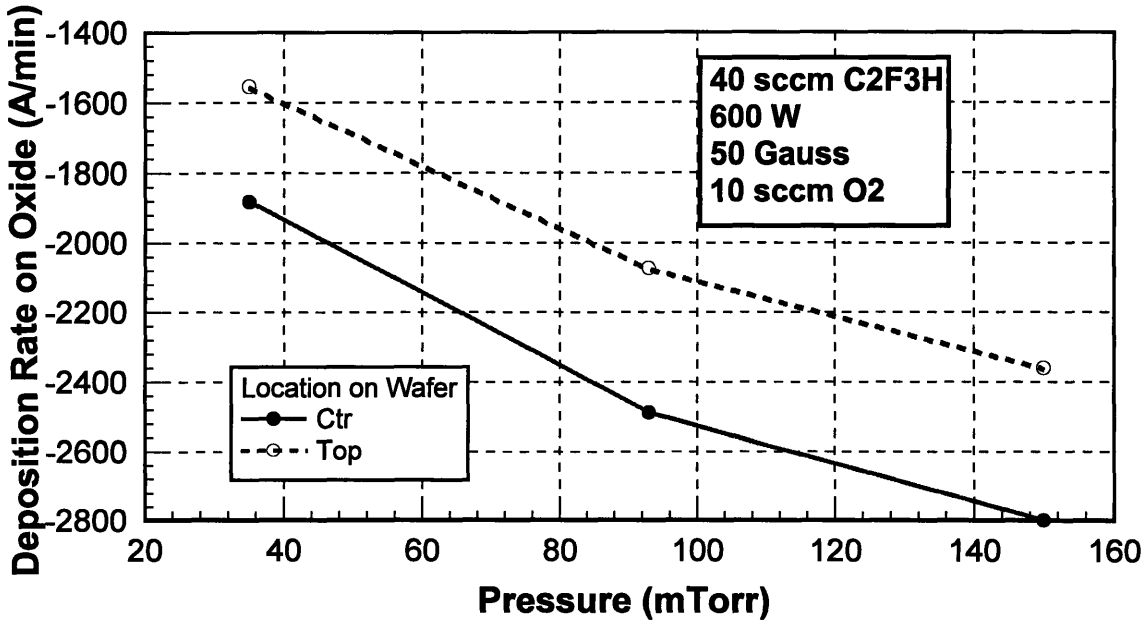

Figure 5.7a

Series # 1a: Effect of pressure on the deposition of polymer on SiO_2 with trifluoroethylene as the process gas. Rates at center and edge (top) locations on the wafer are shown. (The "top" location corresponds to the location of the wafer flat.)

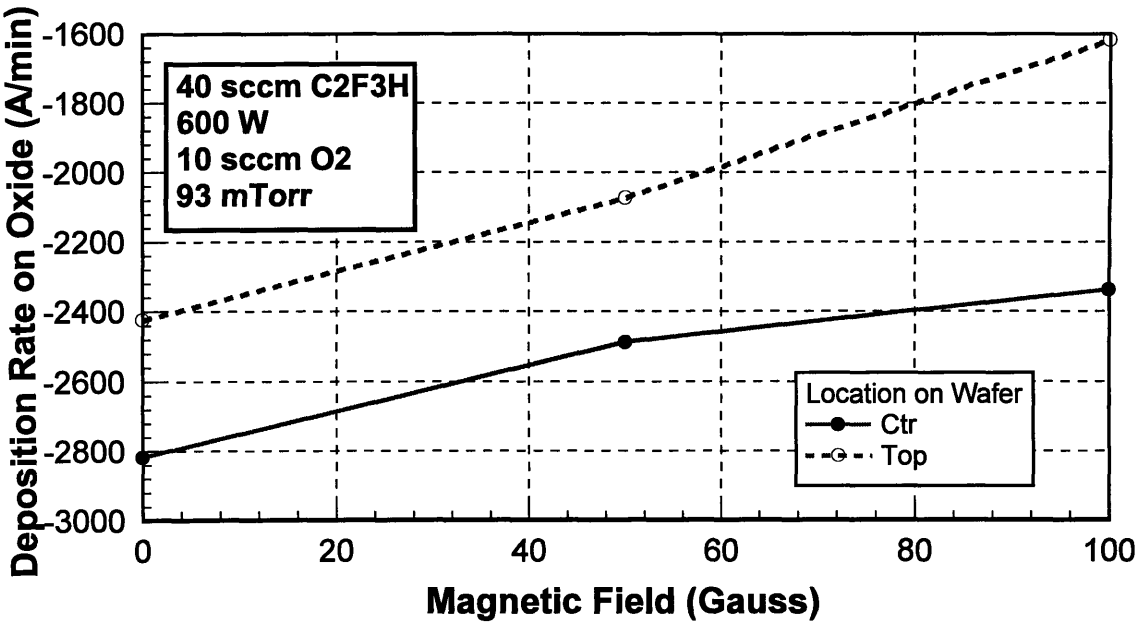

Figure 5.7b

Series # 1b: Effect of magnetic field on the deposition of polymer on SiO_2 with trifluoroethylene as the process gas. Rates at center and edge (top) locations on the wafer are shown.

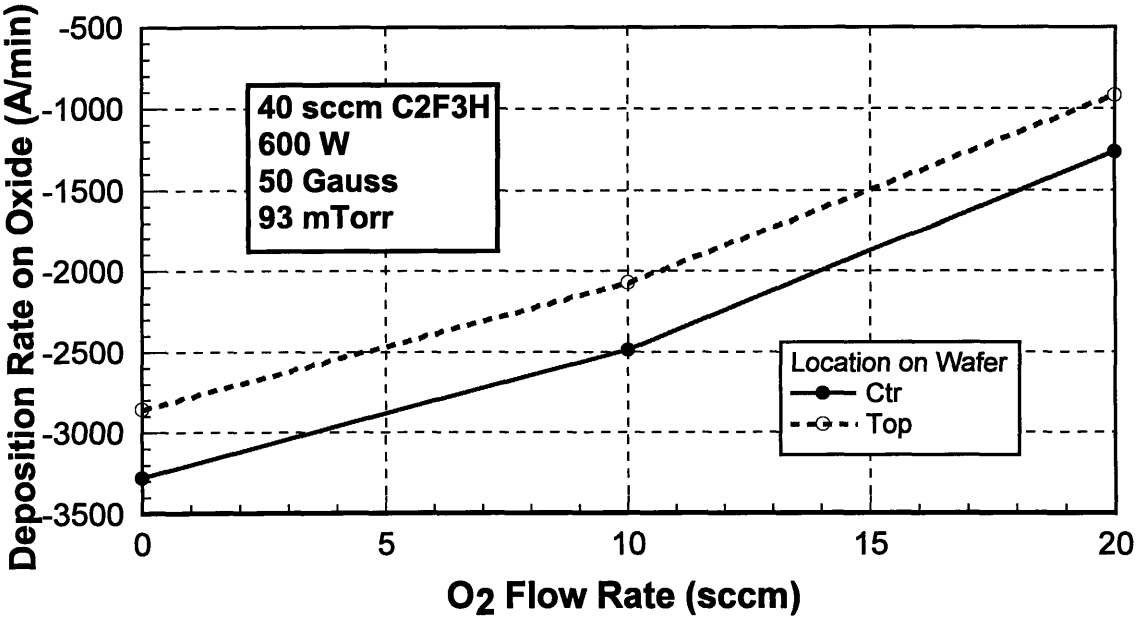

Figure 5.7c

Series # 1c: Effect of oxygen flow on the deposition of polymer on SiO_2 with trifluoroethylene as the process gas. Rates at center and edge (top) locations on the wafer are shown.

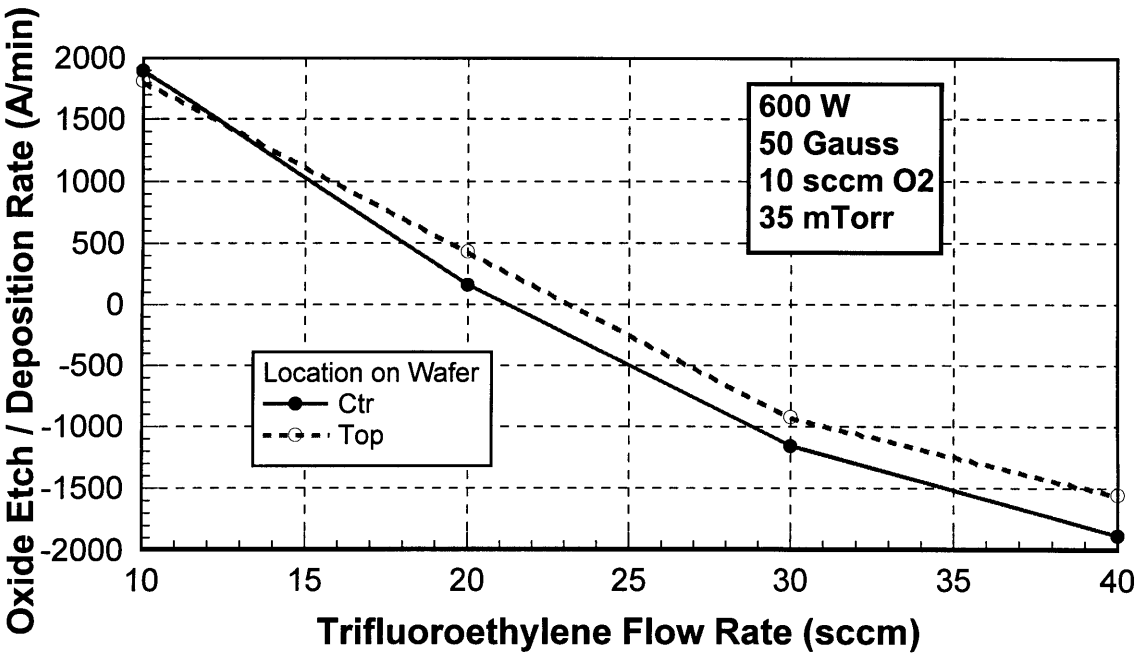

Figure 5.7d

Series # 1d: Effect of trifluoroethylene flow rate on etch rate/polymer deposition rate on SiO_2. Rates at center and edge (top) locations on the wafer are shown

5.2.2 Oxygen Flow Rate Study (Non-Matrix Series # 2-15)

The oxygen flow rate study consisted of 14 experimental series, one for each gas with each of the two types of substrates. Process conditions for this regime (the "low flow/low pressure" or "suppressed polymerization" regime) were chosen on the basis of the results of the previous series. Oxygen flow was varied from 0 to 45 sccm (a 3:1 oxygen : etch gas ratio), with rf power at 600 W, pressure at 35 mTorr, B-field at 50 Gauss, and etch gas flow at 15 sccm. An oxygen clean (900s or more, 200 mTorr, 700 W, 0 Gauss, 60 or 80 sccm O_2, 5 sccm CF_4), but no seasoning step, was carried out before each set of runs with a new gas/substrate combination. In all series, the runs were ordered from high oxygen flow to low oxygen flow. See Section 5.2.5 for the rationale behind this methodology.

It was observed that the etch rate of nitride in octafluoropropane, pentafluoroethane, and both isomers of heptafluoropropane increases markedly with the addition of oxygen, then drops off at higher oxygen flows. The initial increase is explainable by the role oxygen is believed to play in the mechanism cited above, namely the suppression of polymer formation and liberation of fluorine. The decrease at higher etch rates is most likely due to dilution of the fluorine

concentration and/or a transition into a pumping speed limited regime, where at high flows (and hence short residence times) etchant species are exhausted before they can react [71]. The oxide etch rates, on the other hand, exhibit only a monotonic decrease with increased oxygen flow for all four gases. The maximum oxide etch rate obtained is ~2600 Å/min (with C_3F_8), while the maximum observed nitride etch rate is ~2200 Å/min (with C_2F_5H). At 0 sccm oxygen, the oxide:nitride etch rate ratio is highest for all four gases - 3.0 for C_3F_8, 3.5 for 1H- and 2H-C_3F_7H, and 2.2 for C_2F_5H. Between 5 and 10 sccm of oxygen, however, these four gases transition into a regime where nitride etches faster than oxide. See Figures 5.8-11.

The behavior of octafluoropropane appears to be consistent with what was observed in the matrix study. Figures 5.4 and 5.5 show typical octafluoropropane etch behavior in the matrix space: at 40 sccm etch gas flow and 80 mTorr, oxide etch rate in octafluoropropane decreases monotonically with the addition of oxygen over the range of oxygen flows studied (from 0 to 20 sccm), while the nitride etch rate increases monotonically with oxygen over the same range.

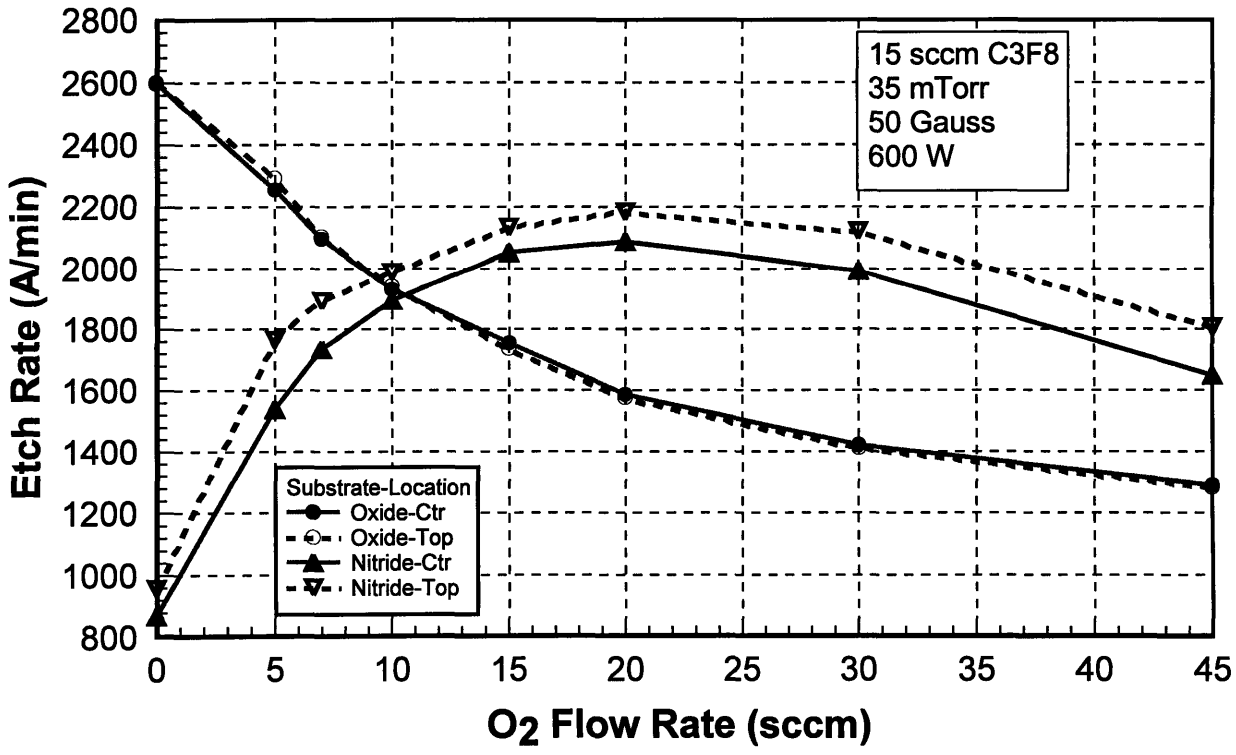

Figure 5.8

Series # 2 & 9: Oxide and nitride etch rate in octafluoropropane in the low flow/low pressure regime.

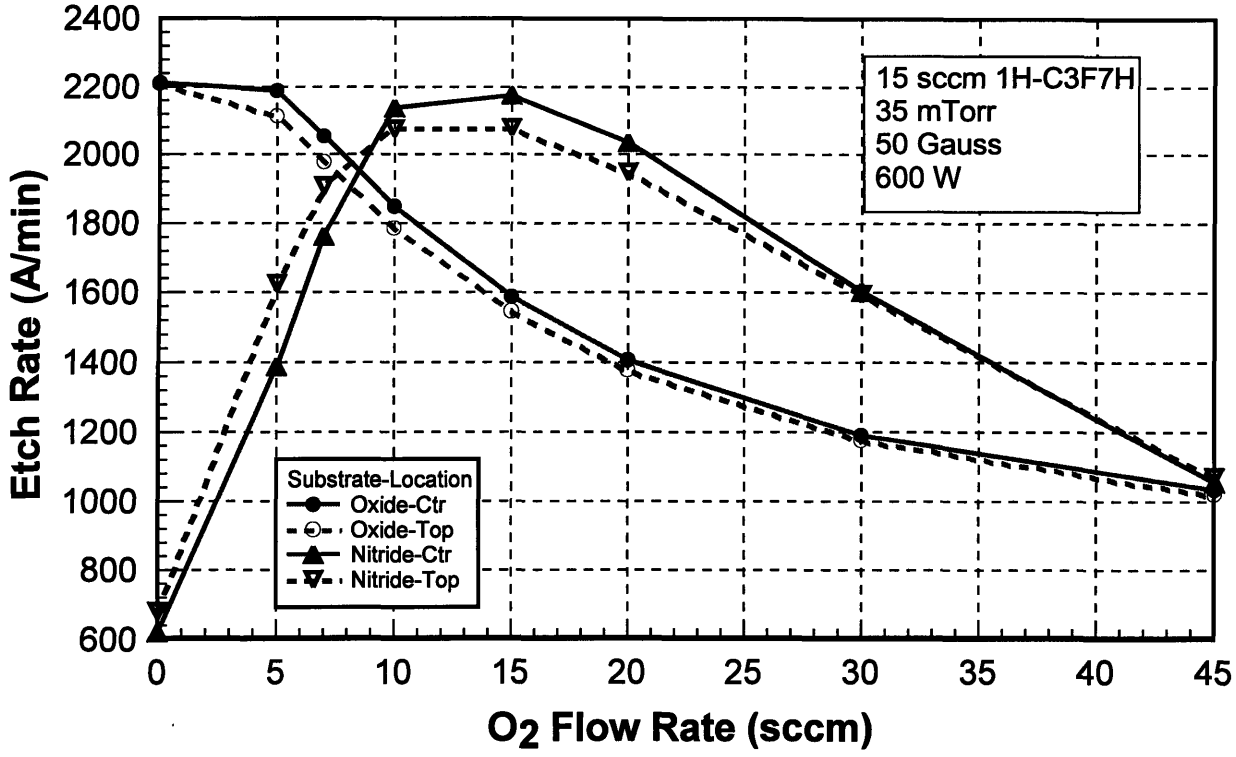

Figure 5.9

Series # 3 & 10: Oxide and nitride etch rate in 1H-heptafluoropropane in the low flow/low pressure regime.

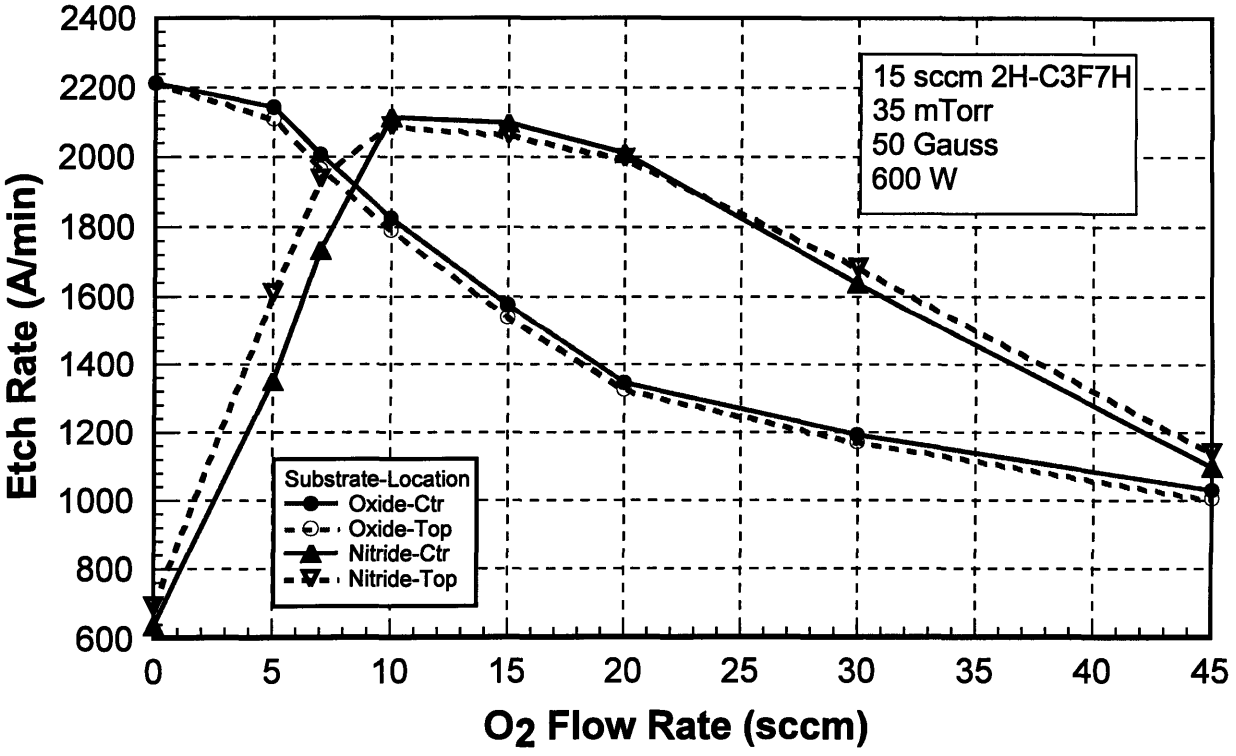

Figure 5.10

Series # 4 & 11: Oxide and nitride etch rate in 2H-heptafluoropropane in the low flow/low pressure regime.

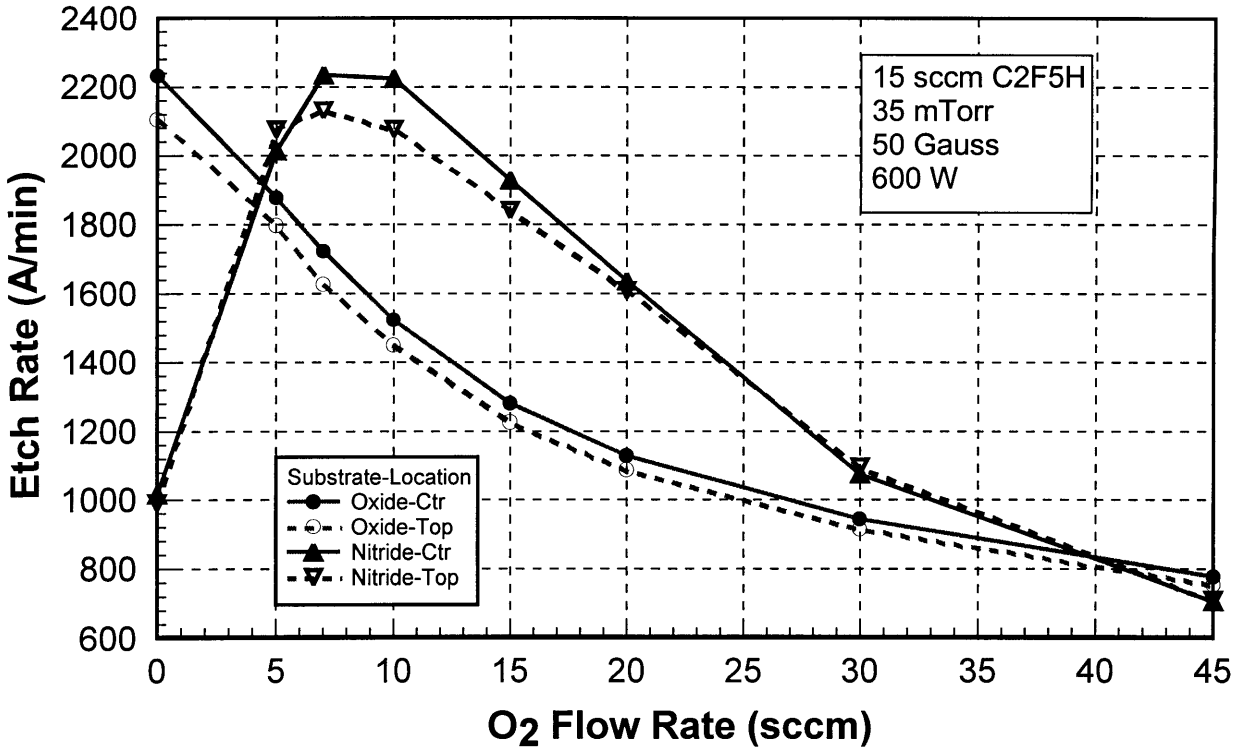

Figure 5.11

Series # 5 & 12: Oxide and nitride etch rate in pentafluoroethane in the low flow/low pressure regime.

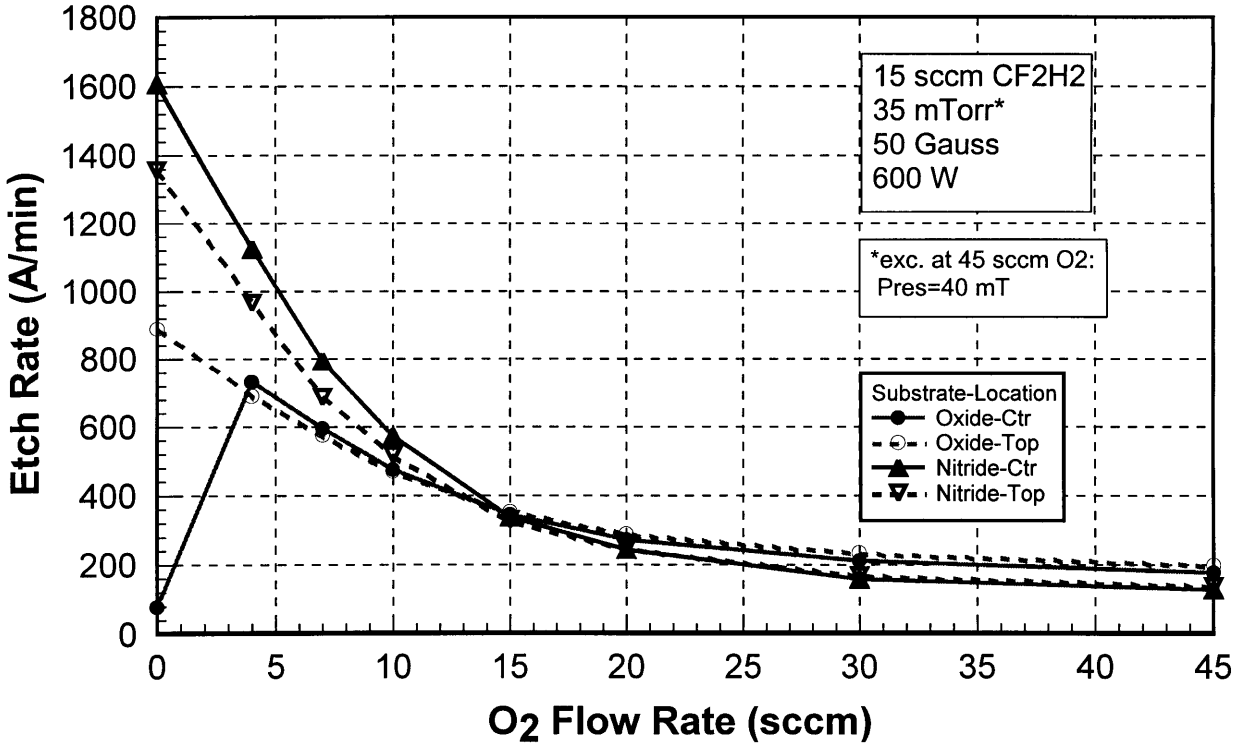

Figure 5.12

Series # 6 & 13: Oxide and nitride etch rate in difluoromethane in the low flow/low pressure regime.

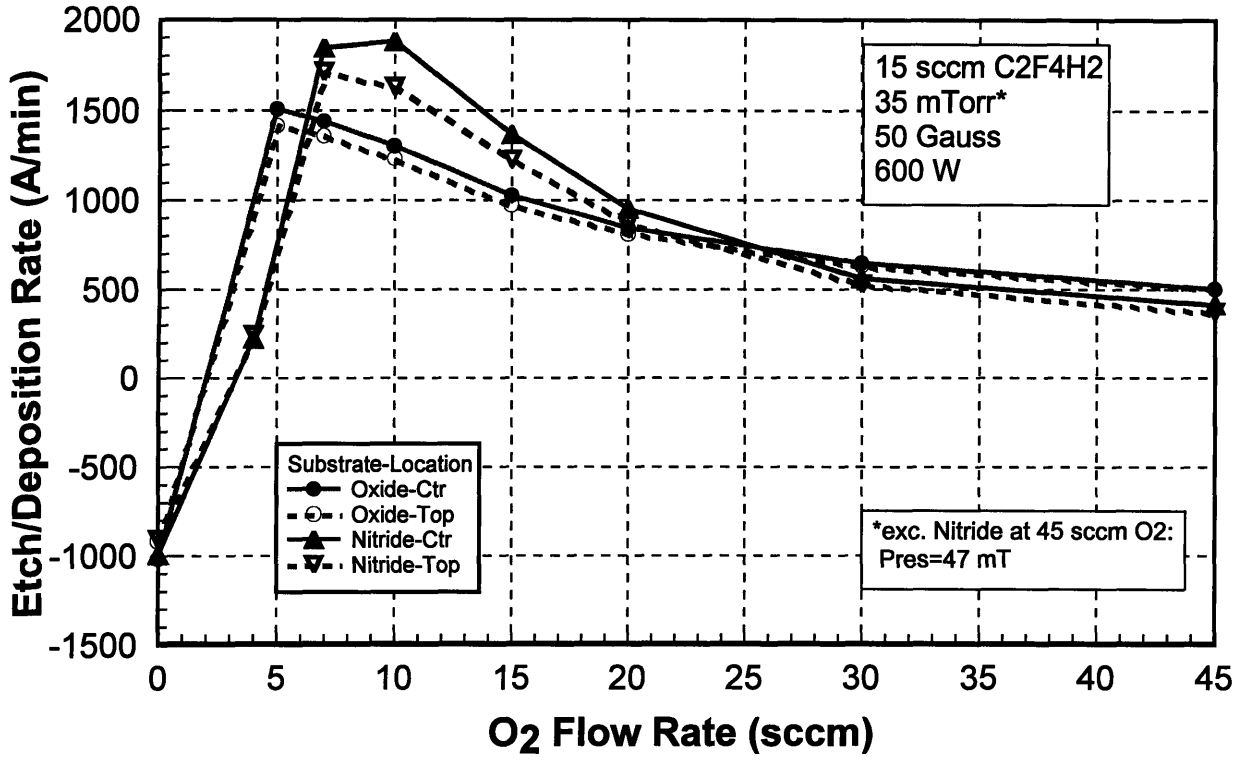

Figure 5.13

Series # 7 & 14: Oxide and nitride etch/dep rate in 1,1,1,2-tetrafluoromethane in the low flow/low pressure regime.

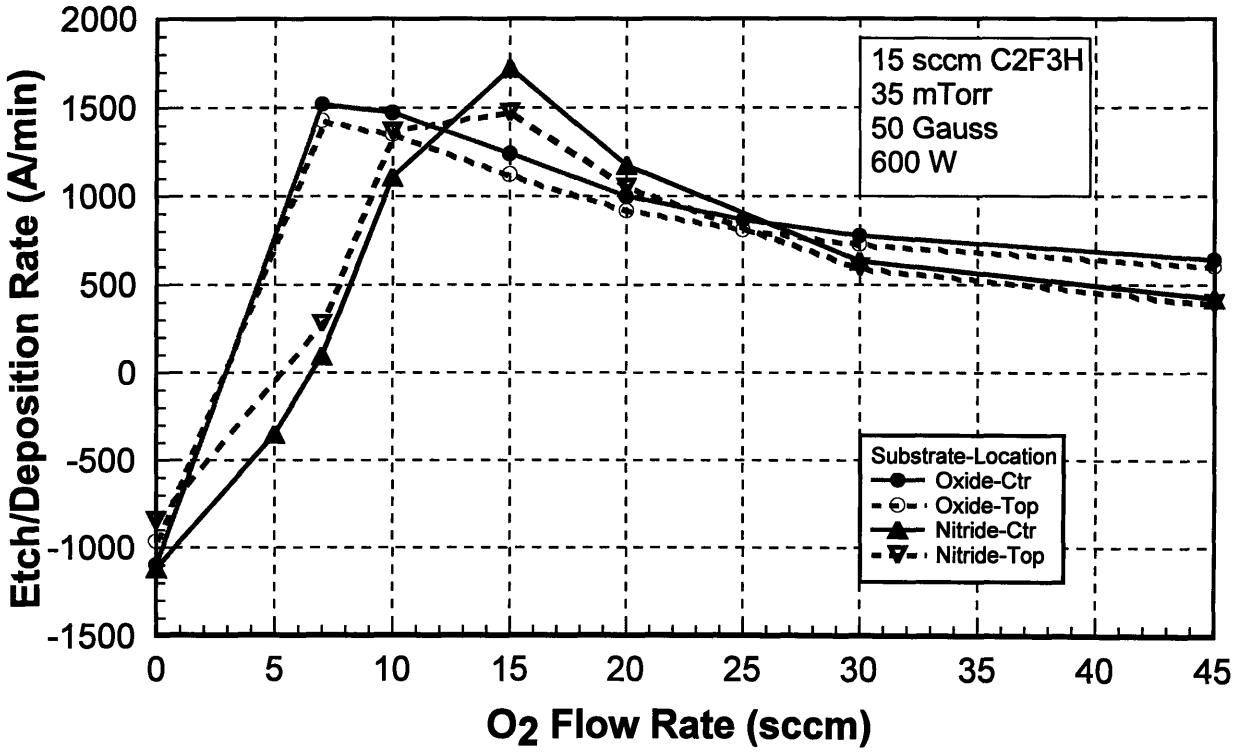

Figure 5.14

Series # 8 & 15: Oxide and nitride etch/dep rate in trifluoroethylene in the low flow/low pressure regime.

As Figure 5.5 indicates, the nitride etch rates of pentafluoroethane and 1H- and 2H-heptafluoropropane at 40 sccm and 80 mTorr increase monotonically with oxygen in the range of oxygen flows studied, which is consistent with the effect seen here. Interestingly enough, however, the oxide etch behavior of these three gases in the present study is in sharp contrast with the earlier results, for at 40 sccm and 80 mTorr, these gases did indeed show a pronounced increase in oxide etch rate with the initial addition to oxygen (see Figure 5.4). This effect was then followed by a leveling-off or decrease in etch rate at higher oxygen flows (oxygen flows were in the range from 0 to 20 sccm).

A tentative explanation for why the addition of oxygen fails to have a beneficial effect for the etching of oxide in these three gases in the 15 sccm, 35 mTorr regime may be tied to the assumption that polymerization kinetics are suppressed in this regime to the point that addition of oxygen is not necessary. This view is consistent with the observation that, in the suppressed polymerization regime, the measured etch rates of all three gases at 0 sccm oxygen (2212 Å/min for both isomers of C_3F_7H, 2232 Å/min for C_2F_5H) are considerably higher than those predicted by the neural network for the 0 sccm condition at 40 sccm, 80 mTorr (435 Å/min for 1H-C_3F_7H, 1450 Å/min for 2H-C_3F_7H, 1820 Å/min for C_2F_5H). It is also interesting that the oxide etch rates for the two isomers of C_3F_7H differ considerably at low oxygen flows in the high flow/high pressure regime, whereas their behavior in the low flow/low pressure regime is practically identical (see Figures 5.9, 5.10). This suggests that, as polymerization kinetics begin to dominate, the molecular structure of the precursor and the pathways by which it dissociates become more important. In any case, a more thorough study of these effects is needed before definitive explanations can be offered.

Of the remaining gases studied - difluoromethane, 1,1,1,2-tetrafluoroethane, and trifluoroethylene - the latter two were found to have predictable behavior in these tests. Without oxygen, $C_2F_4H_2$ and C_2F_3H deposit a polymer film on both oxide and nitride at a rate of approximately 1000 Å/min. Deposition rates on oxide and nitride are roughly the same. Interestingly, while the etch rate profile across the wafer varies widely in runs where net etching is observed (in both matrix and non-matrix experiments), the profile in net deposition runs is invariably "dome-shaped," with the fastest deposition in the center of the wafer. The addition of a few sccm of oxygen moves these gases into a net etch regime. The measured etch rates for

both types of films reach maxima (of 1509 to 1879 Å/min at the center of the wafer) between 5 and 15 sccm, then decrease with higher oxygen flows. See Figures 5.13 and 5.14.

Difluoromethane, on the other hand, does not appear to enter the net deposition regime at all at 15 sccm etch gas flow and 35 mTorr. In the case of nitride, addition of oxygen has no beneficial effect. In the oxide case, etch rate at the edge of the wafer (see Figure 5.12) tracks the trend of the nitride curve, though reaching a maximum of only 889 Å/min at 0 sccm, vs. 1358 Å/min for nitride. In the center of the oxide wafer, however, etching all but ceases at 0 sccm oxygen (Nanospec® measurement indicates a net etch rate of 78 Å/min). The OEI data for this run shows rapid change in film thickness at the beginning of the run, followed by a relatively flat signal, instead of a periodic signal of constant amplitude (seen during a typical etch process) or a decaying periodic signal (seen during a typical deposition process[§§§]). This may indicate that a brief period of etching initially took place, but the etching was then blocked by the competing deposition process. The extreme non-uniformity across the wafer on this run may be the result of depletion of etchant over the center of the wafer

[§§§] The signal decay appears to result from the coating of the chamber viewport on which the camera is mounted with polymer deposit.

5.2.3 Etch Gas Flow Rate Study (Non-Matrix Series # 16, 17)

A two-level study was carried out to evaluate the effect of process gas flow rate on etching and polymer deposition with the three "polymerizing" gases (difluoromethane, 1,1,1,2-tetrafluoroethane, and trifluoroethylene). Etch gas flow rate was varied from 15 sccm to 40 sccm, with power held at 600 W, magnetic field held at 50 Gauss, oxygen flow held at 10 sccm, and pressure held at 35 mTorr. Figures 5.15a and 5.15b show the results for oxide and nitride films, respectively. For comparison purposes, runs were also carried out with the four "non-polymerizing" gases (octafluoropropane, the two heptafluoropropane isomers, and pentafluoroethane) at 15 sccm. The 40 sccm etch gas flow data for these gases was taken from the matrix series.

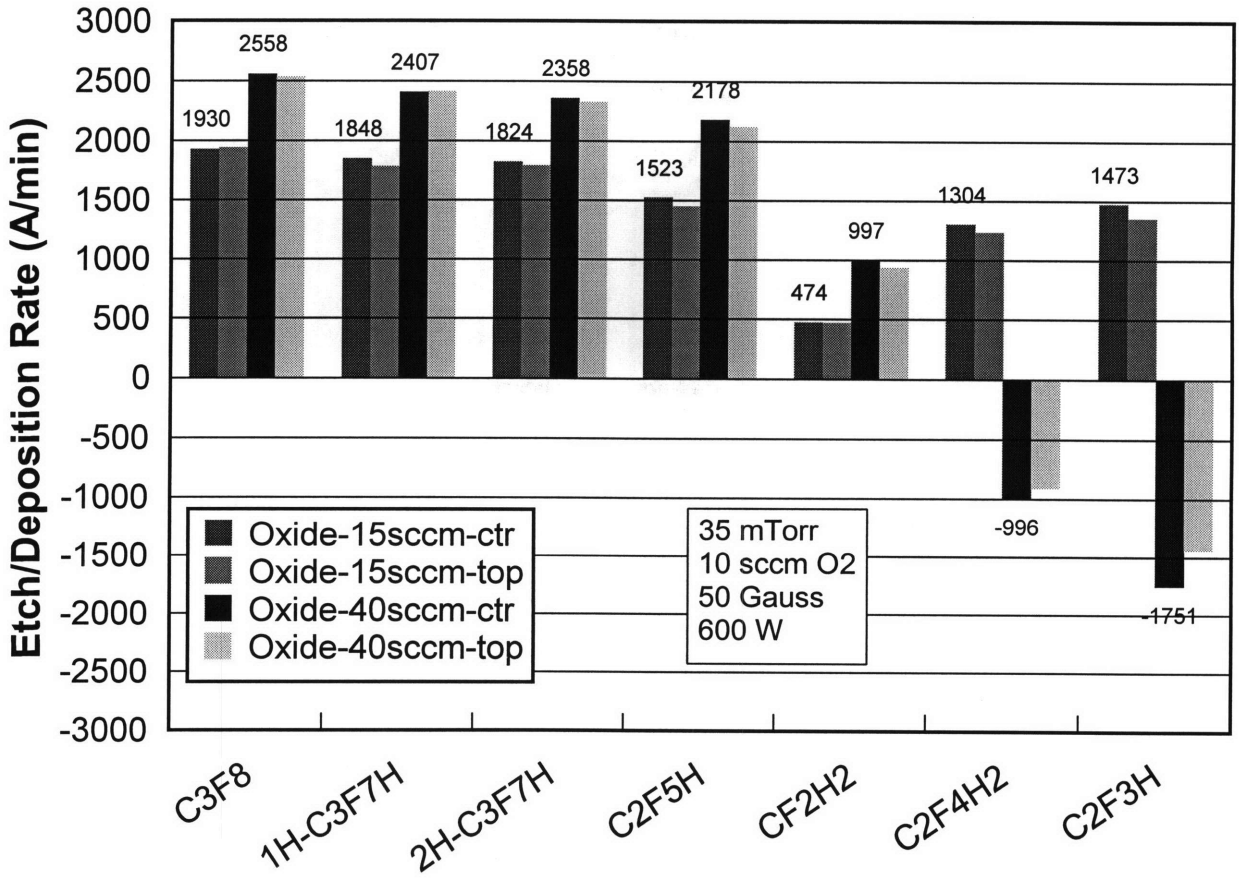

Figure 5.15a

Series # 16: The effect of etch gas flow rate on oxide etch/dep rate.

In the case of the four non-polymerizing gases, decreasing etch gas flow from 40 sccm (matrix star point recipe) to 15 sccm lowers the oxide etch rate but increases the nitride etch rate. One explanation for this suggests that the oxide process is in the etchant generation rate limited flow regime, where increasing etch gas flow still increases etchant species concentrations at the wafer surface, whereas the nitride process finds itself already in the pumping rate limited flow regime, where additional etchant that is generated is pumped out before it can react (see Section 4.2.3 and Figure 4.2).

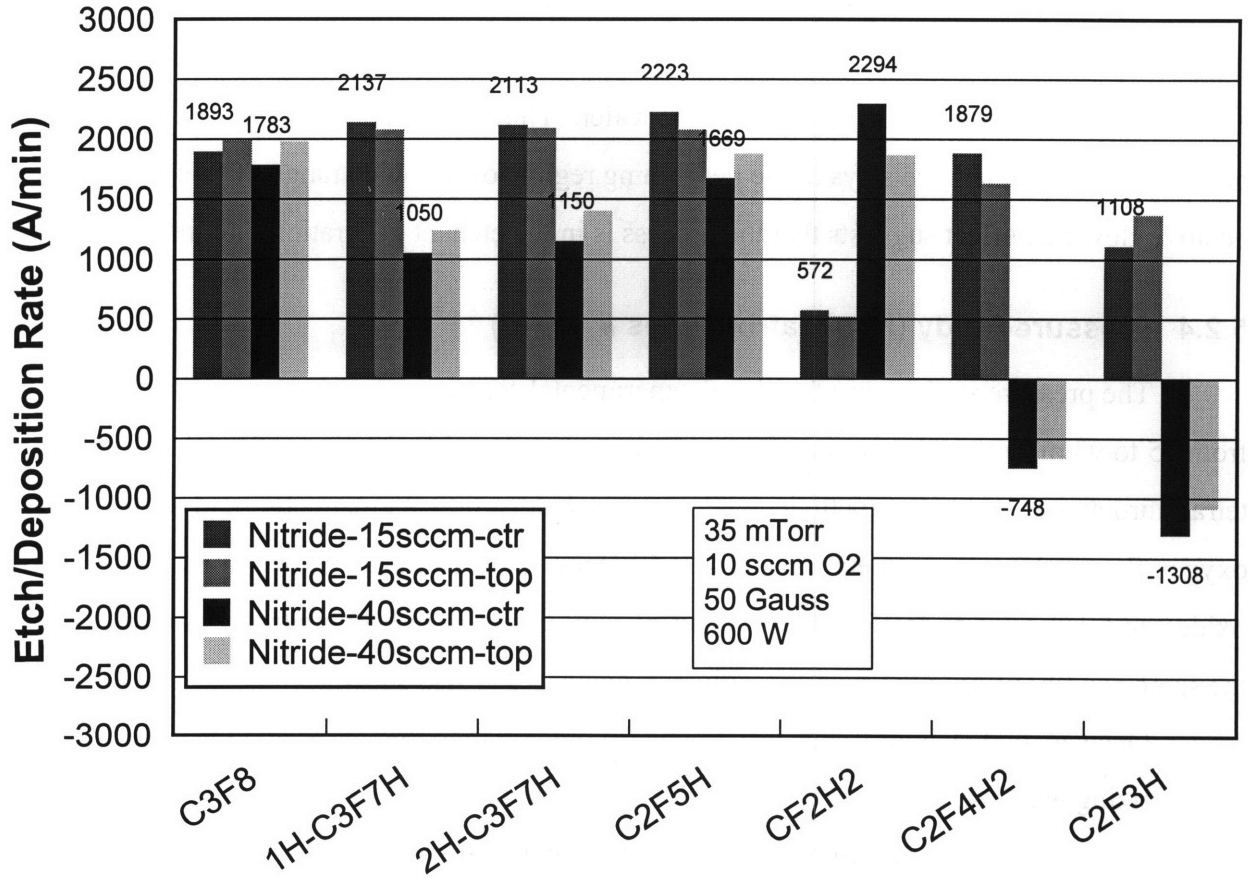

Figure 5.15b

Series # 17: The effect of etch gas flow rate on nitride etch/dep rate.

In the case of tetrafluoroethane and trifluoroethylene, lowering the etch gas flow from 40 sccm to 15 sccm moves both gases from a net deposition regime into a net etch regime. This effect is consistent with what was observed earlier in the trifluoroethylene study (Series # 1d, see

Figure 5.7d). If the same explanation, which invokes relative amounts of etch species versus polymer deposition precursors at each flow condition (see Section 5.2.1), is correct, it will be applicable here as well. For both gases, the deposition rate on oxide appeared to be higher than on nitride.

As was the case in the oxygen flow rate study, difluoromethane behavior does not appear to follow the trends set by either group of gases. Difluoromethane appears to etch both oxide and nitride substrates at both 15 sccm and 40 sccm, with increases in etch gas flow causing increases in etch rate in both cases. The increase seen in the nitride case is much more pronounced. Interestingly, difluoromethane appears to have the lowest observed nitride etch rate of the seven gases (572 Å/min at the center of the wafer) at 15 sccm, but the highest observed etch rate (2294 Å/min) at 40 sccm, at least in the center of the wafer. Thus it would appear that, at low pressures, difluoromethane stays in the net etching regime over a wide range of flows. The positive flow rate effect suggests that the process is in the etchant generation rate limited regime.

5.2.4 Pressure Study (Non-Matrix Series # 18, 19)

The pressure study was a two-level experimental series in which pressure was varied from 35 to 93 mTorr to observe its effect on polymerization with difluoromethane, 1,1,1,2-tetrafluoroethane, and trifluoroethylene. Power was held at 600 W, magnetic field at 50 Gauss, oxygen flow at 10 sccm, and etch gas flow at 40 sccm. The results are shown in Figure 5.16a for oxide and 5.16b for nitride. For the purposes of comparison, data from matrix runs carried out at the same conditions with the four non-polymerizing gases is also shown.

Once again, behavior trends differ between the polymerizing gases and the non-polymerizing gases, as well as between oxide and nitride films. For the gases in the etch regime, it can be seen that, in the case of oxide, the reduction in pressure from 93 to 35 mTorr causes a reduction in etch rate; in the case of nitride, however, the effects of pressure vary from gas to gas. (See individual explanations for each of the gases in Section 5.1.) However, for the gases in the deposition regime, the effect of decreasing pressure is a decrease in polymer deposition rate, which is consistent with the behavior seen in the trifluoroethylene study (Series # 1a, see Figure 5.7a). In the case of difluoromethane, no nitride data exists for the 93 mTorr (*i.e.,* matrix center point) process condition, because of the instability of the process in this regime that was noted

earlier. However, since, as was mentioned earlier, polymerization is known to occur with this gas at the 93 mTorr condition, the effect of decreasing pressure in this case is to move the process from a deposition regime to a net etch regime. Interestingly, while the difluoromethane oxide etch rate at the 35 mTorr condition is slow, the 2294 Å/min nitride etch rate (at the center of the wafer) is the fastest observed, faster even then the corresponding octafluoropropane nitride etch rate. Generally speaking, it appears that in the deposition regime fluoropolymer deposition rates on nitride surfaces appear to be somewhat higher than the corresponding deposition rates on oxide surfaces.

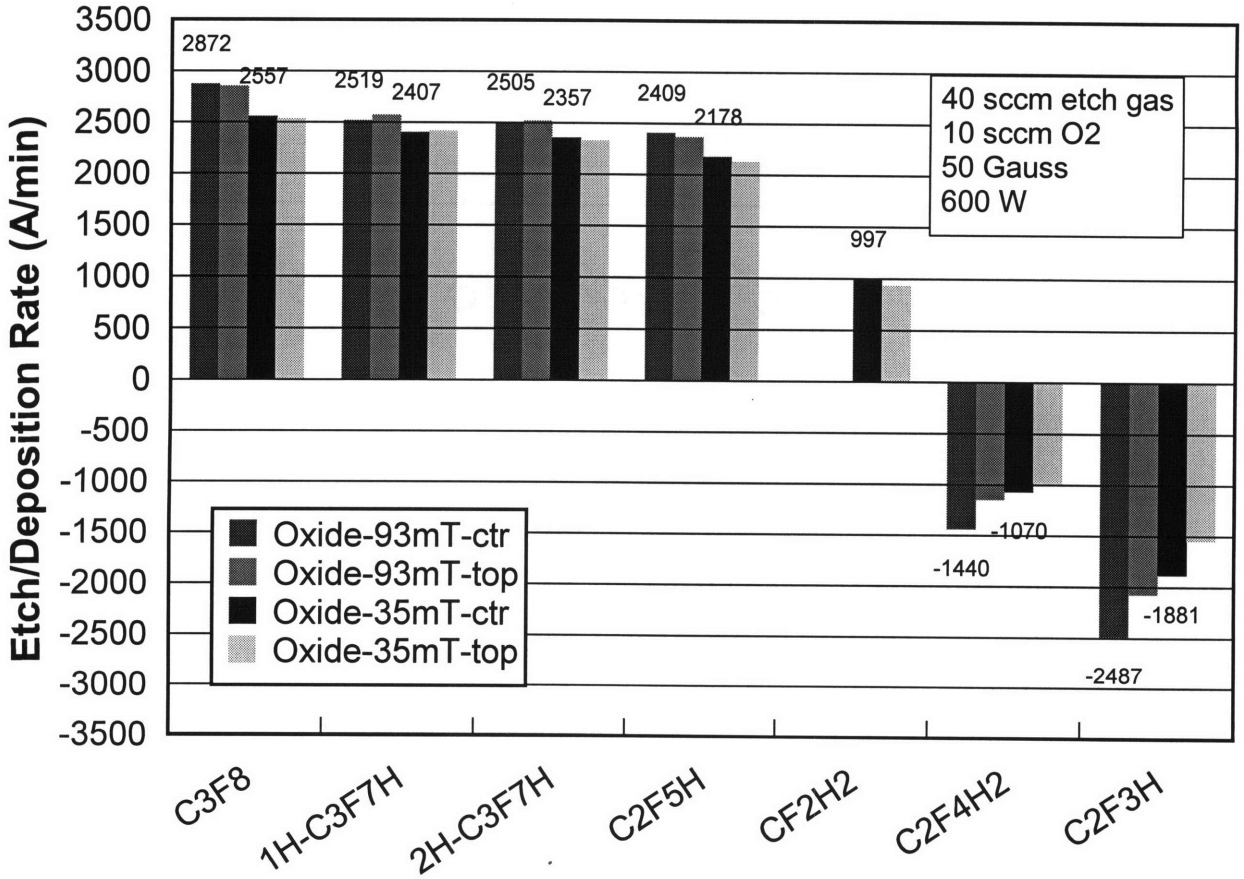

Figure 5.16a

Series # 18: The effect of pressure on oxide etch/dep rate.

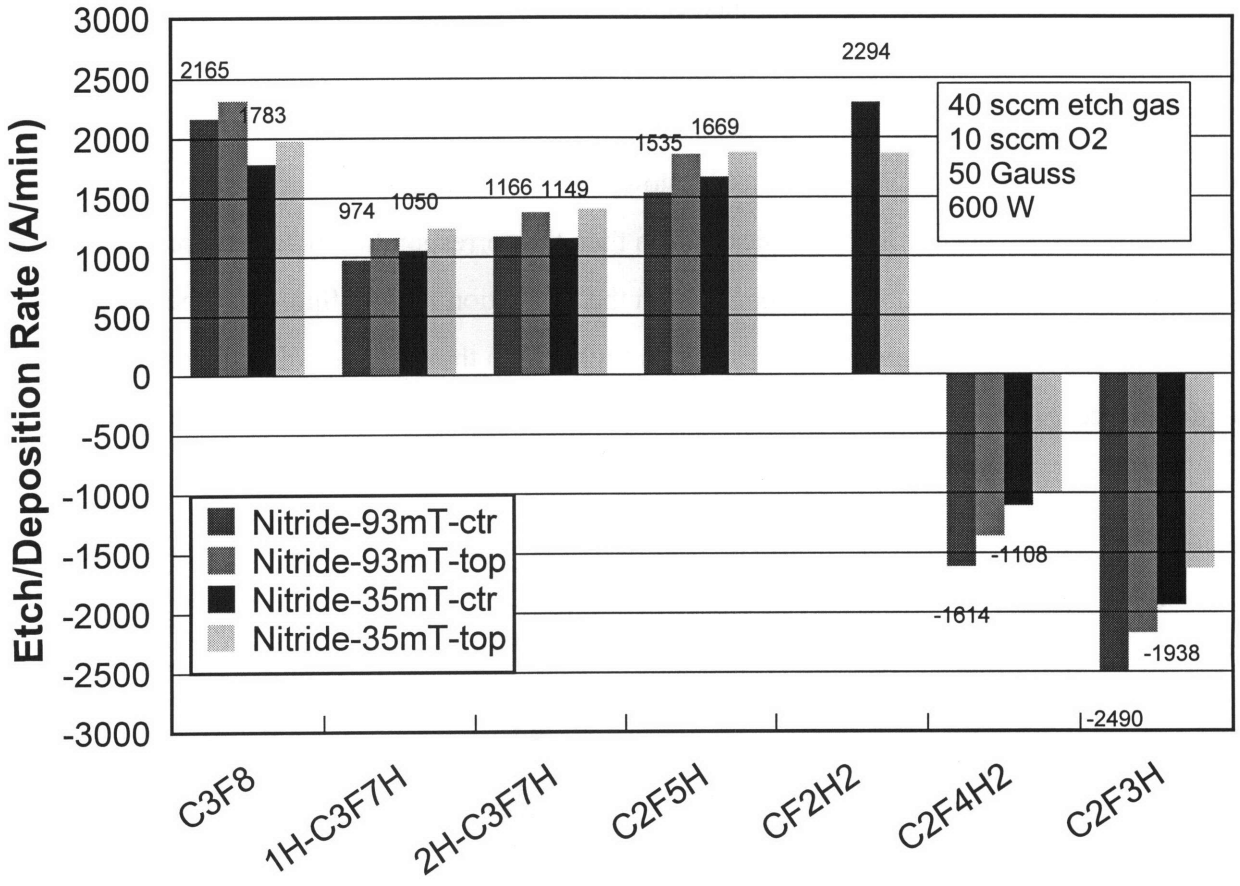

Figure 5.16b

Series # 19: The effect of pressure on nitride etch/dep rate.

5.2.5 Memory Effects in Oxygen Flow Rate Studies (Non-Matrix Series # 20-25)

Three sets of data documenting memory effects, *i.e.,* a change in the process as a function of the chamber's history, have been collected using trifluoroethylene as the process gas. The first set consists of Series # 20, 21, which were taken at 93 mTorr, 40 sccm etch gas flow, 50 Gauss, and 600 W. In Series # 20, the runs were performed in the following order: 10 sccm O_2, 0 sccm, 20 sccm, 30 sccm, 40 sccm, 48 sccm, with other trifluoroethylene runs intervening (some of these runs were also part of Series # 1). The series was run after the chamber had been subjected to an O_2 clean (900s, 200 mTorr, 700 W, 0 Gauss, 80 sccm O_2, 5 sccm CF_4), followed, in turn, by a seasoning step which resulted in net deposition (trifluoroethylene matrix center point recipe, 10 min, blank Si wafer). In Series # 21, the runs were performed in the following order: 48 sccm O_2, 40 sccm, 30 sccm, 20 sccm, 10 sccm, 0 sccm, with no other runs intervening. The series was

run after the chamber had been used for trifluoroethylene runs, followed by a seasoning step which did *not* result in net deposition (the 48 sccm O_2 recipe, 10 min, blank Si wafer). As Figure 5.17a shows, no significant memory effects appear in those runs where net deposition occurred (0, 10, 20 sccm O_2), whereas significant etch rate variation can be seen for the data points in the net etch regime - for instance, up to a 30% drop-off in etch rate at the edge of the wafer (25% at the center) from the first series to the second for the 48 sccm O_2 condition.

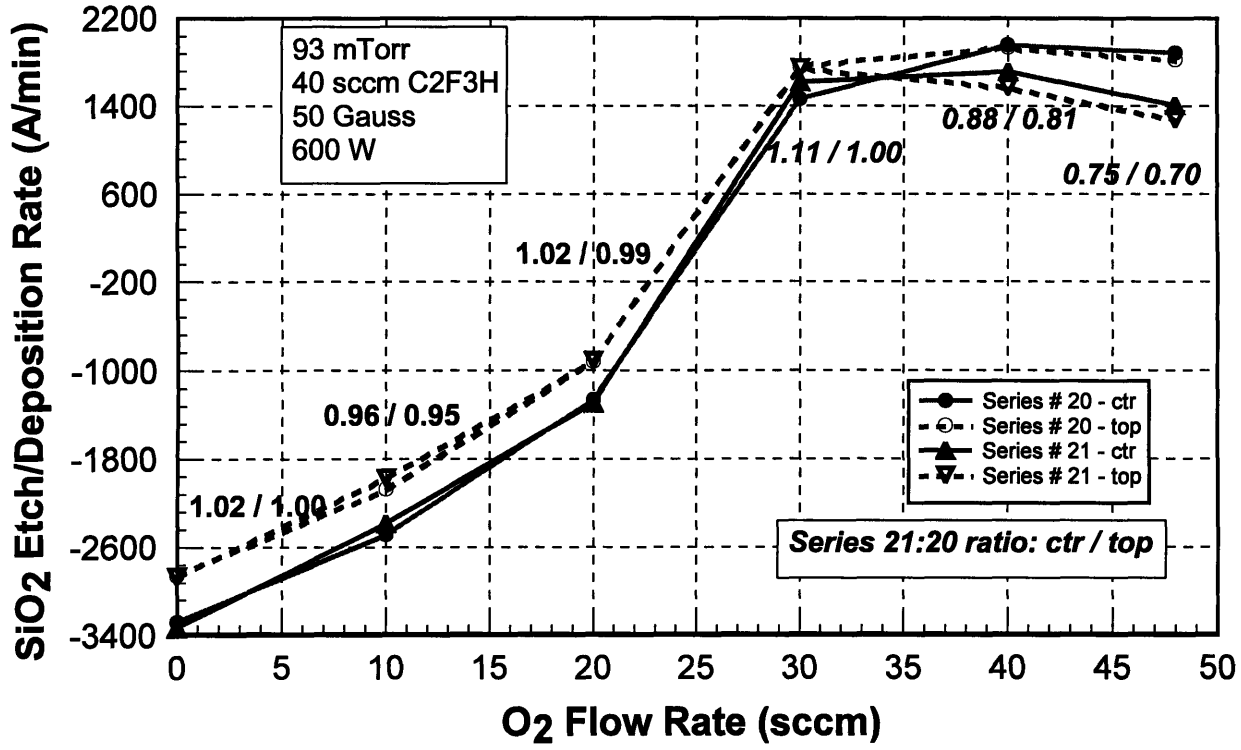

Figure 5.17a

Series # 20, 21: Memory effects with trifluoroethylene: Series # 20 was carried out "low-to-high" (0 to 48 sccm O_2), except for the 10 sccm point, which was run first; Series # 21 was carried out "high-to-low" (48 to 0 sccm O_2). Italicized labels indicate a change of 10% or more.

The explanation for this phenomenon appears to be simple. In the first series (# 20), runs which caused heavy net deposition of fluoropolymer were performed first. They were then followed by runs where higher oxygen content moved the process into a net etch regime. Thus the high oxygen etch runs were being performed in a chamber where the walls were "pre-coated" with polymer residue. The author believes that fluorine was liberated from the fluoropolymer

layer on the chamber surfaces principally by the oxygen in the plasma, which increased the effective concentrations of etchant species from levels that would otherwise be present in a clean chamber. In effect then, the high oxygen runs were performing a chamber clean during the etch process. The increased fluorine concentrations are likely to account for the increase in etch rate over identical data points run in a clean chamber. This hypothesis is borne out by the results from Series # 21. Here the 10 minute 48 sccm O_2 seasoning recipe probably served the role of an oxygen clean (because of the high oxygen flows involved). The high oxygen content, net etch runs that followed were then being performed in a presumably clean chamber and did not benefit from the added fluorine concentrations that were the product of chamber surface deposits. Interestingly, results from runs that yielded net deposition in both series are quite repeatable (see again Figure 5.17a), indicating that the deposition process is relatively insensitive to the condition of the chamber.

Two other sets of data documenting memory effects have been collected, both of which used a trifluoroethylene oxygen flow rate study series as a reference. An oxide set (Series # 22, 23) and a nitride set (Series # 24, 25) were collected. Series # 23 consists of the same runs as Series # 8, while Series # 25 consists of a portion of the runs in Series # 15 (see Figure 5.14). All runs in these series were taken at 35 mTorr, 15 sccm etch gas flow, 50 Gauss, and 600 W. In Series # 22, the runs were performed in the following order: 0 sccm O_2, 10 sccm, 20 sccm, 30 sccm, 40 sccm, 25 sccm, with no other runs intervening. The series was run after the chamber had been used for other trifluoroethylene runs. In Series # 23, the runs were performed in the following order: 45 sccm O_2, 30 sccm, 20 sccm, 15 sccm, 10 sccm, 7 sccm, 0 sccm, with no other runs intervening. The series was run after an oxygen clean (900s, 200 mTorr, 700 W, 0 Gauss, 60 sccm O_2, 5 sccm CF_4). One can see from Figure 5.17b that the 25 sccm point in Series # 22 does not fit the trend marked by the other points in this series. The explanation being offered for this is that the same effect which caused an increase in etch rate due to an increase in fluorine concentrations in Series # 20 was operative here. The 25 sccm run, however, was performed last, after the chamber had already been partially "cleaned" by high oxygen content, net etch runs. Hence the augmentation of fluorine concentrations in the plasma by that time was probably less pronounced, and thus the etch rate increase over the "clean chamber" condition was lower. Series # 23 indeed shows lower rates for those runs in the net etch regime, which is consistent

with the fact that they were being performed in a cleaner chamber. Once again, the rates for the net deposition points are repeatable, indicating that the deposition of fluoropolymer is relatively insensitive to chamber history.

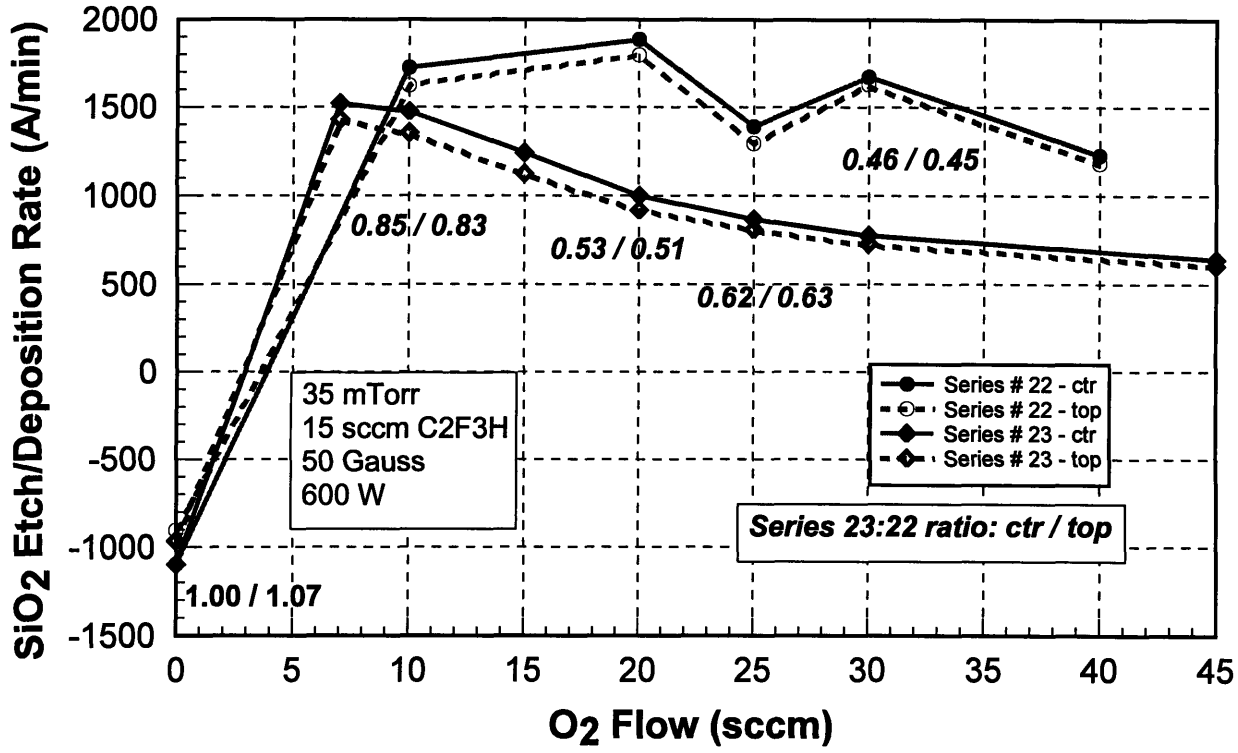

Figure 5.17b

Series # 22, 23: Memory effects with trifluoroethylene: Series # 22 was carried out "low-to-high" (0 to 40 sccm O_2), except for the 25 sccm point, which was run last; Series # 23 was carried out "high-to-low" (45 to 0 sccm O_2). Italicized labels indicate a change of 10% or more.

The above analysis thus suggests that two important factors which affect an etch process with heavily polymerizing gases are 1). whether or not a net deposition seasoning step was performed prior to the experiments, and 2). the order of the runs, *i.e.,* whether runs where polymerization was significant were performed before or after those where polymerization was suppressed. Series # 20, 21, 22, and 24 were taken prior to the inception of the oxygen flow rate study of which Series # 23 and 25 are part. On the basis of the trends seen in Series # 20 and 21, an attempt was made to minimize the effects of the above factors in subsequent runs. For this reason, no seasoning step was used for any of the oxygen flow rate study series; additionally, all

the series in this study were performed in a "high-to-low" order of oxygen flows, to ensure that the runs where polymerization was expected were carried out last.

The third data set, consisting of Series # 24, 25, however, indicates that there may be other factors affecting the repeatability of results with heavily polymerizing gases. Series # 24 was performed after an oxygen clean (1800s, 200 mTorr, 700 W, 0 Gauss, 60 sccm O_2, 5 sccm CF_4), with the runs in the following order: 50 sccm O_2, 45 sccm, 30 sccm, 20 sccm, 10 sccm, 5 sccm, 0 sccm, with no other runs intervening. Results from the 50 sccm and 5 sccm runs are not shown in Figure 5.17c, but they follow the same trend as the other data points. Series # 25 consists of the 45 sccm O_2, 30 sccm, 20 sccm, 10 sccm, and 0 sccm points of Series # 15, which was performed after an oxygen clean (900 s, 200 mTorr, 700 W, 0 Gauss, 60 sccm O_2, 5 sccm CF_4), and which also included 15, 7, and 4 sccm O_2 runs. All runs in this series were carried out in a "high-to-low" order of oxygen flows, as in Series # 24. As Figure 5.17c indicates, despite the fact that both series were run in a "high-to-low" order, after an oxygen clean, and with no seasoning step, significant variation in etch rate is still present at high oxygen flow conditions.

One natural conclusion is that the amount of deposit in the chamber prior to the oxygen clean is a significant factor. If this is the case, then the data suggests that Series # 25 was performed in a "cleaner" chamber than Series # 24, despite the shorter clean time. (Series # 25 was run in the chamber after 1H-heptafluoropropane, a gas which does not exhibit heavy polymerization, whereas Series # 24 was run after trifluoroethylene.) No endpoint for the oxygen clean was used other than a visual inspection of the chamber viewports. It may be the case then that reliably endpointing the duration of the oxygen cleans (*e.g.,* through an optical emission method) or simply using considerably longer clean times to ensure that the chamber is indeed returned to a polymer-free condition would provide for greater process repeatability with the heavily polymerizing gases. In any case, if any of these gases are to be employed in an actual process, careful attention will need to be paid to chamber condition in order to guarantee that process drift is minimized.

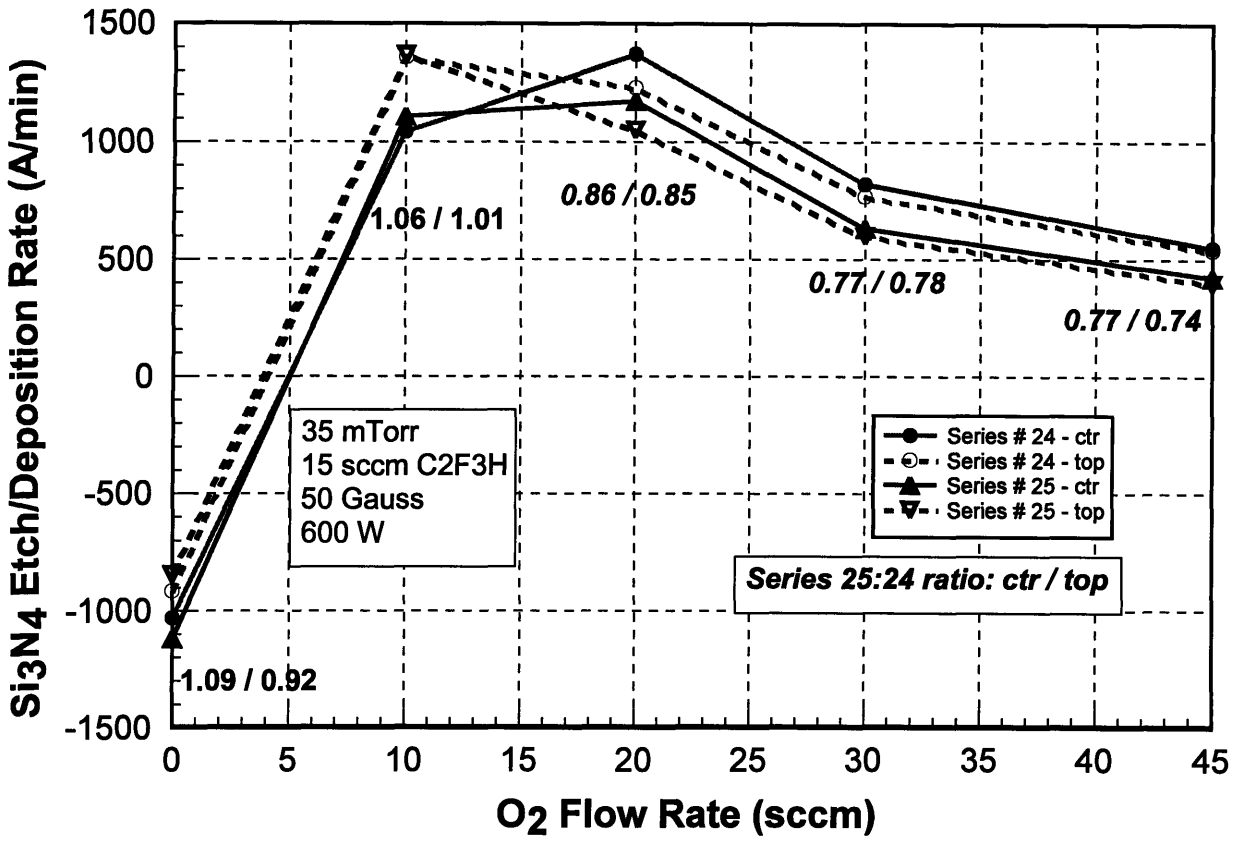

Figure 5.17c

Series # 24, 25: Memory effects with trifluoroethylene: Both these series were carried out "high-to-low" (45 to 0 sccm). Italicized labels indicate a change of 10% or more.

5.3 Auger Electron Spectroscopy Data

Limited Auger electron spectroscopy (AES) tests were carried out on wafers from the following runs: 1,1,1,2-tetrafluoroethane, matrix center point, SiO_2 substrate; 1,1,1,2-tetrafluoroethane, matrix center point, blank Si substrate; and 1H-heptafluoropropane, 93 mTorr, 50 Gauss, 0 sccm O_2, 40 sccm etch gas, 600 W, SiO_2 substrate (2 wafers). Tests with all samples indicate the presence of both carbon and fluorine on the surface. The carbon:fluorine ratios of the films were not established quantitatively, but the tests did present sufficient evidence to confirm the presence of a fluoropolymer layer on these wafers. The presence of carbon and fluorine in a surface layer on the wafers exposed to tetrafluoroethane is to be expected, as a thick film was found on both the silicon and oxide substrates after the process (the deposition rates were calculated to be 1150 Å/min and 1440 Å/min at the top and center locations on the SiO_2

wafer, and 1433 Å/min and 1605 Å/min at the top and center locations on another Si wafer run under the same conditions). Somewhat more interesting, however, is the presence of a surface layer with a similar composition on the 1H-heptafluoropropane SiO_2 wafers. These runs were performed at a set of process conditions which are conducive to polymerization; however, net etching at an average rate of approximately 350 Å/min was observed. The results indicate that, under these conditions, a fluoropolymer residue is left on the wafers during the etch process. Further AES work may be useful in determining the extent to which process gas identity and process conditions affect the composition and the amount of this residue on wafer surfaces in hydrofluorocarbon etch processes.

5.4 Summary

Six hydrofluorocarbon gases (1H- and 2H-heptafluoropropane, pentafluoroethane, difluoromethane, 1,1,1,2-tetrafluoroethane, and trifluoroethylene) were examined for their ability to etch silicon dioxide and silicon nitride films in an Applied Materials Precision 500 etch tool. Octafluoropropane, a perfluorinated gas, was used as a reference. To the author's knowledge, 1H- and 2H-heptafluoropropane and trifluoroethylene had not previously been examined in a dielectric etch application. All seven gases were found to be capable of etching both types of substrates under the correct set of conditions. The first three gases, along with octafluoropropane, were evaluated in a designed experiment matrix study. Neural network software was utilized in the analysis of the data. The etch behavior of these four gases varied noticeably from gas to gas, but over large regions of the parameter space, the two heptafluoropropane isomers and pentafluoroethane were capable of etching both substrates at rates comparable to those of octafluoropropane. Generally speaking, octafluoropropane yielded the fastest etch rates for most process conditions in the matrix parameter space. However, the fact that the other three gases offered comparable performance over a wide range of conditions, at least in terms of etch rate, should be taken as encouraging. Moreover, no significant memory effects (*i.e.*, process drifts) due to a change in chamber condition were noted with these gases, indicating that these chemistries do not polymerize very heavily, leaving large amounts of polymeric residue in the chamber.

The remaining three chemistries, difluoromethane, 1,1,1,2-tetrafluoroethane, and trifluoroethylene, on the other hand, were found to polymerize heavily at pressures and etch gas flow rates at which the other gases etched readily. Etching of oxide and nitride with these gases was achieved at lower pressures and flows. All seven gases were evaluated in non-matrix experiments in this low pressure/low etch gas flow regime. Oxide and nitride etch rate as a function of oxygen flow was studied. Additional, more limited tests were also carried out with all seven gases to establish the effects of pressure and etch gas flow rate on the process. In addition to this, a number of tests were carried out with trifluoroethylene in particular, in which the effects of various process variables on polymerization behavior were studied, along with the effect of chamber condition on the etch process. In general, oxide and nitride etch rates observed for difluoromethane, 1,1,1,2-tetrafluoroethane, and trifluoroethylene were considerably lower than those of the other gases. Thus, while these compounds may have some limited application in wafer patterning processes where polymerizing behavior is desirable for selectivity or anisotropy considerations, their use in chamber cleaning processes, which take place at high pressures and flow rates, relative to those typical of patterning processes, is unlikely. On the other hand, 1H- and 2H-heptafluoropropane and pentafluoroethane once again were found to have oxide and nitride etch behavior similar to that of octafluoropropane. These gases were found to exhibit the same trends as octafluoropropane, as well as comparable etch rates under the conditions studied. These results suggest then that these gases may indeed be promising as viable etchants of dielectrics and further work is warranted to test the feasibility of their use in wafer patterning and chamber cleaning applications.

6 Conclusions and Plans for Future Work

The evaluation of the first set of PFC replacement candidates - hydrofluorocarbons - has been completed. Three of the gases evaluated, 1H-heptafluoropropane, 2H-heptafluoropropane, and pentafluoroethane, have shown themselves to be promising as potential replacements, based on a comparison of their performance with that of octafluoropropane. From a global warming standpoint, they are not ideal candidates, as they still possess measurable GWPs (see Section 3.2.1, Table 3.1). However, the global warming impact of these gases is likely to be lower than that of PFCs. Since these gases were tested in an etch tool, some degree of success in using them for wafer patterning applications may be expected. Since they were found to exhibit little polymerizing behavior, they might also be expected to be able to serve as replacements in a chamber cleaning application. However, this extrapolation cannot be made solely on the basis of the data presented here. Testing of these gases in a PECVD tool as well as testing them again in an etch tool, but this time in an attempt to develop actual process recipes, are the logical next steps. A key aspect of this work will be the analysis of the process effluent in these tests. The methodology for this stage of the alternative chemistries project has been outlined in Sections 1.3.3 and 1.3.4

The six gases tested in the study described in this work represent one of three families of potential PFC replacements, the others being unsaturated fluorocarbons and iodofluorocarbons. In addition to further tests with the three chemistries listed above, future work will involve the evaluation of the substances in the remaining two families (see Chapter 3 for a list) using experimental procedures like the ones in this work. An important modification to the matrix for future work may be the inclusion of process gas flow rate as a fourth variable, at the price of a lengthier experimental scheme. When the most promising candidates are identified in each of the other two families, they too will be examined in the application specific tests described in Sections 1.3.3 and 1.3.4. Finally, once promising replacements for either the wafer patterning or the PECVD chamber cleaning application have been tested at MIT, the next step will be to ensure that they are beta tested in an industrial setting. To this end, continued close contact with the semiconductor industry will be essential.

References

1 W. Worth, "The SEMATECH PFC Strategy/Technology Update," *Proceedings of SEMICON/West 1995: Perfluorocompound Technical Update*, 1995, pp.71-77.

2 Personal communication with various microelectronic manufacturers and semiconductor equipment vendors, 1994, 1995.

3 M. A. K. Khalil, "Global Warming Review", *Proc. SIA/SSA/SEMATECH Global Warming Symposium*, Science and Policy Section, Paper #2, 1994.

4 _____, Intergovernmental Panel on Climate Change (IPCC), "Climate Change: The IPCC Scientific Assessment," 1990.

5 L. Marinilli and W. Worth, "Global Warming: A White Paper on the Science, Policies, and Control Techniques that Impact the U.S. Semiconductor Industry," SEMATECH Technology Transfer Report # 93112074A-TR, 1994.

6 _____, Intergovernmental Panel on Climate Change (IPCC), "Radiative Forcing of Climate Change - The 1994 Working Report of the Scientific Assessment Working Group of IPCC," 1994.

7 W. Worth, SEMATECH, personal communication, June 1995.

8 G. Sherwood, 3M, "C_3F_8 for CVD Cleaning," presented at SRC Technology Transfer Course, MIT, December 1995.

9 J. Langan, Air Products and Chemicals, "Process Optimization as a Strategy to Minimize the Environmental Impact of the Gases used in PECVD Chamber Cleaning," presented at SRC Technology Transfer Course, MIT, December 1995.

10 M. T. Mocella, "Long-Lived and Greenhouse Gases in the Semiconductor Industry: A Review of Science, Policy, and Technology," *Journal of the Semiconductor Safety Association*, December, 1994, p. 16.

11 _____, US Environmental Protection Agency, "U.S. Climate Change Action Plan," 1993.

12 _____, US Environmental Protection Agency, "PFC Emission Reduction Partnership for the Semiconductor Industry: Memorandum of Understanding," 1996.

13 _____, DuPont Fluoroproducts, "Zyron®-116 Global Business Policy," distributed at the SSA/SEMATECH/SIA Semiconductor PFC Workshop, February, 1996.

14 L. Beu, "Greenhouse Gas User Strategies," *Proceedings of SEMICON/West 1995: Perfluorocompound Technical Update*, 1995, pp.51-56.

15 *The National Technology Roadmap for Semiconductors*, , Semiconductor Industry Association (SIA), 1994.

16 S. Karecki, B. Tao, R. Reif, "Alternative Chemistries for Wafer Patterning and PECVD Chamber Cleaning," *Proceedings of SEMICON/West 1995: Perfluorocompound Technical Update*, 1995, pp.91-97.

17 T. J. Dalton, W. T. Conner, and H. H. Sawin, "Interferometric Real-Time Measurements of Uniformity for Plasma Etching," *Journal of the Electrochemical Society*, Vol. 141, No. 7, July 1994, pp. 1893-1900.

18 I. Tepermeister, W. T. Conner, T. Alzaben, H. Barnard, K. Gehlert, and D. Scipione, "In Situ Monitoring of Product Wafers," *Solid State Technology*, March, 1996, pp.63-68.

19 S. Wolf and R. N. Tauber, *Silicon Processing for the VLSI Era, Volume 1: Process Technology*, Lattice Press, Sunset Beach, CA, 1986.

20 S. M. Sze, *VLSI Technology, Second Edition*, McGraw-Hill Publishing Company, New York, NY, 1988.

21 R. C. Jaeger, *Introduction to Microelectronic Fabrication*, Addison-Wesley Publishing Company, Reading, MA, 1990.

22 S. K. Ghandhi, *VLSI Fabrication Principles - Silicon and Gallium Arsenide, Second Edition*, John Wiley & Sons, Inc., New York, NY, 1994.

23 S. Wolf and R. N. Tauber, *op. cit.*, p. 198.

24 S. Wolf and R. N. Tauber, *op. cit.*, p. 182.

25 S. M. Sze, *op. cit.*, p.249.

26 S. Wolf and R. N. Tauber, *op. cit.*, p. 191.

27 J. E. Nulty, P. S. Trammel, "Self-Aligned Contact (SAC) Dry Etch Process for 0.5 μm SRAM Technology," *Proc. of the American Vacuum Society, 41st Nat'l Symposium*, 1994.

28 H. H. Sawin and L. R. Reif, *Plasma Processing for Microelectronic Fabrication: Plasma Deposition, Etching, and Sputtering of Thin Films for VLSI*, unpublished.
29 B. Chapman, *Glow Discharge Processes - Sputtering and Plasma Etching*, John Wiley & Sons, Inc., New York, NY, 1980, p. 52.
30 D. L. Flamm and J. A. Mucha, "Plasma Etching," from *Chemistry of the Semiconductor Industry*, S. J. Moss and A. Ledwith, (eds.), Chapman and Hall, New York, NY, 1987, pp.343-390.
31 J. W. Butterbaugh, L. D. Baston, and H. H. Sawin, "Measurement and Analysis of Radio Frequency Glow Discharge Electrical Impedance and Network Power Loss," *Journal of Vacuum Science and Technology A*, Vol. 8, No. 2, 1990, pp. 916-923.
32 M. A. Lieberman and R. A. Gottscho, "Design of High Density Plasma Sources for Materials Processing," unpublished.
33 C. Stone, Novellus systems, Inc., personal communication, April, 1995.
34 J. Cook, LAM Research, personal communication, April, 1995.
35 B. Chapman, *op. cit.*, pp. 51-57.
36 B. Chapman, *op. cit.*, Chapter 4.
37 B. Chapman, *op. cit.*, Chapter 5.
38 B. Chapman, *op. cit.*, pp. 156-160.
39 S. Maniv, "Modeling for rf discharge characteristics", *Journal of Appl. Physics*, Vol. 63, No. 4, February 1988, pp. 1022-1031.
40 R. C. Jaeger, *op cit.*, p.15.
41 D. L. Flamm, V. M. Donnelly, and D. E. Ibbotson, "Basic Chemistry and Mechanisms of Plasma Etching," *Semiconductor International*, April, 1983, pp. 136-143.
42 J. W. Coburn, "Plasma-Assisted Etching," *Plasma Chemistry and Plasma Processing*, Vol. 2, No. 1, 1982, pp. 1-41.
43 D.R. Sparks, "Plasma Etching of Si, SiO_2, Si_3N_4, and Resist with Fluorine, Chlorine, and Bromine Compounds," *Journal of the Electrochemical Society,* Vol. 139, No. 6, June 1992, pp. 1736-1741.
44 W.E. Frank and T. Chabert, "Dry Etching of Single-Crystal Silicon Trench in Hydrogen Iodide Containing Plasma," *Journal of the Electrochemical Society*, Vol. 140, No. 2, February 1993, pp. 490-495.
45 J. A. Mucha, "The Gases of Plasma Etching: Silicon-Based Technology," *Solid State Technology*, March, 1985, pp. 123-127.
46 J. W. Coburn and H. F. Winters, "Plasma Etching - A Discussion of Mechanisms," *Journal of Vacuum Science and Technology*, Vol. 16, No. 2, 1979, pp. 391-403.
47 D. L. Flamm and V. M. Donnelly, "The Design of Plasma Etchants," *Plasma Chemistry and Plasma Processing*, Vol. 1, No. 4, 1981, pp. 317-363.
48 J. Dulak, B. J. Howard, and C. Steinbrüchel, "Etch mechanism in the Reactive Ion Etching of Silicon Nitride," *Journal of Vacuum Science and Technology A,* Vol. 9, No. 3, 1991, pp. 775-778.
49 N. Hayasaka, H. Okano, Y. Horiike, "Highly Selective Etching of Si_3N_4 over SiO_2 Employing a Downstream Type Reactor," *Solid State Technology*, April, 1988, pp. 127-130.
50 S. Wolf and R. N. Tauber, *op. cit.*, p. 192.
51 R. C. Jaeger, *op. cit.,* p. 136.
52 P. Mahal, "C_3F_8 Etch Process Development Report," Novellus Systems, Inc. San Jose, CA, 1995.
53 D. L. Flamm, University of California, Berkeley, personal communication, May 1996.
54 M.C. Olewine, "Alternative Etch Chemistries and Optimization Studies for Dielectric Reactor Cleaning," *Global Warming Symposium (SEMATECH)*, 1994.
55 V. Mohindra, H.H. Sawin, M. T. Mocella, J.M. Cook, J. Flanner, and O. Turmel, "Alternatives to Perfluorocompounds as Plasma Processing Gases: SiO_2 Etching Using C_2F_5H and $C_2F_4H_2$," *Proceedings of the Tenth Symposium on Plasma Processing, Proceedings Volume 94-20 of the Electrochemical Society,* 1994, pp. 300-310.
56 Material Safety Data Sheet information from various gas manufacturers.
57 S. Solomon, J. B. Burkholder, A. R. Ravishankara, and R. R. Garcia, "Ozone Depletion and Global Warming Potentials of CF_3I," *Journal of Geophysical Research,* Vol. 99, No. D10, 1994, pp. 20929-20935.

58 _____, "Scientific Assessment of Stratospheric Ozone: 1989," World Meteorological Organization, Global Ozone Research and Monitoring Project - Report #20, 1989.
59 Tsang, W., NIST, personal communication, March, 1995.
60 Bliznetsov, V. N., O. P. Gutshin, V. V. Yachmenev, "Reactive ion etching of deep trenches in silicon", Proceedings of SPIE International Conference of Microelectronics, Vol. 1783, 1992, pp. 584-589.
61 DuPont Haskell Laboratory data, February, 1996.
62 Joubert, O., G.S. Oehrlein, and Y. Zhang, "Fluorocarbon high-density plasmas. V. Influence of aspect ratio on the etch rate of silicon dioxide in an electron cyclotron resonance plasma", *Journal of Vacuum Science and Technology, A*, Vol. 12, No. 3, 1994, p. 658.
63 Bell, F.H., O. Joubert, G.S. Oehrlein, Y. Zhang, and D. Vender, "Investigation of selective SiO_2-to-Si etching in an inductively coupled high-density plasma using fluorocarbon gases", *Journal of Vacuum Science and Technology, A*, Vol. 12, No. 6, 1994, p. 3095.
64 _____, *Precision 5000 Operations and Programming, Revision C* - Manual, Applied Materials, Santa Clara, CA, March, 1994, p. 2-5.
65 T. J. Dalton, "Pattern Dependencies in the Plasma Etching of Polysilicon," Ph.D. Thesis, Massachusetts Institute of Technology, Dept. of Chemical Engineering, Sept., 1994, p.168.
66 T. J. Dalton, *op cit.*, pp. 149-150.
67 T. J. Dalton, *op cit.*, pp. 364-365.
68 T. J. Dalton, *op cit.*, p. 161.
69 B. Chapman, *op. cit.*, pp. 330-337.
70 B. Chapman, *op. cit.*, pp. 352.
71 T. J. Dalton, *op. cit.*, pp. 334-339.
72 T. J. Dalton, *op. cit.*, p. 154, p. 339.
73 G. Y. Yeom and M. J. Kushner, "Magnetic Field Effects on Cylindrical Magnetron Reactive Ion Etching of Si/SiO_2 in CF_4 and CF_4/H_2 Plasma," *Journal of Vacuum Science and Technology A*, Vol. 7, No. 3, 1989, pp. 987-992.
74 T. J. Dalton, *op. cit.*, p. 164, p. 167, pp. 338-339.
75 T. J. Dalton, *op. cit.*, p.363.
76 T. J. Dalton, *op. cit.*, p.153.
77 T. J. Dalton, *op. cit.*, Chapter 5.
78 _____, *1000-IS Full Wafer Imagining Interferometer* - Manual, Low Entropy Systems, Inc., Boston, MA, 1995.
79 M-M. Chen and Y. H. Lee, "Optical Emission from Reactive Fluorocarbon-Oxygen Plasma," *Proceedings of the Electrochemical Society*, Vol. 83-10, 1983, p.3-10.
80 R. d'Agostino, F. Cramarossa, V. Colaprico, and R. d'Etolle, "Mechanisms of Etching and Polymerization in Radiofrequency Discharges of CF_4-H_2, CF_4-C_2F_4, C_2F_6-H_2, C_3F_8-H_2," *Journal of Applied Physics*, Vol. 54, No. 3, 1983, p.1284-1288.
81 P. J. Astell-Burt, J. A. Cairns, A. K. Cheetham, and R. M. Hazel, "A Study of the Deposition of Polymeric Material onto Surfaces from Fluorocarbon RF Plasmas," *Plasma Chemistry and Plasma Processing*, Vol. 6, 1986, p. 417.
82 D. C. Montgomery, *Design and Analysis of Experiments (3rd Edition)*, John Wiley & Sons, Inc., New York, NY, 1991.
83 R. V., Hogg and J. Ledolter, *Applied Statistics for Engineers and Physical Scientists*, Macmillian Publishing Co., New York, NY, 1992.
84 R. H. Myers and D. C. Montgomery, *Response Surface Methodology: Process and Product Optimization Using Designed Experiments*, John Wiley & Sons, New York, NY, 1995.
85 W. J. Diamond, *Practical Experiment Designs for Scientists and Engineers Second Edition*, Van Nostrand Reinhold, New York, NY, 1989.
86 S. Ghosh, editor, *Statistical Design and Analysis of Industrial Experiments*, Marcel Dekker, Inc., New York, NY, 1990.
87 T. J. Dalton, *op. cit.*, p. 165.
88 T. J. Dalton, personal communication, February, 1996.
89 T. J. Dalton, *op. cit.*, p.138-139.

90 M. T. Mocella, J. A. Bondur, T. R. Turner, "Etch Process Characterization Using Neural Network Methodology: a Case Study," *SPIE Proceedings: "Process Module Metrology, Control and Clustering,"* Vol. 1594, 1991, p. 232.

91 _____, *NNAPER User Guide, Version 3.0*, E. I. du Pont de Nemours and Company, Wilmington, DE, 1993.

92 L. M. Loewenstein, "Selective Etching of Silicon Nitride Using Remote Plasmas of CF_4 and SF_6," *Journal of Vacuum Science and Technology A*, Vol. 7, No. 3, 1989, pp. 686-690.

93 P. E. Clarke, D. Field, A. J. Hydes, D. F. Klemperer, and M. J. Seakins, "Mass Spectrometric Studies of Plasma Etching of Silicon Nitride," *Journal of Vacuum Science and Technology B*, Vol. 3, No. 6, 1985, pp. 1614-1619.

94 G. Turban, "Basic Phenomena in Reactive Low Pressure Plasmas Used for Deposition and Etching - Current Status," *Pure & Applied Chem.*, Vol. 56, No. 2, 1984, pp. 215-230.

Appendix 1: NNAPER Models of Matrix Experiments

C3F8 oxide (100 Gauss)

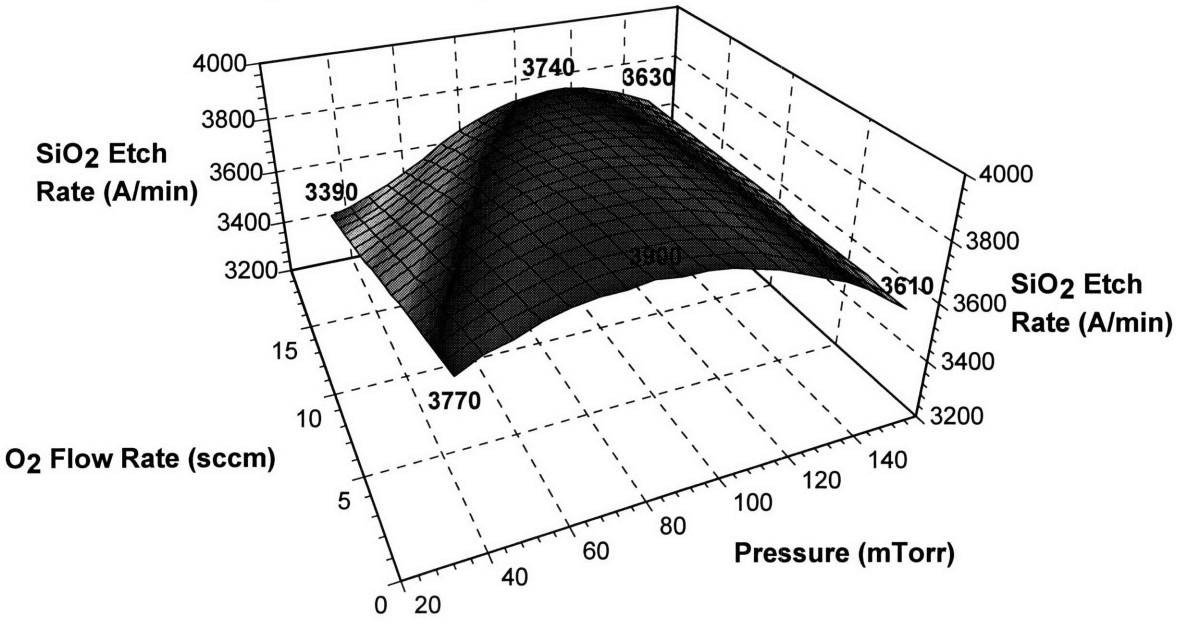

C3F8 oxide (50 Gauss)

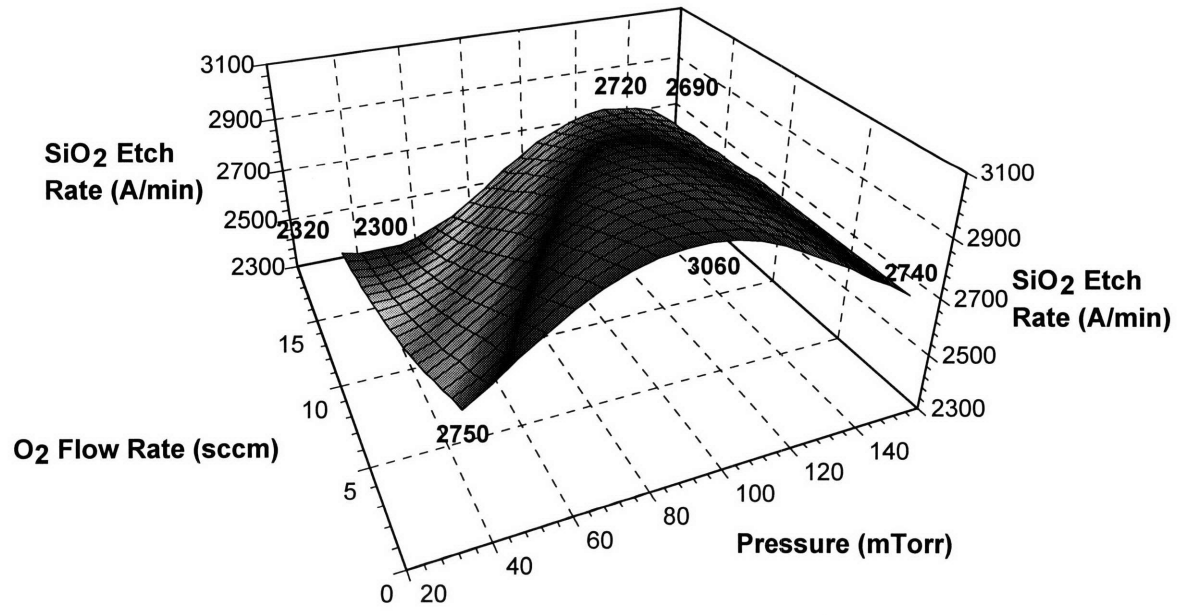

Figure A1.1

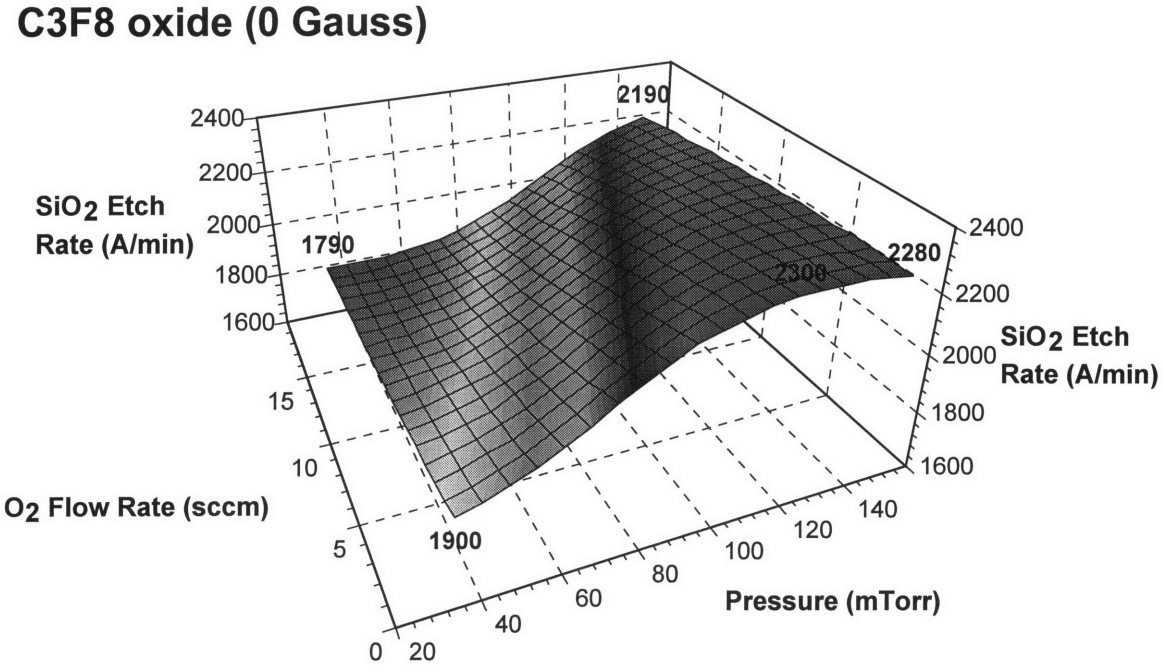

Figure A1.1

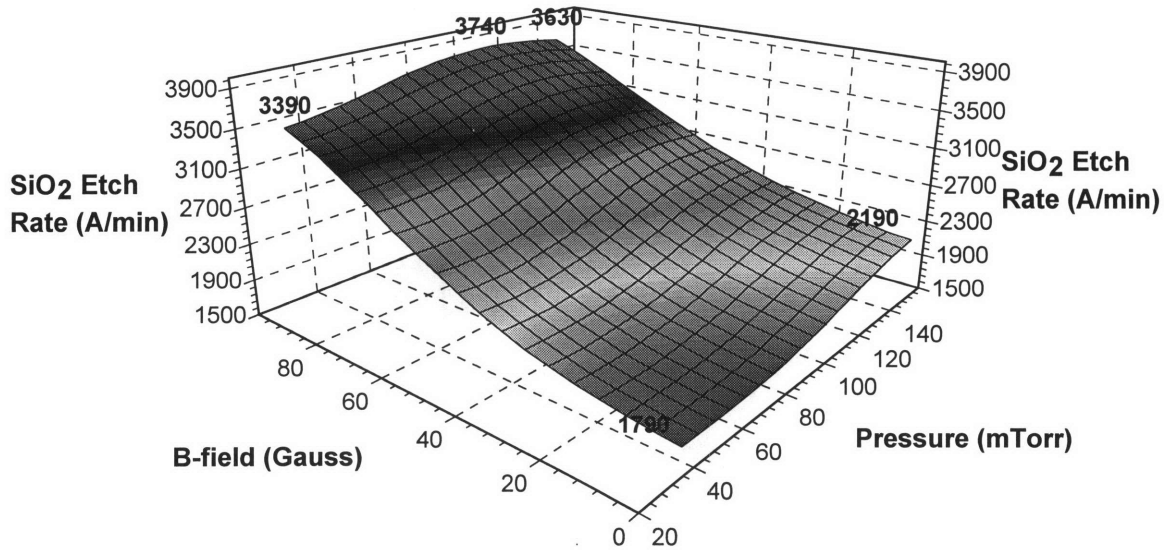

Figure A1.2

C3F8 oxide (10 sccm O2)

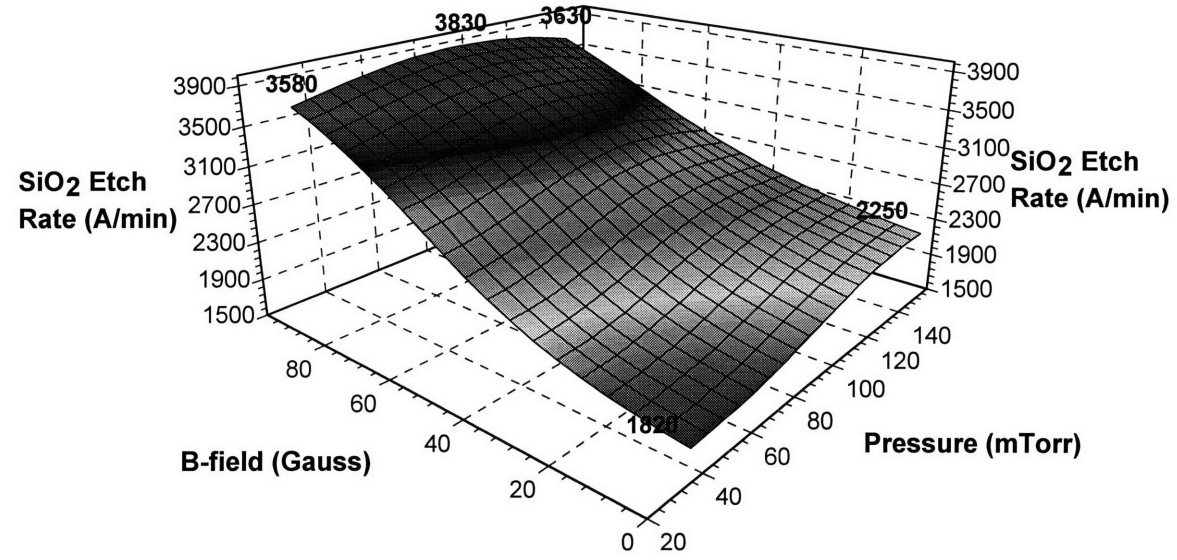

C3F8 oxide (0 sccm O2)

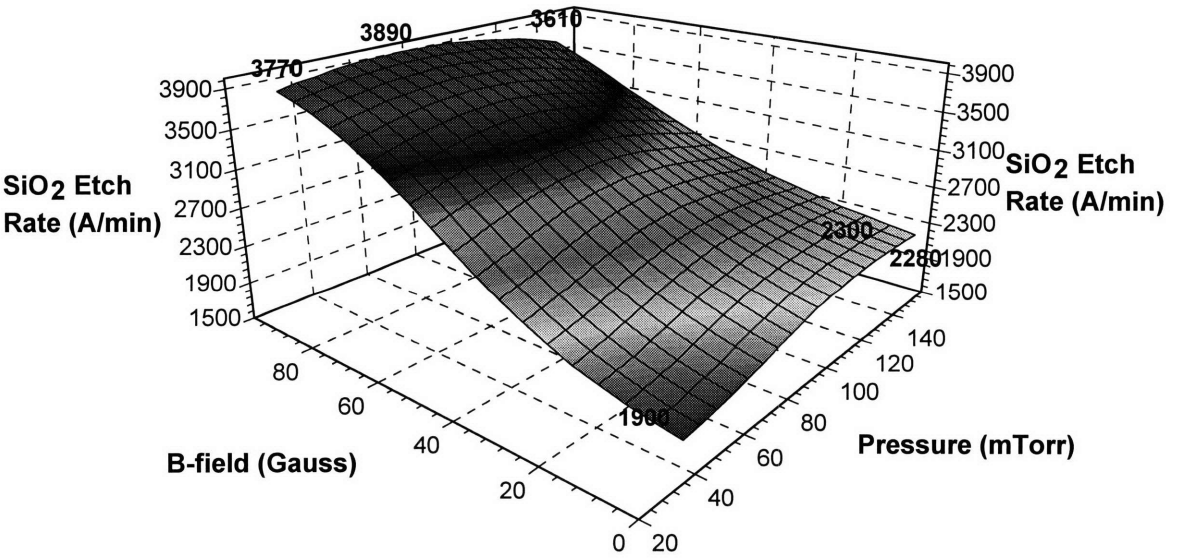

Figure A1.2

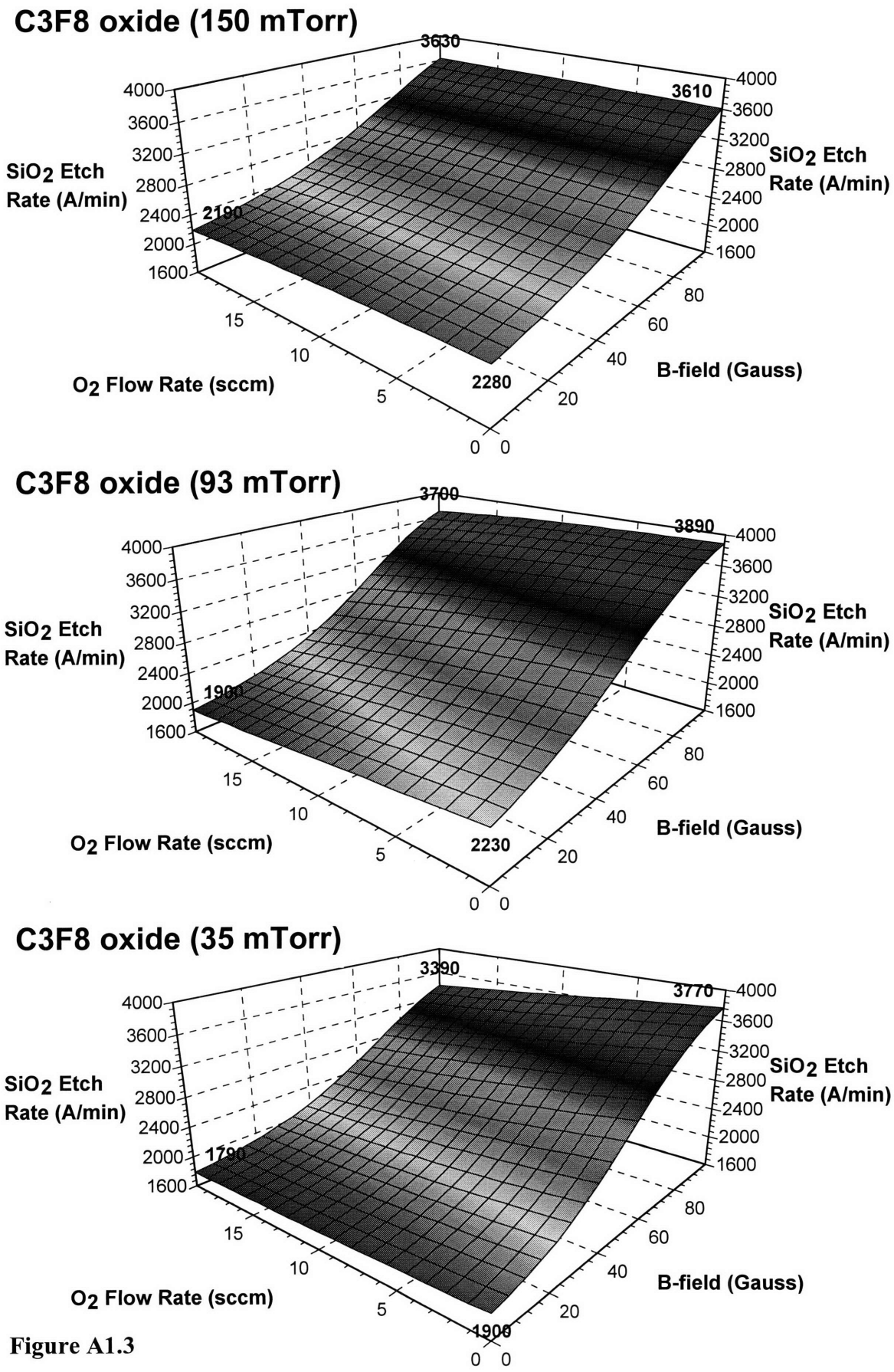
C3F8 oxide (150 mTorr)
3630
3610
2190
2280
SiO2 Etch Rate (A/min)
O2 Flow Rate (sccm)
B-field (Gauss)
C3F8 oxide (93 mTorr)
3700
3890
1900
2230
SiO2 Etch Rate (A/min)
O2 Flow Rate (sccm)
B-field (Gauss)
C3F8 oxide (35 mTorr)
3390
3770
1790
1900
SiO2 Etch Rate (A/min)
O2 Flow Rate (sccm)
B-field (Gauss)

Figure A1.3

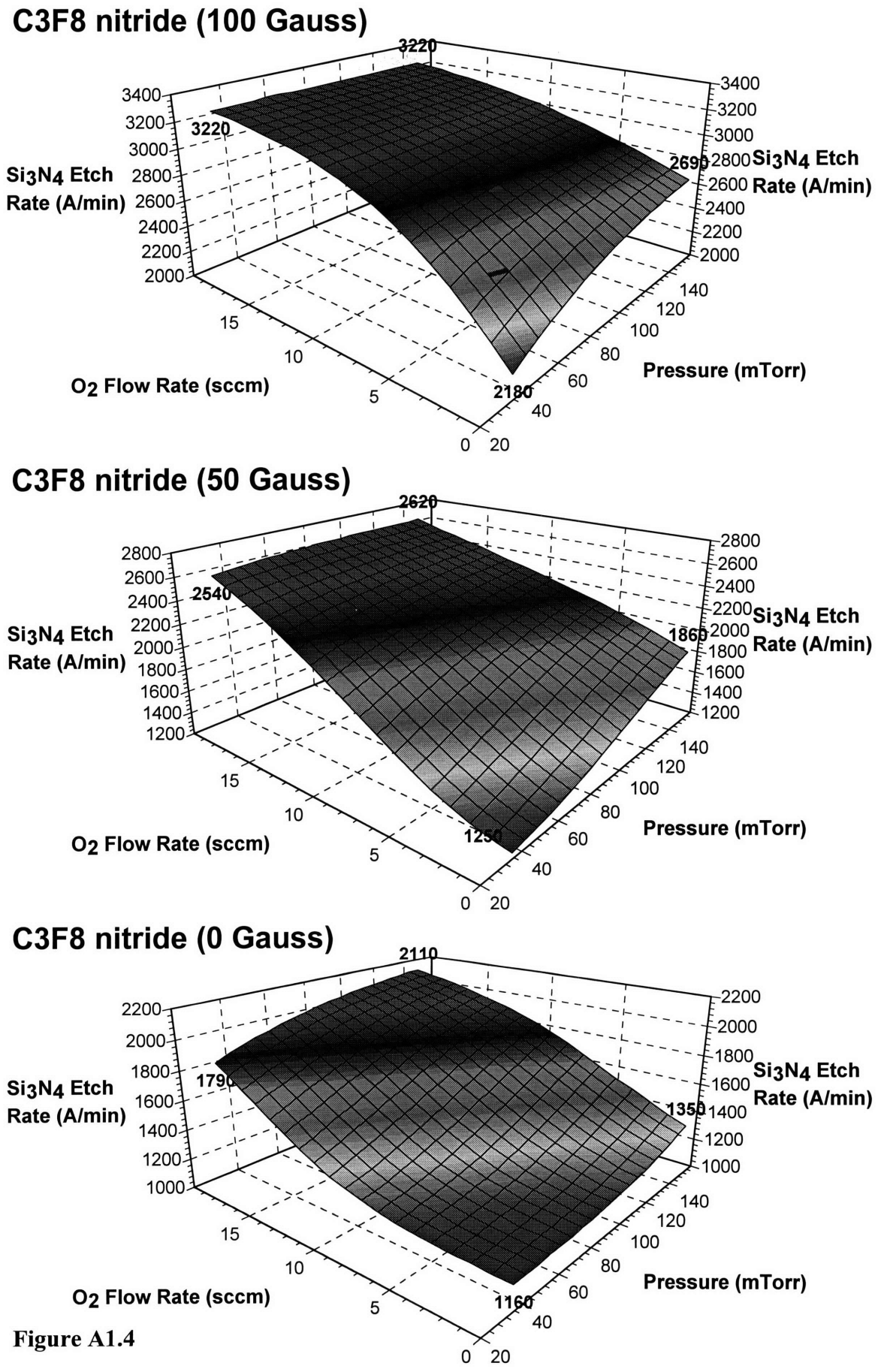
C3F8 nitride (100 Gauss)
3220
3400
3200
3000
2800
2600
2400
2200
2000
Si3N4 Etch Rate (A/min)
2690
2180
15
10
5
0
O2 Flow Rate (sccm)
20
40
60
80
100
120
140
Pressure (mTorr)
C3F8 nitride (50 Gauss)
2620
2800
2600
2400
2200
2000
1800
1600
1400
1200
2540
1860
1250
C3F8 nitride (0 Gauss)
2110
2200
2000
1800
1600
1400
1200
1000
1790
1350
1160

Figure A1.4

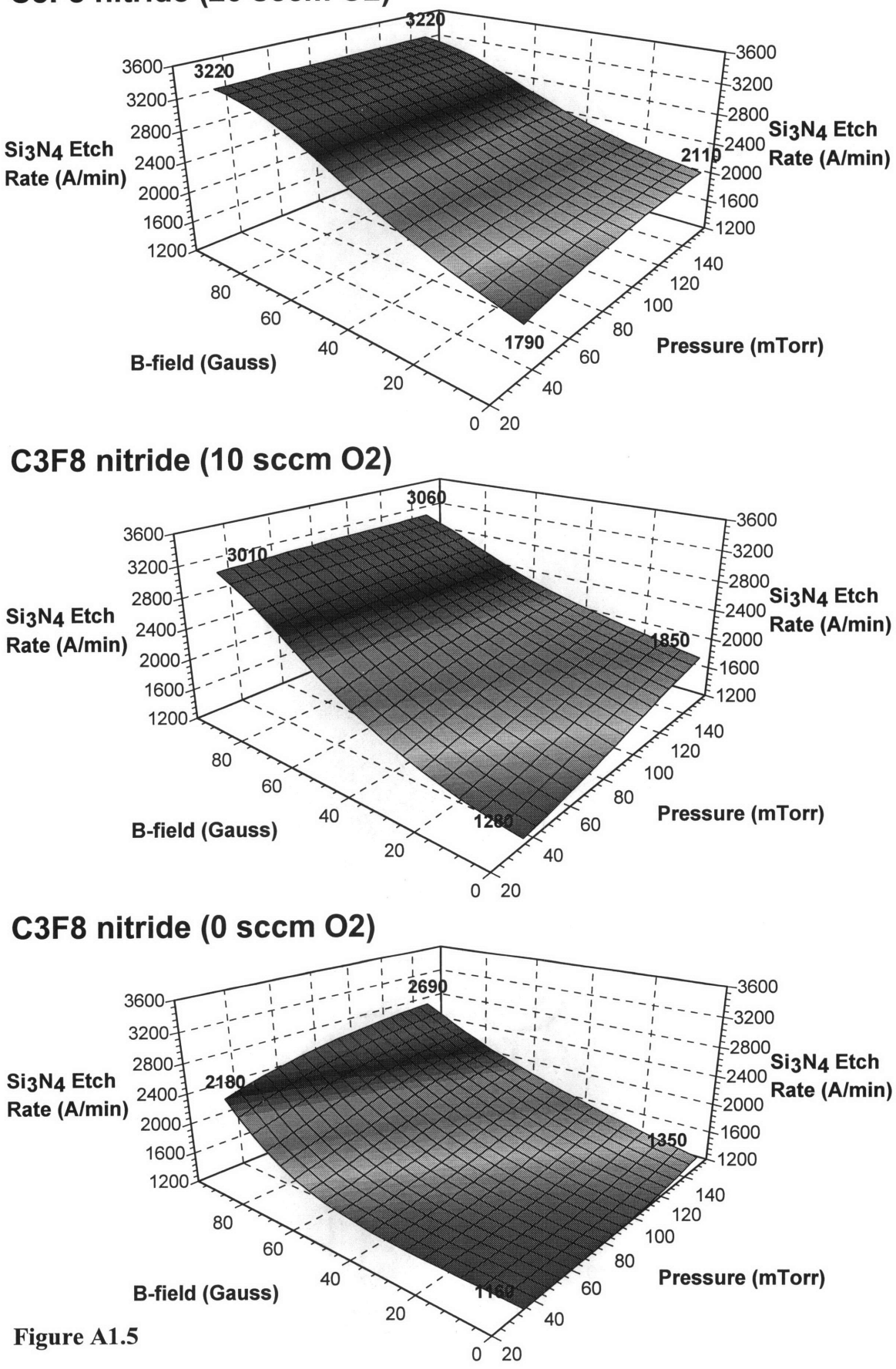
C3F8 nitride (20 sccm O2)
3220
3220
2110
1790
Si3N4 Etch Rate (A/min)
B-field (Gauss)
Pressure (mTorr)
C3F8 nitride (10 sccm O2)
3060
3010
1850
1280
Si3N4 Etch Rate (A/min)
B-field (Gauss)
Pressure (mTorr)
C3F8 nitride (0 sccm O2)
2690
2180
1350
1160
Si3N4 Etch Rate (A/min)
B-field (Gauss)
Pressure (mTorr)

Figure A1.5

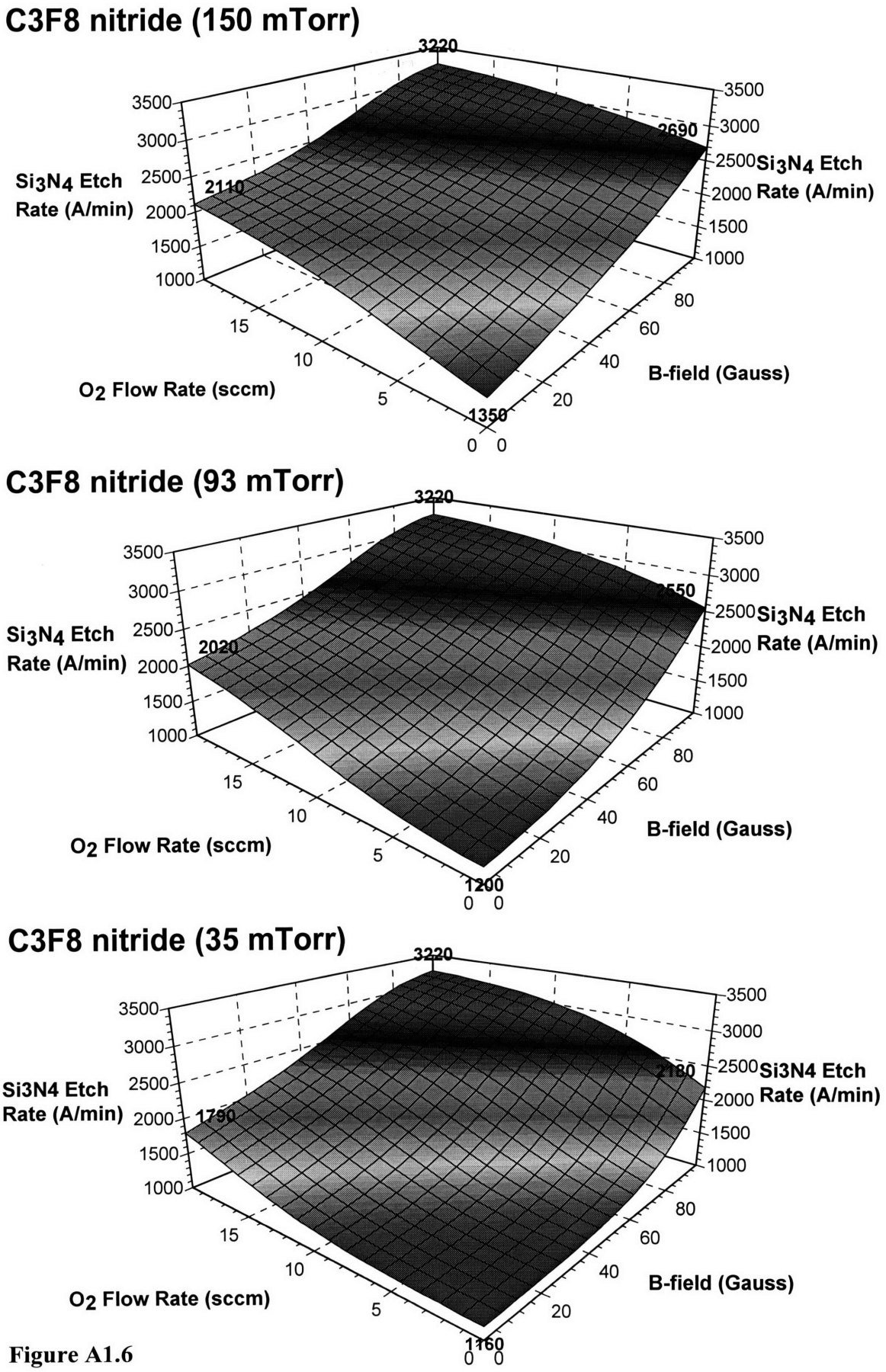
C3F8 nitride (150 mTorr)
3220
3500
3000
2500
2000
1500
1000
Si3N4 Etch
Rate (A/min)
2110
2690
1350
15
10
5
0
O2 Flow Rate (sccm)
0
20
40
60
80
B-field (Gauss)
C3F8 nitride (93 mTorr)
3220
2020
2550
1200
C3F8 nitride (35 mTorr)
3220
Si3N4 Etch
Rate (A/min)
1790
2180
1160

Figure A1.6

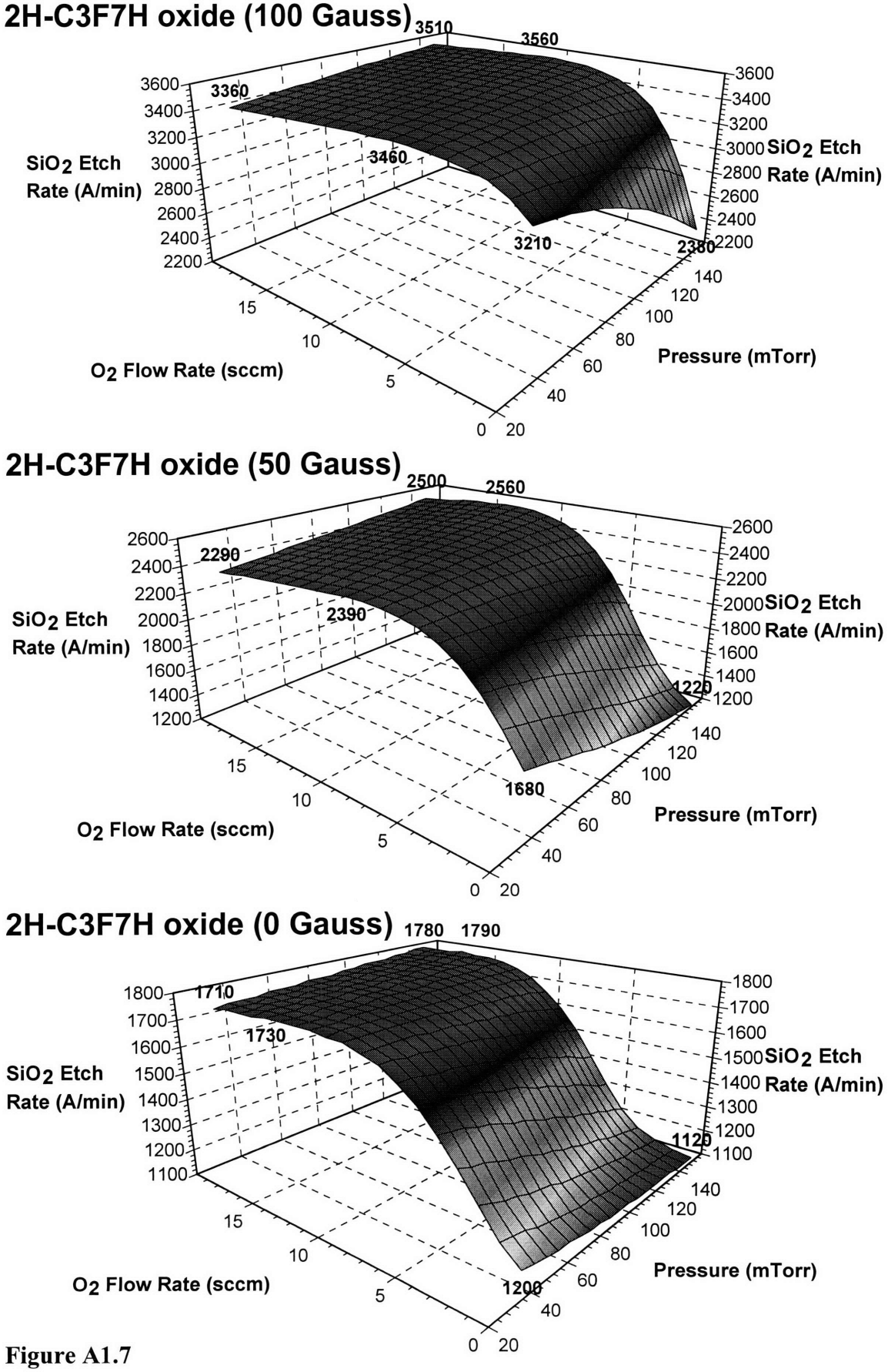
2H-C3F7H oxide (100 Gauss)
3510
3560
3360
3460
3210
2380
3600
3400
3200
3000
2800
2600
2400
2200
SiO2 Etch Rate (A/min)
O2 Flow Rate (sccm)
Pressure (mTorr)
0
5
10
15
20
40
60
80
100
120
140
2H-C3F7H oxide (50 Gauss)
2500
2560
2290
2390
1680
1220
2600
2400
2200
2000
1800
1600
1400
1200
2H-C3F7H oxide (0 Gauss)
1780
1790
1710
1730
1200
1120
1800
1700
1600
1500
1400
1300
1200
1100

Figure A1.7

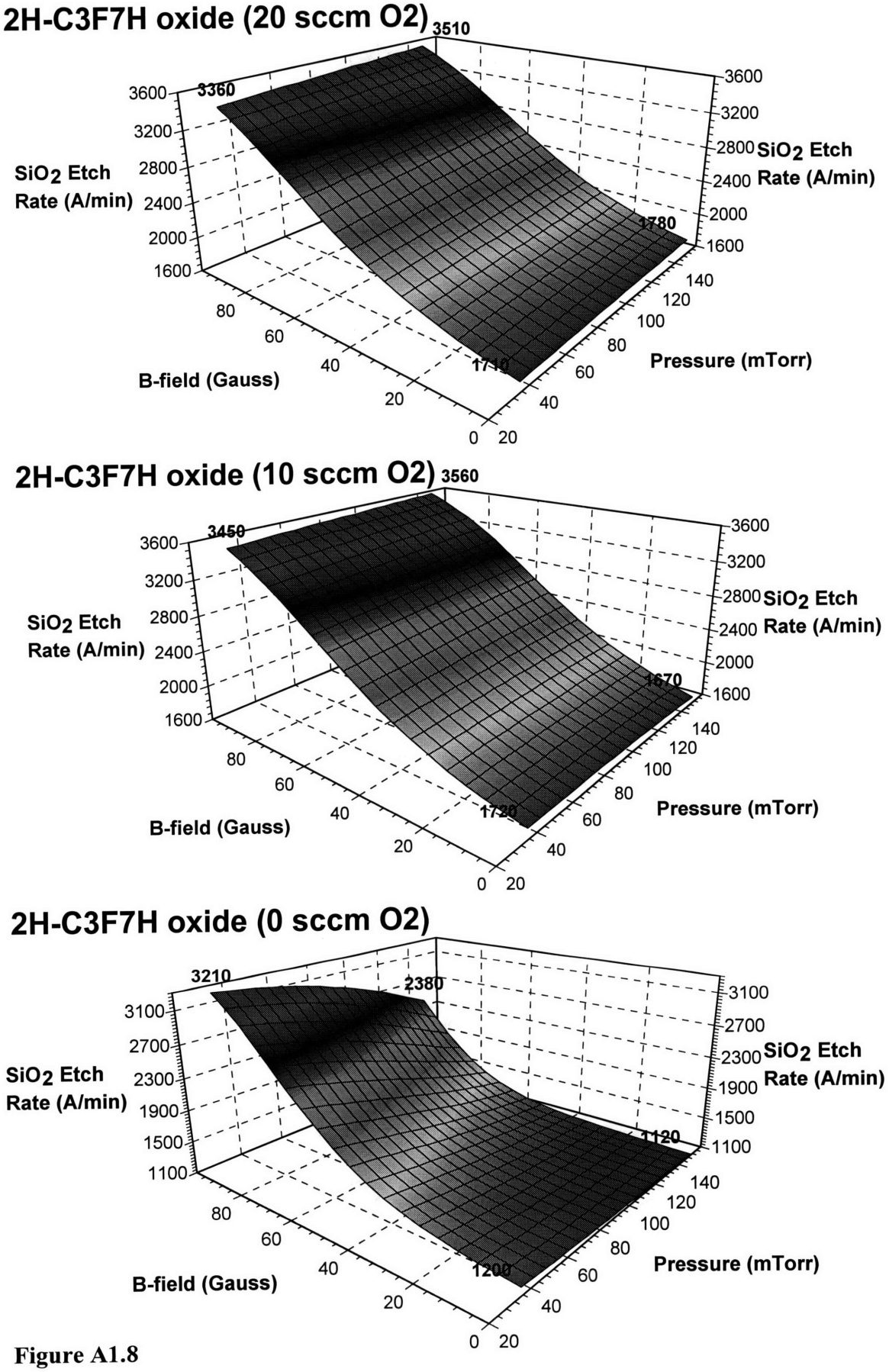
2H-C3F7H oxide (20 sccm O2)
3510
3360
1780
1710
SiO2 Etch Rate (A/min)
B-field (Gauss)
Pressure (mTorr)
2H-C3F7H oxide (10 sccm O2)
3560
3450
1670
1720
SiO2 Etch Rate (A/min)
B-field (Gauss)
Pressure (mTorr)
2H-C3F7H oxide (0 sccm O2)
3210
2380
1120
1200
SiO2 Etch Rate (A/min)
B-field (Gauss)
Pressure (mTorr)

Figure A1.8

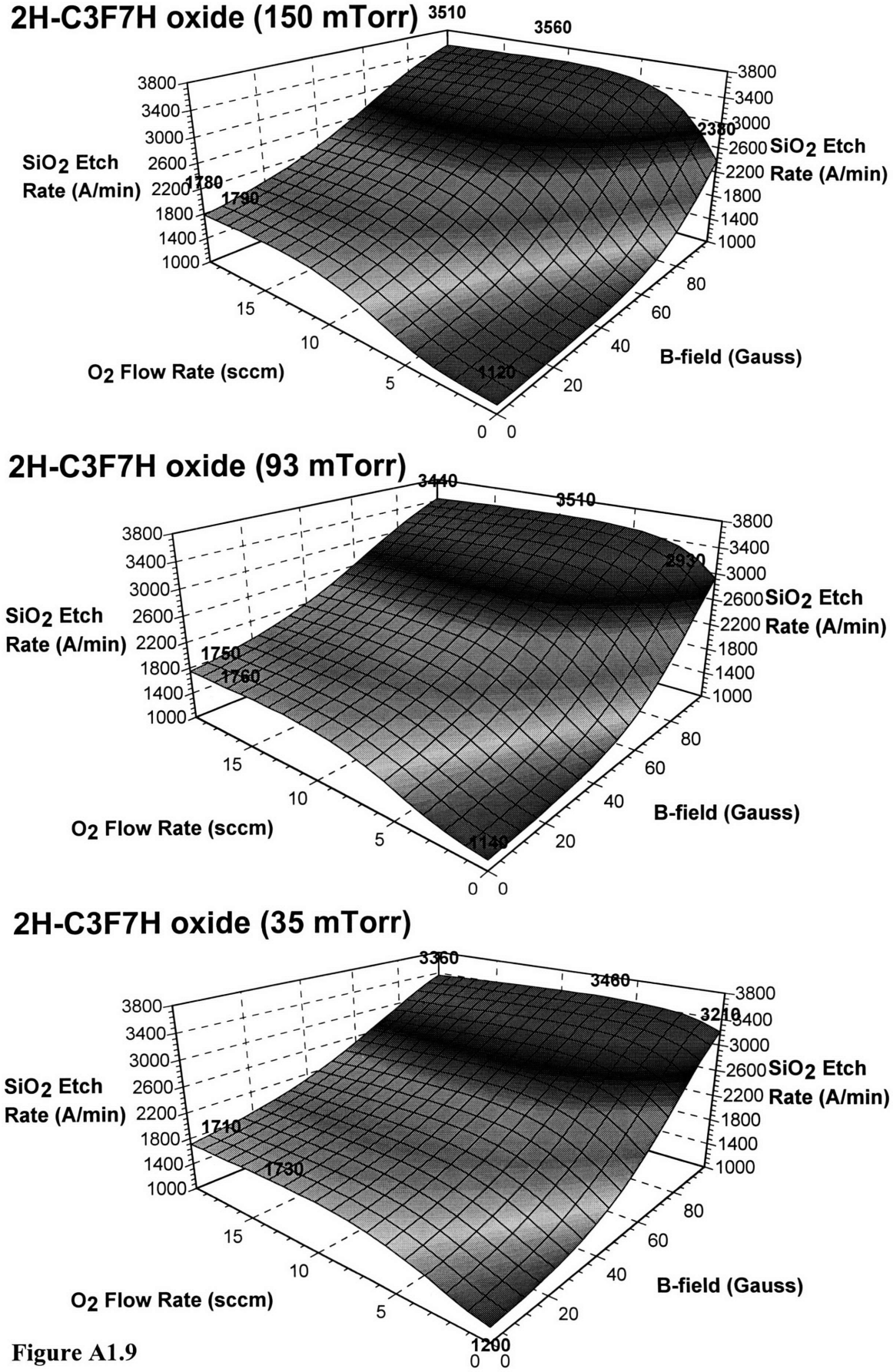
2H-C3F7H oxide (150 mTorr)
3510
3560
3800
3400
3000
2600
2200
1800
1400
1000
SiO2 Etch
Rate (A/min)
1780
1790
2350
SiO2 Etch
Rate (A/min)
15
10
5
0
O2 Flow Rate (sccm)
1120
0
20
40
60
80
B-field (Gauss)
2H-C3F7H oxide (93 mTorr)
3440
3510
2930
1750
1760
1140
2H-C3F7H oxide (35 mTorr)
3360
3460
3210
1710
1730
1200

Figure A1.9

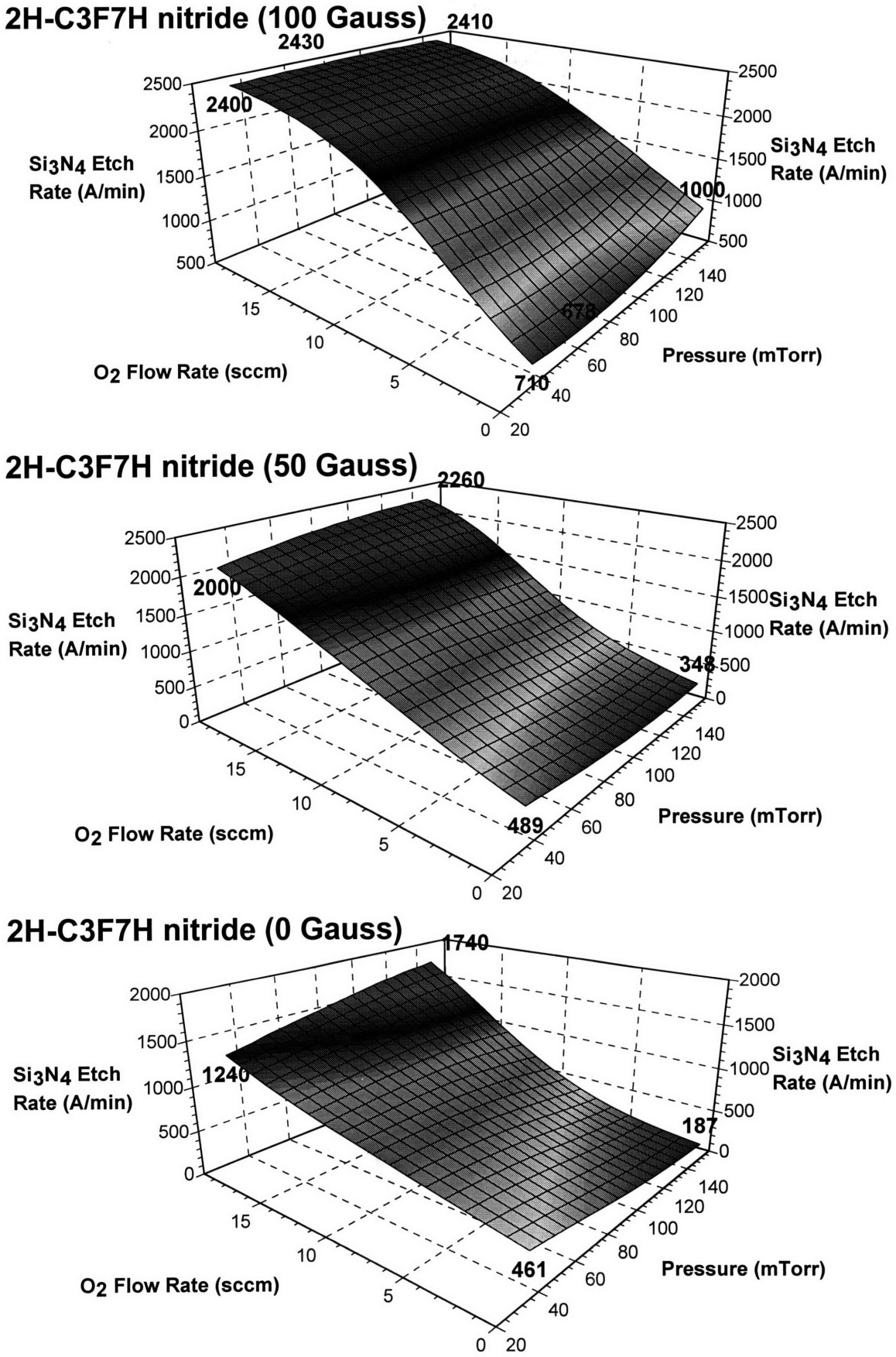
2H-C3F7H nitride (100 Gauss)
2410
2430
2400
1000
678
710
Si3N4 Etch Rate (A/min)
O2 Flow Rate (sccm)
Pressure (mTorr)
2H-C3F7H nitride (50 Gauss)
2260
2000
348
489
Si3N4 Etch Rate (A/min)
O2 Flow Rate (sccm)
Pressure (mTorr)
2H-C3F7H nitride (0 Gauss)
1740
1240
187
461
Si3N4 Etch Rate (A/min)
O2 Flow Rate (sccm)
Pressure (mTorr)

Figure A1.10

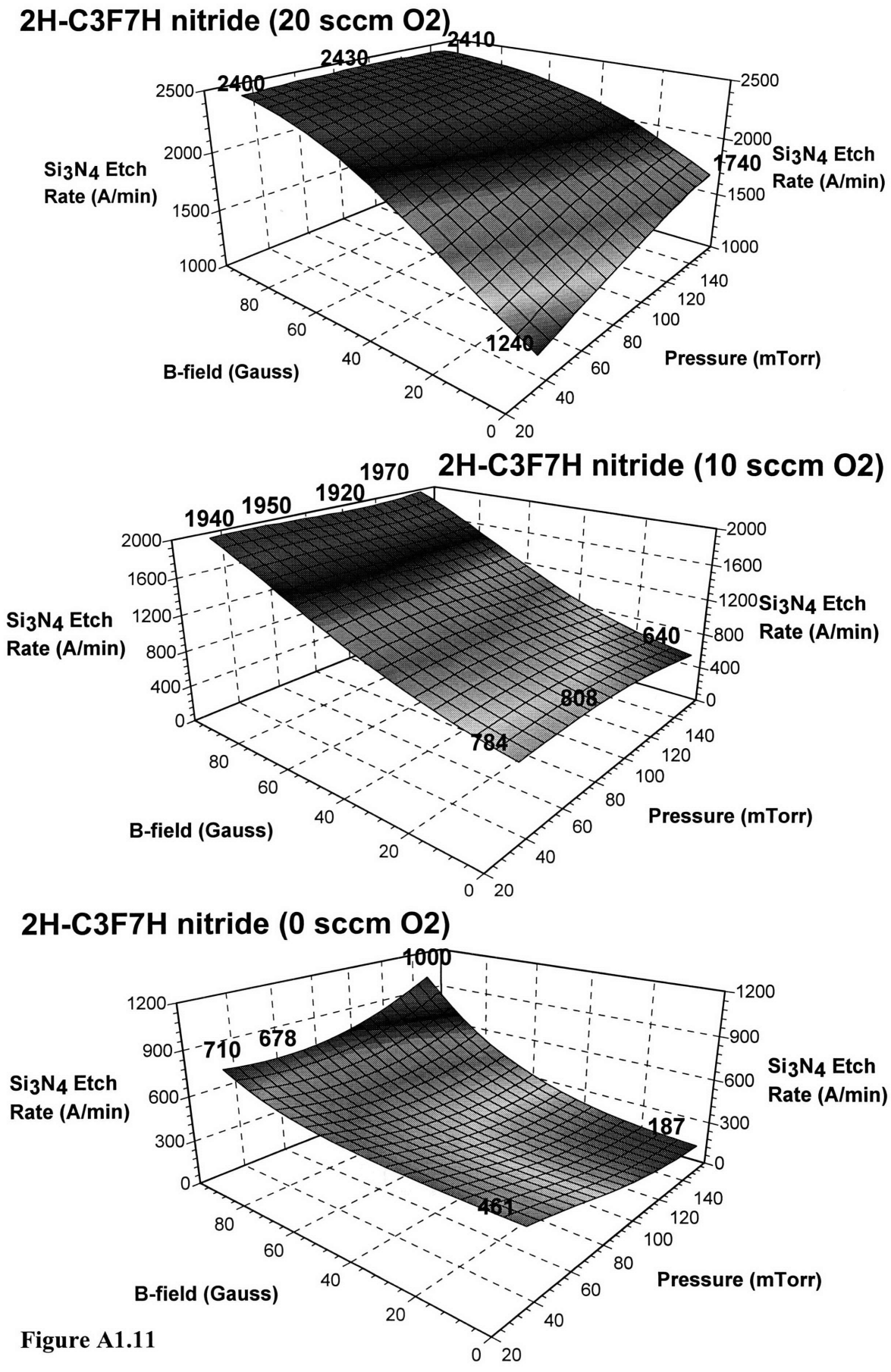
2H-C3F7H nitride (20 sccm O2)
2410
2430
2400
2500
2000
1500
1000
Si3N4 Etch Rate (A/min)
1740
1240
B-field (Gauss)
Pressure (mTorr)
2H-C3F7H nitride (10 sccm O2)
1970
1940
1950
1920
2000
1600
1200
800
400
0
Si3N4 Etch Rate (A/min)
640
808
784
B-field (Gauss)
Pressure (mTorr)
2H-C3F7H nitride (0 sccm O2)
1000
1200
900
600
300
0
Si3N4 Etch Rate (A/min)
710
678
187
461
B-field (Gauss)
Pressure (mTorr)

Figure A1.11

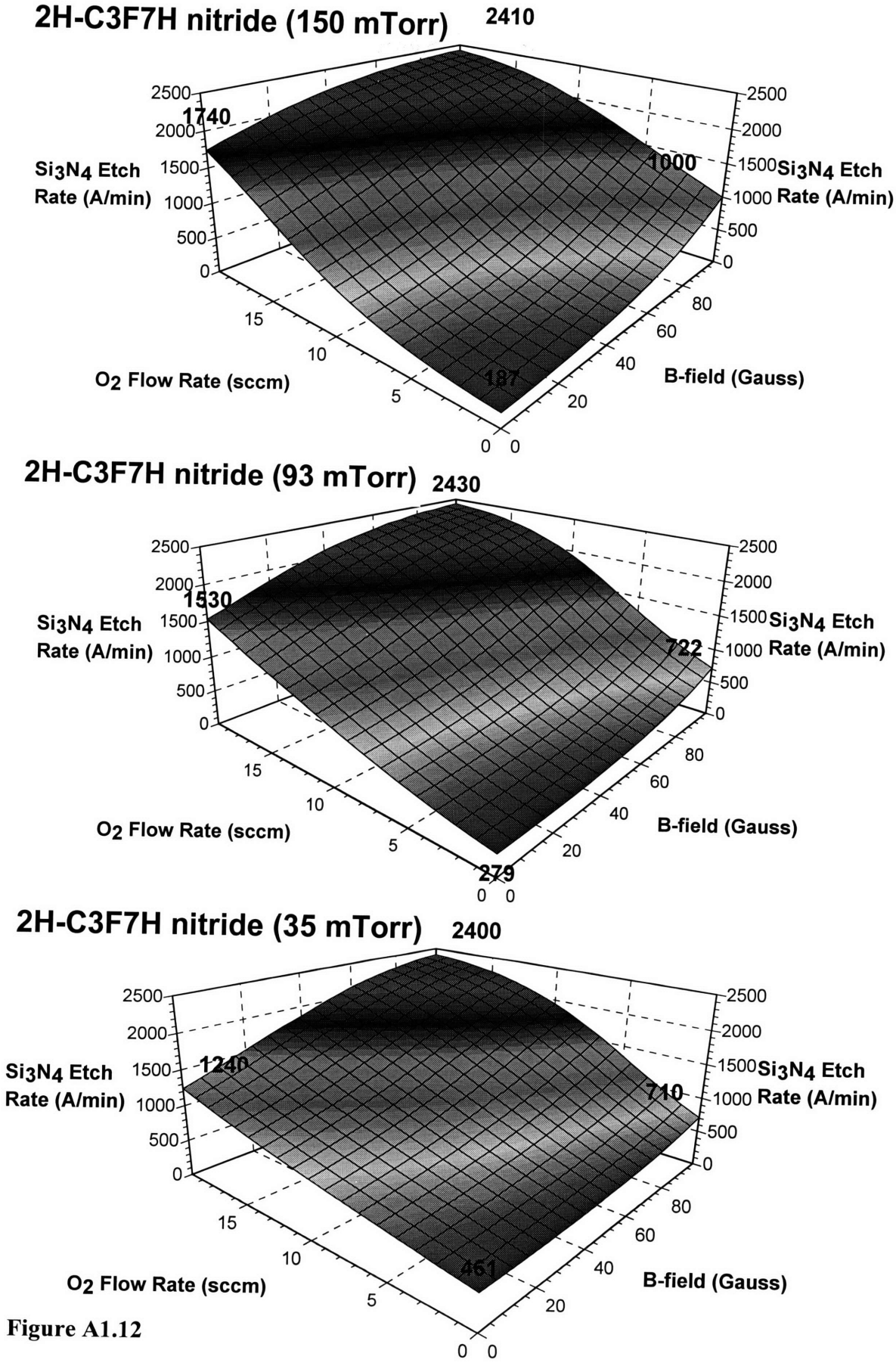
2H-C3F7H nitride (150 mTorr)
2410
1740
1000
187
Si3N4 Etch Rate (A/min)
O2 Flow Rate (sccm)
B-field (Gauss)
2H-C3F7H nitride (93 mTorr)
2430
1530
722
279
Si3N4 Etch Rate (A/min)
O2 Flow Rate (sccm)
B-field (Gauss)
2H-C3F7H nitride (35 mTorr)
2400
1240
710
461
Si3N4 Etch Rate (A/min)
O2 Flow Rate (sccm)
B-field (Gauss)

Figure A1.12

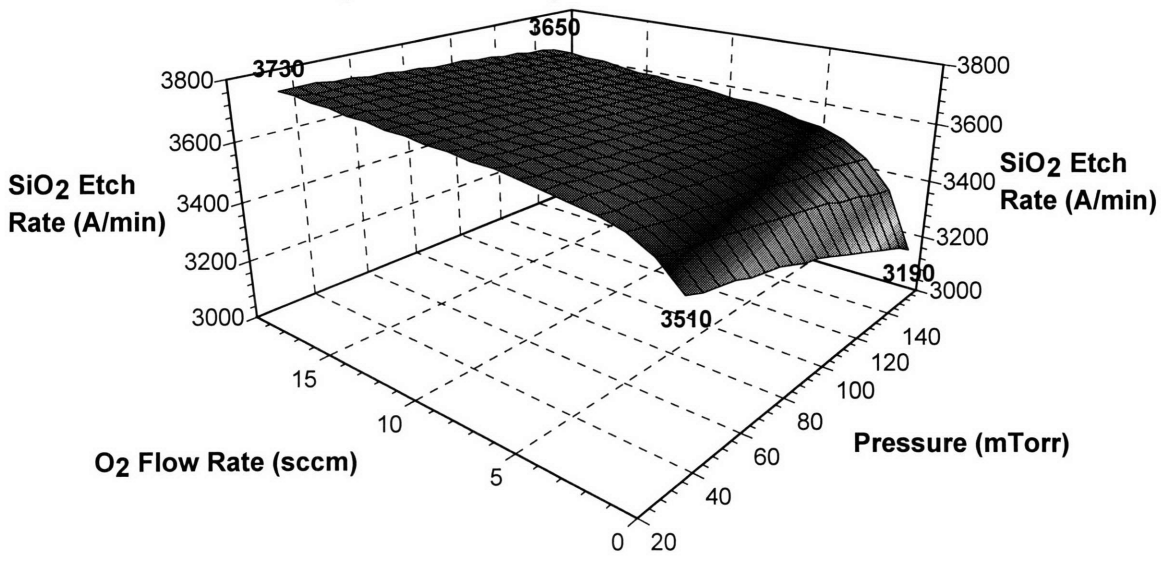
1H-C3F7H oxide (100 Gauss)
3650
3730
3800
3600
3400
3200
3000
SiO2 Etch
Rate (A/min)
3800
3600
3400
3200
3000
SiO2 Etch
Rate (A/min)
3190
3510
15
10
5
0
O2 Flow Rate (sccm)
20
40
60
80
100
120
140
Pressure (mTorr)

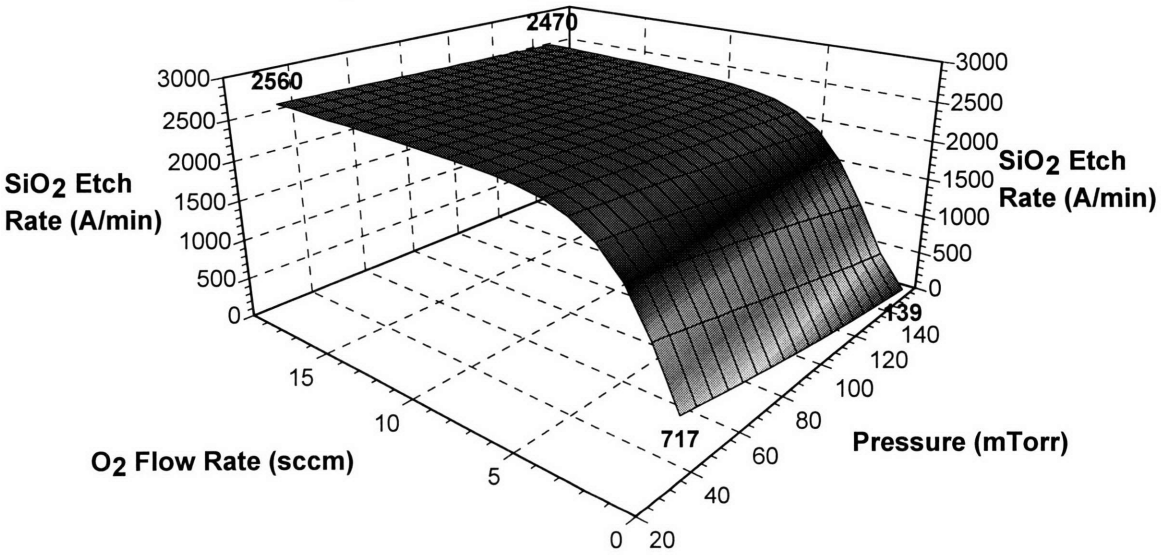
1H-C3F7H oxide (50 Gauss)
2470
2560
3000
2500
2000
1500
1000
500
0
SiO2 Etch
Rate (A/min)
3000
2500
2000
1500
1000
500
0
SiO2 Etch
Rate (A/min)
-139
717
15
10
5
0
O2 Flow Rate (sccm)
20
40
60
80
100
120
140
Pressure (mTorr)

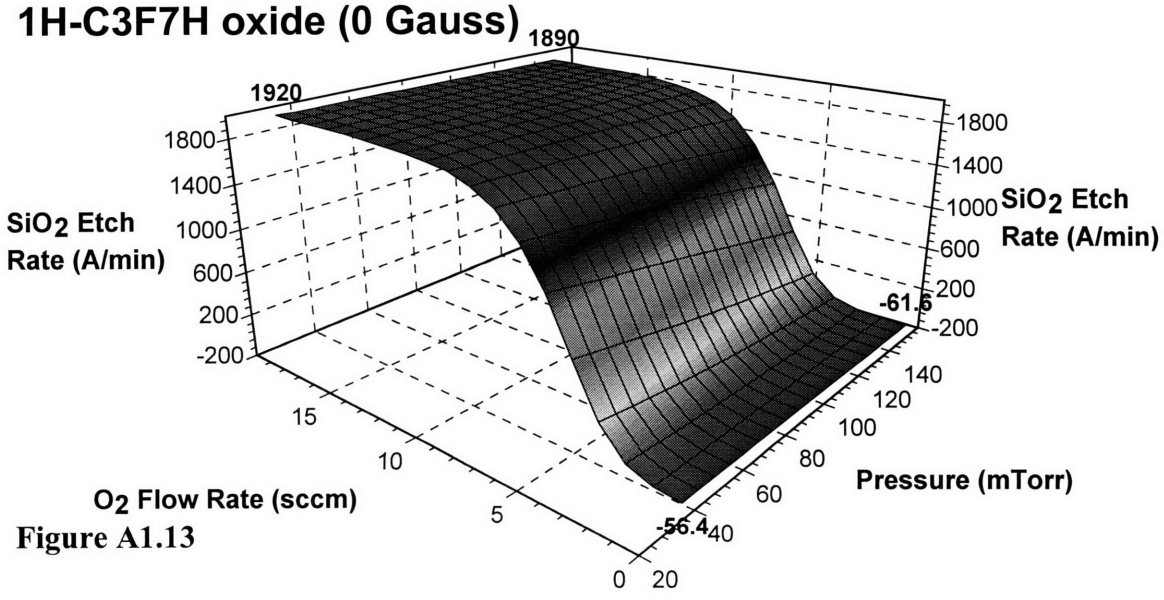
1H-C3F7H oxide (0 Gauss)
1890
1920
1800
1400
1000
600
200
-200
SiO2 Etch
Rate (A/min)
1800
1400
1000
600
200
-200
SiO2 Etch
Rate (A/min)
-61.6
-56.4
15
10
5
0
O2 Flow Rate (sccm)
20
40
60
80
100
120
140
Pressure (mTorr)

Figure A1.13

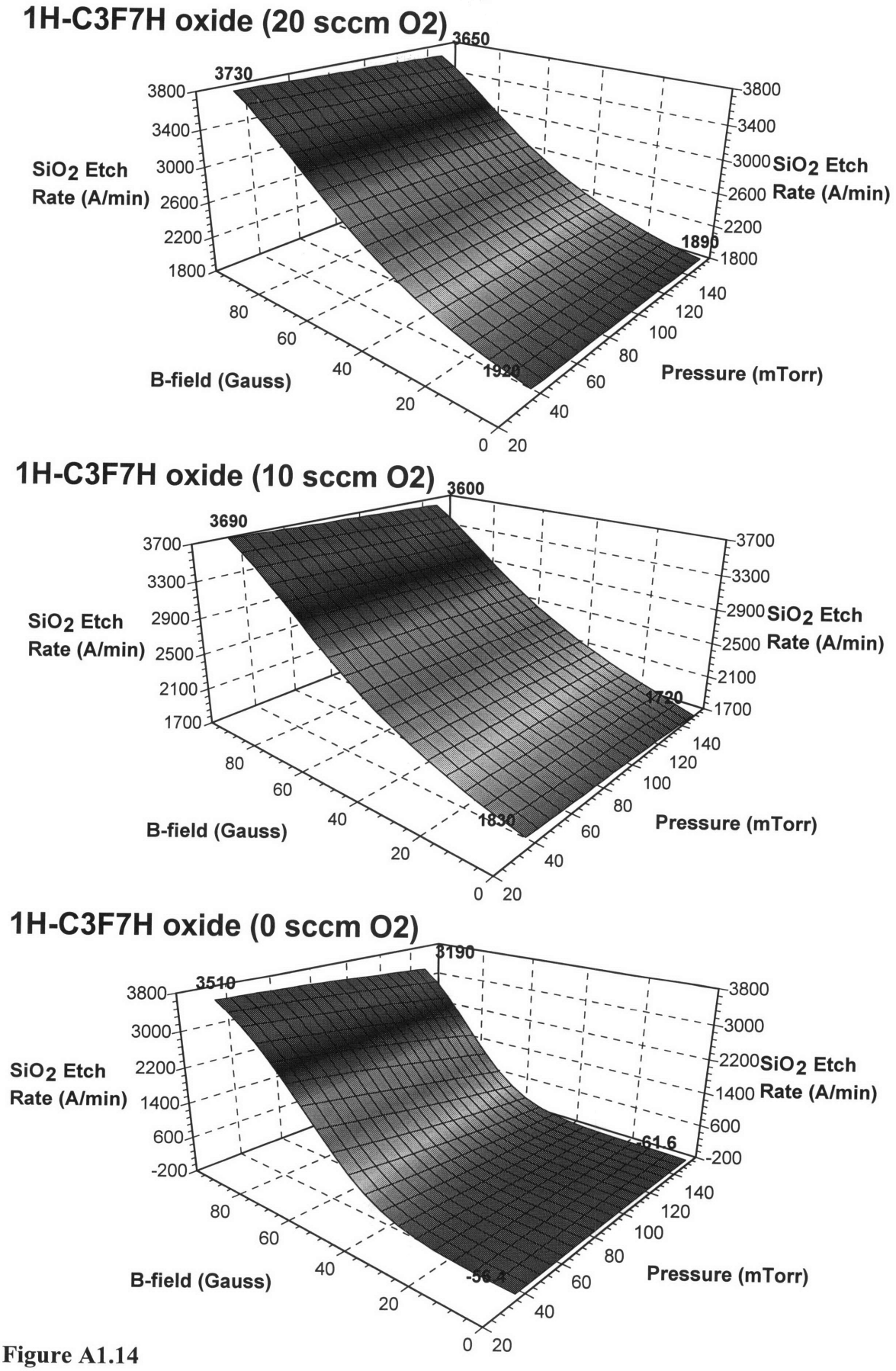
1H-C3F7H oxide (20 sccm O2)
3650
3730
3800
3400
3000
2600
2200
1800
SiO2 Etch
Rate (A/min)
1890
80
60
40
20
0
B-field (Gauss)
20
40
60
80
100
120
140
Pressure (mTorr)
1H-C3F7H oxide (10 sccm O2)
3600
3690
3700
3300
2900
2500
2100
1700
SiO2 Etch
Rate (A/min)
1720
1830
1H-C3F7H oxide (0 sccm O2)
3190
3510
3800
3000
2200
1400
600
-200
SiO2 Etch
Rate (A/min)
61.6
-56.4

Figure A1.14

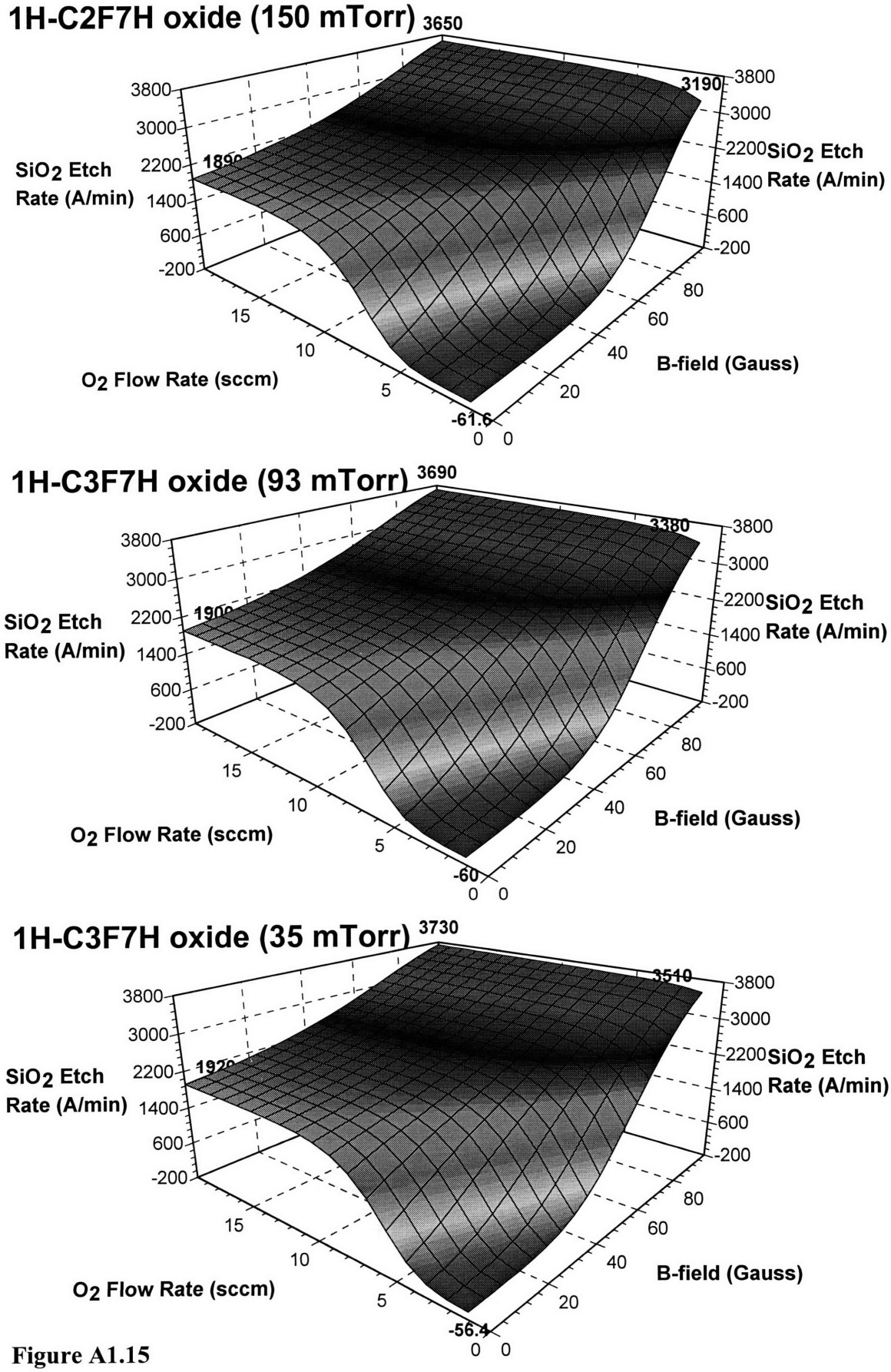
1H-C2F7H oxide (150 mTorr)
3650
3800
3000
2200
1890
1400
600
-200
SiO2 Etch
Rate (A/min)
15
10
5
0
O2 Flow Rate (sccm)
0
20
40
60
80
B-field (Gauss)
3190
-61.6
3800
3000
2200
1400
600
-200
SiO2 Etch
Rate (A/min)
1H-C3F7H oxide (93 mTorr)
3690
3800
3000
2200
1900
1400
600
-200
SiO2 Etch
Rate (A/min)
15
10
5
0
O2 Flow Rate (sccm)
0
20
40
60
80
B-field (Gauss)
3380
-60
3800
3000
2200
1400
600
-200
SiO2 Etch
Rate (A/min)
1H-C3F7H oxide (35 mTorr)
3730
3800
3000
2200
1920
1400
600
-200
SiO2 Etch
Rate (A/min)
15
10
5
0
O2 Flow Rate (sccm)
0
20
40
60
80
B-field (Gauss)
3510
-56.4
3800
3000
2200
1400
600
-200
SiO2 Etch
Rate (A/min)

Figure A1.15

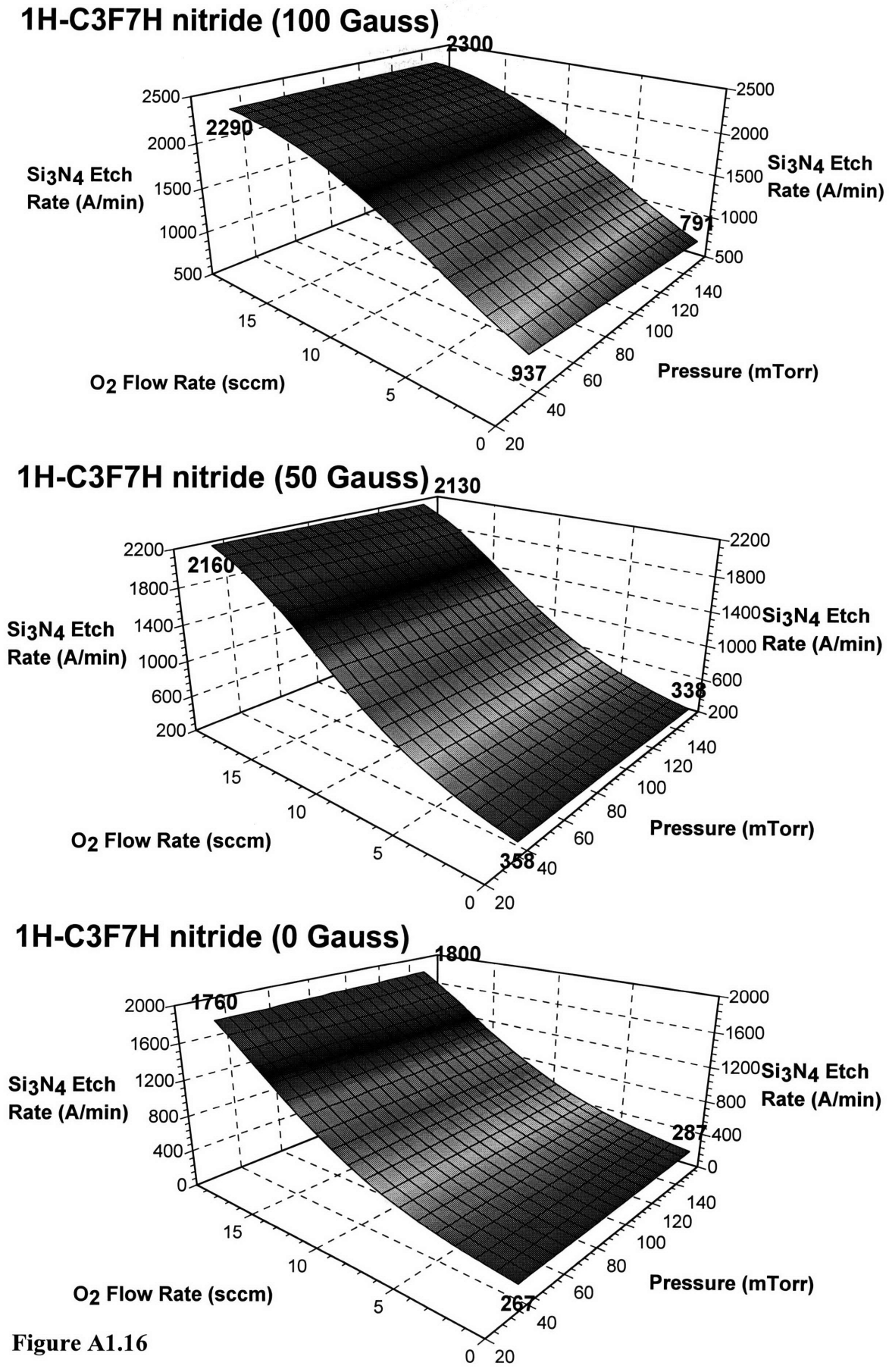
1H-C3F7H nitride (100 Gauss)
2300
2290
791
937
Si3N4 Etch Rate (A/min)
O2 Flow Rate (sccm)
Pressure (mTorr)
1H-C3F7H nitride (50 Gauss)
2130
2160
338
358
Si3N4 Etch Rate (A/min)
O2 Flow Rate (sccm)
Pressure (mTorr)
1H-C3F7H nitride (0 Gauss)
1800
1760
287
267
Si3N4 Etch Rate (A/min)
O2 Flow Rate (sccm)
Pressure (mTorr)

Figure A1.16

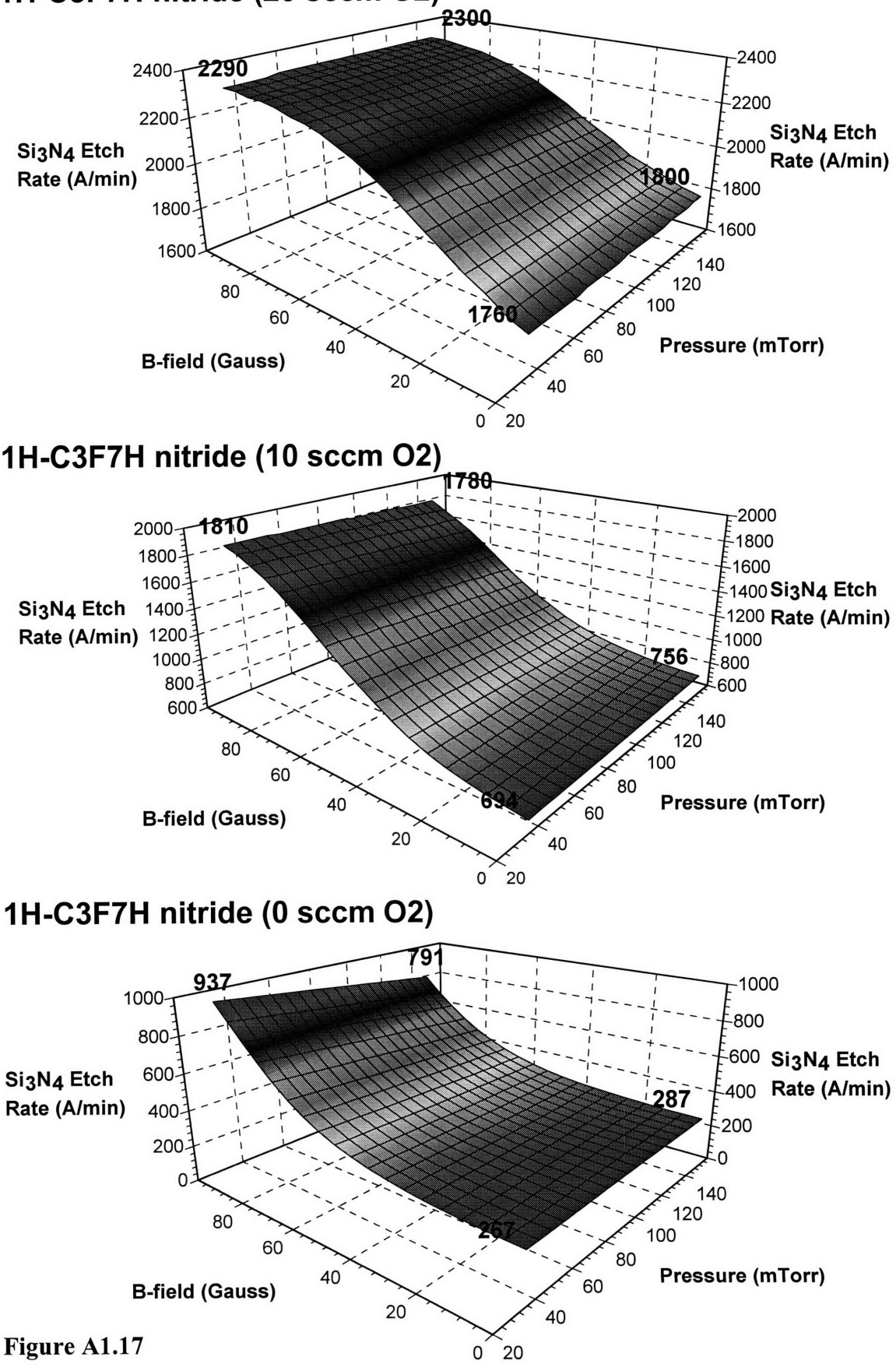
1H-C3F7H nitride (20 sccm O2)
2300
2290
1800
1760
Si3N4 Etch Rate (A/min)
B-field (Gauss)
Pressure (mTorr)
1H-C3F7H nitride (10 sccm O2)
1780
1810
756
694
Si3N4 Etch Rate (A/min)
B-field (Gauss)
Pressure (mTorr)
1H-C3F7H nitride (0 sccm O2)
791
937
287
257
Si3N4 Etch Rate (A/min)
B-field (Gauss)
Pressure (mTorr)

Figure A1.17

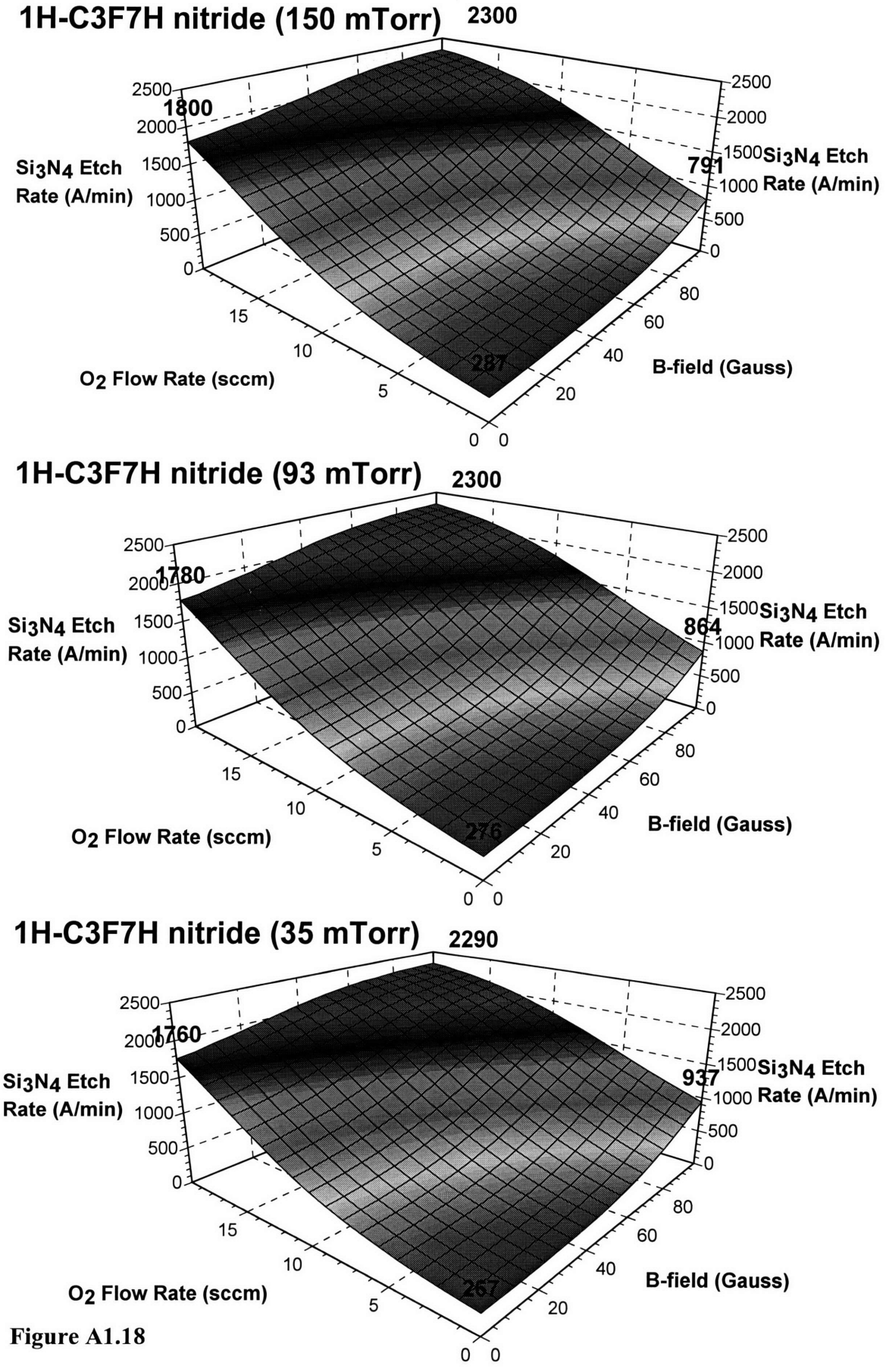
1H-C3F7H nitride (150 mTorr)
2300
1800
791
287
Si3N4 Etch Rate (A/min)
O2 Flow Rate (sccm)
B-field (Gauss)
1H-C3F7H nitride (93 mTorr)
2300
1780
864
276
Si3N4 Etch Rate (A/min)
O2 Flow Rate (sccm)
B-field (Gauss)
1H-C3F7H nitride (35 mTorr)
2290
1760
937
267
Si3N4 Etch Rate (A/min)
O2 Flow Rate (sccm)
B-field (Gauss)

Figure A1.18

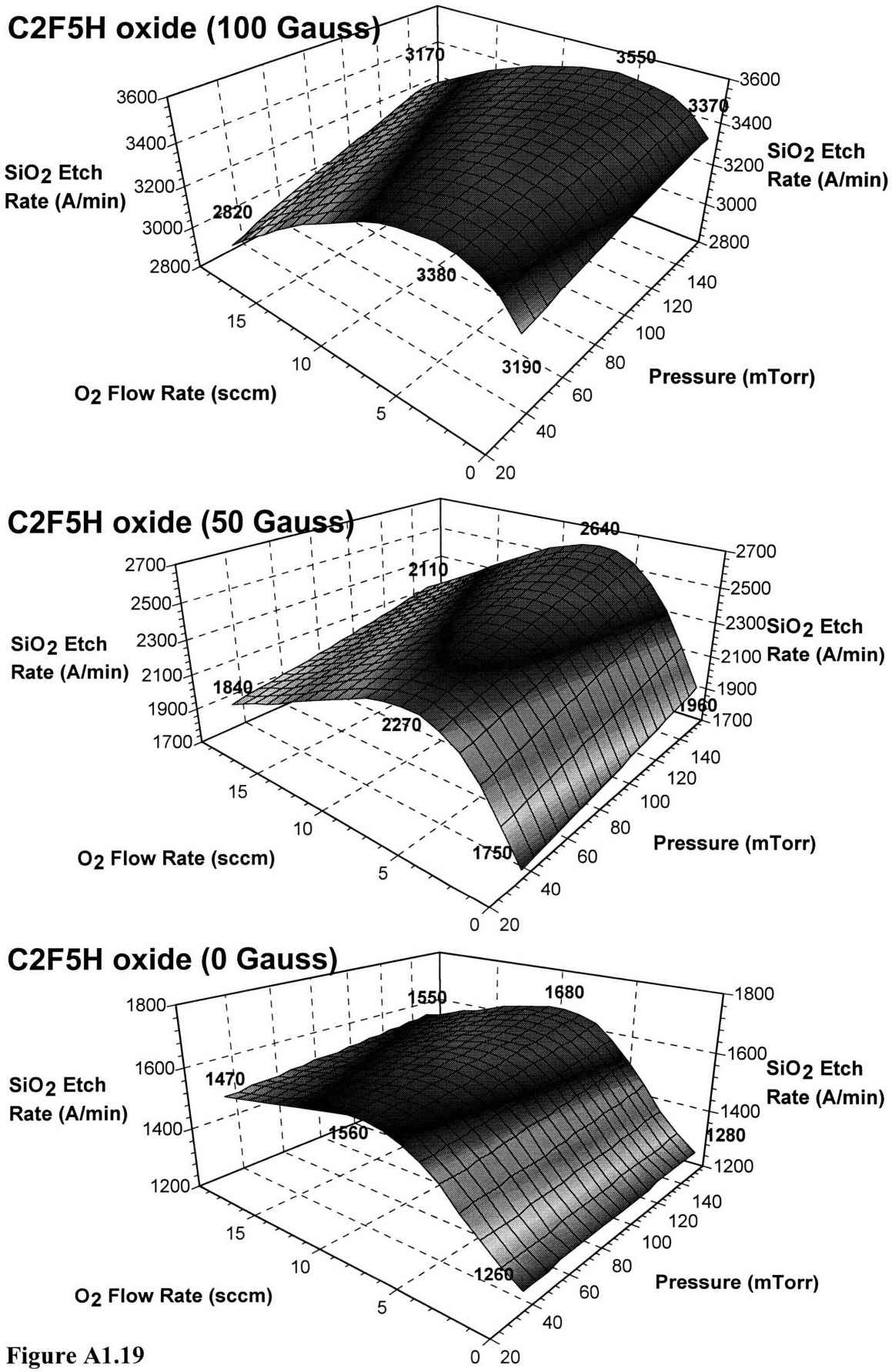
C2F5H oxide (100 Gauss)
SiO2 Etch Rate (A/min)
3600
3400
3200
3000
2800
3170
3550
3370
2820
3380
3190
O2 Flow Rate (sccm)
0
5
10
15
Pressure (mTorr)
20
40
60
80
100
120
140
C2F5H oxide (50 Gauss)
SiO2 Etch Rate (A/min)
2700
2500
2300
2100
1900
1700
2640
2110
1840
2270
1960
1750
O2 Flow Rate (sccm)
Pressure (mTorr)
C2F5H oxide (0 Gauss)
SiO2 Etch Rate (A/min)
1800
1600
1400
1200
1550
1680
1470
1560
1280
1260
O2 Flow Rate (sccm)
Pressure (mTorr)

Figure A1.19

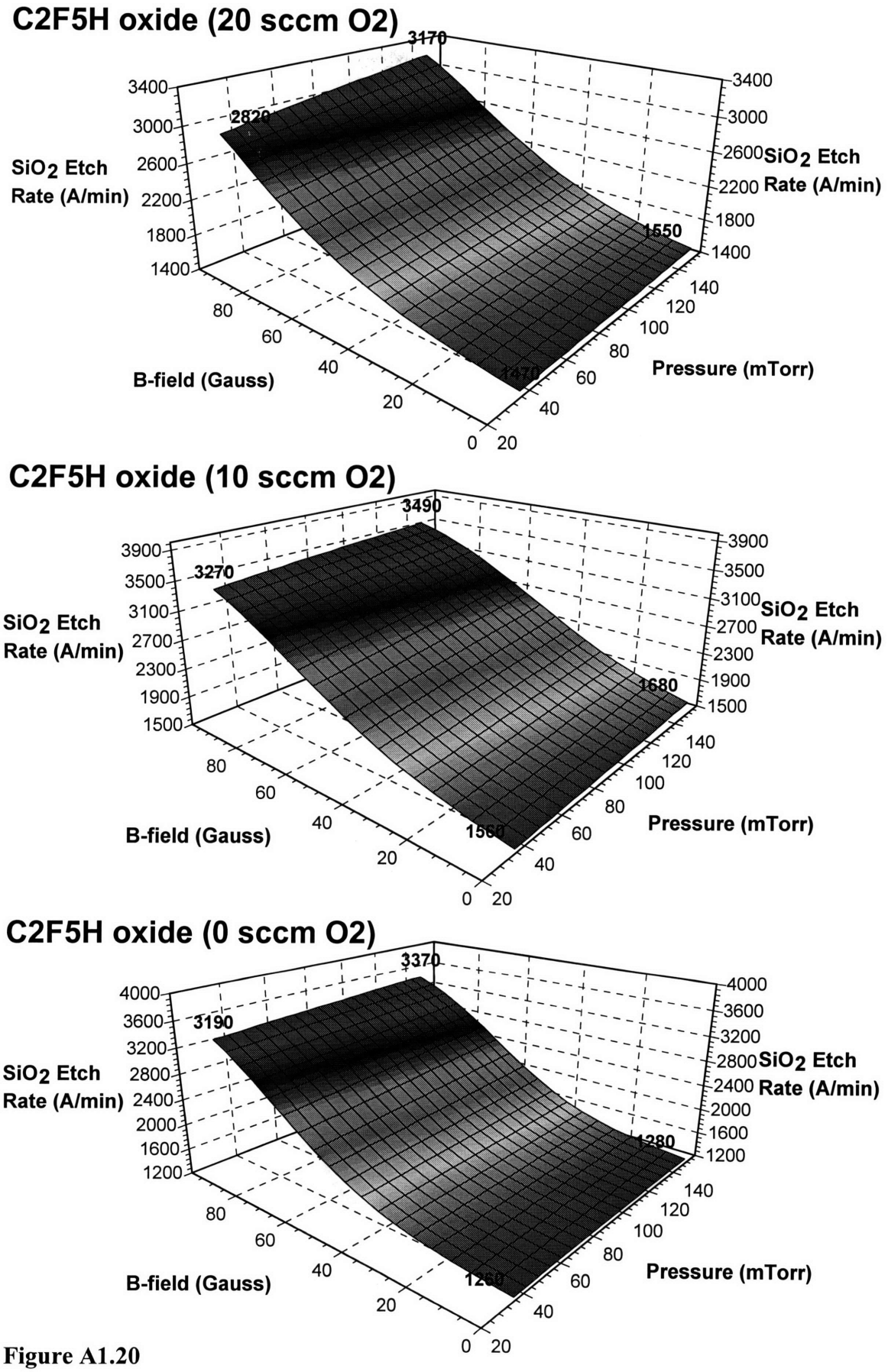
C2F5H oxide (20 sccm O2)
3170
2820
1550
1470
3400
3000
2600
2200
1800
1400
SiO2 Etch Rate (A/min)
80
60
40
20
0
B-field (Gauss)
20
40
60
80
100
120
140
Pressure (mTorr)
C2F5H oxide (10 sccm O2)
3490
3270
1680
1560
3900
3500
3100
2700
2300
1900
1500
SiO2 Etch Rate (A/min)
B-field (Gauss)
Pressure (mTorr)
C2F5H oxide (0 sccm O2)
3370
3190
1280
1260
4000
3600
3200
2800
2400
2000
1600
1200
SiO2 Etch Rate (A/min)
B-field (Gauss)
Pressure (mTorr)

Figure A1.20

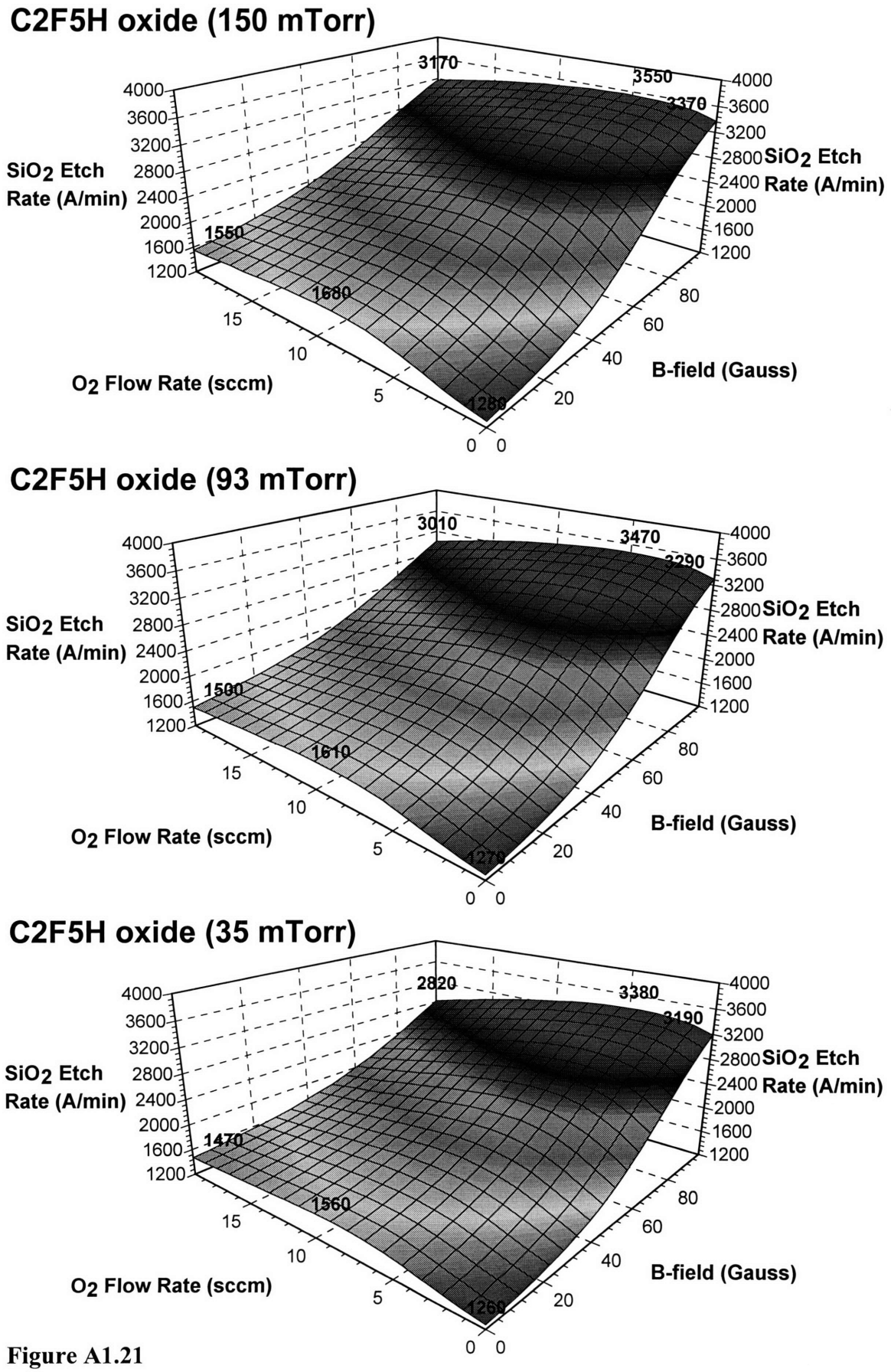
C2F5H oxide (150 mTorr)
3170
3550
3370
1550
1680
1280
4000
3600
3200
2800
2400
2000
1600
1200
SiO2 Etch Rate (A/min)
O2 Flow Rate (sccm)
B-field (Gauss)
0
5
10
15
20
40
60
80
C2F5H oxide (93 mTorr)
3010
3470
3290
1500
1610
1270
C2F5H oxide (35 mTorr)
2820
3380
3190
1470
1560
1260

Figure A1.21

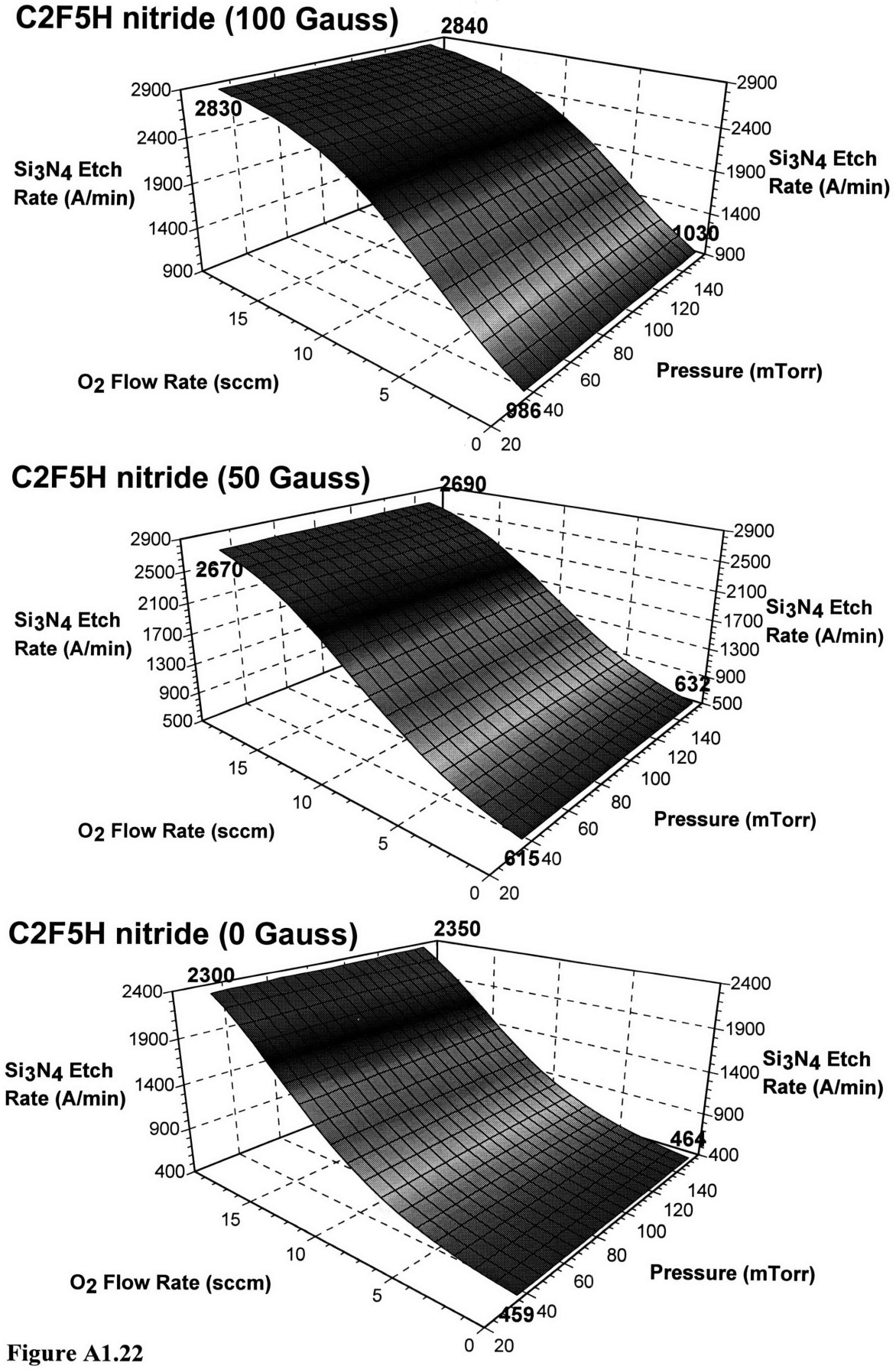
C2F5H nitride (100 Gauss)
2840
2830
1030
986
2900
2400
1900
1400
900
Si3N4 Etch Rate (A/min)
O2 Flow Rate (sccm)
Pressure (mTorr)
0
5
10
15
20
40
60
80
100
120
140
C2F5H nitride (50 Gauss)
2690
2670
632
615
2900
2500
2100
1700
1300
900
500
Si3N4 Etch Rate (A/min)
O2 Flow Rate (sccm)
Pressure (mTorr)
C2F5H nitride (0 Gauss)
2350
2300
464
459
2400
1900
1400
900
400
Si3N4 Etch Rate (A/min)
O2 Flow Rate (sccm)
Pressure (mTorr)

Figure A1.22

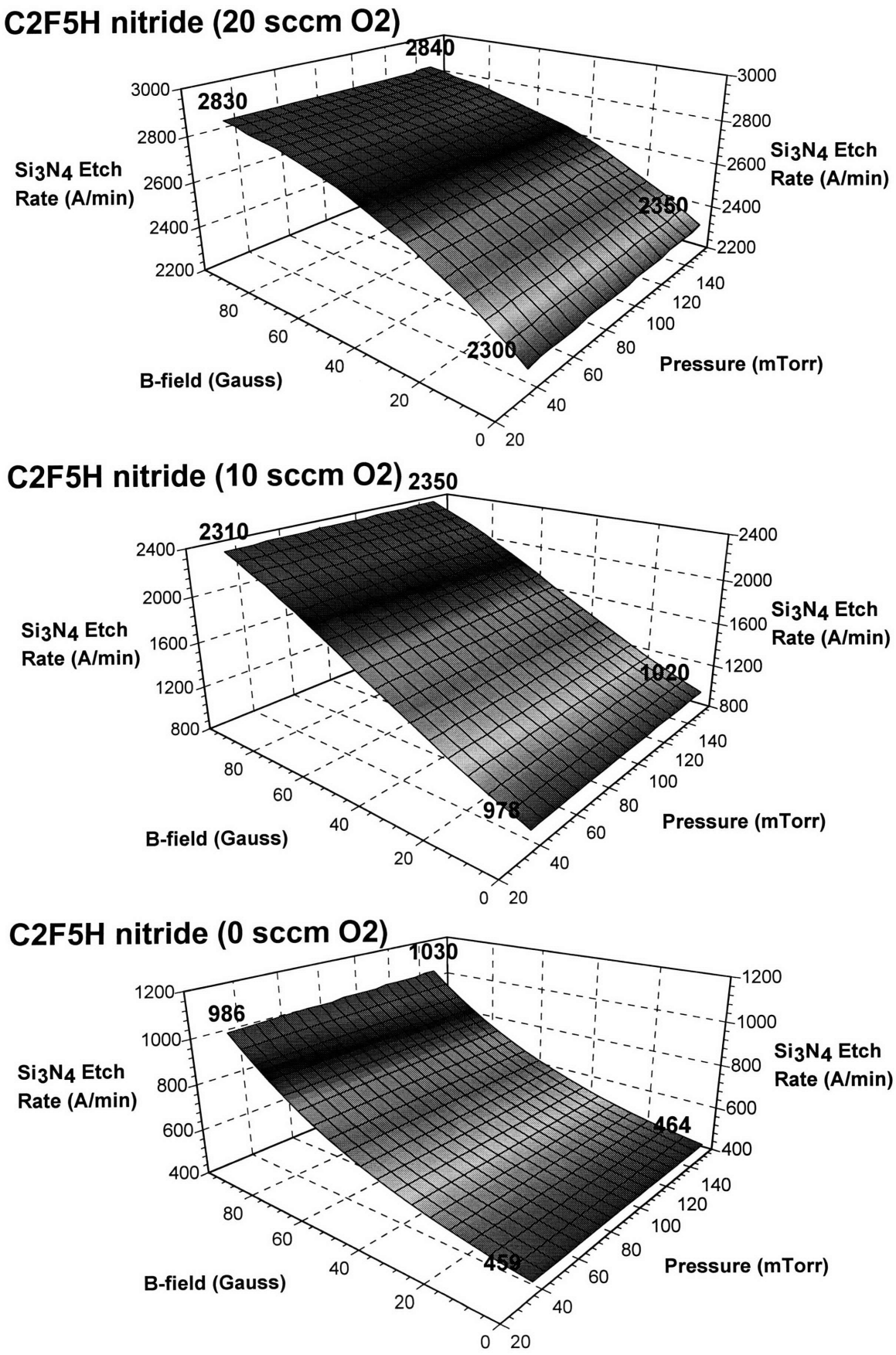
C2F5H nitride (20 sccm O2)
2840
2830
2350
2300
3000
2800
2600
2400
2200
Si3N4 Etch Rate (A/min)
B-field (Gauss)
Pressure (mTorr)
C2F5H nitride (10 sccm O2)
2350
2310
1020
978
2400
2000
1600
1200
800
Si3N4 Etch Rate (A/min)
B-field (Gauss)
Pressure (mTorr)
C2F5H nitride (0 sccm O2)
1030
986
464
459
1200
1000
800
600
400
Si3N4 Etch Rate (A/min)
B-field (Gauss)
Pressure (mTorr)
0
20
40
60
80
100
120
140

Figure A1.23

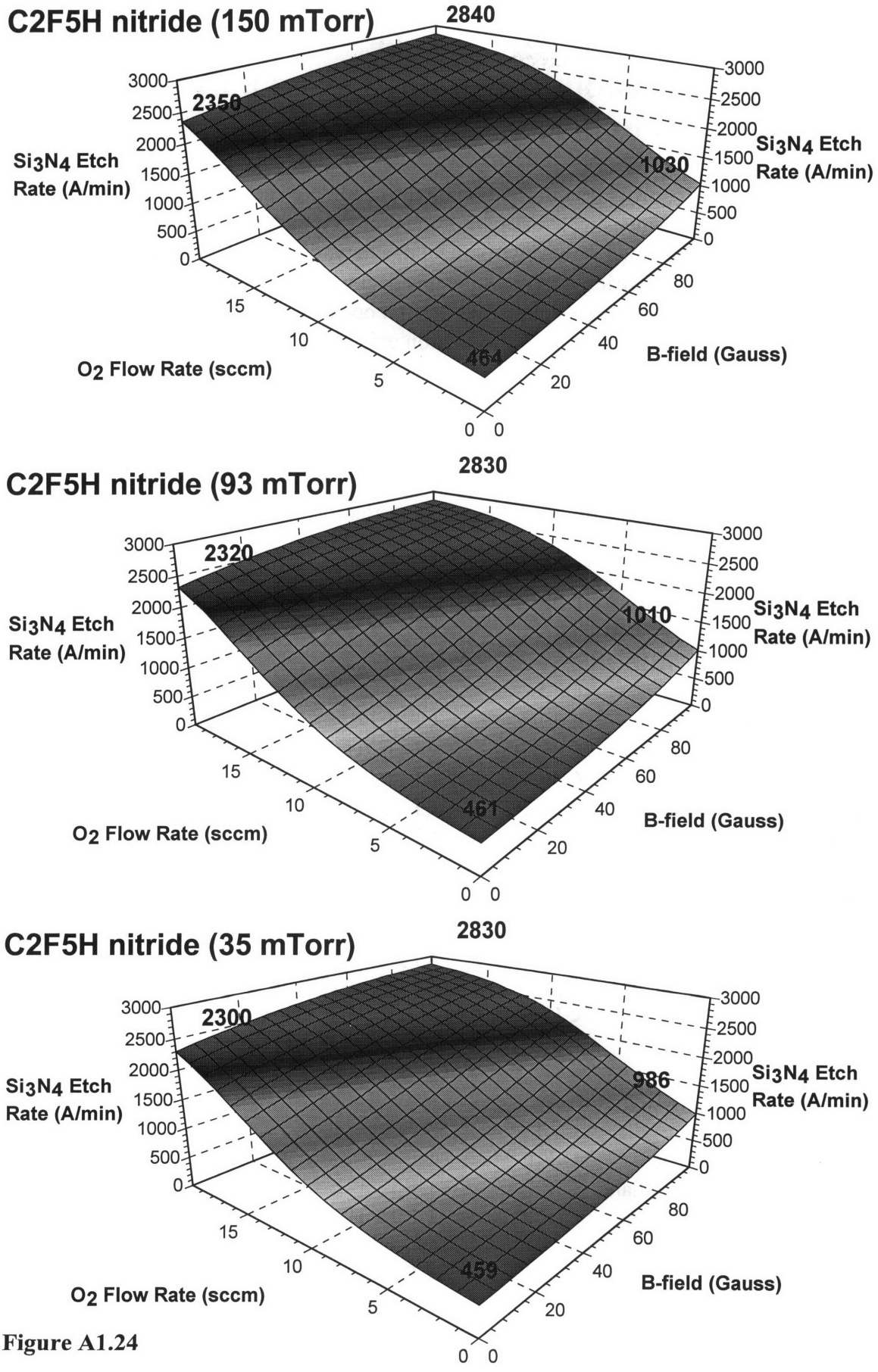
C2F5H nitride (150 mTorr)
2840
2350
1030
464
2830
Si3N4 Etch Rate (A/min)
O2 Flow Rate (sccm)
B-field (Gauss)
C2F5H nitride (93 mTorr)
2320
1010
461
2830
Si3N4 Etch Rate (A/min)
O2 Flow Rate (sccm)
B-field (Gauss)
C2F5H nitride (35 mTorr)
2300
986
459
Si3N4 Etch Rate (A/min)
O2 Flow Rate (sccm)
B-field (Gauss)

Figure A1.24

Appendix 2: Environmental, Health, and Safety Information on Replacement Candidates

This appendix provides information on the candidate chemistries that are being investigated or will be investigated as part of the project on alternative chemistries for PFC replacement. Included is the environmental, safety, and health data that the author is aware of for these chemistries. Areas where this data is lacking are also noted. It should be noted that a number of these chemistries has not been well researched from an ESH standpoint and thus only incomplete information exists for these compounds.

TECHNICAL RESULTS AND DATA

The candidate chemistries fall into three general families: hydrofluorocarbons (HFCs), unsaturated fluorocarbons (FCs), and iodofluorocarbons (IFCs). The specific chemistries are listed below.

NAME	FORMULA	LINE FORMULA
HYDROFLUOROCARBONS		
Difluoromethane	CF_2H_2	
Pentafluoroethane	C_2F_5H	CF_3-CF_2H
1,1,1,2-Tetrafluoroethane	$C_2F_4H_2$	CF_3-CFH_2
2H-Heptafluoropropane	C_3F_7H	CF_3-CFH-CF_3
1H-Heptafluoropropane	C_3F_7H	CF_2H-CF_2-CF_3
Trifluoroethylene	C_2F_3H	CF_2=CFH
UNSATURATED FLUOROCARBONS		
Hexafluoropropylene	C_3F_6	CF_3-CF=CF_2
Hexafluoro-2-butyne	C_4F_6	CF_3-C≡C-CF_3
Hexafluoro-1,3-butadiene	C_4F_6	CF_2=CF-CF=CF_2
Hexafluorocyclobutene	c-C_4F_6	CF_2-CF_2-CF=CF-
Octofluoro-2-butene	C_4F_8	CF_3-CF=CF-CF_3
IODOFLUOROCARBONS		
Iodotrifluoromethane	CF_3I	
Iodopentafluoroethane	C_2F_5I	CF_3-CF_2I
1,2-Diiodotetrafluoroethane	$C_2F_4I_2$	CF_2I-CF_2I
1-Iodoheptafluoropropane	C_3F_7I	CF_2I-CF_2-CF_3
2-Iodoheptafluoropropane	C_3F_7I	CF_3-CFI-CIF_3
Iodotrifluoroethylene	C_2F_3I	CF_2=CFI

Specific etch performance, environmental, safety, and health information for each compound is given below. Performance information is summarized from listed sources. Global warming potentials are taken from reports from the IPCC and Air Products, except for CF_3I, where global warming potential and ozone depletion potential for is taken from: S. Solomon, J. B. Burkholder, A. R. Ravishankara, and R. R. Garcia, "Ozone Depletion and Global Warming Potentials of CF_3I," *Journal of Geophysical Research,* Vol. 99, No. D10, 1994, pp. 20929-20935. Health and safety information is summarized from Materials Safety Data Sheets. Finally, compounds containing fluorine only, unlike bromine, chlorine, and iodine compounds, are not believed to be ozone depleters; therefore no ODP entry is given for HFCs and unsaturated FCs.

HYDROFLUOROCARBONS

Difluoromethane CF_2H_2

CAS # 75-10-5

Etch Performance: Has been examined in combination with other HFCs and PFCs for its ability to promote polymer deposition during etching of silicon dioxide. Used in both low and high density plasma source systems.

Source(s):
ARAI, TSUJIMOTO, and TACH, "DEPOSITION IN DRY-ETCHING GAS PLASMAS,"
JAP. J. APPL. PHYS., 31, 2011 (1992).

GOTOH, and KURE, "ANALYSIS OF POLYMER FORMATION DURING SIO(2) MICROWAVWE
PLASMA ETCHING," JPN. J. APPL. PHYS., 34, 2132 (1995).

KADOMURA, "ETCHING GAS AND METHOD," JPN. KOKAI TOKKYO KOHO JP 61,142,744(1986) (TO SONY), and CHEM. ABSTR., 105, 217533 (1986).

LAMM, and CARRASCO, "HYDROFLUOROCARBON PLASMA SUBMICRON SILICON DIOXIDE
ETCH IN AN AXISYMMETRIC STATIC MAGNETRON," VACUUM, 45, 555 (1994).

MARKS, WONG, KESWICK, and YANG, "OXIDE ETCHING FROM INTEGRATED CIRCUIT
WITH HIGH SELECTIVITY," JPN. KOKAI TOKKYO KOHO JP 06 29, 256 (1994) (TO
APPLIED MATERIALS) and CHEM. ABSTR., 121, 193405 (1994).

NABESHIMA, and TAMAKI, "METHOD OF DRY ETCHING," U.S. PATENT 5, 296, 095
(1994) (TO MATSUSHITA ELECTRIC).

SHIN, "PROCESS FOR DRY ETCHING A SILICON NITRIDE LAYER," U.S. PATENT
5,180,466 (1993) (TO FUJITSU)).

TATEIWA, and TSUJI, "ETCHING CHARACTERISTICS OF PLASMA CVD POLYMERS,"
PROC. 1988 DRY PROCESS SYMP., 74 (1988).

Global Warming Potential: 580 (100 year ITH)

Lifetime: 6 years

Safety: Stable. Flammable; flash point not determined. Incompatible with strong oxidizers (alkali metals). Hazardous decomposition products are HF, CO, and CO(2). No hazardous polymerization.

Health: May cause skin, eye, and respiratory irritation. Narcotic effect. Large exposure can cause damage to heart. 8 Hour TWA:10000 PPM. Not listed as carcinogen by IARC, NTP, or OSHA.

Pentafluoroethane C_2F_5H, CF_3-CF_2H

CAS # 354-33-6

Etch Performance: Has been examined alone for the etching of patterned silicon dioxide films in both low density and high density etching systems. Has also been examined in combination with CF(4) to improve selectivity during silicon dioxide etching in a high density etcher. Has been examined for PECVD chamber cleaning applications, but etch rate deemed to slow.

Source(s) in Literature:

LAMM, and CARRASCO, "HYDROFLUOROCARBON PLASMA SUBMICRON SILICON DIOXIDE
ETCH IN AN AXISYMMETRIC STATIC MAGNETRON," VACUUM, 45, 555 (1994).

MOCELLA, "MATURE AND EMERGING ENVIRONMENTAL ISSUES IN PLASMA PROCESSING:
CFC'S AND PFC'S," PROC. 19TH TEGAL PLASMA SEMINAR, 11 (1993).

MOHINDRA, SAWIN, MOCELLA, COOK, FLANNER, and TURMEL, "ALTERNATIVES TO
PERFLUOROCOMPOUNDS AS PLASMA PROCESSING GASES: SIO(2) ETCHING USING
C(2)F(5)H AND C(2)F(4)H(2)," PROC. ELECTROCHEM. SOC., 94-20, 300 (1994).

OLEWINE, "ALTERNATIVE ETCH CHEMISTRIES AND OPTIMIZATION STUDIES FOR
DIELECTRIC REACTOR CLEANING," PROC. SIA/SSA/SEMATECH GLOBAL WARMING
SYMPOSIUM, ALTERNATIVES/OPTIMIZATION/RECOVERY SECTION, PAPER #3 (1994).

Global Warming Potential: 3,200 (100 year ITH)

Lifetime: 36 years

Safety: Stable. Not flammable. Incompatible with alkali or alkaline earth metals. Hazardous decomposition (by flame) products are HF and possibly carbonyl fluoride. No hazardous polymerization.

Health: Gross exposure may cause dizziness, confusion, uncoordination, drowsiness, or unconsciousness. May cause irregular heat beat. Systemic toxicity through skin contact appears unlikely. Increased susceptibility to persons with pre-existing disease of the cardiovascular system. Not tested for eye or skin irritation. Has very low toxicity (acts like anesthetic). PEL(OSHA):none established, TLV(ACGIH):none established, AEL(DuPont):1000 ppm, 8 and 12 hr. TWA, WEEL (AIHA):1000 ppm, 4900 mg/m3, 8hr. TWA. Inhalation: 4 hour, ALC, rat: > 709,000 ppm. Not listed as carcinogen by IARC, NTP, OSHA, or ACIGH.

1,1,1,2-Tetrafluoroethane C_2F_4H, CF_3-CFH_2

CAS # 811-97-2

Etch Performance: Has been examined alone for the etching of patterned silicon dioxide films in both low density and high density etching systems. Has also been examined in combination with CF(4) to improve selectivity during silicon dioxide etching in a high density etcher.

Source(s):

LAMM, and CARRASCO, "HYDROFLUOROCARBON PLASMA SUBMICRON SILICON DIOXIDE
ETCH IN AN AXISYMMETRIC STATIC MAGNETRON," VACUUM, 45, 555 (1994).

MOCELLA, "MATURE AND EMERGING ENVIRONMENTAL ISSUES IN PLASMA PROCESSING:
CFC'S AND PFC'S," PROC. 19TH TEGAL PLASMA SEMINAR, 11 (1993).

MOHINDRA, SAWIN, MOCELLA, COOK, FLANNER, and TURMEL, "ALTERNATIVES TO
PERFLUOROCOMPOUNDS AS PLASMA PROCESSING GASES: SIO(2) ETCHING USING
C(2)F(5)H AND C(2)F(4)H(2)," PROC. ELECTROCHEM. SOC., 94-20, 300 (1994).

O'NEILL and SINGH, "ULTRAVIOLET ABSORPTION SPECTROSCOPY FOR THE DETECTION
OF CF2 IN HIGH-DENSITY PLASMAS," J. APPL. PHYS., 76, 5967 (1994).

Global Warming Potential: 1,300 (100 year ITH)

Lifetime: 14 years

Safety: Stable. Not flammable. Incompatible with alkali and alkaline earth metals. Hazardous decomposition (open flame) products are HF and possible carbonyl fluoride. No hazardous polymerization.

Health: Gross exposure may cause dizziness, confusion, uncoordination, drowsiness, or unconsciousness. May cause irregular heartbeat. Increased susceptibility to persons with pre-existing disease of the cardiovascular and nervous systems. May be slight eye and skin irritant. Has very low toxicity (acts like anesthetic). PEL(OSHA):none established, TLV(ACGIH):none established, AEL(DuPont):1000 ppm, 8 and 12 hr. TWA, WEEL (AIHA):1000 ppm, 4900 mg/m3, 8hr. TWA. Inhalation: 4 hour, ALC, rate: 567,000 ppm. Not listed as carcinogen by IARC, NTP, OSAH, or ACIGH. According to a DuPont MSDS, for a two year study, a concentration of 50,000 ppm produced an increase in late-occurring benign testicular tumors, testicular hyperplasia, and testicular weight. The no-effect-level for this study was 10,000 ppm. Slight fetotoxicity observed, but only at levels that produced other toxic effects in adults. No change in reproductive performance in male rats. No genetic damage observed in bacterial or mammalian cell cultures, or in animals.

2H-Heptafluoropropane C_3F_7H, CF_3-CFH-CF_3

CAS # 431-89-0

Etch Performance: No etching use reported.

Global Warming Potential: 3,300 (100 year ITH)

Lifetime: 41 years

Safety: Stable. Not flammable. Incompatible with molten alkali metals and strong oxidizers. Hazardous decomposition products are HF, CO, and CO(2). Thermal decomposition products may include PFIB. No hazardous polymerization.

Health: Little health data. Toxicity not determined. PEL(OSHA): not established, TLV(ACGIH): not established. Not listed as carcinogen by NTP, IARC, or OSHA.

1H-Heptafluoropropane C_3F_7H, CF_2H-CF_2-CF_3

CAS # 2252-84-8

Etch Performance: No etching use reported.

Global Warming Potential: not determined

Lifetime: not determined

Safety: Stable. Not flammable. Hazardous decomposition products are HF, CO, and CO(2). Thermal decomposition products may include PFIB. No hazardous polymerization.

Health: Little health data. Toxicity not determined. PEL(OSHA):not determined, TLV(ACGIH):not determined. Not listed as carcinogen by NTP, IARC, or OSHA.

Trifluoroethylene C_2F_3H, CF_2=CFH

CAS # 359-11-5

Etch Performance: No etching use reported.

Global Warming Potential: not determined

Lifetime: not determined

Safety: Stable. Flammable (flash limits not determined). Inhibited with dipentene (<1%). May react explosively with oxygen. Incompatible with peroxides, radical forming conditions, halogens, and halogen halides. Hazardous decomposition products are carbonyl fluoride, HF, CO, CO(2), and perfluoroisobutylene. Hazardous polymerization occurs.

Health: Little health data. Toxicity not determined. May be harmful if inhaled, ingested, or by skin absorption. PEL(OSHA):not established, TLV(ACGIH):not established. Not listed as carcinogen by NTP, IARC, or OSHA.

UNSATURATED FLUOROCARBONS

Hexafluoropropylene C_3F_6, CF_3-CF=CF_2

CAS # 116-15-4

Etch Performance: Has been examined in combination with HFCs and other unsaturated FCs for selective silicon dioxide etching in low and high density plasma systems.

Sources:
BELL, JOUBERT, OEHRLEIN, ZHANG, and VENDER, "INVESTIGATION OF SELECTIVE
SIO(2)-TO-SI ETCHING IN AN INDUCTIVELY COUPLED HIGH-DENSITY PLASMA USING
FLUOROCARBON GASES," J. VAC. SCI. TECHNOL. A, 12, 3095 (1994).

COBURN and WINTERS, "UTILIZING SATURATED AND UNSATURATED HALOCARBON GASES
IN PLASMA ETCHING TO INCREASE ETCH OF SIO2 RELATIVE TO SI," U.S. PATENT
4,162,185 (1979) (TO IBM).

HICHIN, NAKAYAMA, and TANNO, "DRY ETCHING OF A SILICON FILM ON A SEMICONDUCTOR SUBSTRATE," JPN. KOKAI TOKKYO KOHO JP 61,133,630 (1986) (TO
MATSUSHITA ELECTRIC) and CHEM. ABSTR., 105, 236904 (1986).

OEHRLEIN, ZHANG, JOUBERT, VENDER, HAVERLAG, BELL, and KIRMSE, "HIGH-DENSITY PLASMA ETCHING OF SILICON DIOXIDE AND SILICON USING
FLUOROCARBON GASES," PROC. 19TH TEGAL PLASMA SEMINAR, 1 (1993).

Global Warming Potential: not determined

Lifetime: not determined

Safety: Stable. Flammable limits: LEL: 2.6, UEL: 21.7. Matheson describes C(3)F(6) as nonflammable at RT and AP. Incompatibilities: active metals. Hazardous decomposition products may include CO(2), CO, COF(2) and HF. No hazardous polymerization. Reacts with C2F4 + air to form explosive peroxides. Anhydrous C(3)F(6) is not corrosive to most common metals of construction; moist C(3)F(6) hydrolyzes slowly and creates corrosive conditions.

Health: Inhalation can cause central nervous system depression. Symptoms of exposure may include dizziness, cardiac arrhythmia, incoordination. Inhalation of large quantities of this material may also cause liver and kidney damage.

LC50: 750 ppm 4 hours (mouse)
LC50: 20,000 mg/m3 2 hours (rat)
LC50: 2800 ppm 4 hours (rat)
LC50: 11,200 mg/m3 4 hours (rat)
PEL (OSHA):none established, TLV (ACGIH): none established.
OEL (Russia): STEL 5 mg/m3 (Jan 93)

Not listed as carcinogen by IARC, NTP, or OSHA.

Hexafluoro-1,3-butadiene C_4F_6, CF_2=CF-CF=CF_2

CAS # 685-63-2

Etch Performance: No etching use reported.

Global Warming Potential: not determined

Lifetime: not determined

Safety: Stable. Not flammable. Incompatibilities: strong oxidizers, acids, possibly air, oxygen. Hazardous decomposition products may include CO(2), CO, COF(2) and HF. No hazardous polymerization.

Health: Little health data. Toxicity has not been determined. May be harmful if inhaled, ingested or by skin absorption. PEL (OSHA):none established, TLV (ACGIH): none established. Not listed as carcinogen by IARC, NTP, or OSHA.

Hexafluoro-2-butyne C_4F_6, CF_3-C≡C-CF_3

CAS # 692-50-2

Etch Performance: No etching use reported.

Global Warming Potential: not determined

Lifetime: not determined

Safety: Stable. Flammable. Incompatibilities: strong oxidizers, active metals. Hazardous decomposition products may include CO(2), CO, COF(2) and HF. No hazardous polymerization. Forms explosive mixtures in air.

Health: Highly toxic by inhalation. May cause severe irritation to nose and upper respiratory system. May cause skin and eye irritation. "In a DuPont study, six rats exposed to 220 ppm of this material during nose-only exposures died. 5 of 6 rats exposed to 55 ppm died either during or immediately after exposure. All six rats survived a 4 hour exposure to 20 ppm." (PCR MSDS) Symptoms of exposure may include difficulty breathing, headache, chest pain, cardiac arrhythmia, and unconsciousness. May aggravate existing heart conditions. PEL (OSHA):none established, TLV (ACGIH): none established. Not listed as carcinogen by IARC, NTP, or OSHA.

Hexafluorocyclobutene C_4F_6, CF_2-CF_2-CF=CF-

CAS # 697-11-0

Etch Performance : Has been examined alone for the etching of silicon dioxide in a low density plasma system.

Source(s):
YANAGIDA, "DRY ETCHING METHOD," U.S. PATENT 5,338,399 (1994) (TO SONY
CORP.).

Global Warming Potential: not determined

Lifetime: not determined

Safety: Stable. Not flammable. Incompatibilities: strong oxidizers, acids, air, oxygen. Hazardous decomposition products may include CO(2),

CO, COF(2), perfluoroisobutene, and HF. No hazardous polymerization.

Health: Highly toxic by inhalation. Inhalation may cause unconsciousness, dizziness, nausea, and vomiting.

LCLo: 50,000 ppm (inhalation mouse)
LC50: 50 ppm (unknown test animal)
PEL (OSHA):none established, TLV (ACGIH): none established.

Not listed as carcinogen by IARC, NTP, or OSHA.

Octafluoro-2-butene C_4F_8, CF_3-CF=CF-CF_3

CAS # 360-89-4

Etch Performance: The literature search reports the use of C(4)F(8). No indication of which C4F8 isomer was used is given. Some of the sources are listed below.

Source(s):
AKIMOTO, FURUOYA, HARASHIMA, and IKAWA, "ANALYSIS OF FLUOROCARBON FILM
DEPOSITED BY C4F8/CO GAS PLASMA," PROC. ELECTROCHEM. SOC., 94-20, 311
(1994).

FUKASAWA, NAKAMURA, SHINDO, and HORIIKE, "HIGH RATE AND HIGH SELECTIVITY
SIO(2) ETCHING EMPLOYING INDUCTIVELY COUPLED PLASMA," PROC. 15TH DRY
PROCESS SYMP., 103 (1993).

FUKASAWA, NAKAMURA, SHINDO, and HORIIKE, "HIGH RATE AND HIGHLY SELECTIVE
ETCHING EMPLOYING INDUCTIVELY COUPLED PLASMA," JPN. J. APPL. PHYS., 33,
2139 (1994).

GAMBINO, OHIWA, DOBUZINSKY, ARMACOST, YOSHIKAWA, and CUNNINGHAM, "A
SI(3)N(4) ETCH STOP PROCESS FOR BORDERLESS CONTACTS IN 0.25 MICRON
DEVICES," PROC. 12TH VMIC, 558 (1995).

GOTOH and KURE, "ANALYSIS OF POLYMER FORMATION DURING SIO2 MICROWAVWE
PLASMA ETCHING," JPN. J. APPL. PHYS., 34, 2132 (1995).

HISADA, NAKAMURA, and HOSOKI, "HIGHLY SELECTIVE ETCHING OF AN SIO(2) FILM
TO A METAL LAYER," PROC. ELECTROCHEM. SOC., 94-20, 320 (1994).

NOJIRI and IGUCHI, "ELECTRON CYCLOTRON RESONANCE PLASMA ETCHING OF
SILICON DIOXIDE FOR DEEP-SUBMICRON ULTRALARGE SCALE INTEGRATIONS,"
J. VAC. SCI. TECHNOL. B, 13, 1451 (1995).

NOJIRI, IGUCHI, KAWAMURA, and KADOTA, "MICROWAVE PLASMA ETCHING OF
SILICON DIOXIDE FOR HALF-MICRON ULSI'S," EXT. ABSTR. CONF. SOLID STATE
DEV. MATER., 21, 153 (1989).

(NO AUTHOR DISCLOSED), "GAS PLASMA ETCHING METHOD," JPN. KOKAI TOKKYO
KOHO JP 80 61,027(1980) (TO CHO LSI GIJUTSU KINKYU KUMIAI) and CHEM. ABSTR., 93, 141980 (1980).

Global Warming Potential: not determined

Lifetime: not determined

Safety: Stable. Not flammable. Incompatibilities: powdered metals, alkali or alkaline earth metals. Hazardous decomposition products may include CO(2), CO, possibly COF(2) and HF. No hazardous polymerization. Anhydrous octafluoro-2-butene is not corrosive to common metals of construction. In contact with water, it is hydrolyzed slowly and will create corrosive conditions.

Health: Little health data. Toxicity has not been determined. May be harmful if inhaled, ingested or by skin absorption. LCLo: 6100 ppm / 4 hours (rat). Exposure to 6100 ppm for 4 hrs causes mild irritation in rats; higher concentrations produce CNS signs (decrease in activity and convulsions). Symptoms of exposure may include light-headedness, giddiness, shortness of breath, possible narcosis, possible cardiac arrhythmia at high concentrations. PEL (OSHA):none established, TLV (ACGIH): none established. Not listed as carcinogen by IARC, NTP, or OSHA.

IODOFLUOROCARBONS

Iodotrifluoromethane CF_3I

CAS # 2314-97-8

Etch Performance: Has been examined in combination with SF(6) for trench etching of silicon in a low pressure, batch diode system.

Source(s):
BLIZNETSOV, GUTSHIN, and YACHMENEV, "REACTIVE ION ETCHING OF DEEP
TRENCHES IN SILICON," PROC. SPIE, 1783, 584 (1992).

Global Warming Potential: < 5 (20 year ITH)

Lifetime: 0.0026 years (about 1 day)

Ozone Depleting Potential: < 0.008 (conservatively), probably < 0.0001

Safety: Stable. Not flammable. May be incompatible with strong oxidizing agents, alkali metals. Hazardous decomposition products may include CO, CO(2), HI, and HF. No hazardous polymerization. May generate iodine upon exposure to light.

Health: Little health data. Toxicity has not been determined. May be harmful if inhaled, ingested or by skin absorption. May cause cardiac arrhythmia. Irritant to the skin, eyes, mucous membranes, and respiratory tract. PEL (OSHA):none established, TLV (ACGIH): none established. Not listed as carcinogen by IARC, NTP, or OSHA.

Other: B.P.: -22.5 C. Vapor Pressure: 85 psia @ 20 C.

Iodopentafluoroethane C_2F_5I

CAS # 354-64-3

Etch Performance: No etching use reported.

Global Warming Potential: not determined, expected to be negligible.

Lifetime: not determined

Ozone Depleting Potential: not determined

Safety: Stable. Not flammable. May be incompatible with strong oxidizing agents, possibly aluminum. Hazardous decomposition products may include CO, CO(2), Iodine, Perfluorobutane, HI, and HF. No hazardous polymerization. May generate iodine upon exposure to light.

Health: Little health data. Toxicity has not been determined. May be harmful if inhaled, ingested or by skin absorption. Irritant to the skin, eyes, mucous membranes, and respiratory tract. PEL (OSHA):none established, TLV (ACGIH): none established. Not listed as carcinogen by IARC, NTP, or OSHA.

Other: B.P.: 12-13 C. Vapor pressure: 35 psia @ 20 C, 738.9 mmHg @ 10 C.

Iodotrifluoroethylene C_2F_3I, CF_2=CFI

CAS # 359-37-5

Etch Performance: No etching use reported.

Global Warming Potential: not determined, expected to be negligible

Lifetime: not determined

Ozone Depleting Potential: not determined

Safety: Stable. Not flammable. May be incompatible with acids, active metals. Hazardous decomposition products may include CO, CO(2), possibly COF(2), HI, and HF. No hazardous polymerization. May generate iodine upon exposure to light.

Health: Little health data. Toxicity has not been determined. May be harmful if inhaled, ingested or by skin absorption. Irritant to the skin, eyes, mucous membranes, and respiratory tract. PEL (OSHA):none established, TLV (ACGIH): none established. Not listed as carcinogen by IARC, NTP, or OSHA.

Other: B.P.: 30 C (liquid at room temperature). Vapor pressure: not determined.

1-Iodoheptafluoropropane C_3F_7I, CF_2I-CF_2-CF_3

CAS # 754-34-7

Etch Performance: No etching use reported.

Global Warming Potential: not determined, expected to be negligible

Lifetime: not determined

Ozone Depleting Potential: not determined

Safety: Stable. Not flammable. May be incompatible with strong oxidizing agents. Hazardous decomposition products may include CO, CO(2), HI, and HF. No hazardous polymerization. May generate iodine upon exposure to light.

Health: Little health data. Toxicity: ihl-mouse LC50: 404 g/m3 / 2 H. May be harmful if inhaled, ingested or by skin absorption. Irritant to the skin, eyes, mucous membranes, and respiratory tract. PEL (OSHA):none established, TLV (ACGIH): none established. Not listed as carcinogen by IARC, NTP, or OSHA.

Other: B.P.: 40 C (liquid at room temperature). Vapor pressure: not determined.

2-Iodoheptafluoropropane C_3F_7I, CF_3-CFI-CF_3

CAS # 677-69-0

Etch Performance: No etching use reported.

Global Warming Potential: not determined, expected to be negligible

Lifetime: not determined

Ozone Depleting Potential: not determined

Safety: Stable. Not flammable. May be incompatible with strong oxidizing agents. Hazardous decomposition products may include CO, CO(2), HI, and HF. No hazardous polymerization. May generate iodine upon exposure to light.

Health: Little health data. Toxicity has not been determined. May be harmful if inhaled, ingested or by skin absorption. Irritant to the

skin, eyes, mucous membranes, and respiratory tract. PEL (OSHA):none established, TLV (ACGIH): none established. Not listed as carcinogen by IARC, NTP, or OSHA.

Other: B.P.: 38 to 40 C (liquid at room temperature). Vapor pressure: 7.12 psi @ 20 C, 23.29 psi @ 55 C.

1,2-Diiodotetrafluoroethane $C_2F_4I_2$, CF_2I-CF_2I

CAS # 354-65-4

Etch Performance: No etching use reported.

Global Warming Potential: not determined, expected to be negligible

Lifetime: not determined

Ozone Depleting Potential: not determined

Safety: Stable. Not flammable. May be incompatible with strong oxidizing agents. Hazardous decomposition products may include CO, CO(2), iodine, HI, and HF. No hazardous polymerization. May generate iodine upon exposure to light.

Health: Toxic by inhalation in rats: ihl-rat: 33 ppm (acute lethal concentration); produces skin necrosis in rabbits in 48 hours; irritant to eyes in test animals: observation of test animals at 24 hrs showed severe redness, moderate iritis and mild corneal opacity. Severe irritant to the skin, eyes, and possibly mucous membranes and respiratory tract. PEL (OSHA):none established, TLV (ACGIH): none established. Not listed as carcinogen by IARC, NTP, or OSHA.

Other: B.P.: 112-113 C (liquid at room temperature). Vapor pressure: not determined.

Appendix 3: Gases Used in This Study

Table A3.1: Supplementary Information on the Experimental Gases

Gas Name	CAS #	Supplier	Purity (%)	Lot #	Product #	Gas Conversion Factor Used (N_2)**
Octafluoropropane	76-19-7	3M	99+	-	-	0.17
1H-Heptafluoropropane	2252-84-8	PCR, Inc.	99.4	93-3297	17310-4	0.21
2H-Heptafluoropropane	431-89-0	PCR, Inc.	99.8	92-2359	13163-1	0.22
			99.0	95-1311		0.21
Pentafluoroethane	354-33-6	DuPont	99.99	-	-	0.29
1,1,1,2-Tetrafluoroethane	811-97-2	DuPont	99.994	-	-	0.33
Difluoromethane	75-10-5	PCR, Inc.	99.9	95-0795	10002-4	0.61
Trifluoroethylene*	359-11-5	PCR, Inc.	99.9	95-0534	10210-3	0.40

*inhibited with <0.1% dipentene
**as determined by built-in MFC calibration routine on Precision 5000